The Impact of ADAM17 Inhibition on L-selectin in Murine Influenza Virus Infection

Sophie Gabrielle Reed

Thesis presented for the award of PhD (Doctor of Philosophy) at Cardiff University

Division of Infection and Immunity, School of Medicine,
Cardiff University

September 2022

Acknowledgments

I would firstly like to say a huge thank you to my wonderful supervisory team: Ann, Vera, and Augustin. The support and guidance you have given me over the past four years has been second to none. I was an extremely naïve undergraduate student when you first met me, and I hope you agree that I have come a long way since. You have all set such a remarkable example of what a career in research science can hold, and I hope to follow in your footsteps.

Thank you to all of the collaborators who have provided me with reagents and guidance throughout my PhD; Professor Henry Kwok (University of Macau), Dr Dimitar Nikolov and Dr Nayanendu Saha (Sloan Kettering Institute), Professor Ian Humphreys (Cardiff University), Professor Phil Taylor (Cardiff University). And thank you to my funders; BBSRC and GlaxoSmithKline for funding my PhD research.

Thanks to all the amazing members of the Ager lab, past and present. We have made a great team and I will miss you all dearly. Thank you to all the wonderful lifelong friends I have made along the way- special mention to Shayda, Ellie, Ana, Emma, Lauder, Federica, Hannah T, Aisling and Muireann for providing endless laughter, support, and friendship (often along with cocktails!). I couldn't have asked for a more welcoming department to do my PhD in, and I will remember this time fondly.

Thank you to my always supportive family and friends from home who have motivated me throughout my studies and have always made me feel very proud of my achievements. Last but certainly not least, thank you to my wonderful, kind, and caring boyfriend Oliver who has had to put up with endless talk about L-selectin and ADAM17 for the last four years! Thank you for your continued help with calculations, proof-reading, tech support and always believing in me even when I didn't believe in myself. You're my biggest motivation and supporter and I couldn't have done this without your love and encouragement. I hope to return the favour of getting you to the end of your PhD next!

Abstract

L-selectin (CD62L) is a homing molecule on leucocytes. Previously, L-selectin maintenance on CD8 cytotoxic T lymphocytes (CTLs) improved homing to sites of virus infection and subsequent viral clearance in mouse models of influenza A virus (IAV) infection. This finding led us to believe that L-selectin could be a therapeutic target in viral infection. There are currently no pharmacological agents available which directly block the cleavage of L-selectin, however, 'A disintegrin and metalloproteinase 17' (ADAM17) proteolytically cleaves L-selectin from the cell surface. Anti-ADAM17 antibodies were tested for their ability to block shedding of L-selectin in CD8 T cells *in vitro*, and candidate A9(B8) was chosen to take forward to mouse studies with a 50% maximal inhibitory concentration (IC_{50}) of $\geq$261 nM for L-selectin shedding. 10 mg/kg of A9(B8) did not reduce X31 IAV burden in mice over a 7-day infection. 15 mg/kg of A9(B8) was only able to block L-selectin shedding *in vivo* 6 hours post-administration; this was diminished by 4 days. Transgenic ADAM17 inhibition was then tested *in vivo* for effects on X31 IAV virus clearance using $ADAM17^{-/-}$ and $ADAM17^{+/+}$ chimeric mice. Whilst L-selectin was maintained on the cell surface of $ADAM17^{-/-}$ CD8 T cells, these mice did not have reduced X31 titres 5 days post-infection. This timepoint may be too early to investigate T cell-dependent virus clearance and requires further investigation. Furthermore, ADAM17 chimeras revealed a novel role for ADAM17 in homeostatic shedding of L-selectin in B cells, but not T cells. Further *in vitro* studies showed that A9(B8) was less effective at blocking L-selectin shedding from B cells than T cells. However, A9(B8) was more effective at blocking TNF-α shedding with an IC_{50} of $\geq$75 nM. Together, these studies demonstrate that the proteolytic activity of ADAM17 is differentially controlled in T and B cells and is substrate dependent.

Table of contents

List of Tables

List of Figures

Table of Abbreviations

ADAM10/17	A disintegrin and metalloproteinase 10/17
ADCC	Antibody-dependent cellular cytotoxicity
AEC	3-amino-9-ethylcarbazole
AM	Alveolar macrophage
ANOVA	Analysis of variance
APC	Antigen presenting cell
APC-Cy7	Allophycocyanin-cy7
BAL	Bronchoalveolar lavage
BALF	Bronchoalveolar lavage fluid
BCR	B cell receptor
BSA	Bovine serum albumin
B6	C57BL/6J mouse
CCL	Chemokine ligand
CCR	Chemokine receptor
CD	Cluster of differentiation
cDNA	Complementary deoxyribonucleic acid
CD62L	L-selectin
CTL	CD8 cytotoxic T lymphocyte
CXCL	Chemokine ligand
CXCR	Chemokine receptor
DC	Dendritic cell
ddH_20	Double distilled water
DDT	Dithiothreitol
DLBCL	Diffuse large B cell lymphoma
DMEM	Dulbecco's modified eagle medium
DMF	Dimethyl formamide
DMSO	Dimethyl sulfoxide
ECD	Extracellular domain
EDTA	Ethylenediaminetetraacetic acid
EGF(R)	Epidermal growth factor (receptor)
ELISA	Enzyme-linked immunosorbent assay
EM	Electron microscopy
ER	Endoplasmic reticulum
FA	Formaldehyde
FasL	Fas ligand
FCS	Foetal calf serum
FITC	Fluorescein isothiocyanate
FMO	Fluorescence minus one
GAPDH	Glyceraldehyde-3-phosphate dehydrogenase
GlyCAM-1	glycosylation-dependent cell adhesion molecule-1
GM-CSF	Granulocyte-macrophage colony-stimulating factor
GPCR	G-coupled protein receptors
HA	Haemagglutinin
HER2	Human epidermal growth factor 2
HEV	High endothelial venule
HRP	Horseradish peroxidase
H17	E61-13-H17 (H3N2) influenza A virus
IAV	Influenza A virus
ICAM-1/2	Intercellular cell-adhesion molecule-1/2
ICD	Intracellular domain
IC_{50}	50% maximal inhibitory concentration

IFN(-α,β,γ)	Interferon-alpha, beta, gamma
Ig	Immunoglobulin
IL-1β	Interleukin 1-beta
IL-2	Interleukin 2
IL-6	Interleukin 6
IL-10	Interleukin 10
IL-12p70	Interleukin 12p70
IP-10	Interferon-gamma-inducible protein 10
i.p.	Intraperitoneal
i.v.	Intravenous
JAM	Junction adhesion molecule
KC	Keratinocyte derived chemokine
KLF2	Kruppel-like factor 2
LAG3	Lymphocyte activation gene-3
LD	Live/dead
LFA-1	Leucocyte function-associated antigen-1
LOD	Limit of detection
LPS	Lipopolysaccharide
LΔP	Mouse that resists L-selectin proteolytic cleavage and transcriptional silencing on T cells
Mac-1	Macrophage antigen 1
MAdCAM-1	Mucosal vascular addressin cell-adhesion molecule 1
MALT	Mucosal associated lymphoid tissue
MAPK	Mitogen-activate protein kinase
MCP-1	Monocyte chemoattractant protein-1
MDCK	Madin Darby canine kidney cells
Med LN	Mediastinal lymph node
MFI	Mean fluorescence intensity
MHC-I/II	Major histocompatibility complex class 1/2
MMP	Matrix metalloproteinase
mRNA	Messenger ribonucleic acid
NA	Neuraminidase
NALT	Nasal associated lymphoid tissue
NSCLC	Non-small cell lung cancer
NFW	Nuclease free water
NK cell	Natural killer cell
NP	Nucleoprotein
PAO	Phenylarsine oxidase
PBS	Phosphate-buffered saline
PDAC	Pancreatic ductal adenocarcinoma
PDI	Protein disulfide isomerase
PE	Phycoerythrin
PE-Cy7	Phycoerythrin-cy7
PerCP-Cy5.5	Peridinin chlorophyll protein-cy5.5
Pfu	Plaque forming unit
PI3Kδ	Phosphoinositide-3-kinase-delta
PKC	Protein kinase C
PMA	Phorbol 12-myristate 13-acetate
PNAd	Peripheral lymph node addressin
PRR	Pattern recognition receptor
PR8	A/PuertoRico/8/34 (H1N1) influenza A virus
PSGL1	P-selectin glycoprotein-1
Rag$^{-/-}$	Recombinase activation gene knockout mouse
RANTES	Regulated upon Activation, Normal T Cell Expressed and Presumably Secreted

RBC	Red blood cell
ROS	Reactive oxygen species
RPMI	Rosewell Park memorial institute medium
RT-qPCR	Reverse transcription quantitative polymerase chain reaction
scFv	Short chain variable fragment
SCR	Short consensus repeat
SDS-PAGE	Sodium dodecyl-sulfate polyacrylamide gel electrophoresis
SEM	Standard error of the mean
SPF	Specific pathogen-free
S1P(R)	Sphingosine-1-phosphate (receptor)
TACE	Tumour necrosis factor alpha converting enzyme
T_{CM}	Central memory T cells
TCR	T cell receptor
T_{EM}	Effector memory T cells
T_{FH}	T follicular helper cells
TGF-α	Transforming growth factor alpha
TIM-3	T cell immunoglobulin and mucin gene 3
TIMP-1/3	Tissue inhibitor of metalloproteinase-1/3
TLR	Toll like receptor
TMD	Transmembrane domain
TNF-α	Tumour necrosis factor alpha
TNFRI/11	(TNF)-receptor 1/2
TRAIL	(TNF)-related apoptosis inducing ligand
T_{reg}	Regulatory T cell
T_{SCM}	Stem cell memory T cell
VCAM-1/2	Vascular cell adhesion molecule-1/2
VE-Cadherin	Vascular-endothelial cadherin
VLA-4	Very late antigen-4
vRNA	Viral ribonucleic acid
vRNP	Viral ribonucleoprotein
X31	H3N2/A-X31 influenza A virus

Chapter One

Introduction

1. Introduction

1.1 The immune system

The immune system is the body's defence against infections, cancer, and tissue damage. We are constantly challenged by pathogens within our environment, which are confronted by our immune response. The immune system consists of numerous cell types, each with their own unique function to protect the host. The molecules they produce and the specialised immune organs with which they interact aid in the effectiveness of this defence strategy (Murphy and Weaver 2017).

There are four main tasks the immune system must fulfil to protect its host. Firstly, it must recognise the presence of pathogens or cancerous cells. This is conducted by the first defence line of the immune system; the innate immune system. Secondly, effector functions must be engaged to try and eliminate the infection or threat. To further protect the host, the immune system must thirdly control itself to prevent allergies and autoimmune diseases. An overactive immune system can be harmful to the host; thus, the immune system must be tightly regulated. The concluding major task is to create immunological memory. This involves the adaptive immune system, which functions to protect the host against additional infections by the same pathogen in future. This adaptive arm of the immune system is the target for vaccinations (Murphy and Weaver 2017).

Pluripotent haematopoietic stem cells in the bone marrow develop into either a common lymphoid or myeloid progenitor. These progenitor cells are precursors to the white cells of the immune system called leucocytes. Common myeloid progenitors also give rise to thrombocytes and erythrocytes (Murphy and Weaver 2017).

The innate immune system is the first defence line within the body and consists of various cell types such as granulocytes, monocytes, and dendritic cells (DCs) developing from the common myeloid progenitor cells. The adaptive immune system is involved in long lasting, immunological memory and consists of T and

B lymphocytes (T and B cells) which mature from the common lymphoid progenitor cells (Murphy and Weaver 2017).

Throughout the body there are specialised lymphoid tissues and organs which have their own unique functions within the immune system. The cells of the immune system are all derived from precursor cells in the bone marrow which can either differentiate within the bone marrow itself, or the thymus in the case of T cells, which are both primary lymphoid organs. These mature cells leave their primary lymphoid organs and survey the body for pathogen either within tissues or the blood. The spleen and lymph nodes (LNs) are secondary lymphoid organs, which act as sites of immune surveillance lymphocyte activation (Murphy and Weaver 2017).

1.2 The adaptive immune system

The adaptive immune system is the second line of defence to invading pathogens within the body. If the innate immune system becomes unable to eliminate a pathogen, the adaptive response is initiated. Two key features of this response are antigen specificity and long-lasting memory (Murphy and Weaver 2017).

There are 2 major types of cells within the adaptive immune system: T and B lymphocytes. Both cell types have a cell surface receptor, a T cell receptor (TCR) and B cell receptor (BCR) respectively, which are antigen specific. These cells will survey the body as naïve lymphocytes until encountered by a corresponding antigen which stimulates activation and differentiation into effector cells (Murphy and Weaver 2017).

Effector T cells can be either cytotoxic CD8 cells, helper CD4 cells or regulatory CD4 cells. Cytotoxic CD8 T lymphocytes (CTLs) are involved with direct killing of infected cells, whereas helper T cells orchestrate signals to other cells of the immune system such as B cells and macrophages to improve efficiency of the response. Regulatory T cells help with the control of the immune response to

minimise overactivation which is harmful to the host (Murphy and Weaver 2017).

B cells differentiate into plasma cells upon antigen recognition which secrete antibodies with the same antigen specificity as the BCR. Antibodies/ immunoglobulins (Igs) have key roles in neutralising and destroying pathogens. Aiding in phagocytosis, initialising the complement system via Fc receptors, and blocking mucosal binding are some of the effector functions of antibodies (Murphy and Weaver 2017).

Immunological memory is a vital feature which provides long lasting protection to the host against a specific pathogen. Memory T and B cells will develop after exposure to an antigen and reside in tissues or the blood for a significant amount of time. Therefore, if this pathogen is encountered again, a population of antigen-specific cells will readily differentiate into effector cells to provide an enhanced immune response upon second exposure (Murphy and Weaver 2017).

1.3 T cells

1.3.1 T cell development and differentiation

T lymphocytes develop from common lymphoid progenitors derived from pluripotent haematopoietic stem cells in the bone marrow. Common lymphoid progenitors will leave the bone marrow and migrate to the thymus where they will undergo clonal selection and differentiation into mature naïve T cells.

T cells go through distinct stages of differentiation starting with double negative ($CD4^-CD8^-$) thymocytes. Mature T cells contain a TCR which will recognise peptide sequences in an MHC molecule to allow activation and effector functions. Each TCR consists of an alpha (α) and beta (β) chain (or gamma (γ) and delta (δ) chains for $\gamma\delta$ T cells) which requires a high level of variety to create a diverse population of T lymphocytes in each host. Immunological diversity of antigen recognition allows for a successful immune response against invading pathogens. This diversity is created by rearrangement of the

variable (V), diversity (D) and joining (J) gene segments of the TCR chains and is coined 'VDJ recombination'. VDJ rearrangement of the β chain of the TCR occurs during the double negative stage of differentiation. Cells then differentiate into double positive (CD4+CD8+) thymocytes where VDJ recombination of the α chain of the TCR is initiated and a complete TCR is created. However, this variety in TCR specificity can result in self-antigen recognition. Therefore, after gene arrangement, T cells will go through rigorous clonal selection and deletion (positive and negative selection) to ensure TCRs do not attack host tissues or cells. During the double positive stage, positive selection is initiated to select for thymocytes with low-affinity self-peptide recognition. Subsequently, a CD4 or CD8 phenotype is then selected, and these cells become single positive thymocytes. These cells will then undergo negative selection to remove T cells that strongly recognise self-peptides.

Once matured and clonally selected, naïve T cells will recirculate to the secondary lymphoid organs via the blood and lymphatics. Secondary lymphoid organs are the spleen, LNs and mucosal associated lymphoid tissue (MALT) which function for immunosurveillance and homeostatic purposes (Murphy and Weaver 2017).

1.3.2 Cytotoxic CD8 T cells

Cytotoxic CD8 T cells are a type of effector T cell known as 'CTLs' and have key roles in controlling pathogens and cancers. Naïve CD8 T cells differentiate in response to antigenic stimulation by an antigen presenting cell (APC), which is recognised by their clonotype of TCR. In addition to co-stimulatory molecules, this will result in proliferation and clonal expansion of the CD8 T cell and differentiation into an effector phenotype. Once a CTL phenotype has been adopted, the cell will change expression of several cell surface molecules to allow migration to sites of infection. This is described in more detail in section 1.8 onwards. The role of a CTL is to detect pathogenic peptide-MHC on infected cells and carry out cytotoxic actions to kill the infected cell (apoptosis), limit pathogenesis and promote survival. CTLs carry out programmed cell death via cytokine and cytotoxic granule release. Cytokines like interferon gamma (IFN-γ) and granules which contain proteins such as

perforin and granzymes, trigger apoptosis pathways within the target cell to reduce pathogenic spread. CTLs have a fundamental role in the control of viral infections (Murphy and Weaver 2017).

1.4 Viruses

Viruses are small intracellular parasites which can infect animals, plants, or microorganisms. Many viruses, including influenza A virus (IAV) are unable to self-replicate and require a host to survive, by inserting their genome into the host cells' replication machinery to create new virions. A virus consists of a protein capsid with nucleoproteins (NPs) which encloses the viral genome to form a nucleocapsid. This can be contained inside the envelope of glycoproteins and a lipid bilayer in some viruses. This complete particle is known as a virion (Gelderblom 1996).

Viruses that can infect humans are categorised into 21 families based on their biochemical composition, morphology, and method of replication. 70% of viruses use RNA as their genetic material such as coronaviruses, retroviruses and orthomyxoviruses. These viruses have higher mutation rates than DNA viruses and adapt rapidly to new hosts. Adenoviruses and herpesviruses are among DNA viruses which infect humans. Each family has its own unique structure, mode of pathogenesis and mechanism of disease in humans varying from respiratory disease, gastrointestinal disease, and disease of the nervous system (Gelderblom 1996).

Highly pathogenic viruses have the ability to cause worldwide pandemics such as Spanish Influenza (H1N1) in 1918, Swine Influenza (H1N1) in 2009 and the most recent SARS-CoV-2 (COVID-19) pandemic. Due to the increasing possibility of future pandemics whereby there are no vaccines or anti-viral drugs available, investigating immune responses and therapeutics that target the immune system are both fundamental, to limit virus induced pathology and boost immune-mediated destruction of virus infected cells.

1.4.1 Influenza viruses

Influenza viruses are of the orthomyxovirus family and can be categorised into types A, B, C and D. Influenza D is primarily found within cattle, whilst influenza C is known to cause only mild illness in humans (Influenza (Seasonal). 2018). Types A and B cause seasonal epidemics each year, however, only the A subtype has resulted in a worldwide pandemic to date. Influenza virus is a significant health burden throughout the world, causing up to 650,000 deaths per year (Influenza (Seasonal). 2018). Typical influenza virus infection presents with respiratory symptoms such as cough, sore throat, and rhinitis as well as fever, headache, and myalgia. In severe cases, which mainly occur in the elderly and those with pre-existing conditions, pneumonia can occur leading to sepsis and organ failure (Influenza (Seasonal). 2018). Annual vaccinations are recommended for the public but predicting circulating strains can be highly challenging with such a dynamic virus. IAV is known to cause higher mortality than other influenzas, so is therefore more researched.

Influenza viruses are RNA viruses which use negative, single-strand RNA as their genetic material. The IAV genome is concealed within 8 viral ribonucleoprotein (vRNP) segments. Viral RNA (vRNA) secured within the nucleocapsid, is flanked at one end by polymerase complexes PB1, PB2 and PA. The segmented nucleocapsids are enclosed by the matrix protein (M1) and lipid bilayer which is coated in haemagglutinin (HA) and neuraminidase (NA) glycoproteins with M2 membrane ion channels (Blümel et al. 2009), (Figure 1.1 A). IAVs are further categorised by their HA and NA expression. There are currently 18 HAs and 11 NAs identified, with 120 combinations of HA and NA molecules being found naturally circulating, to date. H1N1 and H3N2 are among the most common circulating seasonal strains in humans (Kosik and Yewdell 2019).

1.4.2 Influenza virus replication

Influenza virus enters the host through the respiratory tract. The HA glycoprotein has receptor binding and membrane fusion capabilities to allow entry into host cells. The HA receptor binding domain binds sialylated glycoconjugates on the host cell surface. This triggers endocytosis of the virion

into the cell. Once inside the cell, the virion is trafficked towards the endosome, where acidic pH causes a conformational change in HA via activation of the M2 protein. This confirmational change exposes the HA ‘fusion peptide’, which embeds into the endosomal membrane. This causes the M2 protein channel to allow the inside of the virion to sense pH changes. This leads to release of vRNPs from the M1 protein. Further HA conformational changes creates a ‘fusion pore’ to allow vRNPs to be released into the cytosol of the cell. Importin-α and importin-β will then transport vRNPs into the nucleus where vRNAs will be transcribed into mRNA by the viral RNA polymerases (PB1, PB2, PA). mRNAs are subsequently exported from the nucleus to be transcribed into vRNPs via cytosolic or endoplasmic reticulum (ER) associated ribosomes. The vRNPs are then transported to the budding region of the plasma membrane by Rab11 for assembly into a complete virion. Virion release from the bud is then catalysed by NA; removal of sialic acid residues prevents HA binding and subsequent virion release from the cell for further host infection (Dou et al. 2018), (Figure 1.1 B).

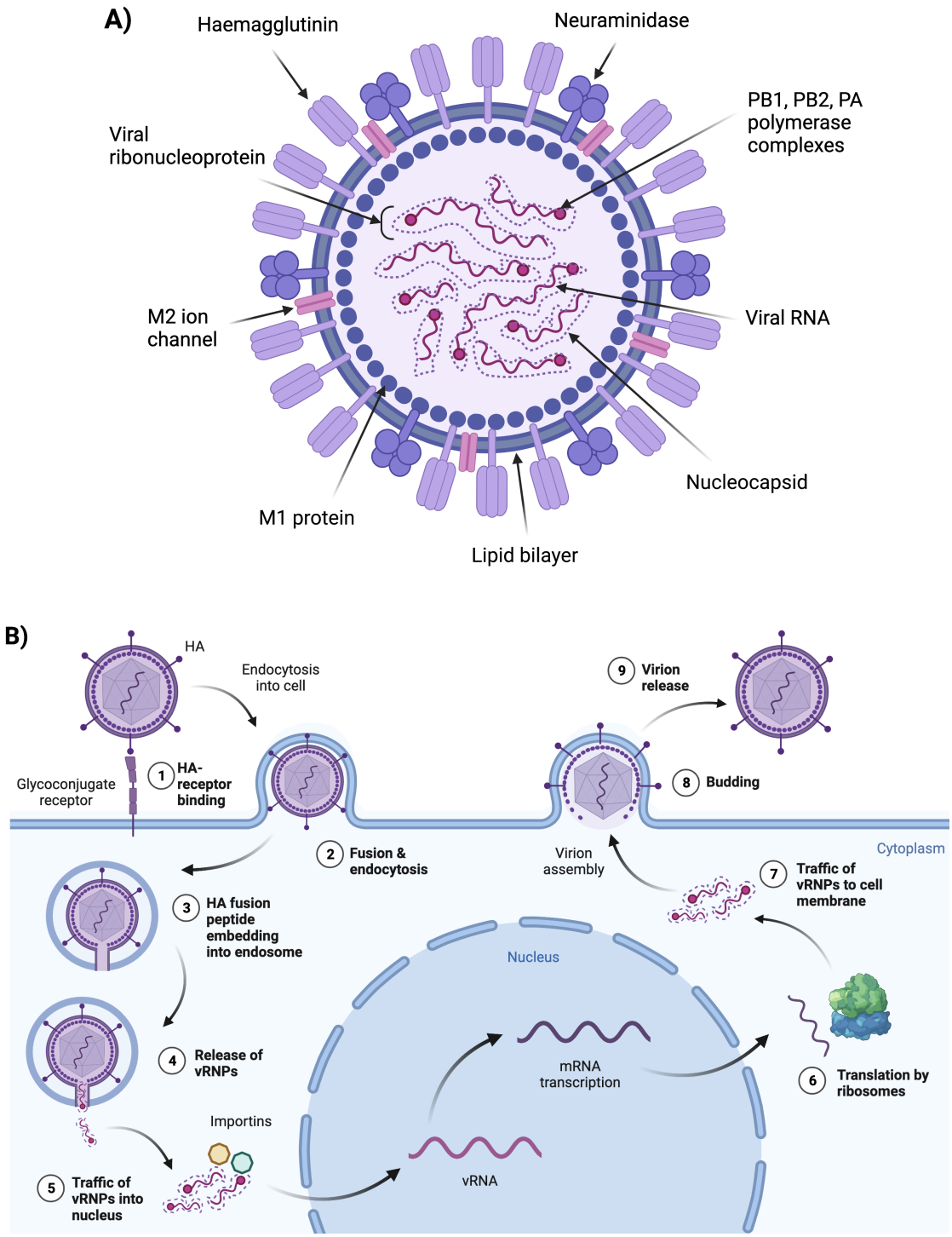

Figure 1.1. Influenza virus virion structure and life cycle. A) Influenza virus virion structure; 8 viral ribonucleoprotein (vRNP) complexes each consisting of an RNA genome segment wrapped around viral nucleoproteins, concealed within a nucleocapsid, flanked at one end by polymerase complexes PB1, PB2 and PA. The segmented vRNPs are enclosed by the matrix protein (M1) and lipid bilayer which is coated in haemagglutinin (HA) and neuraminidase (NA) glycoproteins, with M2 membrane ion channels. **B)** 1. Viral HA binds sialylated glycoconjugates on the host cell surface. 2. Endocytosis of the virion into the cell. 3. Acidic pH inside endosome causes conformational change in HA via activation of the M2 protein channel. Exposure of the HA 'fusion peptide', which embeds into the endosomal membrane,

causing M2 to allow the inside of the virion to sense pH changes. A ‘fusion pore’ from further pH-dependent HA confirmational changes occurs. 4. Release of vRNPs into the host cell. 5. Importin-α and importin-β transport vRNPs into the nucleus where viral RNAs (vRNAs) are transcribed by the viral RNA polymerases (PB1, PB2, PA) into mRNA. 6. Translation of mRNAs into proteins via ribosomes. 7. Viral proteins are trafficked from the endoplasmic reticulum to the budding region of the plasma membrane where they assemble into a complete virion. 8. Budding of the membrane which is required for scission of the viral envelope from the cell. 9. Virion release from the bud catalysed by NA; removal of sialic acid residues prevents HA binding and subsequent virion release from the cell for further infection (Dou et al. 2018). Figure created using Biorender.com.

1.4.3 IAV Tissue Tropism

As mentioned above, the influenza HA glycoprotein on the virion surface has receptor binding and membrane fusion capabilities to allow entry into host cells. This happens mainly in the respiratory tract. The HA receptor binding domain binds sialylated glycoconjugates on the host cell surface. α2,3 or α2,6 sialic acid (N-acetyl neuraminic acid) linkages are preferentially targeted by HA in humans (Stevens et al. 2006).

Epithelial cells (pneumocytes in the alveoli) are one of the first cells contacted by IAV within the respiratory tract, making them highly susceptible to initial infection. In animal and human lung tissue sections, IAV strains H1N1 and H3N2 demonstrated preferential binding to type I pneumocytes, while H5N1, H5N9, and H6N1 bound to type II pneumocytes (Van Riel et al. 2007). *Ex vivo* infection of human lung explants showed association of viral antigen with type II pneumocytes for H5N1, H1N1 and H3N2 strains (Weinheimer et al. 2012).

Alveolar macrophages (AMs) are the resident population of phagocytes present in the lungs, which have roles in homeostasis and defence against pathogens. Evidence from *ex vivo* studies on primary human cells suggests that AMs can also become directly infected by IAV, but to a much lesser extent than epithelial cells (Travanty et al. 2015), (Ettensohn et al. 2016). However, mouse AMs are more susceptible to direct infection with up to 90% of primary murine AMs becoming infected, dependent on IAV strain (Londrigan et al. 2015). As well as AMs, a range of immune cells such as monocytes, DCs, neutrophils, natural killer (NK) cells, eosinophils and B cells are found to be directly infected by IAV in humans (Hou et al. 2012), (Österlund et al. 2010), (Zhao et al. 2008), (Mao et al. 2009), (Dougan et al. 2013), and mice (Hao et al. 2008), (Guo et al. 2009), (Samarasinghe et al. 2017). Some studies suggest this can be abortive infection, whereby the cells infected do not produce functional IAV virions (Guo et al. 2009), (Dougan et al. 2013). Other studies suggest these cells may be ‘productively infected’ and able to migrate and disseminate the virus to other organs or tissues (Zhao et al. 2008). This could be a mode of infection for blood vessel endothelial cells, however, there is limited data available to suggest

endothelial cells become infected in mammals (Nguyen-Van-Tam 2010). H5N1 vRNAs have been found in peripheral blood and rectum of patients who died of the virus (de Jong et al. 2006), as well as detectable virus in multiple organs including the brain, spleen, and intestine of H5N1 infected ferrets (Govorkova et al. 2005). Further complications such as myocarditis, stroke, encephalitis, acute kidney injury (AKI) and rhabdomyolysis among others, have been documented in severe influenza cases (Sellers et al. 2017). However, it is currently unclear whether these complications are a direct effect of virus on the organs themselves, or whether it is a secondary effect causes by a heightened immune response (Sellers et al. 2017).

1.5 Mouse models for influenza virus research

In early studies, pigs, ferrets, and mice were found to be excellent models for studying influenza virus *in vivo* (Shope 1935). Due to accessibility, cost, husbandry requirements, ease of handling, experimental numbers and availability of species-specific reagents, mice have been adopted as a key model for *in vivo* influenza virus research. Immune responses are comparable between humans and mice, with strong inflammatory responses being the trigger for disease associated lung pathology (Tumpey et al. 2005). Mice exhibit similar histological and pathological changes in the respiratory tract to humans with IAV (Shope 1935), however, clinical signs of influenza vary greatly between species (Bouvier and Lowen 2010). Key symptoms in humans include fever, myalgia, headache, and respiratory symptoms such as cough or congestion, whereas in mice anorexia, hypothermia and lethargy are prevalent (Bouvier and Lowen 2010). A further notable difference between human and mouse IAV infection is that influenza presents itself primarily as an upper respiratory tract infection in mild to moderate disease in humans, whereas in mice it predominantly affects the lower respiratory tract (Bouvier and Lowen 2010), (Van Riel et al. 2007).

Mouse adapted strains of influenza are required for effective infection and replication in mice, due to lack of α2,6 sialic acid receptors on mouse lung epithelial cells (Ibricevic et al. 2006). The most commonly used strains of IAV

are H1N1 strains A/PuertoRico/8/1934 (PR8), A/WSN/1933 (WSN) or H3N2 strain A/X-31 (X31). However, these strains are not circulating human isolates and therefore, may not be clinically relevant. Pathogenicity of IAV and susceptibility to infection also varies greatly depending on mouse strain (Srivastava et al. 2009).

Recent investigations into the use of specific pathogen-free (SPF) mice for biomedical research has questioned the translational potential to human disease. Mice which live in the wild were found to mirror the human immune system much more closely than lab-bred strains of mice (Rosshart et al. 2019). Lab-bred mice co-housed with wild mice were found to have transcriptional signatures similar to humans when challenged with influenza vaccination, compared to lab-bred mice (Fiege et al. 2021). This suggests SPF-housed in-bred strains of mice used in research may not be beneficial for effectively representing the 'dirty' way in which humans live, undergoing constant challenge to the immune system.

On the contrary, a recent study concluded that laboratory mice are an excellent model for discovering much needed genetic biomarkers for influenza virus infection (Kollmus et al. 2018). Additionally, mice have been used for preliminary *in vivo* studies of multiple anti-viral drugs which are now approved in humans such as amantadine, rimantadine, Tamiflu®, Relenza® and peramivir (Davies et al. 1964), (Rabinovich 1972), (Mendel et al. 1998), (von Itzstein et al. 1993), (Sidwell et al. 2001). These findings suggest mouse models are pivotal in the discovery of therapeutics for controlling IAV infection in humans.

1.6 Innate immune responses to IAV infection and immunopathology

Both the innate and adaptive immune responses are required to eliminate IAV infection. The first barriers to infection are physical defences such as mucous lining the respiratory tract which contains glycosylated mucins to limit virus binding to respiratory epithelium (Zanin et al. 2016), (Dou et al. 2018).

Once physical barriers are breached, the virus will infect the airway epithelium, kill the infected cells, and trigger the innate immune response.

The immune response is a finely tuned mechanism which functions to elicit inflammation and cytotoxicity to kill an invading pathogen, whilst releasing anti-inflammatory factors to limit host tissue damage. This response can sometimes become imbalanced leading to extensive pathology to the host, or inability to control infection. Due to the clear roles of innate immunity in both clearing IAV infection and causing pathology, manipulating leucocyte homing *in vivo* may be a difficult challenge. The implicated immune cells in IAV infection and their roles in immunoprotection and immunopathology are summarised in table 1.1.

Table 1.1 Innate leucocytes recruited to the lungs during murine IAV infection and their roles in immunoprotection and immunopathology. Leucocytes with crucial roles in influenza virus A (IAV) infection are listed, along with the timepoints of maximal accumulation in the lung. Roles in immunoprotection and immunopathology to the host in IAV infection are listed. IFN; interferon, NETosis; neutrophil extracellular trap(osis), CTL; CD8 cytotoxic T lymphocyte, ROS; reactive oxygen species.

Leucocyte	Peak lung accumulation in IAV infection	Immunoprotection roles	Immunopathology roles
Monocyte	5 days (Lin et al. 2008).	Pro-inflammatory cytokine production (Sprenger et al. 1996), differentiation into dendritic cells (Hou et al. 2012).	Excessive pulmonary inflammation and tissue damage leading to mortality (Lin et al. 2014).
Alveolar macrophage	2 days (Nakanishi Yumi Hashimoto et al. 2007).	Phagocytosis of infected cells (Hashimoto et al. 2007), prevention of epithelial cell infection (Cardani et al. 2017).	Excessive pulmonary inflammation and tissue damage leading to mortality (Snelgrove et al. 2008).
Dendritic cell	10 days (Lin et al. 2008).	Type I IFN production (Cella et al. 1999), activation and recruitment of antigen-specific T cells (Lin et al. 2008).	Excessive pulmonary inflammation and tissue damage leading to mortality (Aldridge et al. 2009).
Neutrophil	3-5 days (Tate et al. 2008).	Pro-inflammatory cytokine production (Tate et al. 2008), phagocytosis of infected cells (Hashimoto et al. 2007), anti-bacterial granule release and NETosis to limit viral replication (Tripathi et al. 2014), recruitment of CD8 T cells (Lim et al. 2015).	Excessive pulmonary inflammation, ROS production (Akaike et al. 1990) and tissue damage leading to mortality (Brandes et al. 2013).

Natural killer cell	2-4 days (Leung and Leung 1981), 6 days (Carlin et al. 2018).	Pro-inflammatory cytokine production (Monteiro et al. 1998), cytotoxicity of IAV infected cells (Leung and Leung 1981), recruitment of dendritic cells and T cells to mediastinal lymph node (Ge et al. 2012), enhancement of CTL responses (Kos and Engleman 1996).	Excessive lung inflammation, increased phagocyte, and neutrophil recruitment (Abdul-Careem et al. 2012).

1.7 Adaptive immune responses to IAV infection

1.7.1 Roles of the draining lymph nodes

The mediastinal lymph nodes (med LNs) are the lung draining LNs in both humans and mice. They function to harbour immune cells for immunosurveillance, antigen priming and adaptive immune cell activation to limit infection spread. The med LN in mice increases in both size and cellularity within 48 hours of IAV infection, due to rapid activation of the immune response (Coro et al. 2006). Within the upper airways, cervical LNs and nasal associated lymphoid tissue (NALT) are the draining LNs.

Activation of the adaptive immune response to IAV relies on APCs such as $CD11b^{low/neg}CD103^{+}$ DCs to survey the lungs, phagocytose virus particles and upregulate chemokine receptor 7 (CCR7) (Förster et al. 1999). They then enter afferent lymphatics via CCR7 interaction with chemokine ligands 19 and 21 (CCL19, CCL21) and are transported to the draining LNs (Luther et al. 2000). Within the draining LNs, naïve CD4 and CD8 T cells recruited from the blood steam via high endothelial venules (HEVs), circulate in the paracortex (T cell zone) where they survey peptide-MHC (major histocompatibility complex) on DCs. DCs carrying IAV peptides will present the epitope on MHC-I or MHC-II, and an antigen-specific TCR on a T cell will bind the MHC, along with its corresponding CD8 or CD4 co-receptor. Recognition of foreign peptide sequences through this process will initiate the adaptive arm of the immune system (Figure 1.2).

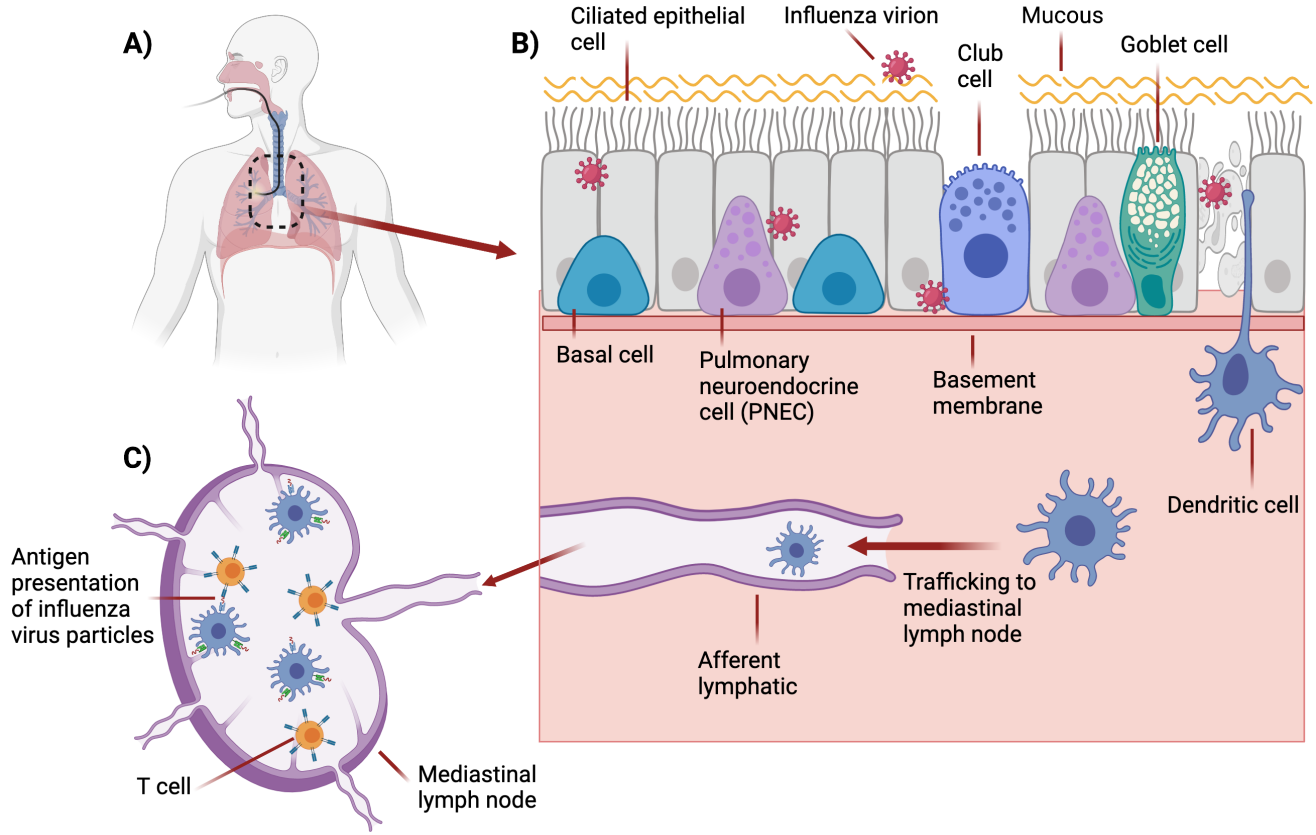

Figure 1.2. Influenza infection of airway epithelium leads to activation of the innate, then adaptive immune response in the mediastinal lymph node. A) The human respiratory system with the trachea and bronchi circled. **B)** Human airway epithelial layer consisting of ciliated epithelial cells, club cells, goblet cells, basal cells, and pulmonary neuroendocrine cells (PNEC) with basement membrane. Influenza virions infect epithelial cells, resulting in cell death. Dendritic cells (DCs) take up dead or live virus particles and traffic in afferent lymphatics to mediastinal lymph nodes. **C)**

Within mediastinal lymph node, DCs present antigen to T cell receptors (TCRs) on T cells via major histocompatibility complex I or II (MHC-I or MHC-II), leading to T cell activation and differentiation, inducing the adaptive arm of the immune system. Figure created using Biorender.com.

1.7.2 Roles of T lymphocytes in IAV infection

Following activation and differentiation in LNs, cytokine secreting CD8 CTLs downregulate CCR7 which recognises CCL19 and CCL21 expressed within HEV and paracortex, as well as downregulating L-selectin (CD62L) (Förster et al. 1999), (Luther et al. 2000), (Mobley and Dailey 1992). This is accompanied by upregulation of sphingosine-1-phosphate receptor (S1PR) which senses high levels of its ligand of sphingosine-1-phosphate (S1P) in lymph, allowing egress from the LN via efferent lymphatics and release into the bloodstream (Benechet et al. 2016). CTLs also upregulate various inflammation-associated chemokine receptors (e.g., CXCR3, CCR5) allowing subsequent recruitment to the site of infection to carry out cytotoxic responses (Bromley et al. 2008).

CD8 T cells are found to begin accumulation in the lungs of mice on day 5 of IAV infection in mice, and peak around day 10 (Miao et al. 2010). This is also found to correlate with viral clearance (Miao et al. 2010), (Moskophidis and Kioussis 1998). CTLs directly kill IAV-infected cells via cytotoxic granules and controlled apoptosis, limiting viral replication and making them a key component of a successful immune response against influenza virus. Upon recognition of an infected cell, CTLs will release perforin to create pores in the cell membrane, allowing granzymes A and B, also released by CTLs, to induce cell death. Expression of tumour necrosis factor (TNF)-related apoptosis inducing ligand (TRAIL) and Fas ligand (FasL) can also activate death receptors within infected cells, resulting in programmed cell death (Topham et al. 1997). These ‘killer’ mechanisms protect against further viral infection and replication within the host.

CD8 T cells have been shown as vital in murine IAV infection, as mice lacking CD8 T cells have a much higher mortality rate against H1N1 IAV than wild-type mice (Bender et al. 1992). However, there is conflicting evidence to the role of CD8 T cells in IAV infection, as CTLs produce the anti-inflammatory cytokine interleukin 10 (IL-10) to limit excessive inflammation and lung injury in murine IAV infection and have been found to be protective in mild infection, yet can be pathogenic in severe infection (Sun et al. 2009), (Moskophidis and Kioussis

1998). Complete depletion of all lymphocytes in mice ($Rag^{-/-}$) is lethal in IAV infection, suggesting that the innate immune system alone is insufficient to clear influenza virus infection (Wu et al. 2010).

Naïve CD4 T cells are also activated within the draining LNs in IAV infection via the TCR binding to MHC-II bound IAV peptides on APCs. CD4 T cells are classed as 'T-helper cells' (Th) and differentiate into a Th1 phenotype during viral infection driven by the transcription factor T-bet (Szabo et al. 2000). This initiates release of IFNγ, TNF-α and IL-2 (Szabo et al. 2000). Primary roles of CD4 T cells during IAV infection include regulating CD8 T cell responses and stimulating B cell responses (Kumamoto et al. 2011), (Moser 2015). A subset of CD4 T cells will migrate away from the med LN to carry out effector functions in the lungs, whilst a subset of $CXCR5^{+}$ CD4 T cells deemed 'T follicular helper cells' (T_{FH}), will migrate to the B cell zone to engage antigen presenting B cells. This results in antibody production, plasma cell and memory B cell generation (Moser 2015). Antigen-specific CD4 T cells are detectable in the lungs of IAV infected mice 7 days post-infection, peaking at 10 days (Hornick et al. 2019). In the lungs of IAV infected mice, the predominant subset of CD4 T cells are Th1 cells, however, T regulatory cells (T_{regs}) and T_{FH} cells are present in fewer numbers (Hornick et al. 2019). CD4 T_{regs} are found to have important roles in dampening inflammatory responses during IAV infection, by reducing monocyte and macrophage accumulation (Antunes and Kassiotis 2010).

'Memory' T cells are T cells that persist after infection to prevent recurring disease. Their function is to proliferate upon reinfection to mount an antigen-specific response quickly, to eliminate a pathogen faster than in a primary infection. Memory T cells in IAV infection have been shown to be cross-reactive in both humans (Lee et al. 2008) and mice (Effros et al. 1977), providing valuable protection against heterosubtypic strains of influenza virus. They can be broadly divided into $CCR7^{HI}CD62L^{HI}$ central memory T cells (T_{CM}) that survey secondary lymphoid organs, and $CCR7^{LO}CD62L^{LO}$ effector memory T cells (T_{EM}) that survey tissues (Sallusto et al. 1999). Further to this, memory T cells can be further divided into tissue resident (T_{RM}) and stem cell memory T cells (T_{SCM}). T_{RM}s reside in the tissue where the primary infection occurred and are the most efficacious population of memory T cells in a secondary IAV

challenge (Wu et al. 2014). T_{SCM} are a newly defined population of 'stem like' memory T cells with self-renewing capabilities (Gattinoni et al. 2011). However, the function T_{SCM} are yet to be understood in the context of IAV infection.

1.7.3 Roles of B lymphocytes in IAV infection

B cells are another arm of the adaptive immune response, primarily involved in antibody production against foreign pathogens. Neutralising antibodies bind directly to IAV virions via HA epitopes, to limit host cell binding and infectivity, rendering the virus inactive. Non-neutralising antibodies also have indirect immunoprotective roles such as facilitating memory CD8 T cell expansion, complement activation, antibody-dependent cellular cytotoxicity (ADCC) and phagocytosis of infected cells (Rangel-Moreno et al. 2008), (Padilla-Quirarte et al. 2019). B cells are key in generating immune protection from IAV vaccines, as memory CD8 T cells alone are found not to protect mice against secondary heterosubtypic IAV challenge (Rangel-Moreno et al. 2008). As early as 48 hours post-infection in mice, extrafollicular plasmablast cells secrete antibodies IgG, IgM and IgA, and in humans plasmablast levels peak in the blood on day 7 (Coro et al. 2006), (Huang et al. 2014). Later in infection, germinal centre B cells turn into long-lived plasma cells and memory B cells which may protect against subsequent IAV infections (Padilla-Quirarte et al. 2019), (Lam and Baumgarth 2019).

1.8 The role of lymphocyte homing in adaptive immune responses to IAV

As described, leucocytes function to protect the host from virus infections. To detect and eradicate these threats, both innate and adaptive immune cells must travel to sites of infection, as well as to draining LNs or other lymphoid organs, in a tightly controlled manner. Leucocyte homing is controlled by different types of receptors on the leucocyte surface which bind to their respective ligands on blood vessel or HEV endothelium. This enables leucocytes to stably adhere to blood vessels and transmigrate the vessel wall to enter tissues. Leucocyte-endothelial cell interactions are stringently controlled to

ensure leucocytes migrate to where they are needed, such as to the lungs and med LNs in influenza infection, without causing excessive build-up of leucocytes and lung pathology.

Most *in vivo* research into leucocyte homing is carried out in mice, whilst the majority of *in vitro* research is carried out using cultured human endothelial cells such as human umbilical vein endothelial cells. Some, but not all homing receptor-ligand interactions are conserved across species and collectively, this research can be used to predict mechanisms used by leucocytes for trafficking in humans. The next sections will describe the general principles underlying leucocyte homing and summarise the receptors and ligands that control homing of T cells to LNs and virus infected lungs.

1.8.1 The multistep adhesion cascade of leucocyte homing

The multi-step adhesion cascade describes the sequence of adhesive interactions that regulate the recruitment of leucocytes from the bloodstream into tissues (also known as homing) and involves selectins, integrins and chemokines. The first step involves leucocyte tethering to the endothelium, which leads to slow rolling of the cell. Leucocytes then undergo arrest, and finally extravasation across the endothelial cell lining and vascular basement membrane to enter tissues (Springer 1994).

Selectins are type I transmembrane glycoproteins; P-selectin is found on platelets and endothelium, E-selectin is found only on endothelium and L-selectin is only on leucocytes. E- and P-selectins bind sialyl-lewis X (sLe^x) epitopes on scaffold proteins such as P-selectin glycoprotein ligand 1 (PSGL1) and CD44, whereas L-selectin binds to sulfated sLe^x on proteins such as CD34, podocalyxin and glycosylation-dependent cell adhesion molecule-1 (GlyCAM-1). These interactions initiate the tethering and rolling of cells on vasculature. Chemokine binding to glycosaminoglycans on activated endothelium further activates the slow-rolling leucocyte via G-protein coupled receptor (GPCR) activation of leucocytes. For example, CCR7 on leucocytes binding to CCL21 or CCL19 on HEV endothelium is key in T cell homing to LNs, whereas CXCR5 binding to CXCL13 is key in B cell homing to LNs. Chemokine and selectin

binding also trigger inside-out signalling, which results in high-affinity, stabilised integrin expression. Integrins are cell surface receptors such as $\alpha4\beta7$, leucocyte function-associated antigen 1 (LFA-1), very late antigen-4 (VLA-4) and macrophage antigen-1 (Mac-1) which bind molecules such as mucosal vascular addressin cell-adhesion molecule 1 (MAdCAM-1), and immunoglobulin superfamily members intercellular cell-adhesion molecule-1 (ICAM-1) and vascular cell-adhesion molecule-1 (VCAM-1). Once rolling cells are arrested by integrins, cells will begin to migrate through the endothelium, basement membrane and pericytes to reach their destination via one of two routes; paracellular or transcellular transmigration. Leucocyte engagement of junction adhesion molecules (JAMs); JAM-A, JAM-B, JAM-C, CD31 or CD99 will dissociate the binding of two adjacent endothelial cells. Vascular-endothelial cadherin (VE-cadherin) is also required to be released from the endothelium for this dissociation; these processes result in paracellular migration of the leucocyte between endothelial cells. Transmigration between a single endothelium cell, known as transcellular migration, can also occur via F-actin containing podosomes on the leucocyte which allow transit through the endothelial cell cytoplasm. Migration through the basement membrane occurs at areas of low-density matrix proteins, which co-localise with gaps between adjacent pericytes, to allow the cell to reach the site of infection or LN via chemotaxis (Springer 1994), (Ager 2012), (Ley et al. 2007), (Figure 1.3).

A disintegrin and metalloproteinase 17 (ADAM17) is a transmembrane enzyme responsible for the cleavage of over 80 cell surface molecules (Moss and Minond 2017). Early *in vitro* studies with hydroxamate metalloproteinase inhibitors such as Ro 31-9790 and endogenous ADAM protease inhibitors such as tissue inhibitor of metalloproteinases-3 (TIMP-3) highlighted a potential role for ADAM17 in leucocyte homing (Faveeuw et al. 2001). ADAM17-dependent ectodomain cleavage controls the expression of several cell trafficking proteins such as L-selectin on leucocytes and VLA-4 and VCAM-1 on endothelial cells. Studies using genetically modified leucocytes suggested roles for ADAM17 and shedding of L-selectin in innate immune cell recruitment *in vivo* (Hafezi-Moghadam et al. 2001) and for ADAM17 and L-selectin shedding in monocyte transendothelial migration *in vitro* (Rzeniewicz et al. 2015). The roles of L-

selectin shedding and ADAM17 in lymphocyte homing will be covered in more detail in sections 1.11 onwards.

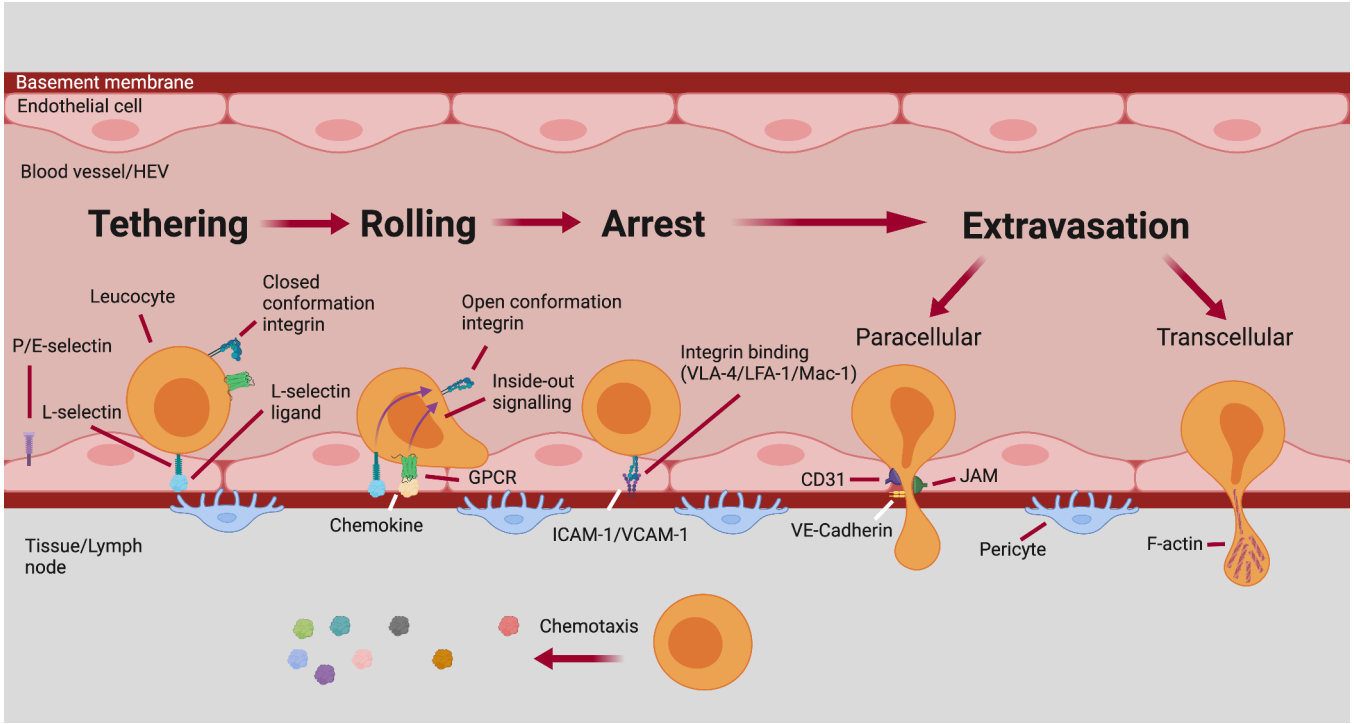

Figure 1.3. Leucocyte adhesion cascade within blood vessel/HEV. Leucocytes are recruited to lymph nodes or inflamed tissues from high endothelial venules (HEVs) or inflamed blood vessels in a series of 4 major steps. Leucocytes tether to endothelium via the transmembrane receptors P-, E- or L-selectin which bind vascular addressins such as P-selectin glycoprotein 1 (PSGL1), CD44 or peripheral lymph node addressin (PNAd). Leucocytes then slowly roll across the endothelium and encounter chemokines which bind G-protein coupled receptors (GPCRs). These events result in an inside-out signalling cascade stabilising integrin expression on the leucocyte such as leucocyte function-associated antigen 1 (LFA-1), very late antigen-4 (VLA-4) and macrophage antigen-1 (Mac-1) which bind mucosal vascular addressin cell-adhesion molecule 1 (MAdCAM-1), and immunoglobulin superfamily members intercellular cell-adhesion molecule-1 (ICAM-1) and vascular cell-adhesion molecule-1 (VCAM-1) on the endothelial cell surface. This causes arrest of the leucocyte onto the endothelium, ready for the final step of extravasation into the lymph node/tissue

via paracellular or transcellular transmigration. Paracellular migration occurs via leucocyte interaction with junction adhesion molecules and release of VE-cadherin which allows the leucocyte to pass between two endothelial cells. Transcellular migration occurs via F-actin rich podosomes on leucocytes passing through the cytoplasm of a single endothelial cell. Figure created using Biorender.com.

1.8.2 T Lymphocyte homing to lymph nodes and lungs during IAV infection

Each organ or tissue requires the expression of a unique set of homing molecules on vasculature and leucocytes to allow for optimal cell recruitment. Homing pathways vary depending on whether the secondary lymphoid organ is peripheral or mucosal. The majority of studies of *in vivo* peripheral and mucosal lymphocyte homing pathways have been carried out on naïve mice; physiological changes to cell trafficking during infection and inflammation are comparatively less well understood. However, there are currently no studies identifying T cell homing to the med LN in naïve mice, nor during infection. Due to the med LN being mucosal, it may have similar mechanisms to the mesenteric LN. Therefore, the trafficking mechanisms of T lymphocytes to and from the med LN and lungs during IAV infection is still to be elucidated (Table 1.2).

The lung alveoli contain the largest vascular bed in the body. This is important for both gas exchange and leucocyte recruitment due to the contact this organ has with the outside environment, rendering the lungs vulnerable to infection. There are three major vascular networks associated with respiratory tract infections; HEVs in med LNs, tracheal and bronchial post-capillary vessels and alveolar capillaries, all which must adapt greatly in pulmonary infection to recruit leucocytes (Alon et al. 2020).

Tracheal and bronchial post-capillary vessels in the lungs constitutively express the integrin ligands VCAM-1 and ICAM-2 and various chemokines to allow for transient entry of leucocytes for surveillance. This alters during influenza virus infection whereby P- and E-selectin and inflammatory cytokines such as CXCL1 and CCL5 are upregulated on activated endothelium to promote recruitment of innate and adaptive immune cells. The pro-inflammatory chemokines and cytokines released which cause these endothelial changes are expressed by infected epithelial cells and AMs. During IAV infection, leucocytes upregulate cell surface expression of chemokine receptors such as CCR1, CCR3, CCR5, CXCR3 and integrins VLA-4, LFA-1 and Mac-1 which bind to ligands expressed on the activated endothelium (Alon et al. 2020).

Alveolar capillaries use slightly different cell homing mechanisms to post-capillary venules; selectins are not required for cell adhesion and rolling along this endothelium, however similar chemokine receptors and integrins are expressed on cells trafficking through alveolar capillaries, with the exception of VLA-4 (Alon et al. 2020). These differences are attributed to the narrow diameter of these capillaries, which induces slower leucocyte motility as the majority of segments are narrower than the size of leucocytes trafficking through (Doerschuk et al. 1993), (Alon et al. 2020).

Table 1.2. Adhesion molecules required for T lymphocyte homing. Lymphocyte homing to lymph nodes, Peyer's patches in the gut and lungs in IAV infection require a unique set of adhesion molecules that aid in tethering, rolling and arrest of lymphocytes for cell trafficking. PNAd; peripheral lymph node addressin, CCR7; chemokine receptor 7, CCL19/21; chemokine ligand 19/21, LFA-1; leucocyte function-associated antigen 1, ICAM-1; intercellular cell-adhesion molecule-1, MAdCAM-1; mucosal addressin cell adhesion molecule 1, PSGL1; P-selectin glycoprotein ligand 1, IAV; influenza A virus, VLA-4; very late antigen-4, Mac-1; macrophage antigen-1, VCAM-1; vascular cell-adhesion molecule-1.[1] Required during inflammation/infection.

Location	Selectins	Selectin ligands	Chemokine receptors and ligands	Integrins	Integrin ligands
Peripheral lymph nodes	L-selectin (Gallatin et al. 2006)	PNAd (Streeter et al. 1988)	CCR7, CCL19, CCL21 (Baekkevold et al. 2001), (Stein et al. 2000), (Luther et al. 2000)	LFA-1 (Warnock et al. 1998)	ICAM-1 (Warnock et al. 1998), ICAM-2 (Lehmann et al. 2003)
Mesenteric lymph node	L-selectin (Gallatin et al. 2006)	MAdCAM-1, PNAd (Berg et al. 1993), (Streeter et al. 1988)	CCR7, CCL19, CCL21 (Gunn et al. 1998)	$\alpha4\beta7$ (Wagner et al. 1998), LFA-1 (Berlin-Rufenach et al. 1999)	MAdCAM-1 (Wagner et al. 1998)
Peyer's patches in gut mucosa	P-selectin [1], L-selectin (Kunkel et al. 1998)	PSGL-1, MAdCAM-1 (Haddad et al. 2003)	CCR7, CCL21 (Warnock et al. 2000)	$\alpha4\beta7$ (Berlin et al. 1993), LFA-1 (Berlin-Rufenach et al. 1999)	MAdCAM-1 (Berlin et al. 1993)
Lungs in IAV infection[1]	L-selectin (Mohammed et al. 2016)	Not known	CXCR1, CXCR3, CCR4, CCR5, CXCR6 (Alon et al. 2020)	VLA-4, LFA-1 (Alon et al. 2020)	VCAM-1, ICAM-1 (Alon et al. 2020)

1.9 L-selectin

L-selectin is a type I transmembrane glycoprotein expressed on leucocytes, involved in leucocyte recruitment to LNs and inflamed tissues. L-selectin function is best characterised on T cells, B cells and neutrophils, with T cells being the focus of this thesis. L-selectin is encoded by the gene SELL found on human and mouse chromosome 1. The protein sequence of L-selectin is 77% conserved between humans and mice, with minor differences in amino acid residues in the cytoplasmic tail and extracellular cleavage site (Tedder et al. 1989). The molecular weight of L-selectin varies from 65-100 kDa, depending on cell type, due to differences in glycosylation patterns (Griffin et al. 1990), (Schleiffenbaum et al. 1992), (Watson et al. 1990), (Figure 1.4).

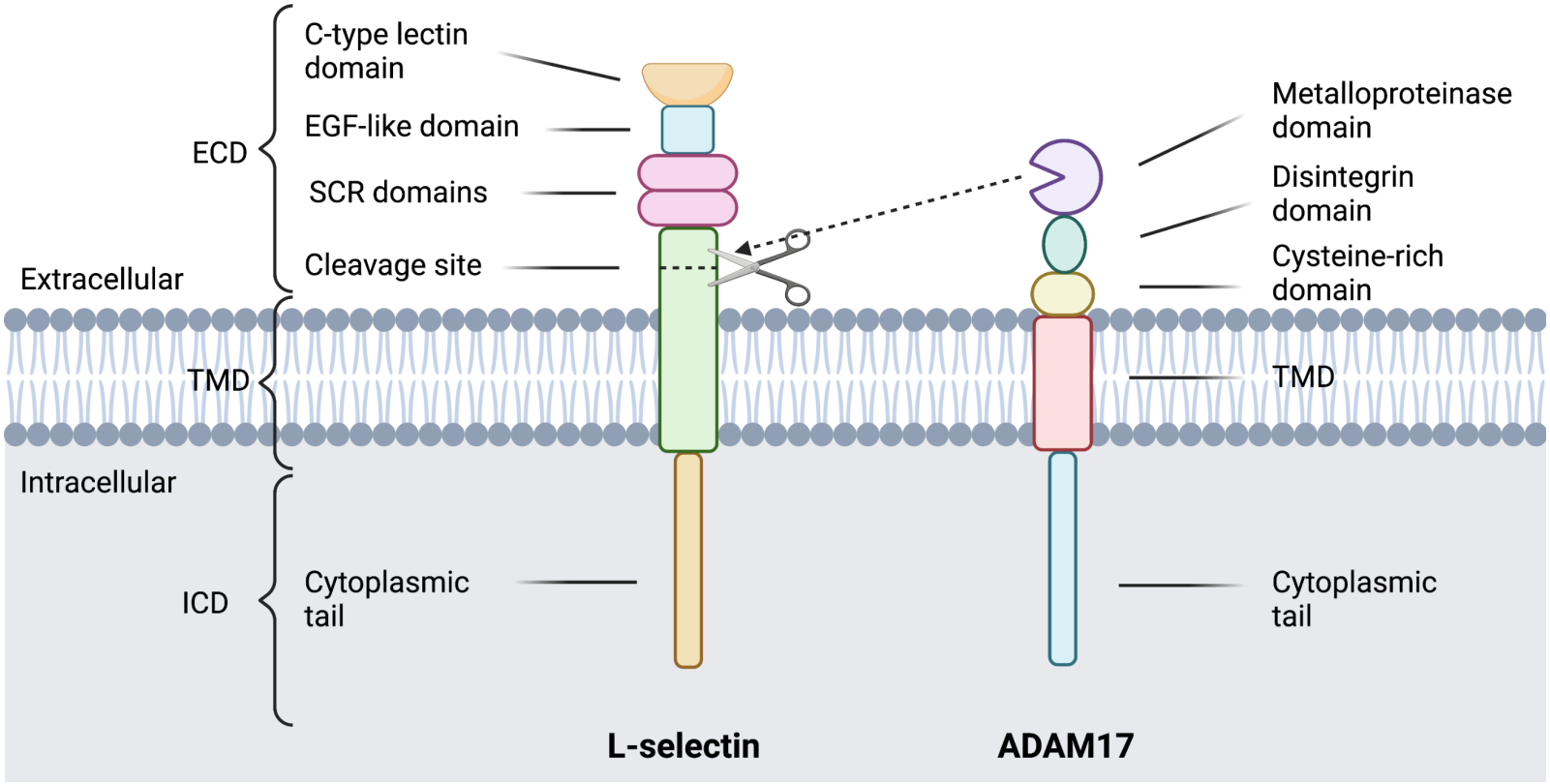

Figure 1.4. The structure of transmembrane glycoprotein L-selectin and enzyme ADAM17. L-selectin is comprised of an intracellular domain (ICD) at the C-terminus which consists of the 17 amino acid cytoplasmic tail, a transmembrane domain (TMD) which spans the cell membrane and an extracellular domain (ECD) involving the C-type lectin domain at the N-terminus, the epidermal growth factor (EGF)-like domain, two short consensus repeat (SCR) domains and the cleavage site. L-selectin is proteolytically shed by ADAM17 which contains an ECD consisting of the metalloproteinase domain, disintegrin domain and cysteine-rich domain which contains the hypervariable region. ADAM17 is then anchored to the cell via the TMD and cytoplasmic tail. Cleavage site whereby ADAM17 cleaves L-selectin via the metalloproteinase domain is shown by scissors/dotted lines. Figure created using Biorender.com.

1.9.1 L-selectin ligands and roles in lymphocyte homing

L-selectin was first discovered as a LN homing receptor in 1983 using antibody clone MEL-14 against mouse L-selectin (Gallatin et al. 1983). MEL-14 was found to block lymphocyte interactions with HEVs *in vitro* and reduced lymphocyte recruitment to peripheral LNs *in vivo* (Gallatin et al. 1983). Further work then characterised vascular addressins such as peripheral lymph node addressin (PNAd), present on peripheral LN HEVs using antibody clone MECA-79. These ligands were found to bind to L-selectin on leucocytes and were necessary for cell homing. However, neither MEL-14 nor MECA-79 blocked lymphocyte homing to gut mucosa Peyer's patches, suggesting a peripheral LN-dependent mechanism (Streeter et al. 1988).

Further work then discovered that there were other ligands for L-selectin, such as MAdCAM-1 in the mesenteric LN of the gut mucosa, and PSGL-1 which binds P- and E-selectin, also (Berg et al. 1993), (Spertini et al. 1996). Many L-selectin ligands have been characterised since, such as CD34, GlyCAM-1, podocalyxin, nepmucin, endomucin which collectively make up 'PNAd' (Puri et al. 1995), (Derry et al. 1997), (Sassetti et al. 1998). L-selectin binds to the glycan ligand 6 sulpho-sLe^x on O and N-linked sugars presented by the protein backbones of these ligands.

L-selectin is able to control leucocyte homing in the absence of P- or E-selectin (Ley et al. 1993). However, mice lacking L-selectin have limited lymphocyte numbers in peripheral LNs, and lymphocytes fail to bind HEVs. Early homing experiments in mice discovered lymphocyte homing to mucosal LNs and Peyer's patches were all reduced in the absence of L-selectin, further signifying the importance of this molecule (Arbonés et al. 1994).

1.9.2 L-selectin in IAV infection

Due to its involvement in lymphoid organ homing, a question to address was whether L-selectin is important for homing to tissues during pathology. L-selectin knockout mice displayed reduced lymphocyte, neutrophil and monocyte recruitment to sites of inflammation, whilst early infection studies first implicated

L-selectin in the immune response by finding that L-selectin knockout mice had impaired neutrophil responses to peritoneal bacterial infection (Tedder et al. 1995), (Arbonés et al. 1994). However, lack of L-selectin expression on activated CTLs suggested that L-selectin was not important in trafficking T cells to sites of infection (Mobley et al. 1994). In more recent times, Ager and colleagues overturned the dogma that L-selectin is solely a LN homing receptor for lymphocytes and a marker of T cell memory; L-selectin was found to have diverse roles in homing to sites of infection, cancer and in T cell proliferation (Mohammed et al. 2016), (Watson et al. 2019), (Mohammed et al. 2019). Ager and colleagues also defined an *in vivo* cyclical expression pattern for L-selectin on CD8 T cells during IAV infection (Mohammed et al. 2016).

The cyclical expression of L-selectin was firstly confirmed *in vitro*, whereby CD8 T cells activated by cognate peptide on APCs completely downregulated L-selectin within 4 hours via proteolytic shedding, with re-expression within 48 hours due to increased L-selectin mRNA expression. 5-7 days later, L-selectin was downregulated again, by a transcriptional silencing-mediated mechanism controlled by phosphoinositide3-kinaseδ (PI3Kδ) (Chao et al. 1997), (Sinclair et al. 2008).

Mohammed *et al*. used lymphocyte homing experiments in mice to determine the role of L-selectin in CD8 T cells during IAV infection. Naïve CD8 T cells which express high levels of L-selectin traffic to the med LN via the leucocyte adhesion cascade described above. L-selectin on lymphocytes binds to PNAd on HEVs which directs the cells to the T cell zone of the LN, where over 90% of CD8 T cells retain their L-selectin expression for immunosurveillance (Mohammed et al. 2016). Following viral infection with PR8, these naïve murine T cells become activated into CTLs by APCs exhibiting viral peptide on MHC-I. This interaction between peptide-MHC-I and the TCR results in the proteolytic cleavage of L-selectin on T cells, where less than 40% of antigen-specific CD8 T cells are L-selectin positive (Mohammed et al. 2016). This mechanism is controlled by ADAM17 ectodomain shedding, a PI3Kδ-mediated process (Sinclair et al. 2008). L-selectin levels begin to increase over the following 48 hours, when the T cells egress the LNs to reach the systemic circulation. By day 4 of infection, roughly 80% of CTLs express L-selectin in the med LN and 60%

in peripheral blood and lungs (Mohammed et al. 2016). L-selectin is downregulated again, being at its lowest in infected tissues by day 8 of infection, where fewer than 5% of antigen-specific CTLs are L-selectin positive (Mohammed et al. 2016). This secondary reduction is controlled by PI3Kδ-mediated transcriptional silencing. PI3Kδ blocks the action of the transcription factor Kruppel-like factor 2 (KLF2), which transcribes the L-selectin gene SELL (Sinclair et al. 2008), (Watson et al. 1990). This identifies an *in vivo* cyclical expression pattern for L-selectin on CD8 T cells which supports previous *in vitro* findings (Chao et al. 1997), (Figure 1.5).

Antibody MEL-14 was historically used to identify L-selectin on leucocytes and has been successful at blocking the functionality of this molecule. During PR8 IAV infection, daily administration of MEL-14 to mice after T cells had been activated inside LNs significantly reduced numbers of influenza-specific CD8 T cells in the lungs on day 8 of infection, suggesting an L-selectin dependent mechanism for CTL trafficking to sites of infection (Mohammed et al. 2016).

To further explore the functional role of L-selectin expression on activated T cells, genetically modified 'LΔP' mice were generated in which ADAM17-resistant L-selectin is expressed on the T cells under a heterologous promoter (Galkina et al. 2003). Using these LΔP mice, maintained L-selectin expression on CTLs was found to improve CD8 T cell homing and subsequent IAV clearance on day 8 in both H1N1 and H3N2 infections (Mohammed et al. 2016). This markedly improved virus clearance in LΔP mice compared to wild-type C57BL/6 (B6) mice, which was further emphasised by poorer virus clearance in L-selectin$^{-/-}$ knockout mice compared to wild-type (Mohammed et al. 2016).

These findings open up a potential avenue of targeting L-selectin pharmacologically to treat IAV or other infections, however, a mechanism of action is required to fully understand downstream effects. Cell activation and differentiation remained the same between LΔP and B6 murine CD8 T cells, suggesting that the superior homing effects are not due to early or increased cell activation (Mohammed et al. 2016). This proposes a cell migration-mediated superiority in LΔP CTLs, in which expression of ligands for L-selectin on endothelium would be key. Traditional ligands for L-selectin; PNAd and

MAdCAM-1, are not detectable in murine IAV infected lungs (unpublished data, Ager lab), suggesting that other ligands not conventionally found in HEVs, or vascular endothelium are responsible for this mechanism.

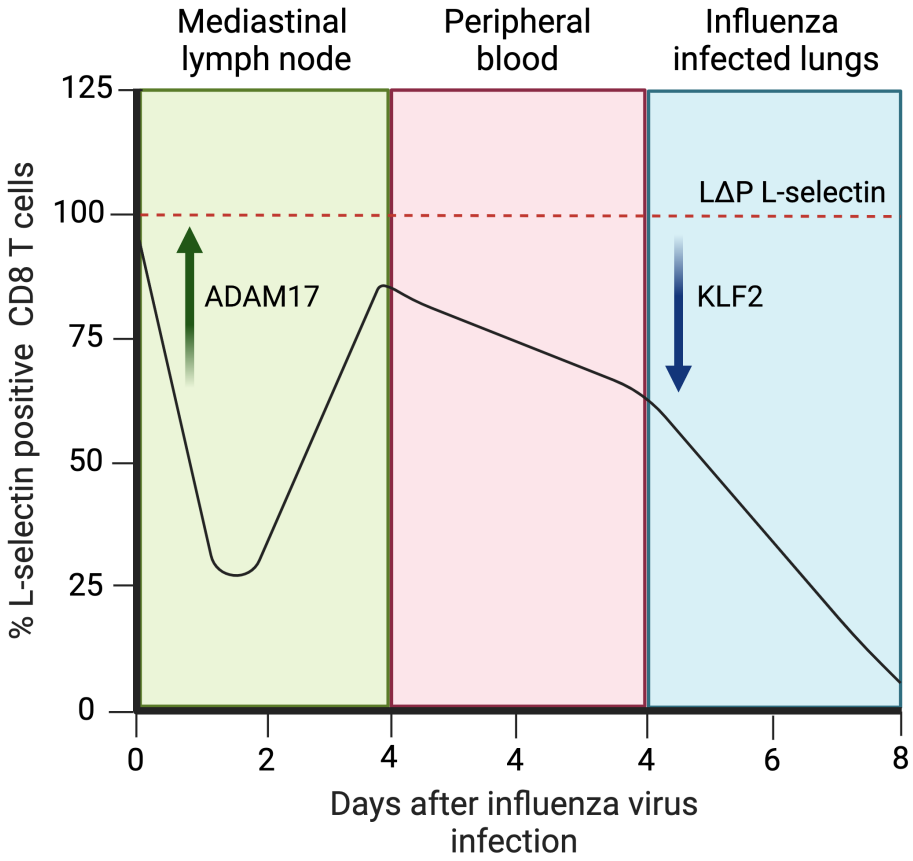

Figure 1.5. Cyclical expression patterns of L-selectin on CD8 T cells during murine influenza virus infection *in vivo*. The black line is the L-selectin expression pattern in wild-type mice. Red dashed line is L-selectin expression pattern in LΔP mice which contain a non-cleavable form of L-selectin that does not undergo transcriptional silencing (Mohammed et al. 2016). The first downregulation of L-selectin is controlled by ADAM17 proteolytic shedding inside lymph nodes. The second downregulation is transcriptional silencing of Kruppel-like factor 2 (KLF2) inside infected tissues (Sinclair et al. 2008). Figure created using Biorender.com.

1.10 ADAMs

ADAMs are a family of type I transmembrane enzymes or 'sheddases' which function to cleave the ectodomains of other transmembrane molecules. Ectodomain shedding is a proteolytic reaction, in which an extracellular domain is removed, leaving a membrane-retained fragment in place. To date, 21 ADAMs have been characterised in humans, with 13 being proteolytically active (Edwards et al. 2008), (Ager 2012). The proteolytically active ADAMs have an active site attached to the metalloproteinase domain for ectodomain shedding (Ager 2012), (Weber and Saftig 2012), (Figure 1.4).

ADAM17 was the first of the ADAMs to be described. It is also known as tumour necrosis factor alpha converting enzyme (TACE), named after its initial discovery in cleaving transmembrane tumour necrosis factor alpha (TNF-α) into soluble TNF-α (Black et al. 1997), (Moss et al. 1997). By using ADAM17 gene knockout mice, the protease was found to be essential for survival, as mice died between embryonic day 17.5 and 1 day post-birth (Peschon et al. 1998). This lethality was attributed to aberrant EGFR signalling (Peschon et al. 1998).

A full-length precursor and a mature form of ADAM17 are detected in cells; ADAMs are synthesised in the ER and matured in the Golgi. iRhom2 transports immature ADAM17 from the ER to the Golgi allowing removal of the pro-domain via proprotein convertase 7 or furin (Schlöndorff et al. 2000). This creates a functional metalloproteinase domain, which is then trafficked to the cell membrane, also by iRhom2 (Schlöndorff et al. 2000). ADAMs are found to predominantly localise to the perinuclear and plasma membranes in order to cleave substrates in *cis* (Schlöndorff et al. 2000). Once at the cell membrane, ADAM17 is further documented to exist in a 'closed/inactive' and 'open/active' confirmation (Takeda et al. 2006). This change to an 'open' confirmation which allows proteolytic shedding, is documented to be a result of disulfide bonds at the disintegrin and cysteine-rich domains (Wang et al. 2009). ADAM17 contains a conserved cysteine-X-X-cysteine motif whereby protein disulfide isomerase (PDI)-mediated thiol disulfides alter its enzymatic activity (Wang et al. 2009). The signalling pathway for ADAM17-dependent proteolytic shedding of

membrane inserted substrates involves stimulation of receptors such as toll like receptors (TLRs), TCRs, GPCRs or pharmacological activation using phorbol esters. This induces mitogen-activated protein-kinase (MAP-kinase)-dependent phosphorylation of the cytoplasmic tail of rhomboid protein iRhom2 (Cavadas et al. 2017). Phosphorylation can occur via an array of proteins, such as protein kinase C (PKC) or PI3Kδ, which is dependent on cell stimuli. These processes result in ADAM17 ectodomain cleavage of other transmembrane proteins (Figure 1.6).

ADAM17 currently has over 80 known substrates including adhesion molecules, chemokines, cytokines, growth factors and receptors (Moss and Minond 2017). Its ‘promiscuous’ activity and role in regulating the bioavailability of various molecules has implicated ADAM17 in cancer, neurological and inflammatory immune conditions, as well as leucocyte recruitment.

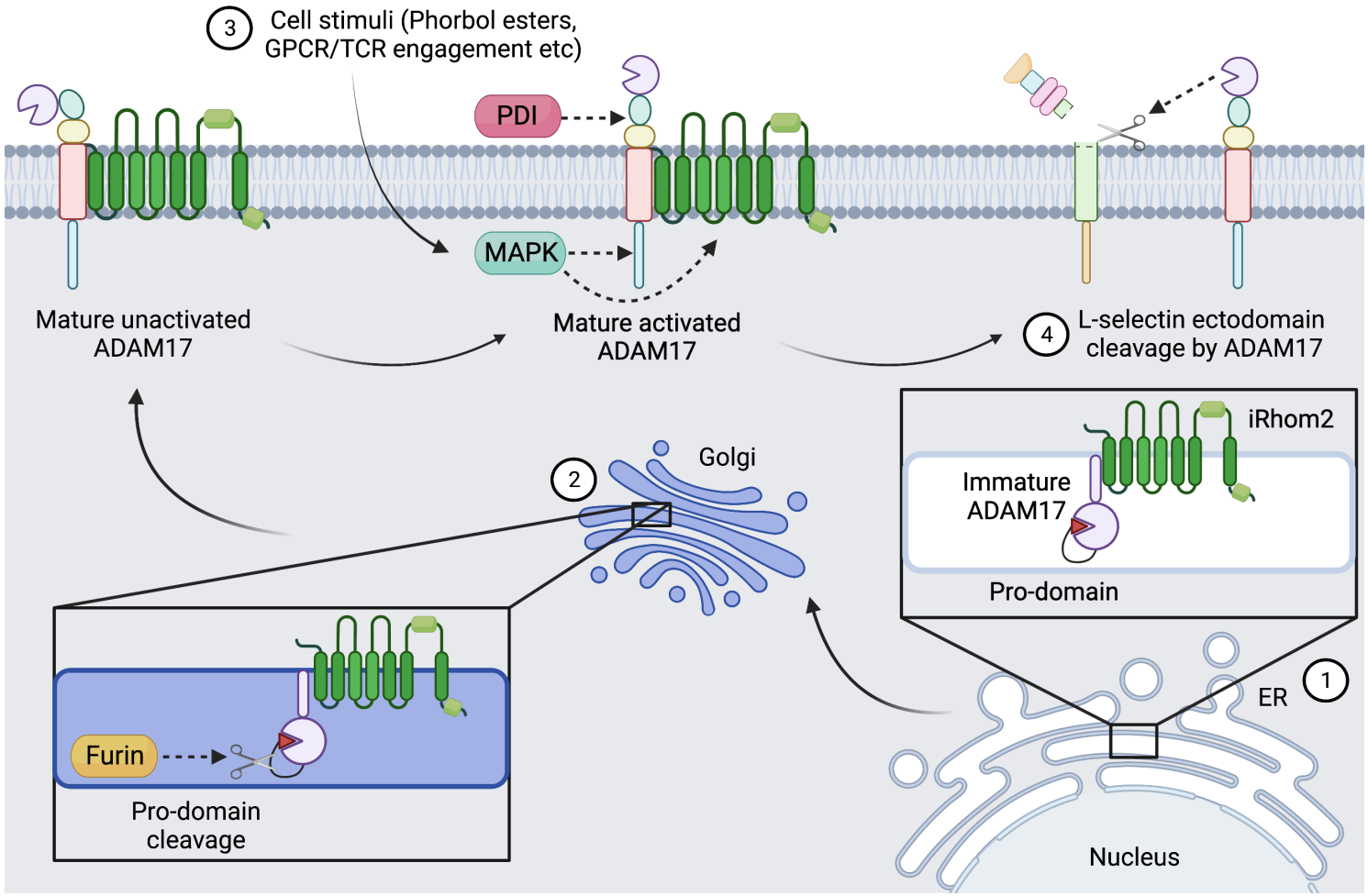

Figure 1.6. ADAM17 maturation and cell surface activation for proteolytic shedding of substrates. 1) A disintegrase and metalloproteinase 17 (ADAM17) is synthesized in the endoplasmic reticulum (ER) where it is chaperoned by iRhom2 in its immature form with pro-domain (Schlöndorff et

al. 2000). **2)** Immature ADAM17 is trafficked to the Golgi where furin mediates pro-domain cleavage to create mature ADAM17. This mature version of ADAM17 is then trafficked to the cell surface in its unactivated form (Schlöndorff et al. 2000). **3)** Cell activation/stimulation caused by phorbol esters such as PMA, G-coupled protein receptors (GPCRs) or T cell receptor (TCR) engagement causes mitogen activated protein kinase (MAPK) phosphorylation of ADAM17 and iRhom2, which will dissociate iRhom2 from ADAM17 (Cavadas et al. 2017). Protein disulfide isomerase (PDI) also oxidises disulfide bonds in the C-xx-C motif in the disintegrin and cysteine-rich domains of ADAM17 to create an active form of ADAM17 (Wang et al. 2009). **4)** Active ADAM17 proteolytically sheds cell surface substrates such as L-selectin. Figure created using Biorender.com.

1.10.1 ADAM17 in immunity

ADAM17 has functions in regulating many cell surface receptors and molecules which influence the immune response to infection. This includes pattern recognition receptors (PRRs) TLR2 and TLR4; other first line defences that detect foreign pathogens during an infection, as well as a number of inflammatory mediators (Table 1.3).

The processes of leucocyte migration and recruitment also involve ADAM17, via cleavage of chemokines and cell adhesion molecules such as ICAM-1, VCAM-1, and L-selectin. These molecules have distinct effects on the cell adhesion cascade which takes place in blood vessels and HEVs, where leucocyte rolling, arrest and transendothelial migration result in leucocyte recruitment to LNs and tissues (Figure 1.3). This is important for both homeostatic immune surveillance, and during infection, where immune cells traffic to sites of inflammation (Ager 2012).

1.10.2 ADAM17 regulation of TNF-α

TNF-α is a 26 kDa pro-inflammatory cytokine central to orchestrating immune responses but can also cause pathology through excessive inflammation (Solomon et al. 1997), (DeBerge et al. 2013). Cell surface TNF-α exists in a homotrimer and binds to TNFRI and TNFRII to elicit its effector functions such as orchestrating lymphoid tissue structure (Ruuls et al. 2001), cytotoxicity (Perez et al. 1990), (Solomon et al. 1997), B cell activation (Aversa et al. 1993), and T cell activation and proliferation (Grell et al. 1995). Soluble TNF-α is a 17 kDa protein which preferentially binds to TNFRI (Solomon et al. 1997), (Grell et al. 1995). Soluble TNF-α has been shown to have different biological consequences than membrane bound TNF-α such as increasing tumour growth *in vivo*, myeloid cell survival (Ardestani et al. 2013), inflammation (Ruuls et al. 2001), host tissue pathology (DeBerge et al. 2013).

ADAM17 was discovered in 1997 for its cleavage of transmembrane TNF-α into soluble TNF-α (Black et al. 1997), (Moss et al. 1997). Inhibition of ADAM17-mediated cleavage of TNF-α on CD8 T cells improves survival in murine

influenza infection with reduced lung pathology. This was attributed to reduced CXCL2 expression in mouse lungs and therefore reduced inflammatory innate immune cell infiltration (DeBerge et al. 2013). Soluble TNFRII, another substrate of ADAM17 released by CD8 T cells, was also shown to regulate soluble TNF-α levels and therefore regulate inflammation during IAV infection (DeBerge et al. 2015).

The cleavage of TNF-α by ADAM17 was found to be 2250 times more efficient than cleavage of L-selectin (Peschon et al. 1998). This is also supported by findings using TIMP-3; an endogenous matrix metalloproteinase (MMP) inhibitor. Borland *et al*. found that TIMP-3 had an IC_{50} of 0.11 μM for blocking shedding of TNF-α in human monocytes, whereas for blocking L-selectin shedding in human monocytes and lymphocytes, the IC_{50} was 0.39 μM (Borland et al. 1999).

Table 1.3. Substrates of ADAM17 in humans and mice and their functions within the immune system. TLR; Toll like receptor, IL-6/15/23R; interleukin 6/15 receptor, IL-1RII, interleukin 1 receptor II, TNFR-I/II; tumour necrosis factor receptor I/II, TNFα; tumour necrosis factor alpha, IL-1β; interleukin 1 beta, CD154/89; cluster of differentiation 154/89, ICAM-1; intercellular adhesion molecule 1, VCAM-1; vascular adhesion molecule 1, CD44; cluster of differentiation 44, JAM-A; junction adhesion molecule A, EGF; epidermal growth factor, LAG-3, lymphocyte activation gene 3, TIM-3/1/4; T cell immunoglobulin and mucin domain 3/1/4, CD16; cluster of differentiation 16, ACE2; angiotensin converting enzyme 2.

Role within the immune system	ADAM17 Substrate
Pattern recognition	TLR2 (Langjahr et al. 2014), TLR4 (Yang et al. 2018)
Inflammation	IL-6R (Matthews et al. 2003), IL-15R (Budagian et al. 2004), IL-23R (Franke et al. 2016), IL-1RII (Uchikawa et al. 2015), TNFR-I (Peschon et al. 1998), TNFR-II (Crowe et al. 1995), TNF-α (Black et al. 1997), Lymphotoxin-αβ (Young et al. 2010), IL-1β, CD154 (Yacoub et al. 2013), CD89 (Peng et al. 2010), 4-1BB (Nielsen et al. 2016)
Leucocyte adhesion and migration	ICAM-1 (Tsakadze et al. 2006), VCAM-1 (Garton et al. 2003), L-selectin (Peschon et al. 1998), CD44 (Nagano et al. 2004), JAM-A (Koenen et al. 2009)
T cell activation, proliferation, and exhaustion	LAG-3 (Li et al. 2007), TIM-3 (Möller-Hackbarth et al. 2013)
NK cell toxicity	CD16 (Romee et al. 2013)
Viral cell entry	ACE2 (Lambert et al. 2005), TIM-1, TIM-4 (Schweigert et al. 2014)

1.10.3 ADAM17 regulation of L-selectin expression by T cells

ADAM17 was discovered to cleave the ectodomain of the transmembrane homing molecule L-selectin in 1998 (Peschon et al. 1998). ADAM17 cleaves L-selectin at a single site in the 15 amino acid extracellular membrane proximal region into a soluble protein 62-100 kDa in size (Schleiffenbaum et al. 1992). This cleavage is mediated by the metalloproteinase domain of ADAM17 (Ager 2012). The hypervariable region of the cysteine-rich domain in ADAM17 could also regulate L-selectin shedding (Ager 2012). ADAMs 8 and 10 have also been found to cleave L-selectin under certain conditions, however, ADAM17 is the dominant enzyme involved (Gómez-Gaviro et al. 2007), (Le Gall et al. 2009), (Figure 1.4). On T cells, TCR stimulation/cross-linking induces the PI3Kδ pathway and subsequent ADAM17-mediated shedding (Chao et al. 1997), (Kaldjian and Stoolman 1995), (Sinclair et al. 2008). *In vitro*, L-selectin begins to downregulate from T cells from 1-hour post-activation, with 90% shed by 4 hours (Chao et al. 1997).

Mohammed *et al*. found that constitutive shedding of L-selectin on naïve leucocytes is not ADAM17- or ADAM10-mediated; this process is still not fully elucidated. However, shedding of L-selectin on peptide-MHC activated CD8 T cells was found to be ADAM17-dependent and a fundamental mediator of cell proliferation. *In vitro* murine CD8 T cells expressing a shedding-resistant form of L-selectin showed reduced proliferation and CD25 expression compared to wild-type CD8 T cells, when stimulated by cognate peptide. These results were also seen in mice infected with vaccinia virus *in vivo*, whereby wild-type CD8 T cells clonally expanded 8-times more than CD8 T cells expressing a shedding-resistant mutant of L-selectin (Mohammed et al. 2019). These results demonstrate the functional relevance of ADAM17-mediated cleavage of L-selectin at sites of immune activity and illustrate non-homing related effects which have implications for T cell function. Although the maintenance of L-selectin on CD8 T cells is shown to improve homing to sites of virus infection and subsequent viral clearance, lack of proteolytic shedding may reduce early lymphocyte proliferation and impede the initial adaptive immune response to infection (Mohammed et al. 2016), (Mohammed et al. 2019).

1.10.4 ADAM17 in infection

Due to its diverse array of substrates, it is no surprise that ADAM17 plays an important role in controlling infection. Impairing ADAM17 function in a murine model of bacterial peritonitis enhanced both L-selectin and TNF-α cell surface expression on neutrophils which increased neutrophil recruitment to the peritoneum, reduced bacterial load and improved survival (Long et al. 2010). Neutrophils expressing a non-cleavable form of L-selectin alone were found to confer an advantage in early neutrophil recruitment in bacterial peritonitis, but not in bacterial clearance. This suggests that substrates of ADAM17 other than L-selectin may contribute to this protection (Long et al. 2012). Conversely, ADAM17-dependent shedding of L-selectin is required for neutrophils to clear *Klebsiella pneumoniae* infection from the lungs of mice (Cappenberg et al. 2019). Alternately, there was no role for ADAM17 found in T cells in murine *Listeria monocytogenes* bacterial infection (Link et al. 2017). ADAM17 deficient T cells from $Adam17^{fl/fl}$×$CD4cre^{+}$ mice did not have altered clearance of *Listeria monocytogenes* bacterial infection compared to $Adam17^{fl/fl}$×$CD4cre^{-}$ mice (Link et al. 2017). This suggests different requirements for ADAM17 and L-selectin shedding in bacterial infection depending on leucocyte, pathogen, and target tissue.

ADAM17 was found to contribute to lung pathology in murine IAV infection via cleavage of CD8 T cell TNF-α which induced CXCL2 expression on lung epithelium, leading to heightened inflammatory cell infiltration (DeBerge et al. 2013). Inhibition of CD8 T cell ADAM17 in this mouse model reduced lung injury and improved survival (DeBerge et al. 2013). ADAM17 cleavage of TNFRII on CD8 T cells was also found to reduce bioavailability of circulating soluble TNF-α in IAV infection (DeBerge et al. 2015).

L-selectin is distinctively known not just as a marker of leucocyte homing, but also a marker of T_{CM}. There is evidence to suggest that ADAM17-controlled L-selectin shedding is required for effective CD8 T cell memory responses to recurrent virus infection in mice. Mice containing non-shedding LΔP L-selectin on lymphocytes conferred delayed protection against secondary virus challenge. Influenza-specific CD8 memory T cell quantity and distribution were

similar between wild-type and LΔP mice, apart from within LNs where LΔP mice contained more cells. Upon secondary challenge, the recruitment of CD8 memory T cells to the site of infection was comparable between groups, as well as cell differentiation, the only other difference observed bar viral clearance kinetics, was that LΔP memory CD8 T cells expressed higher IFN-γ and TNF-α levels (Richards et al. 2008). These results are contrasting to findings in primary IAV infection, suggesting L-selectin plays different roles in CTLs compared to memory CD8 T cells in virus infection.

1.10.5 Pharmaceutical agents to block ADAM17

Due to the indication of roles for ADAM17 in several diseases, it has become a pharmaceutical target (Table 1.4). Small molecule inhibitors have been developed, such as dual ADAM10 and ADAM17 inhibitor INCB7839/Aderbasib, which is currently being tested in clinical trials for paediatric glioma as well as diffuse large B cell lymphoma (DLBCL) in combination with rituximab, post autologous haematopoietic cell transplant (ClinicalTrials.gov 2014), (ClinicalTrials.gov 2020). Other small molecule inhibitors against ADAM17 such as BMS 561392/DPC-333 and Apratastat/TMI-005 are also available, however, these are known to have off-target effects on other matrix metalloproteinases (MMPs) and failed to progress through clinical trials due to toxicity and efficacy concerns (Qian et al. 2007), (Thabet and Huizinga 2006).

Further efforts to find specific inhibitors of ADAM17 have focused on developing monoclonal antibodies. Short-chain variable fragment (scFv) clones against ADAM17 epitopes have been identified using phage display technology, then developed into full length antibodies. D1(A12) is a human anti-ADAM17 'cross-domain' IgG antibody which contains the variable heavy (V_H) chain of a human IgG antibody that binds a non-catalytic domain of ADAM17, and the variable light (V_L) chain that binds to the catalytic domain of ADAM17 (Tape et al. 2011). D1(A12) has been efficacious in reducing tumour growth in a xenograft mouse model using human ovarian cancer cell line IGROV1-Luc (Richards et al. 2012).

There have also been efforts to create antibodies that recognise both mouse and human ADAM17. MEDI3622 is a mouse and human cross-reactive anti-ADAM17 antibody, formatted onto a human IgG1 framework (Rios-Doria et al. 2015). MEDI3622 is one of the few ADAM17 antibodies that has been tested in a mouse model of infection. Administration of MEDI3622 before induction of polymicrobial peritoneal sepsis reduced sepsis score, bacterial load, and mortality rates, which were improved further in combination with antibiotic treatment (Mishra et al. 2020). This was associated with increased recruitment of neutrophils to the peritoneum and reduced inflammatory cytokine production (Mishra et al. 2020).

A9(B8) is another mouse and human cross-reactive anti-ADAM17 antibody, formatted on a IgG2 framework (Kwok et al. 2014). A9(B8) underwent biochemical and cellular investigation and was found to be a successful inhibitor of ADAM17 with an IC_{50} of 84 nM in a quenched-fluorescent peptide cleavage assay (Kwok et al. 2014). A9(B8) was also characterised as an allosteric inhibitor, as it did not bind the catalytic domain of ADAM17, although the direct binding site has not yet been determined (Kwok et al. 2014).

A9(B8) had an IC_{50} of 72 nM for blocking soluble TNF-α release from the PANC-1 pancreatic cancer cell line (Ye et al. 2017). A9(B8) has been further tested for its efficacy in a non-small cell lung cancer (NSCLC) model; dual-efficacy was seen with epidermal growth factor receptor tyrosine kinase inhibitors (EGFR-TKI) erlotinib/gefitinib in an *in vitro* NSCLC cell line (Yang et al. 2019). *In vivo* pharmacokinetic analysis of A9(B8) demonstrated a half-life of 13 hours for A9(B8), with a terminal half-life of 10.5 days and no reported toxicity concerns (Ye et al. 2017). A9(B8) treatment significantly attenuated tumour formation in the *Pdx1Cre*;*Kras*^{G12D};*Trp53*$^{fl/+}$ pancreatic ductal adenocarcinoma (PDAC) mouse model, with a significant reduction in circulating levels of ADAM17 substrates TNF-α and amphiregulin (Ye et al. 2017).

D8P1C1 is one of the latest human and mouse cross-reactive anti-ADAM17 antibodies to be created, with a human IgG1 structure (Saha et al. 2022). The binding site of D8P1C1 was mapped to the catalytic domain of ADAM17 using

negative stain electron microscopy. D8P1C1 was first tested for inhibition of tumour cell proliferation *in vitro* and found to reduce the growth of seven different cancer cell lines up to 70% (Saha et al. 2022). However, D8P1C1 was found to bind preferentially to an 'active confirmation' ADAM17 found on tumour cells, compared to ADAM17 found on HEK293T cells (Saha et al. 2022). This is contrasting to MEDI3622 which the authors used to demonstrate binding to any ADAM17 confirmation (Saha et al. 2022). D8P1C1 caused a 78% tumour reduction in a mouse xenograft model of triple negative breast cancer, and 45% tumour reduction in an ovarian cancer xenograft model (Saha et al. 2022). No toxicity was seen with this treatment at a dosage of 15 mg/kg or 60 mg/kg and suggests a promising pharmacological intervention (Saha et al. 2022).

A9(B8) and D8P1C1 are yet to be tested for their binding to leucocyte ADAM17, effects on L-selectin and effects on any infection-related diseases. However, with the encouraging results seen with MEDI3622 and high affinity for ADAM17 inhibition, these antibodies may be promising to test in mouse models of infection.

Toxicity and efficacy issues with small molecule ADAM17 inhibitors led to discontinuation of human trials. This may not be a surprising finding since patients with mutations in ADAM17 have serious clinical conditions. Twins identified to have a loss-of-function mutation of ADAM17 suffered severe skin infections, bowel lesions and cardiomyopathy, with one twin dying at age 12 from myocarditis (Blaydon et al. 2011). Another individual was identified with a frameshift mutation in ADAM17, leading to similar symptoms and death at 10 months due to recurrent sepsis (Bandsma et al. 2015).

Table 1.4. ADAM17 inhibitors and disease models tested. ADAM17 inhibitor drugs, their formulations and published research into treatment of various disease models *in vitro* and *in vivo* using mouse models or human clinical trials. scFv; small chain variable fragment, NSCLC; non-small cell lung cancer, HNSCC; head and neck squamous cell carcinoma, DLBCL; diffuse large B cell lymphoma, HCT; haematopoietic cell transplant.

Drug name	Formulation	*In vitro* models	Mouse models	Human trials
INCB7839/ Aderbasib	Small molecule inhibitor	HER2+ breast cancer with trastuzumab (Liu et al. 2006).	High-grade glioma xenograft tumour model (Venkatesh et al. 2017).	Phase I; paediatric glioma (ClinicalTrials.gov 2020).
				Phase I/II; DLBCL in combination with rituximab, post autologous HCT (ClinicalTrials.gov 2014).
			HER2+ breast cancer xenograft tumour model with trastuzumab (Liu et al. 2006).	Phase I; HER2+ metastatic breast cancer with trastuzumab (Friedman et al. 2010).
BMS-561392/ DPC-333	Small molecule inhibitor	NSCLC (Baumgart et al. 2010).	Collagen-induced arthritis (CIA) model (Grootveld 2003).	Phase II rheumatoid arthritis (Grootveld 2003).
			Autoimmune hepatitis (Sharma et al. 2013).	
		Alzheimer's (Kim et al. 2008).	Acute colitis (Maddox 2015).	
			Alzheimer's (Kim et al. 2008).	
			Spinal cord injury (Vidal et al. 2013).	
			SARS-CoV-2 (Lartey et al. 2021).	

TMI-005/ Apratastat	Small molecule inhibitor	Polycystic kidney disease (Gooz et al. 2014).	NSCLC (Sharma et al. 2016).	Phase II rheumatoid arthritis (Thabet and Huizinga 2006).
JTP-96193	Small molecule inhibitor		Type 2 diabetes & diabetic peripheral neuropathy (Maekawa et al. 2019).	
D1(A12)	Human IgG antibody	HNSCC (Huang et al. 2014b).	Ovarian xenograft tumour model (Richards et al. 2012).	
		Triple negative breast cancer (Caiazza et al. 2015).		
A9(B8)	Humanised mouse IgG2 antibody	NSCLC with erlotinib/gefitinib (Yang et al. 2019).	Pancreatic cancer (Ye et al. 2017).	
MEDI3622	Humanised mouse IgG1 antibody	Colorectal cancer (Dosch et al. 2015).	Head and neck & colorectal xenograft tumour models (Dosch et al. 2017).	
		Ovarian cancer & Burkitt's lymphoma (Mishra et al. 2018).	Polymicrobial sepsis (Mishra et al. 2020).	
D8P1C1	Humanised mouse IgG1 antibody	Ovarian cancer, breast cancer, colon cancer, glioma, NSCLC (Saha et al. 2022).	Ovarian cancer & triple negative breast cancer (Saha et al. 2022).	

1.11 Conclusion

IAV is a clinically relevant virus which circulates yearly, causing significant morbidity and mortality worldwide. The immune response to IAV infection requires a multitude of cells from both the innate and adaptive immune system to orchestrate protection to the host. Leucocyte homing to LNs and tissues is fundamental for immunosurveillance and response to pathogens. This underpins the clearance of IAV, as cells must traffic to the correct tissues and organs to effectively eradicate the infection. Several selectins, chemokine receptors, integrins and their ligands co-ordinate this migration, with L-selectin being one of the most researched and the first homing receptor linked directly to improving virus clearance.

L-selectin and ADAM17 have clear fundamental roles in controlling the migration of leucocytes during infection (Mohammed et al. 2016), (Arbonés et al. 1994), (DeBerge et al. 2013), (Long et al. 2010). However, the mechanisms behind the protective effects seen by blocking L-selectin shedding and/or ADAM17 function are still to be fully elucidated. New unidentified ligands for L-selectin are prime candidates for this mechanism; these ligands may be present in inflamed HEV, peripheral blood vessels or in infected tissues and may help guide leucocytes to infected organs to elicit cytotoxic responses. There is yet to be clear understanding of the regulation of cell surface L-selectin by ADAM17. Understanding of mature ADAM17 cell surface expression patterns alongside transcription and translation of the L-selectin gene SELL are required *in vivo*. The translatability of murine data must also be tested, as there are limited primary human data available on functional L-selectin expression on leucocytes. Primary human data available suggest L-selectin may have crucial roles in T_{EM} homing (Sallusto et al. 1999), as well as in T cell responses during HIV infection (Giuliani et al. 2018).

There are several approaches being used to pharmacologically inhibit ADAM17 in various diseases from infection to autoimmune diseases and cancer. A major downfall with targeting ADAM17 is the off-target effects resulting from the promiscuity of this protein; many substrates will be impacted which may have undesired effects in patients. Other therapeutic avenues must be considered

such as genetic modification and infusion of autologous T cells or drugs that selectively target the ADAM17 cleavage site of L-selectin.

1.12 Hypothesis and aims

The overarching hypothesis for this body of work is that ADAM17 inhibition in mouse models of IAV infection will result in improved CD8 T cell homing to sites of virus infection (lungs) and subsequent viral clearance, via an L-selectin dependent mechanism (Figure 1.7).

The aims for the work presented within each results chapter of this thesis are as follows:

Chapter Three

1. To characterise anti-ADAM17 antibody candidates as pharmacological inhibitors to L-selectin shedding *in vitro*.

Chapter Four

2. To investigate the effects of pharmacological inhibition of ADAM17 on L-selectin shedding in IAV infection *in vivo*.

Chapter five

3. To investigate the effects of genetic ablation of ADAM17 proteolytic activity in lymphocytes on L-selectin shedding in IAV infection *in vivo*.

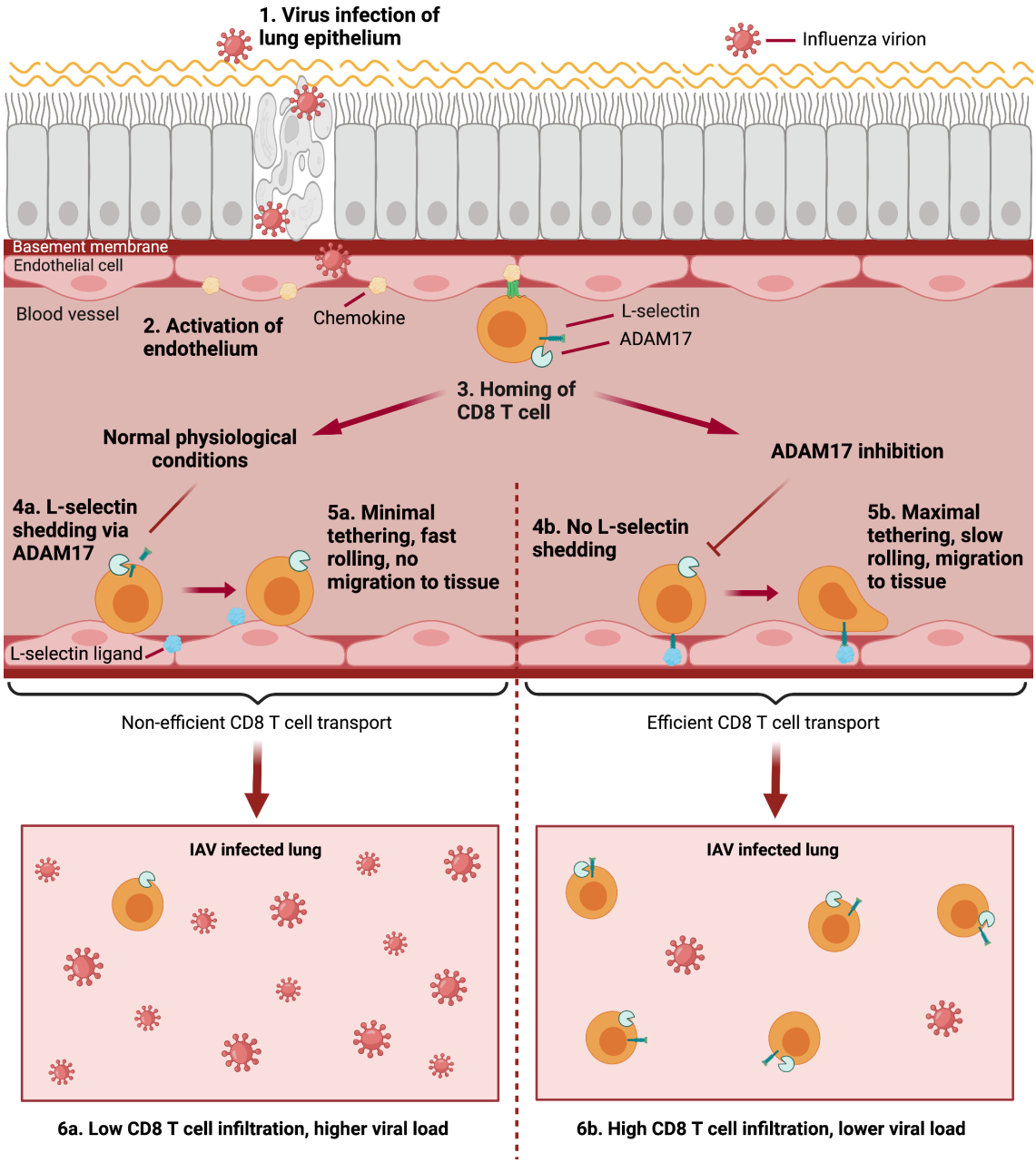

Figure 1.7. The role of ADAM17-mediated control of L-selectin in CD8 T cell homing in IAV infection. 1) Influenza virions infect airway epithelium. **2)** Epithelial infection results in activation of blood vessel endothelial cells and expression of chemokines. **3)** During homing, CD8 T cells become activated by chemokines, stimulating a disintegrin and metalloproteinase 17 (ADAM17). This leads to two possible outcomes depending on the level of ADAM17-dependent shedding of L-selectin. Under normal conditions: **4a)** L-selectin will become proteolytically cleaved by ADAM17. **5a)** Loss of L-selectin ectodomain results in minimal CD8 T cell tethering and rolling along endothelium. T cells fail to migrate to influenza A virus (IAV) infected tissue. **6a)** IAV infected lungs will contain lower CD8 T cell infiltration and will therefore result in higher viral load. When ADAM17 dependent L-selectin shedding is inhibited: **4b)** Blocking ADAM17 function retains L-selectin expression on the surface of CD8 T cells. **5b)** L-selectin binding to its ligand allows maximal CD8 T cell tethering and rolling along endothelium. T cells migrate to IAV infected tissue. **6b)** IAV infected lungs will contain higher CD8 T cell infiltration and will therefore result in lower viral load (Mohammed et al. 2016). Figure created using Biorender.com.

Chapter Two

Materials and Methods

2. Materials and Methods

2.1 Cell culture

2.1.1 Cell cryopreservation

Confluent cells were frozen in a 1 mL solution of 10% (v/v) dimethyl sulfoxide (DMSO)/foetal calf serum (FCS) at a concentration of $3x10^6$ cells/mL. Cells were placed into a labelled cryovial and placed into a 'Mr Frosty™' freezing container (ThermoFisher) for -80°C storage at a freezing rate of -1°C per minute. 1 day later cells were transferred to liquid nitrogen for long term storage.

2.1.2 Cell thawing

Cells were removed from liquid nitrogen storage and placed onto dry ice for transport. Cryovials were immediately placed in 37°C water bath for rapid thawing. Once thawed, 1 mL cell solution was added to 20 mL of pre-warmed DMEM media (Gibco) supplemented with 10% FCS, 100 IU/mL penicillin, 100 µg/mL streptomycin and 1 mM sodium pyruvate (D10) and centrifuged at 500 *g* for 5 minutes. Supernatant was removed, cells were resuspended in pre-warmed D10 media and placed into T25 or T75 flask for culturing.

2.1.3 Adherent cell passaging

All cell culturing was carried out in sterile conditions in a class II laminar flow cabinet. Once cells reached 80-100% confluency, media was removed from the flask and washed with phosphate buffered saline (PBS) to remove remaining media. Trypsin supplemented with 0.25% EDTA (Gibco) was added to cells and incubated at 37°C in 5% CO_2 in air for several minutes until cells detached from the flask. Pre-warmed D10 media was added to the flask to neutralise trypsin-EDTA, and cells were removed and placed into a 50 mL falcon tube. Cells were centrifuged at 500 *g* for 5 minutes at 37°C. Supernatant

was discarded and cells were resuspended into pre-warmed D10 media and placed into a fresh flask for further culturing.

2.1.4 RAW 264.7 cells

The adherent murine macrophage cell line RAW 264.7 was kindly gifted by Professor Phil Taylor from Cardiff University. These cells were cultured using D10 media and used for the TNF-α shedding assay described in section 2.6.5.

2.1.5 MDCK Luc 9.1 cells

The adherent Manin Darby Canine Kidney (MDCK) Luc 9.1 cell line was kindly gifted by Dr M. Jaber Hossain from the Centers of Disease Control and Prevention (Hossain et al. 2010). These cells were cultured using D10 media. Cells were used for the X31 influenza A virus titre assay described in section 2.4.3.

2.2 Mouse procedures

2.2.1 Mouse strains and housing

Congenic B6.PL-Thy1a/CyJ (Thy1.1) mice were bred in-house. C57BL/6J-CD45.1HomRag2KOHom ($Rag2^{-/-}$) supplied by The Jackson laboratory were also bred in-house. C57BL/6J (B6) and B6.129S7-Rag1tm1Mom/J ($Rag1^{-/-}$) mice were supplied by Charlies River. Mice were housed in S-containers ventilated with HEPA-filtered air. Female Thy1.1 and B6 mice were used for experimentation at 8-12 weeks of age. Female $Rag2^{-/-}$ mice were treated with 10% oral Baytril in drinking water every other week from birth. Female $Rag1^{-/-}$ and $Rag2^{-/-}$ mice were used for X31 IAV experimentation at 16-24 weeks of age. All animal studies were ethically reviewed and carried out in accordance with the Animals (Scientific Procedures) Act 1986 and the GSK Policy on the Care, Welfare and Treatment of Animals. All animal studies were also conducted in compliance to Cardiff University guidelines under project licence (PPL) number P2FB675AB.

2.2.2 Anti-ADAM17 antibody A9(B8) administration

Human/mouse cross-reactive ADAM17 inhibitor antibody; A9(B8), was kindly provided by Professor Henry Kwok (University of Macau) at a stock concentration of 2.6 mg/mL and stored at -80^{o}C. Mice were treated with 10 mg/kg or 15 mg/kg of A9(B8), injected intraperitoneally (i.p.), or intravenously (i.v.) via the tail vein. A9(B8) was administered in a volume of 9.5 mL/kg PBS, either 24 hours or 1 hour prior to X31 IAV infection.

2.2.3 Human IgG2 isotype control antibody administration

A human IgG2 isotype control antibody (Bio X Cell, BE0301) was stored at 4^{o}C. Antibody was dosed at 10 mg/kg and was administered via i.p. injection in a volume of 9.5 mL/kg to mice 24 hours prior to X31 infection. This served as an *in vivo* isotype control to A9(B8).

2.2.4 ADAM17 chimera mice generation

Female Rag1$^{-/-}$ or Rag2$^{-/-}$ mice were irradiated with 5 Gy and given ElectroGel electrolyte replenisher (Bio-Serv) for 2 weeks post-irradiation. 24 hours post-irradiation, mice were injected i.v. with either 2x10^{6} ADAM17^{WT} (ADAM17$^{+/+}$) or ADAM17$^{\Delta ZN/\Delta ZN}$ (ADAM17$^{-/-}$) foetal liver stem cells in sterile PBS at a volume of 9.5 mL/kg via the tail vein. Rag2$^{-/-}$ mice were treated with 10% oral Baytril in drinking water every other week from birth. Rag1$^{-/-}$ mice were treated with 10% oral Baytril in drinking water every other week from 1 week prior to stem cell injection. Baytril treatment was stopped for both strains 2 weeks post-stem cell injection.

2.2.5 Tail tipping/bleeding mice

150 µL of peripheral blood was collected via ‘tail tipping’ mice. Briefly, mice were placed into a warming chamber in their home cage at 37^{o}C for $\leq$20 minutes to allow blood vessel dilation. Mice were placed into a restrainer and the tip of the mouse tail was anaesthetised using ethyl chloride spray. The tip of

the tail was removed via scalpel, and 150 µL of peripheral blood was collected into heparinised tubes (VWR, SARS16.443) on ice.

2.2.6 Murine influenza virus infection

Mice were infected with $1x10^3$ or $3x10^3$ plaque forming units (pfu) A/X-31 (H3N2) (X31) in 50 µL sterile PBS. Mice were administered with 1 dose of 50 µL of influenza intranasally, delivered using an automatic pipette. Infection was carried out under general anaesthesia using isoflurane inhalation. Mice were weighed daily and humanely killed by a schedule 1 method on day 4, day 5 or day 7 of infection.

2.3 Harvest and preparation of mouse tissues

2.3.1 Bronchoalveolar lavage (BAL)

Mice were killed via CO_2 inhalation and exsanguination to confirm death. BAL was performed immediately using 500 µL sterile PBS. Briefly, the diaphragm of the mouse was pierced, and the trachea exposed. A small incision was made into the trachea with a scalpel and 0.6 mm tubing was inserted, attached to a 1 mL syringe via a 23 G needle. 500 µL sterile PBS was washed into the lungs. BAL was collected, stored on ice, and centrifuged at 500 *g* for 5 minutes. Supernatant was collected (BAL fluid/BALF) and stored at -80^{o}C for ELISA and multiplex analysis. BAL cells were resuspended in in 1 mL 2% v/v FCS/PBS at 4^{o}C (FACS buffer) and counted using 1 µL of acridine orange/propidium iodide cell viability kit (Labtech, F23001) in the LUNA FL automated fluorescence cell counter (Labtech). Total cell counts per mL and total live cell counts per sample were calculated.

2.3.2 Lungs and Lymph nodes

Mice were killed via CO_2 inhalation and exsanguination to confirm death. Lungs were perfused by injecting 5 mL sterile PBS into the heart using a 5 mL syringe attached to an 18 G needle. Lungs were then harvested into sterile PBS or RNAlater (ThermoFisher, AM7020) on ice. Spleen and mediastinal lymph

nodes were collected into sterile PBS on ice. Lungs were digested using the 'Mouse Lung Dissociation Kit' (Miltenyi Biotech). Briefly, 15 μL of 'enzyme A' and 100 μL of 'enzyme D' were added per lung in gentleMACs C tubes (Miltenyi Biotech) with 2.5 mL of 1x 'buffer S'. Lungs were homogenised using the gentleMACS octo-dissociator with heaters (Miltenyi Biotech) on pre-set program **'**37C_m_LDK_1**'**. Lungs were then washed with 5 mL 1x 'buffer S' and filtered through a 70 μm cell strainer (Greiner Bio-one). Lymph nodes were homogenised through a 70 μm strainer and washed with 5 mL of FACS buffer. Cells were resuspended in FACS buffer and counted using 1 μL of acridine orange/propidium iodide cell viability kit (Labtech) in the LUNA automated cell counter (Labtech). Total cell counts per mL and total live cell counts per sample were calculated.

2.3.3 Spleens

Mice were killed via CO_2 inhalation and cervical dislocation or exsanguination to confirm death. Spleens were collected into sterile PBS on ice. Spleens were homogenised through a 70 μm strainer and treated with 5 mL of 1x RBC lysis buffer (Biolegend) and incubated on ice for 5 minutes. Cells were washed then resuspended in FACS buffer and counted using 1 μL of acridine orange/propidium iodide cell viability kit (Labtech) in the LUNA automated cell counter (Labtech). Total cell counts per mL and total live cell counts per sample were calculated.

2.3.4 Bone marrow

Mice were killed via CO_2 inhalation and exsanguination to confirm death. Femur and tibia bones were removed from the mouse by cutting at hip and foot joints, then at the knee joint to separate. Muscle and skin were removed using a scalpel and discarded. Bones were placed into 5 mL sterile RPMI 1640 media (Gibco), supplemented with 10% FCS, 2 mM L-glutamine and 100 IU/mL penicillin, 100 μg/ml streptomycin (R10) on ice and stored at 4^{o}C overnight. To retrieve bone marrow, the ends of each bone were cut using scissors and the bone marrow was flushed out into a 50 mL falcon tube using 10 mL ice cold R10 in a 10 mL syringe with a 23 G needle. Cells were centrifuged at 500 *g* for

7 minutes at 4°C and supernatant discarded. Cells were resuspended in 1 mL 1x RBC lysis buffer and incubated at 4°C for 5 minutes. Cells were centrifuged again at 500 *g* for 7 minutes and supernatant discarded. Cells were resuspended in 5 mL R10 media and counted using 1 μL of acridine orange/propidium iodide cell viability kit (Labtech) in the LUNA automated cell counter (Labtech). Total cell counts per mL and total live cell counts per sample were calculated.

2.3.5 Sera

Whole blood was collected either via cardiac puncture, whereby mice were killed via CO_2 inhalation and exsanguination to confirm death. A 1 mL syringe with a 23 G needle was used to draw blood directly from the heart. Alternatively, 150 μL of peripheral blood was collected via 'tail tipping' mice as described in section 2.2.5. Blood was collected into 0.5 mL eppendorf tubes and incubated at room temperature for 20 minutes to allow coagulation. Samples were then centrifuged at 1500 *g* for 10 minutes at 4°C. Clear supernatant layer (serum) was removed and stored at -80°C until further use.

2.4 Influenza strain A/X-31 (H3N2)

2.4.1 Virus propagation

Influenza strain A/X-31 (H3N2) (X31) was kindly provided by Professor Ian Humphreys and grown in embryonated chicken eggs. Briefly, 100 μL of $1x10^3$ pfu X31 was administered to day 10 embryos via needle insertion into the side of the egg. Embryos were incubated upright at 37°C for 2-3 days in a humid, non-CO_2 incubator, then killed by incubation at -20°C for 1 hour. The allantoic fluid containing virus was then collected. Allantoic fluid was pooled together and centrifuged at 200 *g* for 5 minutes at 4°C to remove contaminants and stored at 4°C while a titration assay was carried out to determine viral titre of stock.

2.4.2 Mouse lung preparation for influenza virus titre

The left lung lobe from each mouse was homogenised in 1 mL of R10 media using the T 10 basic ULTRA-TURRAX homogeniser (IKA). Lung homogenates were centrifuged at 200 *g* for 10 minutes at 4^{o}C. Supernatant was removed and used for IAV titre assay.

2.4.3 Influenza virus titre assay

Virus within allantoic fluid or lung homogenates were titred using Luc 9.1 MDCK cells and pfu per mL calculated. $1.4x10^5$ Luc 9.1 cells were plated into each well of a 24-well cell bind plate (VWR) in 200 µL serum free RPMI media (Gibco) supplemented with 2 mM L-glutamine and 100 IU/mL penicillin, 100 µg/ml streptomycin. Serial dilutions of X31 virus stock were set-up in a separate 24-well plate; 990 µL serum free RPMI media was added to well number 1 with 10 µL X31 virus (1/100 dilution). Virus or lung homogenate was serially diluted 1 in 2 with serum free RPMI media over the following 4 wells. 200 µL of each dilution was added to the cell bind plate of Luc 9.1 cells. Plates were incubated at 37^{o}C, in 5% CO_2 for 4-6 hours. 300 µL of a methylcellulose-media solution (1-part 2% (w/v) methylcellulose/d$H_2$0 solution (Sigma-Aldrich), 2-parts serum free RPMI) was added to each well and plates were incubated at 37^{o}C, 5% CO_2 for a further 48 hours. Cells were washed with PBS, then fixed with 500 µL of 4% (v/v) formalin/PBS at room temperature for 30 minutes. 250 µL of 0.5% triton X-100 (Sigma-Aldrich) was then added to all wells and incubated for a further 30 minutes. Cells were washed and blocked with 500 µL of 10% (v/v) FCS/PBS for 1 hour at room temperature. Cells were subsequently stained with 200 µL of a 10 µg/mL working concentration of X31 anti-influenza nucleoprotein antibody (Bio-Rad, MCA400) for 90 minutes at room temperature. Cells were again washed and stained with 200 µL of a 1/1000 dilution of anti-mouse IgG-HRP (Bio-Rad, 1721011) secondary antibody at room temperature, in the dark for 90 minutes. Plates were developed using 300 µL of a solution of: 2.5 mL dimethylformamide (DMF), 47.5 mL of 50 nM acetate buffer, one 3-amino-9-ethylcarbazole (AEC) tablet (Sigma-Aldrich) and 25 µL of 30% hydrogen peroxide. Plates were incubated for 30 minutes in the dark, at room temperature. Plates were counted for stained cells under a microscope and total pfu/mL was calculated. Virus was stored at -80^{o}C until use.

2.5 Pharmacological compounds

2.5.1 Anti-ADAM17 antibody A9(B8)

Human/mouse cross-reactive IgG2 ADAM17 inhibitor antibody A9(B8), was kindly provided by Professor Henry Kwok (University of Macau) at a stock concentration of 2.6 mg/mL and stored at -80^{o}C. For *in vitro* titrations, serial dilutions of A9(B8) were prepared at 2x concentrations in FACS buffer or T cell culture media (RPMI (Gibco) 10% FCS, 2 mM L-glutamine, 100 IU/mL penicillin, 100 µg/ml streptomycin, 1x non-essential amino acids (Gibco), 50 µM β-mercaptoethanol (Gibco), 360 IU µL^{-1} human recombinant IL-2). 25 µL of each dilution were added per well and diluted to give a 50 µL final well volume and 1x final concentration.

2.5.2 Anti-ADAM17 antibody D8P1C1

Human/mouse cross-reactive IgG1 ADAM17 inhibitor antibody D8P1C1, was kindly provided by Dr Dimitar Nikolov (Sloan Kettering Institute) at a stock concentration of 1.5 mg/mL and stored at -80^{o}C. For *in vitro* titrations, serial dilutions of D8P1C1 were prepared at 2x concentrations in FACS buffer or T cell media and 25 µL of each dilution were added per well to give a 50 µL final well volume and 1x final concentration.

2.5.3 Anti-ADAM10 antibody 1H5

Human/mouse cross-reactive IgG1 ADAM10 inhibitor antibody 1H5, was kindly provided by Dr Dimitar Nikolov (Sloan Kettering Institute) a stock concentration of 1.5 mg/mL and stored at -80^{o}C. For *in vitro* titrations, serial dilutions of 1H5 were prepared at 2x concentrations in FACS buffer or T cell media and 25 µL of each dilution were added per well to give a 50 µL final well volume and 1x final concentration.

2.5.4 ADAM17 inhibitor TIMP-3

Human recombinant TIMP-3 (R&D systems, 973-TM-MTO) was received at a stock concentration of 0.155 mg/mL and stored at -80°C. For *in vitro* titrations, serial dilutions of TIMP-3 were prepared at 2x concentrations in FACS buffer or T cell media and 25 μL of each dilution were added per well to give a 50 μL final well volume and 1x final concentration.

2.6 Shedding assays and flow cytometry

2.6.1 Anti-CD3/anti-CD28 induced L-selectin shedding assay

Splenocytes were prepared as described in section 2.3.3 and plated at $5x10^5$ cells per well in a U-bottom 96-well plate. Cells were resuspended in 25 μL T-cell culture media. To activate ADAM17, cells were then treated with hamster anti-mouse CD3ε antibody at 200 ng mL^{-1} (BD Bioscience, 553057) and hamster anti-mouse CD28 antibody at 100 ng mL^{-1} (BD Bioscience, 553924), with or without anti-ADAM17/10 antibodies or TIMP-3. After 4 hours of incubation at 37°C in 5% CO_2, cells were centrifuged at 500 *g* for 3 minutes, supernatant collected, and cells washed with 200 μL FACS buffer. Flow cytometric staining and analysis were carried out as described in section 2.6.7.

2.6.2 PMA induced L-selectin shedding assay-whole blood

50 μL of whole blood was plated in U-bottom 96 well plate. Cells were treated with either 5 μM phorbol 12-myristate 13-acetate (PMA) or equal volume of DMSO and incubated at 37°C, 5% CO_2 for 30 minutes to activate ADAM17. Cells were then centrifuged at 500 *g* for 3 minutes, supernatant discarded, and cells washed with 200 μL FACS buffer. Live/dead, antibody staining and analysis for flow cytometry was carried out to determine ADAM17 functionality via levels of L-selectin on lymphocytes in whole blood. Flow cytometric staining and analysis were carried out as described in section 2.6.7.

2.6.3 PMA induced L-selectin shedding assay-sera

Splenocytes were prepared as described in section 2.3.3, and $5x10^5$ cells were resuspended in 7.5 μL of mouse sera and plated in a U-bottom 96 well

plate. Cells were treated with either 5 μM PMA to activate ADAM17, or equal volume of DMSO as a vehicle control. As a positive control, cells resuspended in sera from naïve mice were treated with 7 μM exogenous A9(B8) and 5 μM PMA. Cells were incubated at 37°C, 5% CO_2 for 30 minutes. Cells were then centrifuged at 500 *g* for 3 minutes, supernatant discarded and washed with 200 μL FACS buffer. Live/dead and antibody staining and analysis for flow cytometry were carried out as described in section 2.6.7.

2.6.4 PMA induced L-selectin shedding assay-lymphocytes

Splenocytes were prepared as described in section 2.3.3, and $5x10^5$ cells were resuspended in 22.5 μL FACS buffer and plated in a U-bottom 96 well plate. Cells were treated with either 5 μM PMA to activate ADAM17, or equal volume of DMSO as a vehicle control, with or without anti-ADAM17/10 antibodies or TIMP-3 (R&D Systems). After 30 minutes of incubation at 37°C, 5% CO_2 cells were centrifuged at 500 *g* for 3 minutes, supernatant collected, and cells washed with 200 μL FACS buffer. Flow cytometric staining and analysis were carried out as described in section 2.6.7.

2.6.5 LPS induced TNF-α shedding assay

RAW 264.7 murine macrophage cell line was cultured in D10 media. $5x10^5$ cells were resuspended in 22.5 μL FACS buffer and plated in a U-bottom 96 well plate. Cells were treated with either of 1 μg/mL lipopolysaccharide (LPS) (Sigma-Aldrich) to activate ADAM17, or equal volume of DMEM media as a vehicle control, with or without anti-ADAM17/10 antibodies or TIMP-3 (R&D Systems). After 1 hour of incubation at 37°C, 5% CO_2 cells were centrifuged at 500 *g* for 3 minutes, supernatant collected, and cells washed with 200 μL FACS buffer. Flow cytometric staining and analysis were carried out as described in section 2.6.7.

2.6.6 A9(B8) detection in tissues using goat anti-human IgG-Fc-FITC

Spleen, BAL, lungs, and mediastinal lymph node were prepared as described in section 2.3. Cells were plated at $1x10^6$ cells per well in a U-bottom 96 well plate. Cells were centrifuged at 500 *g* for 3 minutes, supernatant discarded, and lungs and spleen from naïve mice were treated with 7 μM exogenous A9(B8) as a positive control. Cells were incubated at 37°C, 5% CO_2 for 30 minutes. Cells were then centrifuged at 500 *g* for 3 minutes, supernatant discarded and washed with 200 μL FACS buffer. Cells were subsequently stained with live/dead fixable stain aqua and Fc block as in section 2.6.7, then with 100 μL of a 20 μg/mL dilution of goat anti-human IgG-Fc-FITC (Merck, AP113F) in FACS buffer was added per well. Cells were incubated at 4°C for 30 minutes, then centrifuged at 500 *g* for 3 minutes and washed in FACS buffer three times. 100 μL of a 1/100 dilution of normal rat serum (StemCell Technologies) in FACS buffer was added per well. Cells were incubated at 4°C for 15 minutes, then centrifuged at 500 *g* for 3 minutes and supernatant removed. CD8 T cells were stained using rat anti-CD8a antibody and analysed for flow cytometry as described in section 2.6.7.

2.6.7 Flow cytometry

$5x10^5$-$1x10^6$ cells were stained with live/dead fixable dead stain kit aqua (Life Technologies) according to manufacturer instructions. Briefly, a 1 μL/mL solution of live/dead aqua was prepared in sterile PBS and 100 μL was added per well. Cells were incubated at room temperature for 30 minutes in the dark. Cells were centrifuged at 500 *g* for 3 minutes, supernatant discarded, and cell pellets resuspended in 100 μL of 20 μg/mL mouse Fc block (BD Pharmingen) for 5 minutes at 4°C. 50 μL of an antibody cocktail (Table 2.1) diluted in in FACS buffer was added per well. Cells were incubated at 4°C for 30 minutes, then centrifuged at 500 *g* for 3 minutes and supernatant removed. Cells were washed a further three times. Cells were then fixed in 200 μL 4% (v/v) formalin/PBS for 15 minutes at room temperature and centrifuged again, at 500 *g* for 3 minutes. Supernatant was discarded and cells resuspended in 200 μL FACS buffer. Samples were analysed using a FACSCanto II cytometer (BD) and data analysed using FlowJo software (TreeStar Inc). Gating strategy for flow cytometric data is described in figures 2.1, 2.2 and 2.3.

Table 2.1. Antibodies used in flow cytometric staining. All working concentrations stained $5x10^5$ cells per well in a 96-well plate with a volume of 50 µL. All working concentrations of antibody were diluted in 2% (v/v) FCS/PBS (FACS buffer). Cells were incubated with antibody for 30 minutes at 4°C in the dark.

Antibody target antigen	Host species	Clone	Fluorophore conjugate	Stock concentration	Working concentration
Anti-mouse CD8a	Rat	53-6.7	PerCP-Cy5.5	0.2 mg/mL	0.4 µg/mL
Anti-mouse CD4	Rat	GK1.5	APC	0.2 mg/mL	2 µg/mL
Anti-mouse CD19	Rat	6D5	Pe-Cy7	0.2 mg/mL	2 µg/mL
Anti-mouse L-selectin	Rat	MEL-14	APC-Fire^{750}	0.2 mg/mL	0.4 µg/mL
Anti-mouse TNF-α	Rat	MP6-XT22	PE	0.2 mg/mL	2 µg/mL
Anti-mouse CD44	Rat	IM7	FITC	0.5 mg/mL	1 µg/mL
Anti-mouse CD69	Rat	H1.2F3	APC	0.2 mg/mL	0.4 µg/mL
Anti-human IgG-Fc	Goat	N/A	FITC	2 mg/mL	20 µg/mL

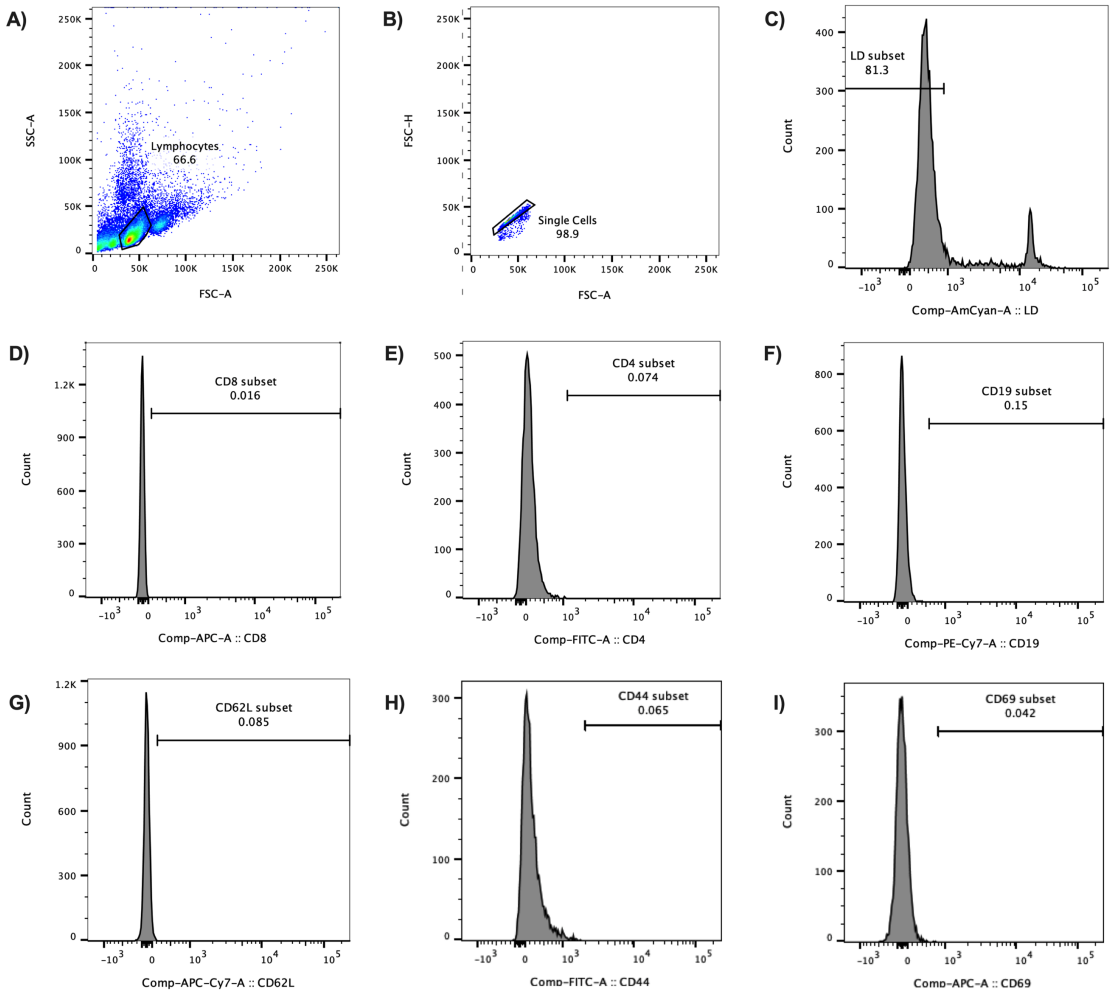

Figure 2.1. Gating strategy for flow cytometric analysis of lymphocyte populations using fluorescence minus one (FMO) gating. A) Lymphocyte gating, forward scatter area (FSC-A) vs side scatter area (SSC-A). **B)** Single cells, FSC-A vs forward scatter height (FSC-H). **C)** Live/dead (LD) gating, LD histogram. **D)** CD8 gating, CD8 FMO histogram. **E)** CD4 gating, CD4 FMO histogram. **F)** CD19 gating, CD19 FMO histogram. **G)** L-selectin (CD62L) gating, CD62L FMO histogram. **H)** CD44 gating, CD44 FMO histogram. **I)** CD69 gating, CD69 FMO histogram. Flow cytometry carried out on FACS Canto II flow cytometer. Analysis carried out using FlowJo (TreeStar Inc).

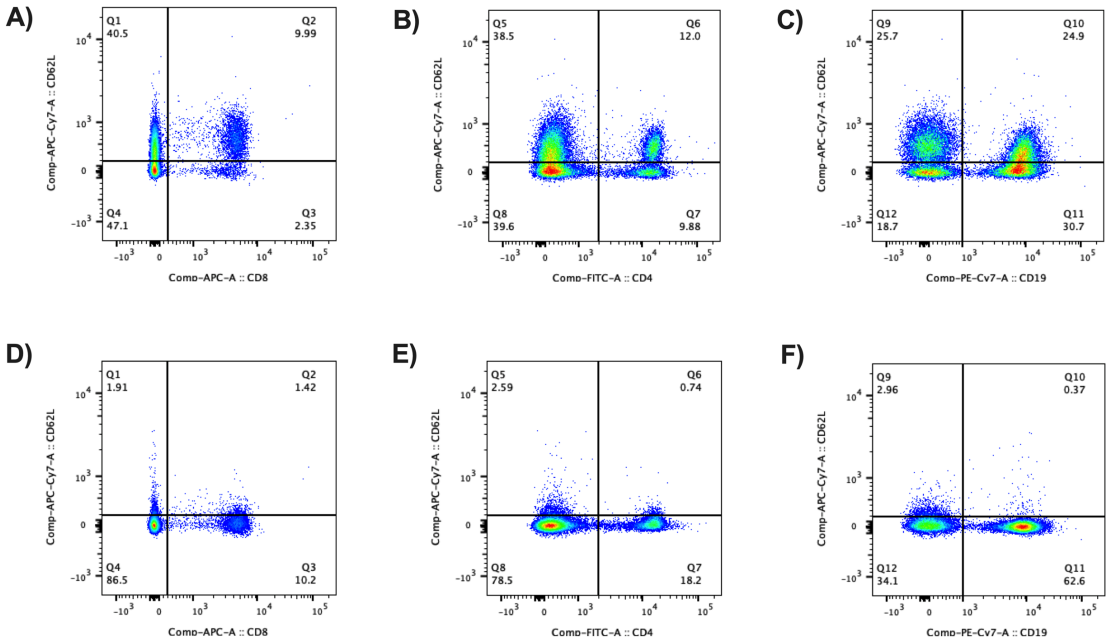

G)

Lymphocyte subset	CD62L MFI DMSO alone	CD62L MFI PMA alone	CD62L MFI PMA + drug/ serum treatment	Percentage CD62L shedding inhibition calculation	Percentage CD62L shedding inhibition
CD8 T cells	521	75	506	(506/521) x 100= 97.1	97.1%
CD4 T cells	260	48	259	(259/260) x 100= 99.6	99.6%
B cells	219	18	179	(179/219) x 100= 81.7	81.7%

Figure 2.2. Representative flow plots for PMA or DMSO control treated lymphocytes to calculate percentage inhibition of L-selectin (CD62L) shedding by ADAM17 inhibitors. A-C) L-selectin expression on unactivated lymphocyte subsets with vehicle control DMSO treatment. Y-axis; L-selectin. **A)** CD8 T cells **B)** CD4 T cells **C)** CD19 B cells. **D-F)** L-selectin expression on PMA activated lymphocyte subsets. Y-axis; L-selectin. **D)** CD8 T cells **E)** CD4 T cells **F)** CD19 B cells. **G)** Table representing how percentage inhibition of L-selectin shedding was calculated. Mean fluorescence intensity (MFI) of L-selectin was calculated from live cells. 'Vehicle control' DMSO treatment and PMA treatment shown, which sheds L-selectin in an ADAM17-dependent mechanism. Representative L-selectin MFI on lymphocytes with PMA treatment and ADAM17 inhibitor/serum treatment shown. Example percentage inhibition of L-selectin calculation shown in last 2 columns. Flow cytometry carried out on FACS Canto II flow cytometer. Analysis carried out using FlowJo (TreeStar Inc).

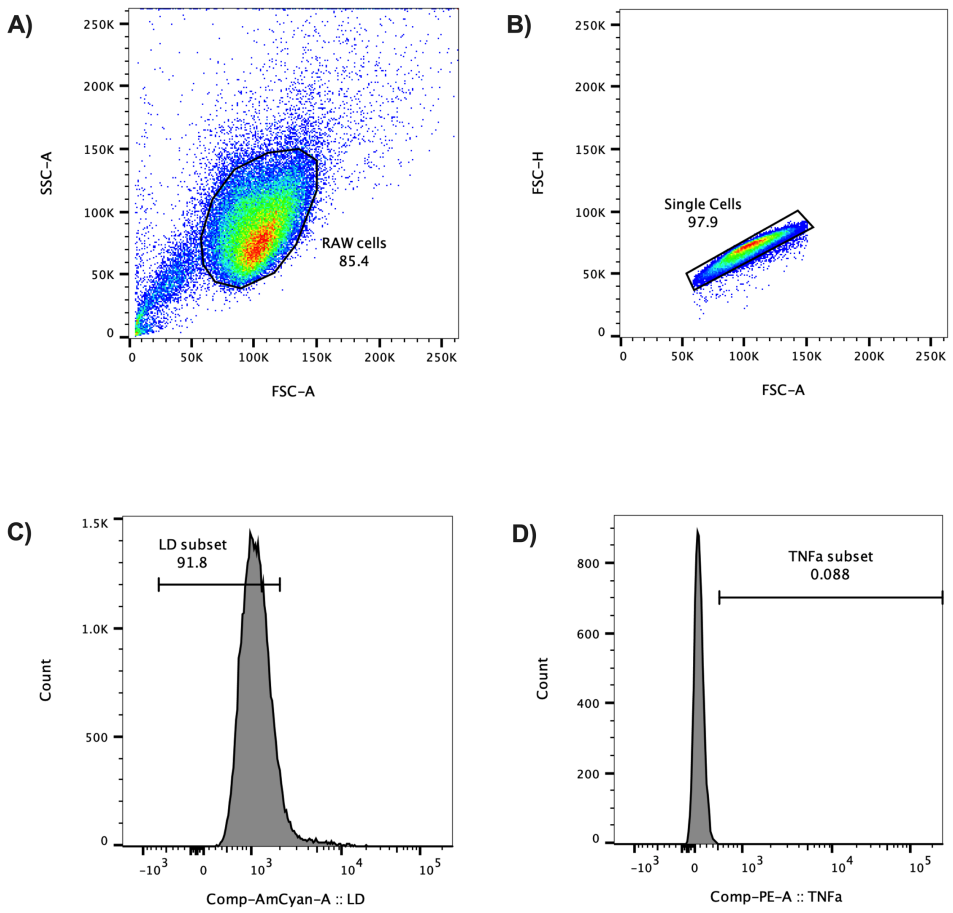

Figure 2.3. Gating strategy for flow cytometric analysis of RAW 264.7 macrophage populations. A) RAW 264.7 macrophage gating, forward scatter area (FSC-A) vs side scatter area (SSC-A). **B)** Single cells, FSC-A vs forward scatter height (FSC-H). **C)** Live/dead (LD) gating, LD histogram. **D)** Tumour necrosis factor-α (TNF-α) gating, TNF-α isotype antibody histogram. Flow cytometry carried out on FACS Canto II flow cytometer. Analysis carried out using FlowJo (TreeStar Inc).

2.7 RT-qPCR

2.7.1 RNA extraction

Virus was quantified from lungs of X31 IAV infected mice using real time quantitative polymerase chain reaction (RT-qPCR). The post caval and inferior lung lobes were collected from mice into RNAlater (ThermoFisher) on ice and further stored at 4^{o}C for a maximum of 1 week for RNA extraction. RNeasy mini kit (Qiagen, 74104) was used for RNA extraction and all steps were carried out at room temperature. $\geq$20 mg lung tissue was placed into 600 µL 'RLT/2-ME' buffer in RNase-free tubes (Starlab) and homogenised using the T 10 basic ULTRA-TURRAX. Samples were centrifuged for 3 minutes at 16,000 *g* in a microcentrifuge (Heraeus). Supernatant was removed by pipetting and an equal volume (600 µL) of 70% ethanol was added to supernatant into a fresh RNase-free tube. 700 µL of this mixture was added to a fresh spin column and 2 mL collection tube provided by the RNeasy kit. Samples were centrifuged for 15 seconds at 9500 *g* and elution was discarded. 700 µL of 'buffer RW1' was added to the spin column, followed by a further centrifugation for 15 seconds at 9,500 *g* and removal of elution. Next, 500 µL of 'RPE buffer' was added to the spin column and tube centrifuged at 9500 *g* for 15 seconds and elution removed again. This step was repeated with a 2-minute centrifugation at 9500 *g*. The spin column was transferred to a fresh collection tube and centrifuged at 16,000 *g* for 1 minute to dry out column. Finally, 40 µL of RNase free water was added to the spin column and centrifuged for 1 minute at 9,500 *g*. This final elution was the RNA. RNA quantity and quality were measured on a NanoDrop 2000/2000c (ThermoFisher Scientific). Absorbance values at 260/280 nm and 230/280 nm wavelengths were measured to assess nucleic acid purity. Values of $\geq$2.0 for 260/280 nm and 2.0-2.2 for 230/280 nm were considered adequately pure.

2.7.2 cDNA synthesis

cDNA was synthesised using the QuantiTect reverse transcription kit (Qiagen, 205311) according to manufacturer instructions. Briefly, 2 µL of 7x gDNA wipeout buffer and 1 µg total RNA were added into an RNase-free

eppendorf and made up to 14 µL with RNase-free water. Eppendorfs were incubated for 2 minutes at 42^{o}C on a heat block, then placed on ice immediately. 4 µL of 5x Quantiscript reverse transcription (RT) buffer, 1 µL RT primer mix and 1 µL of Quantiscript RT were added to each tube and incubated at 42^{o}C for 30 minutes. 80 µL of RNase free water was then added to the samples and they were incubated for 3 minutes at 95^{o}C. cDNA samples were then stored at -20^{o}C until further use.

2.7.3 qPCR

A PCR mastermix was made per primer pair, with 10 µL of Sybr green reagents (Qiagen, 204143), 8 µL nuclease free water (NFW) and 1 µL of forward and reverse primer mix (Sigma-Aldrich) per well. 19 µL of mastermix was added to each well of a V-bottom 96 well plate and 1 µL of cDNA added in triplicate. Plate was analysed using the Quantstudio 3 real time qPCR instrument (ThermoFisher Scientific). Fold increase in mRNA was calculated using the delta-delta-cycle threshold ($2^{-\Delta\Delta Ct}$) method (Schmittgen and Livak 2008). Expression was normalised to glyceraldehyde-3-phosphate dehydrogenase (GAPDH) housekeeping gene expression.

Primers for X31 were designed in house, using the X31 nucleoprotein gene sequence (X31 NP). Mouse GAPDH primers were purchased (PrimerDesign). X31 NP primer sequences: forward 5'-ACTGATGGAGAACGCCAGAA-3', reverse: 5'-TGAGTTCGGTGCACATTTGG-3'.

2.8 Soluble factor analysis via ELISA and Multiplex

2.8.1 Sandwich ELISAs

Sandwich enzyme-linked immunosorbent assay (ELISA) of soluble mouse L-selectin and soluble mouse TNF-α were carried out according to manufacturer instructions using Duoset ELISA kits (R&D systems, DY576, DY410) and Duoset ELISA ancillary reagent kits (R&D systems, DY008). Briefly, 96-well microplates were coated with 100 µL of working concentration of

capture antibody and incubated overnight at room temperature. Plates were washed with 300 µL wash buffer 3 times and blocked with 100 µL reagent diluent (1% (w/v) bovine serum albumin (BSA)/PBS) for 1 hour at room temperature. Plates were washed a further 3 times and 100 µL of cell culture supernatant, sera, BALF or standards were added to the plate. After 2 hours of incubation at room temperature, plates were washed 3 times and 100 µL of working concentration of detection antibody added for a further 2 hours at room temperature. After 3 subsequent washes, 100 µL of working concentration of streptavidin-HRP was added and incubated for 20 minutes in the dark at room temperature. Plates were washed 3 times and 100 µL of substrate solution was added for 20 minutes in the dark at room temperature. 50 µL of stop solution was added to plate. Plates were read for absorbance immediately at 450 nm wavelength using CLARIOstar Plus Microplate Reader.

2.8.2 LEGENDplex Assay

Multiplex assay was carried out using the LEGENDplex Mouse Anti-Virus Response Panel 13-plex (Biolegend, 740621) according to manufacturer instructions. This panel consisted of 13 mouse proteins: IFN-γ, CXCL1 (KC), TNF-α, CCL2 (MCP-1), IL-12p70, CCL5 (RANTES), IL-1β, CXCL10 (IP-10), GM-CSF, IL-10, IFN-β, IFN-α, IL-6. Briefly, 25 µL of diluted standard was added to a V-bottom 96-well plate with 25 µL of matrix A, whilst 1:2 diluted BALF, or sera samples were added to the plate with 25 µL of assay buffer. 25 µL of mixed beads were added to all wells, plate was covered in foil to protect from light and incubated on a plate shaker set at 800 rpm for 2 hours at room temperature. Plate was centrifuged at 250 *g* for 5 minutes, supernatant removed, and plate plotted onto a paper towel. Plate was washed with 200 µL of 1x wash buffer and incubated for 1 minute. Centrifugation and wash step repeated once. After further centrifugation at 250 *g* for 5 minutes and removal of supernatant, 25 µL of detection antibodies were added to each well. Plate was covered with foil to protect from light and placed on a plate shaker at 800 rpm for 1 hour at room temperature. 25 µL of streptavidin-PE was added to each well without washing. Plate was again covered with foil and placed on a plate shaker at 800 rpm for 30 minutes at room temperature. Plate was centrifuged at 250 *g* for 5 minutes and wash step repeated twice. 150 µL of 1x wash buffer

was added to each sample and samples were analysed using the FACS Canto II flow cytometer (BD) and FCS files were analysed using LEGENDplex software (Biolegend).

2.9 SDS-PAGE

2.9.1 Sodium dodecyl sulfate polyacrylamide gel electrophoresis (SDS-PAGE)

For unreduced conditions, 1-5 µg of protein sample was mixed with an equal volume of sample loading buffer. For reduced conditions, reducing sample loading buffer was used, containing 0.5 M dithiothreitol (DTT). Samples and elite pre-stained protein ladder (Generon) were loaded onto a NuPAGE™ 4-12% Bis-Tris Plus Gel (ThermoFisher Scientific) and run in NuPAGE™ MES SDS running buffer (ThermoFisher Scientific) in a Bolt Mini Gel Tank (ThermoFisher Scientific). Gel tank was powered via Bio-Rad Powerpac 200 power supply (Bio-Rad) and run at 200 V for 25 minutes. Gels were removed from casing and stained for 30 minutes. using quick coomassie stain (Generon).

2.10 Statistical analysis

All statistical analyses were carried out using Prism 9.0 software (GraphPad). Normal distribution of data was tested using the Shapiro-Wilk test. To estimate IC_{50}, a non-linear fit curve using the four-parameter logistic equation was generated and IC_{50} values estimated by Prism software. Simple linear regression was used for correlation analyses. For comparing 2 groups with normally distributed data, unpaired students T-test was carried out. For comparing 2 groups with non-normally distributed data, Mann-Whitney test was carried out. For 3 or more groups, one-way analysis of variance (ANOVA) was carried out with Tukey's post-hoc test to directly compare all groups. Error bars on bar graphs represent standard error of the mean ($\pm$SEM). To analyse mouse weight loss, an unpaired student T-test was used at each timepoint. A p value ≤ 0.05 was deemed significant.

2.11 A9(B8) *in vivo* calculations

A9(B8) *in vivo* molar concentrations were calculated to determine circulating levels of antibody (Durbin et al. 1992). Stock of A9(B8) is stored at a concentration of 2.6 mg/mL (17.3 μM).

10 mg/kg dosage

- 10 mg/kg dosage means an average of 200 μg of A9(B8) administered per 20 g mouse in a 200 μL injection.
- Total plasma volume (48.9 +/- 4.4 μL g^{-1}) and extracellular water volume (232 +/- 15 μL g^{-1}) (Durbin et al. 1992).
- Plasma volume + extracellular water volume x average adult female mouse weight

48.9 μL + 232 μL x 20 g = 5618 μL

- Formula weight of A9(B8) x total fluid volume

150000 kDa x 5618 μL = 842,700,000

- Mass of A9(B8) administered / 842,700,000

200 μg / 842,700,000 = 0.000000237 M

0.000000237 M x 1000000000 = 237 nM

- 237 nM concentration *in vivo*

15 mg/kg dosage

- 15 mg/kg dosage means an average of 200 μg of A9(B8) administered per 20 g mouse in a 200 μL injection.
- Mass of A9(B8) / 842,700,000

300 μg / 842,700,000 = 0.000000356 M

0.000000356 M x 1000000000 = 356 nM

- 356 nM concentration *in vivo*

2.12 List of reagents

2.12.1 RPMI and DMEM media

Rosewell Park memorial institute (RPMI) medium was purchased from Gibco and supplemented with 10% FCS (Sigma-Aldrich), 2 nM L-glutamine, 100 IU/mL penicillin, 100 µg/ml streptomycin, 1 mM sodium pyruvate. Dulbecco's Modified Eagle Medium (DMEM) was purchased from Gibco and supplemented with 10% FCS, 100 µg/ml streptomycin, 1 mM sodium pyruvate, 1 mM sodium pyruvate.

2.12.2 T cell media

RPMI medium was supplemented with 10% FCS (Sigma-Aldrich), 2 nM L-glutamine, 100 IU/mL penicillin, 100 µg/ml streptomycin, 1x non-essential amino acids (Gibco) 50 µM β-mercaptoethanol (Gibco), 360 IU μL^{-1} human recombinant IL-2 (Proleukin).

2.12.3 FCS

Foetal calf serum used to supplement media and for freezing was purchased from Sigma-Aldrich and heat inactivated for 30 minutes at 56^{o}C.

2.12.4 Human recombinant interleukin 2

Human recombinant interleukin 2 (IL-2) was purchased from Proleukin and stored at 20 ng/mL in RPMI media. Aliquots were stored at -80^{o}C.

2.12.5 Dimethyl sulfoxide (DMSO)

DMSO was purchased from Sigma-Aldrich and used for cell freezing media (90% FCS, 10% DMSO) or as a vehicle control for PMA.

2.12.6 Mouse lung dissociation kit

Mouse lung dissociation kit was purchased from Miltenyi Biotech (130-095-927) and was used for processing lungs for flow cytometric analysis. Buffer S was supplied as a 20x stock concentration and diluted to 1x using sterile ddH_20 and stored at 4^oC. Enzymes 'A' and 'D' were reconstituted using 'Buffer S' and stored at 40 µL and 110 µL aliquots respectively, at -20^oC. 15 µL of enzyme A and 100 µL of enzyme D were added per lung in gentleMACs C tubes (Miltenyi Biotech, 130-093-237) with 2.5 mL of 1x buffer S. Lungs were homogenised using the gentleMACS octo-dissociator with heaters (Miltenyi Biotech, 130-096-427) on pre-set program **'**37C_m_LDK_1**'**. Lungs were then washed with 5 mL 1x 'buffer S' and filtered through a 70 µm cell strainer (Greiner Bio-one).

2.12.7 RBC lysis buffer

Red blood cell (RBC) lysis buffer was purchased from Biolegend (420301) in a 10x stock. For working concentrations, a 1x dilution was made using sterile double distilled water (ddH_20). RBC lysis buffer was used to lyse RBCs from spleen and whole blood samples from mice.

2.12.8 FACS buffer

FACS buffer was made using 2% v/v sterile FCS/PBS. 50 mL aliquots were created and stored at 4^oC. FACS buffer was used for flow cytometric staining.

2.12.9 Phorbol 12-myristate 13-acetate (PMA)

PMA was purchased from Sigma-Aldrich and reconstituted at 10 mg/mL with DMSO. 5 µL aliquots were stored at -20^oC. PMA was diluted to 500 nM working concentrations using FACS buffer for L-selectin shedding assays on lymphocytes, or 5 µM for whole blood and sera.

2.12.10 Lipopolysaccharide

Lipopolysaccharide (LPS) from Escherichia coli O111:B4 was purchased from Sigma-Aldrich (L2630) to activate TNF-α expression via TLR4 engagement on RAW 264.7 macrophages. LPS was reconstituted at 1 mg/mL in D10 media and diluted to 1 µg/mL in D10 media for working concentrations.

2.12.11 Live/dead (LD) aqua

LD aqua was purchased from Invitrogen (L34957) and each vial was resuspended in 50 µL DMSO, as per manufacturer instructions. 5 µL aliquots were stored at -20^{o}C.

2.12.12 Fc block

Purified NA/LE rat anti-mouse CD16/CD32 (Fc block) was purchased from BD Pharmingen (567021) at a concentration of 0.5 mg/mL and stored at 4^{o}C. Fc block was used to block Fc gamma receptors prior to antibody staining for flow cytometry. FACS buffer was used to dilute to 20 µg/mL working concentration of Fc block, which was added to $1x10^6$ cells for 5 minutes prior to addition of antibody cocktail.

2.12.13 4% formaldehyde fix

37%-40% formalin solution was diluted in sterile PBS to a working solution of 4% formaldehyde (FA) fix. 4% FA fix was used to fix cells for flow cytometric analysis, or to fix Luc 9.1 MDCK cells for IAV titre assay.

2.12.14 Methylcellulose

Methylcellulose (400 CP viscosity) was purchased from Sigma-Aldrich (M0262). A 2% (w/v) methylcellulose solution was created using sterile ddH_20. Solution was autoclaved and stirred overnight at 4^{o}C until fully dissolved. 2% methylcellulose solution was diluted 1:3 with serum free DMEM media for use in the IAV titre assay.

2.12.15 Triton X-100

Triton X-100 was purchased from Sigma-Aldrich (10789704001) and diluted to a 0.5% working concentration in sterile PBS for permeabilisation of cells in IAV titre assay.

2.12.16 3-amino-9-ethylcarbazole (AEC) reagents

AEC tablets were purchased from Sigma-Aldrich (A6926) as a substrate for the horseradish peroxide (HRP) enzyme used in the IAV titre assay. 1 AEC tablet was dissolved in 2.5 mL dimethyl formamide (DMF), 47.5 mL 50 nM sodium acetate buffer was then added along with 25 µL of 30% hydrogen peroxide.

2.12.17 Sodium acetate buffer

50 nM sodium acetate buffer was made by adding 74 mL 0.2 M acetic acid (11.55 mL glacial acetic acid/L), 176 mL 0.2 M Sodium acetate (trihydrate) (27.2 g of sodium acetate trihydrate/L, (Sigma-Aldrich), 750 mL ddH_20. Reagents were mixed thoroughly using a magnetic stirrer at pH5.

Chapter Three

Ectodomain proteolytic shedding of L-selectin and TNF-α by ADAM17

3. Ectodomain proteolytic shedding of L-selectin and TNF-α by ADAM17

3.1 Introduction

L-selectin is a cell adhesion molecule present on leucocytes which aids in leucocyte-endothelial interactions during immune cell recruitment to lymph nodes and inflamed tissues (Ley et al. 2007). Lymphocyte trafficking through specialised high endothelial venules from the bloodstream into lymph nodes and tissues is imperative for a successful immune response, with L-selectin being crucial in this process (Arbonés et al. 1994). More recently, L-selectin maintenance on CTLs has been attributed to improved cell homing to sites of virus infection, and subsequent viral clearance in mouse models of influenza A and vaccinia virus infection (Mohammed et al. 2016). This was discovered using the LΔP transgenic mouse model which has a shedding-resistant mutant of L-selectin selectively expressed on T lymphocytes, which resists transcriptional silencing (Galkina et al. 2003). Additionally, L-selectin maintenance on CTLs in LΔP mice was found to reduce tumour growth of B16 melanoma in mice and was associated with increased expression of the activation marker CD69 on CTLs (Watson et al. 2019). These findings suggest that L-selectin could be used as a pharmacological target to boost the CTL response to virus infection or cancer in mice. However, there is currently no inhibitor available which directly blocks the cleavage site of L-selectin which could be used to inhibit shedding.

ADAM17 is a cell surface enzyme responsible for the ectodomain cleavage of over 80 cell surface substrates, including L-selectin. ADAM17 is also known as TACE, due to its initial discovery of cleaving cell surface TNF-α to generate soluble TNF-α (Black et al. 1997).

In vitro, ADAM17-dependent proteolytic shedding of L-selectin from CD8 T cells is maximal 4 hours post-TCR engagement with an APC presenting a foreign

peptide on MHC-I. Re-expression then occurs within 48 hours via increased L-selectin mRNA expression. 5-7 days later, further downregulation occurs via PI3Kδ controlled transcriptional silencing (Chao et al. 1997), (Sinclair et al. 2008). As aforementioned, there is currently no inhibitor which blocks the cleavage site of L-selectin, therefore, inhibitors of ADAM17 are a promising alternative to investigate the pharmacological maintenance of cell surface L-selectin on CTLs.

TIMP-3 is one of four members of the TIMP family of endogenous inhibitors of zinc-dependent metalloproteinases such as MMPs and ADAMs. TIMP-3 inhibits ADAM17 and has previously been characterised for its ability to block the cleavage of both L-selectin and TNF-α *in vitro* (Borland et al. 1999). TIMP-3 has been published to have an IC_{50} of $\leq$390 nM for inhibiting L-selectin shedding, and a lower IC_{50} value of 110 nM for inhibiting TNF-α shedding (Borland et al. 1999). However, there are newer pharmacological agents available with improved efficacy for inhibiting TNF-α shedding *in vitro,* which are yet to be investigated for their ability to inhibit L-selectin shedding.

A9(B8) is a human and mouse cross reactive anti-ADAM17 monoclonal antibody formulated on a human IgG2 framework. This antibody was generated using phage display technology by Professor Henry Kwok, from whom it was kindly gifted (Kwok et al. 2014). A9(B8) was found to inhibit the shedding of ADAM17 substrate TNF-α at an IC_{50} of 72 nM in the PANC-1 pancreatic cancer cell line *in vitro* (Ye et al. 2017). Due to these data, A9(B8) was selected as a promising candidate to efficiently block ADAM17-mediated ectodomain shedding of L-selectin *in vitro*. A9(B8) has also been found to be efficacious at reducing tumour growth in mouse pancreatic cancer *in vivo*, as well as non-small cell lung cancer *in vitro* (Ye et al. 2017), (Yang et al. 2019).

D8P1C1 is another human and mouse cross reactive anti-ADAM17 monoclonal antibody, which was kindly gifted by Dr Dimitar Nikolov. This antibody was also generated using phage display technology, whereby the Fab region was formulated into a human IgG1 antibody (Saha et al. 2022). D8P1C1 was mapped to bind the catalytic domain of human ADAM17 using negative staining electron microscopy. This antibody successfully inhibited proliferation in a series

of epidermal growth factor receptor (EGFR)/ human epidermal growth factor receptor 2 (HER2) overexpressing tumour cell lines (Saha et al. 2022). D8P1C1 also reduced tumour growth in murine xenograft models of triple negative breast cancer and ovarian cancer (Saha et al. 2022).

A9(B8) and D8P1C1 were therefore deemed as promising candidates for future mouse studies to block *in vivo* L-selectin shedding in mice, as a strategy to replicate previous findings found in L-selectin-genetically modified (LΔP) mice (Mohammed et al. 2016), (Watson et al. 2019).

It is hypothesised that pharmacological ADAM17 inhibition *in vitro* will maintain the expression of cell surface L-selectin on mouse lymphocytes at nanomolar concentrations, as reported for TNF-α shedding with A9(B8) (Ye et al. 2017), and inhibition of tumour cell proliferation with D8P1C1 (Saha et al. 2022).

3.1.1 Aims and Objectives

The aim of this chapter of work was to determine whether anti-ADAM17 antibodies A9(B8) and D8P1C1 inhibit proteolytic shedding of L-selectin on lymphocytes, as a potential pharmacological agent that would replicate the protective effect of LΔP T cells towards viral infections.

Objectives:

- To validate *in vitro* models of L-selectin and TNF-α shedding using murine lymphocytes and macrophages, respectively.
- To determine whether ADAM17 inhibitor antibodies A9(B8) and D8P1C1 inhibit the shedding of L-selectin on T and B lymphocytes *in vitro*, and if so, at which concentrations.
- To compare the effects of ADAM17 inhibition using A9(B8), D8P1C1 and TIMP-3 on both L-selectin and TNF-α shedding.
- To determine which, if any, anti-ADAM17 antibody candidate is most promising to take forward to *in vivo* mouse models, to investigate the effects of pharmacological inhibition of L-selectin shedding during virus infection.

3.2 Results

3.2.1 The effect of pharmacological ADAM17 inhibition on lymphocyte cell surface L-selectin expression *in vitro*

To determine whether anti-ADAM17 antibodies A9(B8) and D8P1C1 inhibit L-selectin shedding from the cell surface of lymphocytes, these compounds were titrated using primary mouse lymphocytes extracted from whole spleens. This was carried out using two different cell activation models which both result in ADAM17-dependent proteolytic cleavage of L-selectin from the cell surface. TIMP-3 was also tested in these cell activation models, as a known inhibitor of ADAM17, along with anti-ADAM10 antibody, 1H5. 1H5 was used as a negative control in this work as ADAM10 has not been implicated in TCR or PMA induced L-selectin shedding (Yan et al. 2016), (Mohammed et al. 2019).

Firstly, a T cell activation model using soluble anti-CD3/anti-CD28 antibodies to induce TCR-dependent L-selectin shedding was tested. Cells were treated with varying concentrations of A9(B8) or D8P1C1 and stained for L-selectin 4 hours post-activation. Concentrations of A9(B8) between 1 nM and 7 μM were chosen due to the report that A9(B8) gave dose-dependent inhibition of TNF-α shedding in vitro starting at 0.5 nM and maximal inhibition at 200 nM and above (Ye et al. 2017). Concentrations of D8P1C1 between 0.8 nM and 5 μM were chosen, as the IC_{50} value for inhibiting proliferation of tumour cell line MDA-MB-231 was reported to be 246 pM (Saha et al. 2022).

There was a dose-dependent blockade of L-selectin shedding with A9(B8) treatment in both CD8 and CD4 T cells after 4 hours of anti-CD3/CD28 stimulation (Figure 3.1). The lowest dose required to see inhibition of L-selectin shedding was 29 nM A9(B8), with maximal inhibition seen at 7 μM in both cell types (Figure 3.1). In CD4 T cells, 7 μM A9(B8) resulted in cell surface L-selectin levels above those on unactivated CD4 T cells (basal levels) (Figure 3.1 B).

D8P1C1 did not show clear dose-dependent inhibition of L-selectin shedding in anti-CD3/CD28 activated CD8 or CD4 T cells (Figure 3.2). Instead, the two highest concentrations of 1.6 μM and 5 μM gave equivalent levels of inhibition of L-selectin shedding (Figure 3.2). Only 66% and 71% of maximal inhibition was reached with D8P1C1 in CD8 and CD4 T cells respectively (Figure 3.2). As expected, the negative control antibody 1H5 against ADAM10 caused no inhibition of L-selectin shedding (Figure 3.2).

ADAM17 inhibitor TIMP-3 partially inhibited TCR induced L-selectin shedding in T cells. At 1 μM TIMP-3, the highest dose tested, L-selectin shedding was inhibited by around 50% in CD8 T cells and 30% in CD4 T cells (Figure 3.3).

Secondly, a pan-cell activation model using PMA to stimulate ADAM17, and subsequent L-selectin shedding was tested in CD8 T cells, CD4 T cells and B cells. Cells were treated with 500 nM PMA and varying concentrations of A9(B8), D8P1C1, 1H5 or TIMP-3. Cells were then stained for L-selectin 30 minutes post-activation. As with the anti-CD3/anti-CD28 activation model, there was a dose-dependent blockade of L-selectin shedding with A9(B8) treatment in all populations (Figure 3.4). 7 μM was required to completely block PMA induced L-selectin shedding on all cell populations analysed (CD8 T cells, CD4 T cells, and B cells) (Figure 3.4). Conversely, there was no inhibition of L-selectin shedding seen with D8P1C1 or 1H5 antibodies (Figure 3.5). ADAM17 inhibitor TIMP-3 was more efficacious at blocking L-selectin shedding in the PMA model, as 1 μM almost completely blocked PMA induced L-selectin shedding in CD8, CD4 and B lymphocytes (Figure 3.6).

A further observation from *in vitro* L-selectin shedding assays carried out, was that CD8 T cells consistently had a higher average L-selectin MFI on unactivated cells, compared to CD4 T cells (Figure 3.1-3.6). For example, with the TCR-induced shedding assay in figure 3.1, the L-selectin MFI on unactivated CD8 T cells was 503 compared to 425 for CD4 T cells (Figure 3.1). The difference between L-selectin levels on unactivated cells and L-selectin levels with anti-CD3/CD28 maximal shedding was also greater for CD8 T cells with an average difference of 503 compared to 370 for CD4 T cells (Figure 3.1).

This was also true regarding the PMA shedding assays (Figure 3.4-3.6) For example, CD8 T cells had the highest starting level of L-selectin with an average MFI of 758, whilst CD4 T cells and B cells had average starting MFIs of 427 and 357 respectively (Figure 3.4). The difference between L-selectin levels on unactivated cells and L-selectin levels with PMA maximal shedding was also greater for CD8 T cells with an average difference of 761 compared to 379 for CD4 T cells and 313 for B cells (Figure 3.4).

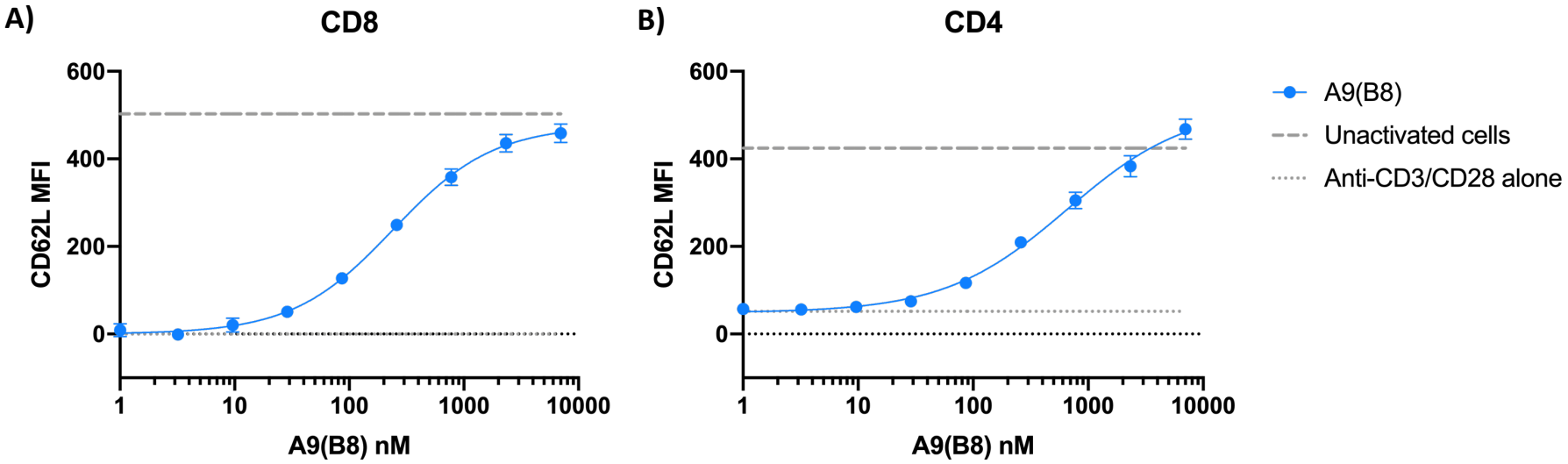

Figure 3.1. Cell surface L-selectin levels on T cells following anti-CD3/anti-CD28 activation and treatment with A9(B8). $5x10^5$ splenocytes were plated, with T cell culture media and anti-CD3/anti-CD28 antibodies to induce cell activation and subsequent L-selectin (CD62L) shedding via ADAM17. Cells were also treated with varying concentrations of A9(B8) from 1 nM-7000 nM. Cells were stained for L-selectin 4 hours later via flow cytometric analysis. Cells were gated on lymphocytes via forward and side scatter profile, single, live cells. **A)** CD8 T cell population **B)** CD4 T cell population. Grey dashed line= Basal MFI of L-selectin on unactivated cells. Grey dotted line= L-selectin MFI with anti-CD3/anti-CD28 activation alone. X-axis shown on $\log_{10}$ scale. Nonlinear regression curve fit. Error bars are $\pm$SEM. n=3.

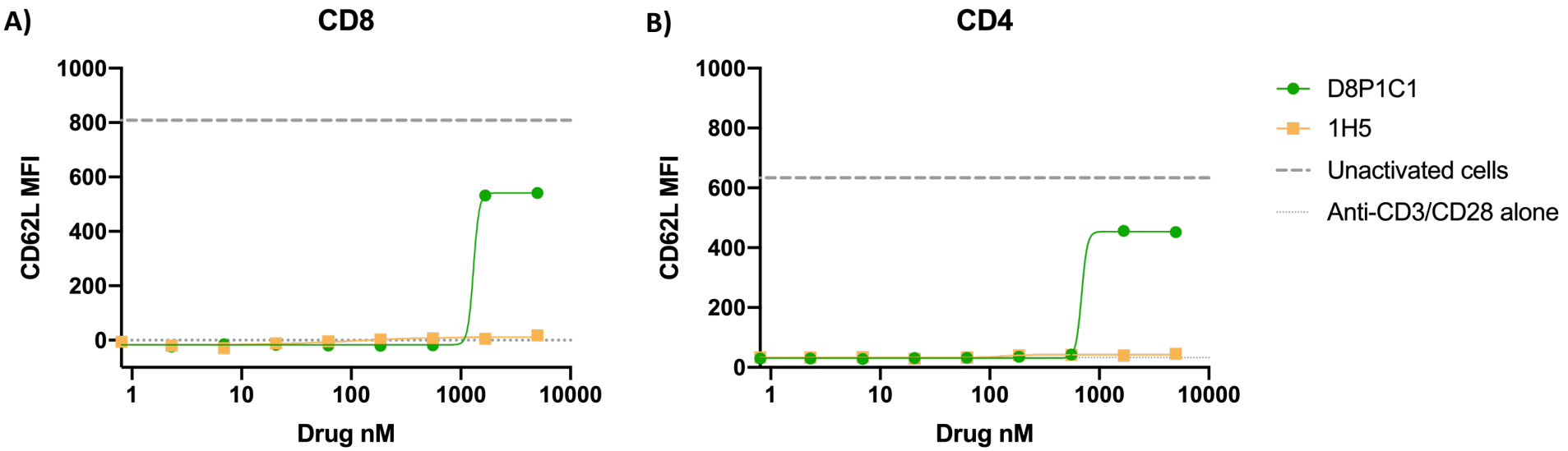

Figure 3.2. Cell surface L-selectin levels on T cells following anti-CD3/anti-CD28 activation and treatment with D8P1C1 or 1H5. $5x10^5$ splenocytes were plated, with T cell culture media and anti-CD3/anti-CD28 antibodies to induce cell activation and subsequent L-selectin (CD62L) shedding via ADAM17. Cells were also treated with varying concentrations of D8P1C1 or 1H5 from 0.8 nM-5000 nM. Cells were stained for L-selectin 4 hours later via flow cytometric analysis. Cells were gated on lymphocytes via forward and side scatter profile, single, live cells. **A)** CD8 T cell population **B)** CD4 T cell population. Grey dashed line= Basal MFI of L-selectin on unactivated cells. Grey dotted line= L-selectin MFI with anti-CD3/anti-CD28 activation alone. X-axis shown on $\log_{10}$ scale. Nonlinear regression curve fit. n=1.

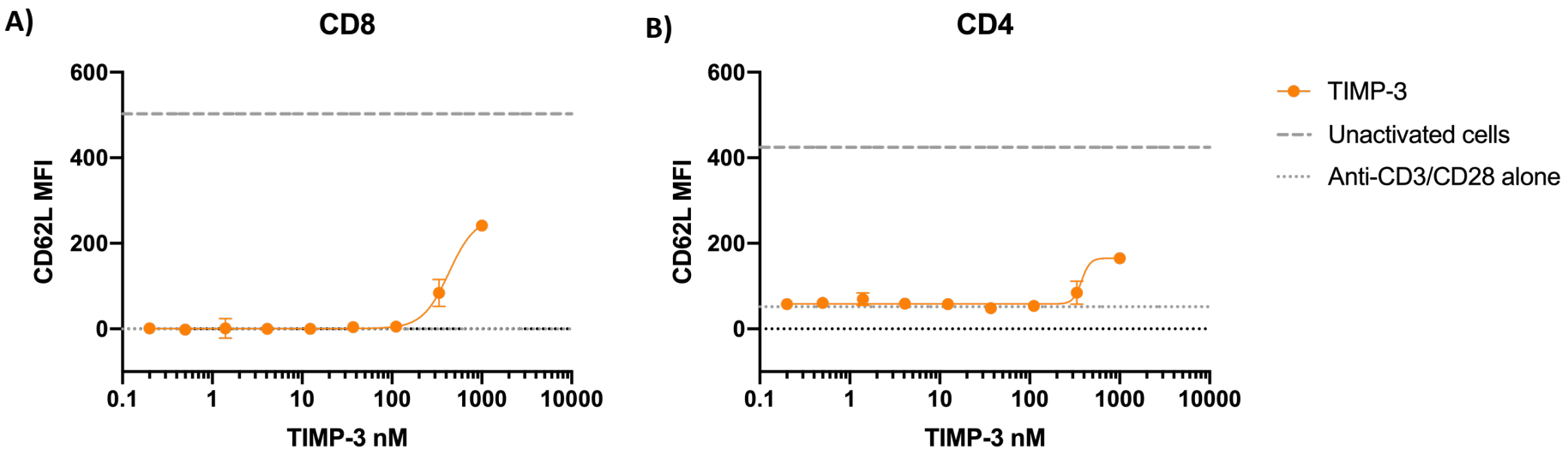

Figure 3.3. Cell surface L-selectin levels on T cells following anti-CD3/anti-CD28 activation and treatment with TIMP-3. $5x10^5$ splenocytes were plated, with T cell culture media and anti-CD3/anti-CD28 antibodies to induce cell activation and subsequent L-selectin (CD62L) shedding via ADAM17. Cells were also treated with varying concentrations of TIMP-3 from 0.2 nM-1000 nM. Cells were stained for L-selectin 4 hours later via flow cytometric analysis. Cells were gated on lymphocytes via forward and side scatter profile, single, live cells. **A)** CD8 T cell population **B)** CD4 T cell population. Grey dashed line= Basal MFI of L-selectin on unactivated cells. Grey dotted line= L-selectin MFI with anti-CD3/anti-CD28 activation alone. X-axis shown on $\log_{10}$ scale. Nonlinear regression curve fit. Error bars are $\pm$SEM. n=3.

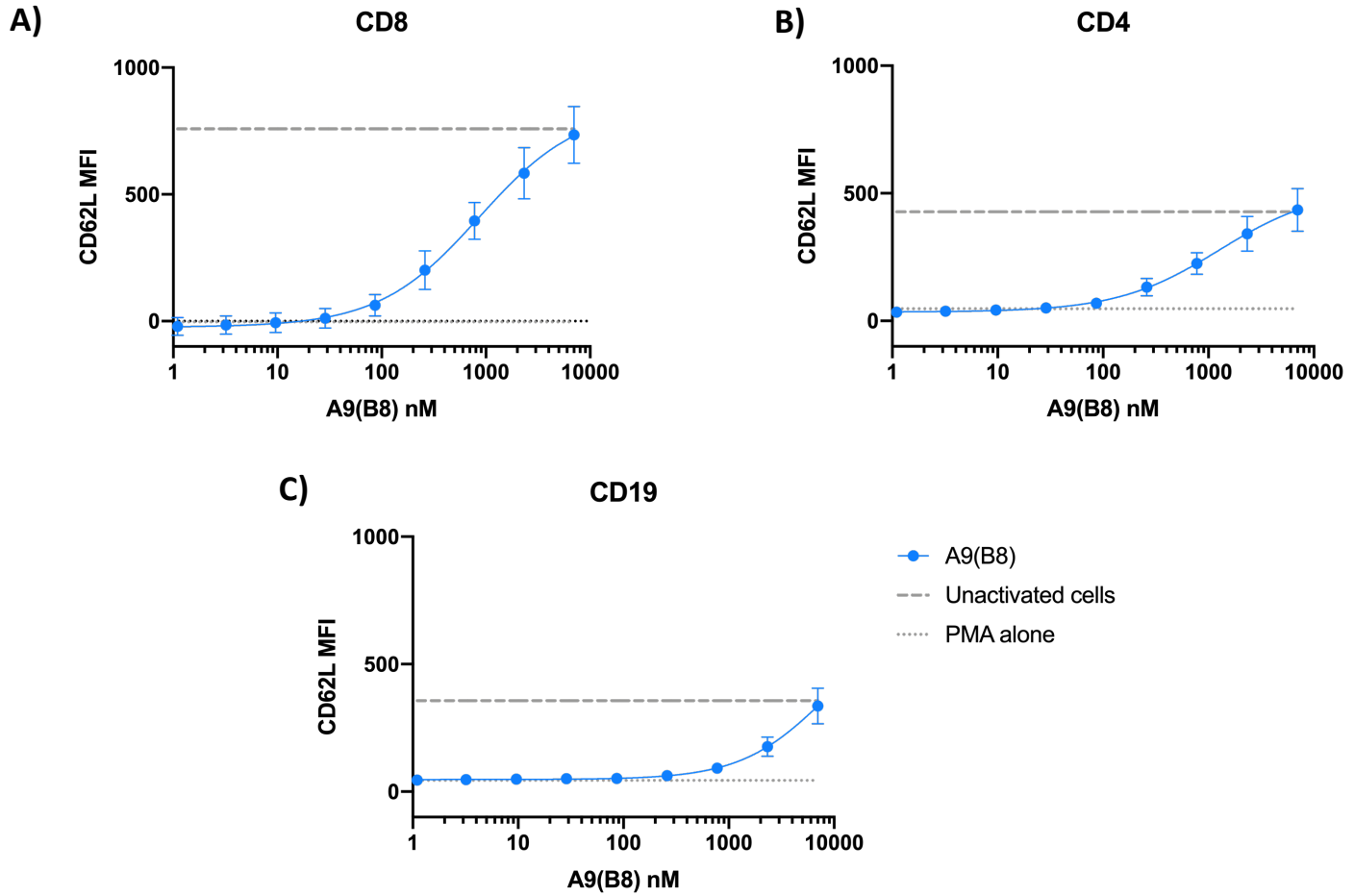

Figure 3.4. Cell surface L-selectin levels on lymphocytes following PMA activation and treatment with A9(B8). $5x10^5$ splenocytes were plated and treated with 500 nM PMA to induce cell activation and subsequent L-selectin (CD62L) shedding via ADAM17. Cells were also treated with varying concentrations of A9(B8) from 1 nM-7000 nM. Cells were stained for L-selectin 30 minutes later via flow cytometric analysis. Cells were gated

on lymphocytes via forward and side scatter profile, single, live cells. **A)** CD8 T cell population. **B)** CD4 T cell population. **C)** B cell population. Grey dashed line= Basal MFI of L-selectin on unactivated cells. Grey dotted line line= L-selectin MFI with 500 nM PMA activation alone. X-axis shown on log_{10} scale. Nonlinear regression curve fit. Error bars are $\pm$SEM. n=5.

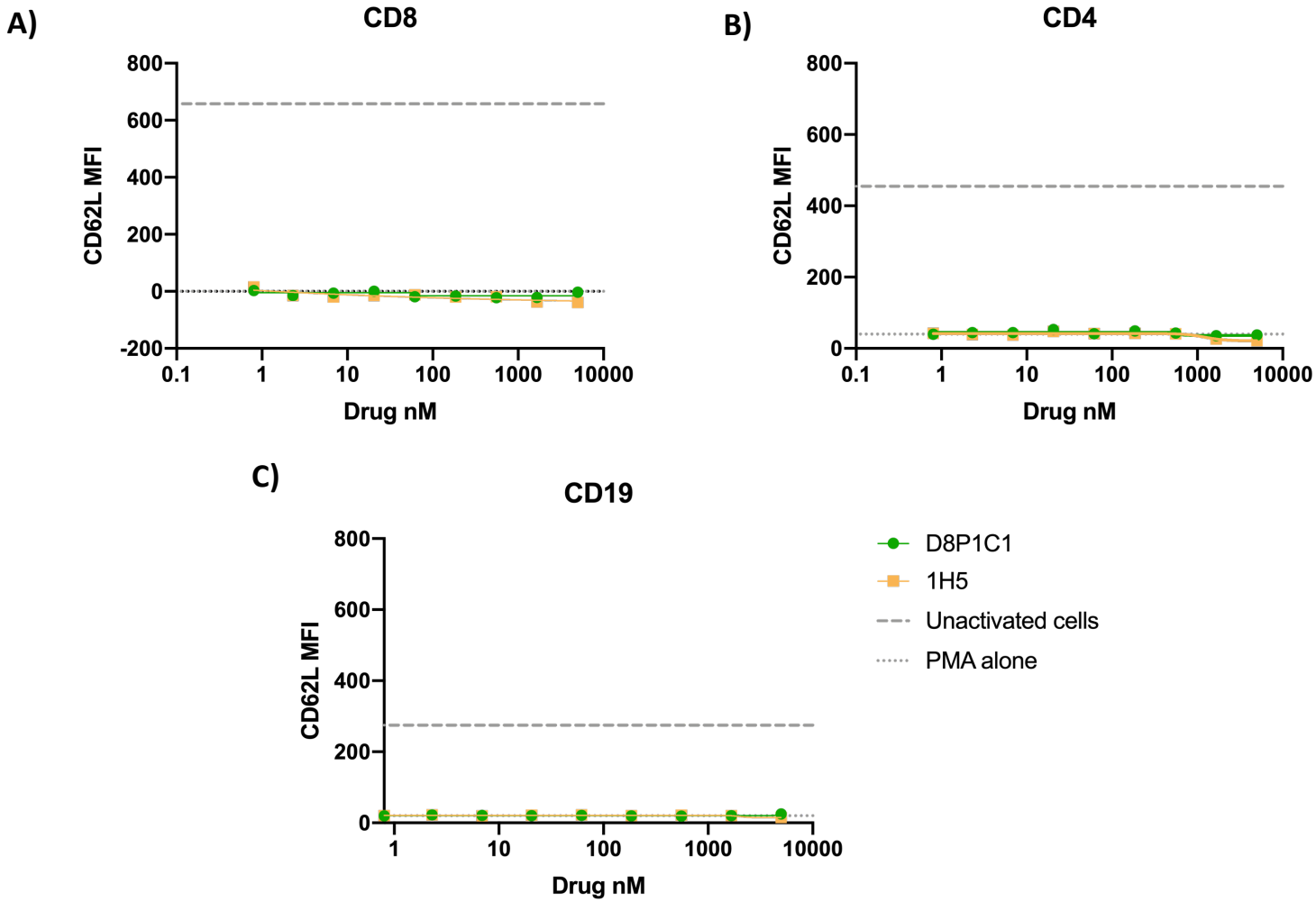

Figure 3.5. Cell surface L-selectin levels on lymphocytes following PMA activation and treatment with D8P1C1 or 1H5. $5x10^5$ splenocytes were plated and treated with 500 nM PMA to induce cell activation and subsequent L-selectin (CD62L) shedding via ADAM17. Cells were also treated

with varying concentrations of D8P1C1 or 1H5 from 0.8 nM-5000 nM. Cells were stained for L-selectin 30 minutes later via flow cytometric analysis. Cells were gated on lymphocytes via forward and side scatter profile, single, live cells. **A)** CD8 T cell population. **B)** CD4 T cell population. **C)** B cell population. Grey dashed line= Basal MFI of L-selectin on unactivated cells. Grey dotted line line= L-selectin MFI with 500 nM PMA activation alone. X-axis shown on $\log_{10}$ scale. Nonlinear regression curve fit. n=1.

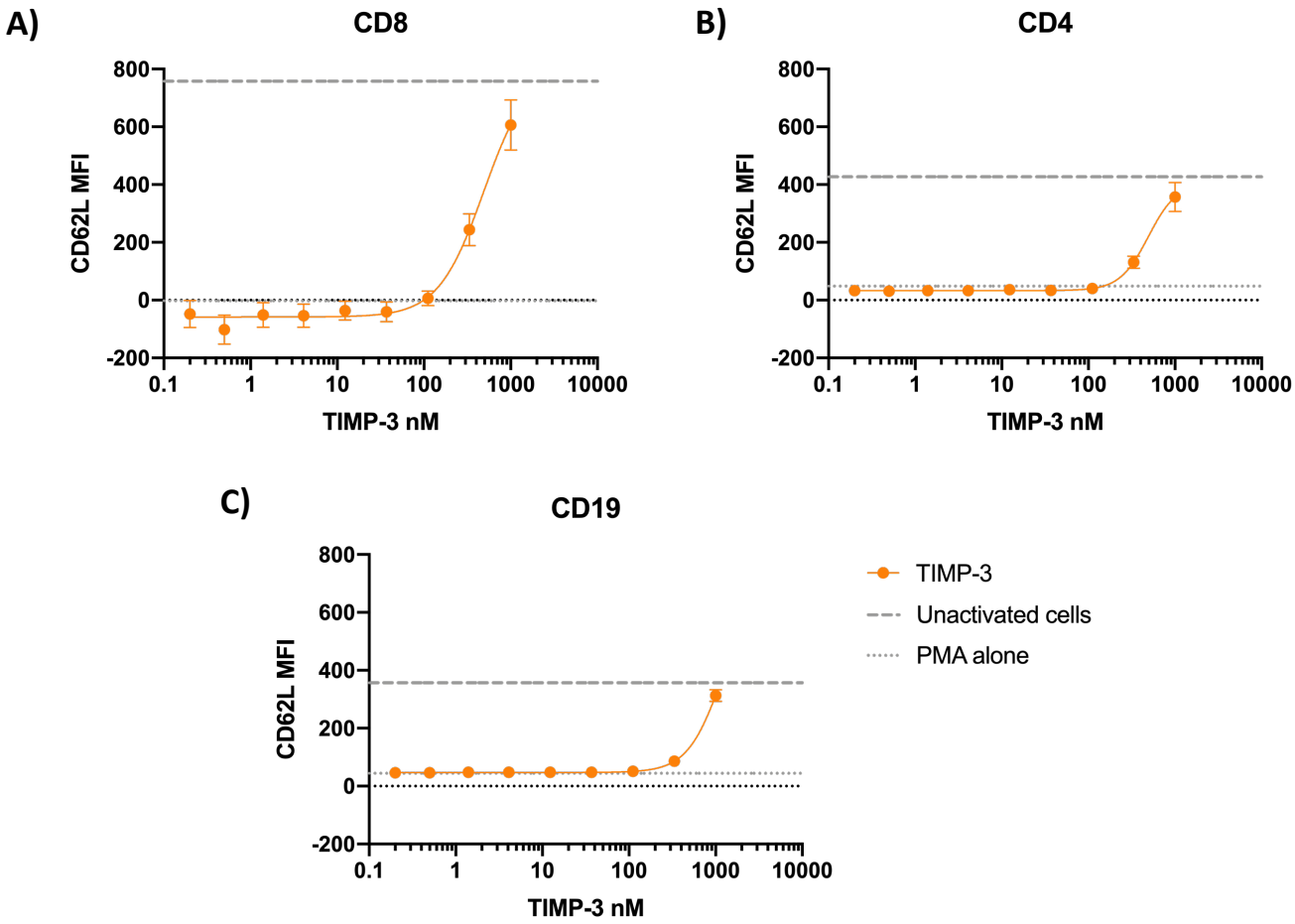

Figure 3.6. Cell surface L-selectin levels on lymphocytes following PMA activation and treatment with TIMP-3. 5x10^5 splenocytes were plated and treated with 500 nM PMA to induce cell activation and subsequent L-selectin (CD62L) shedding via ADAM17. Cells were also treated with varying concentrations of TIMP-3 from 0.2 nM-1000 nM. Cells were stained for L-selectin 30 minutes later via flow cytometric analysis. Cells were

gated on lymphocytes via forward and side scatter profile, single, live cells. **A)** CD8 T cell population. **B)** CD4 T cell population. **C)** B cell population. Grey dashed line= Basal MFI of L-selectin on unactivated cells. Grey dotted line line= L-selectin MFI with 500 nM PMA activation alone. X-axis shown on $\log_{10}$ scale. Nonlinear regression curve fit. Error bars are $\pm$SEM. n=4.

3.2.2 The effect of pharmacological ADAM17 inhibition on macrophage cell surface TNF-α expression *in vitro*

The next step was to determine whether A9(B8) and D8P1C1 inhibit ADAM17-dependent TNF-α shedding from the cell surface in the same manner as they do for inhibiting L-selectin shedding. As unactivated lymphocytes to not produce substantial levels of TNF-α, the murine macrophage 'RAW 264.7' cell line which produces high levels of TNF-α was used. RAW 264.7 cells produce low levels of TNF-α when unactivated, however, this is increased greatly when stimulated with the gram-negative bacteria molecule LPS. LPS is detected by TLR4 inducing both cell surface expression and ADAM17-mediated shedding of TNF-α.

There was a bell-shaped dose-dependent effect of inhibition of TNF-α shedding with increasing doses of A9(B9) in RAW 264.7 cells (Figure 3.7). At 80 nM A9(B8), there was an increase of cell surface expression of TNF-α above the LPS alone threshold, which peaked at roughly 250 nM (Figure 3.7). At concentrations above 1 μM A9(B8) there was a concentration-dependent reduction in cell surface TNF-α that decreased to just above baseline at 7 μM (Figure 3.7 A).

There was a dose-dependent effect of blockade of TNF-α shedding with D8P1C1 (Figure 3.8). At 555 nM there was an increased cell surface level of TNF-α above the LPS alone threshold, which peaked at the maximal dosage of 5 μM (Figure 3.8). There was no inhibition of TNF-α shedding with anti-ADAM10 antibody 1H5 (Figure 3.8). Additionally, there was a dose-dependent effect of blockade of TNF-α shedding with TIMP-3 starting at 100 nM and peaking at 1 μM (Figure 3.9). TIMP-3 and D8P1C1 induced a higher cell surface expression of TNF-α than A9(B8), with an average TNF-α MFI of 4765 at 5 μM D8P1C1 and 4972 at 1 μM for TIMP-3 (Figure 3.8, 3.9). Whilst for A9(B8) the maximal average TNF-α MFI reached was nearly 7x lower at 723 (Figure 3.7).

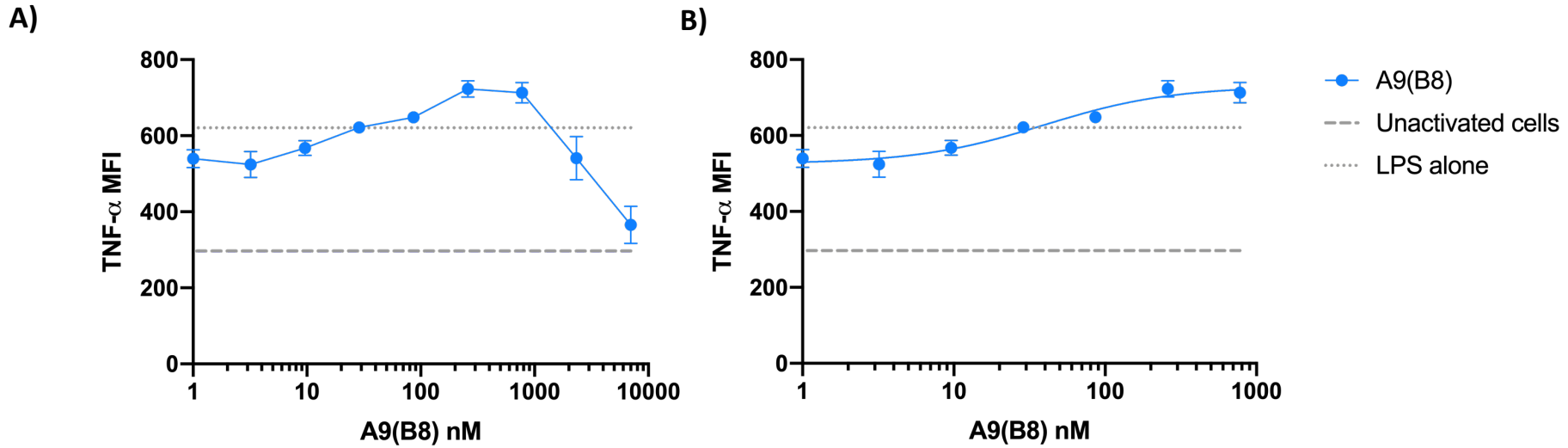

Figure 3.7. Cell surface TNF-α levels on RAW 264.7 macrophages following LPS activation and treatment with A9(B8). $5x10^5$ RAW 264.7 macrophages were plated and treated with 1 μg/mL lipopolysaccharide (LPS) for 1 hour to induce tumour necrosis factor alpha (TNF-α) expression and subsequent shedding via ADAM17. Cells were also treated with varying concentrations of A9(B8) from 1 nM-7000 nM. Cells were stained for TNF-α 1 hour later via flow cytometric analysis. Cells were gated via forward and side scatter profile, single, live cells. **A)** 1 nM-7000 nM A9(B8). X-axis shown on $\log_{10}$ scale. Error bars are ±SEM. n=5. **B)** 1 nM-777 nM A9(B8) data extracted from A. Grey dotted line= TNF-α MFI on cells treated with 1 μg/mL LPS alone. Grey dashed line= Basal TNF-α MFI on unactivated cells. X-axis shown on $\log_{10}$ scale. Nonlinear regression curve fit. Error bars are ±SEM. n=5.

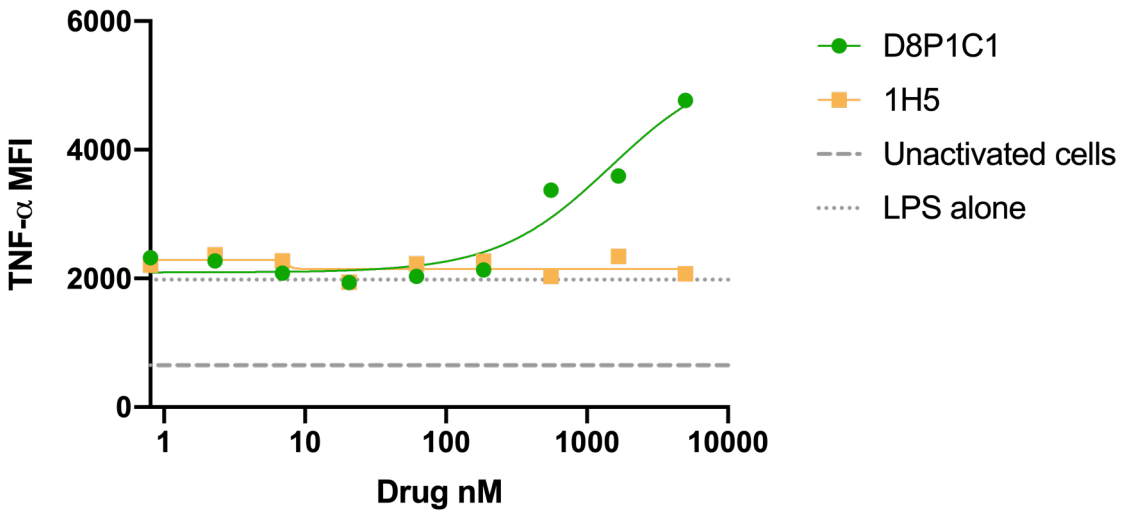

Figure 3.8. Cell surface TNF-α levels on RAW 264.7 macrophages following LPS activation and treatment with D8P1C1 or 1H5. $5x10^5$ RAW 264.7 macrophages were plated and treated with 1 μg/mL lipopolysaccharide (LPS) for 1 hour to induce tumour necrosis factor alpha (TNF-α) expression and subsequent shedding via ADAM17. Cells were also treated with varying concentrations of D8P1C1 or 1H5 from 0.8 nM-5000 nM. Cells were stained for TNF-α 1 hour later via flow cytometric analysis. Cells were gated via forward and side scatter profile, single, live cells. Grey dotted line= TNF-α MFI on cells treated with 1 μg/mL LPS alone. Grey dashed line= Basal TNF-α MFI on unactivated cells. X-axis shown on log_{10} scale. Nonlinear regression curve fit. n=1.

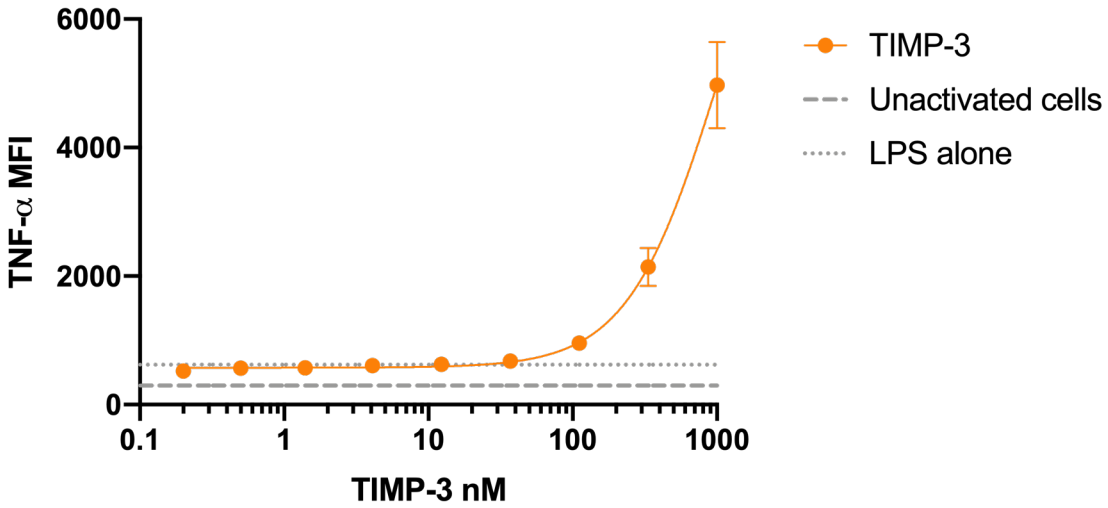

Figure 3.9. Cell surface TNF-α levels on RAW 264.7 macrophages following LPS activation and treatment with TIMP-3. $5x10^5$ RAW 264.7 macrophages were plated and treated with 1 μg/mL lipopolysaccharide (LPS) for 1 hour to induce tumour necrosis factor alpha (TNF-α) expression and subsequent shedding via ADAM17. Cells were also treated with varying concentrations of TIMP-3 from 0.2 nM-1000 nM. Cells were stained for TNF-α 1 hour later via flow cytometric analysis. Cells were gated via forward and side scatter profile, single, live cells. 1 nM-7000 nM TIMP-3. Grey dotted line= TNF-α MFI on cells treated with 1 μg/mL LPS alone. Grey dashed line= Basal TNF-α MFI on unactivated cells. X-axis shown on log_{10} scale. Nonlinear regression curve fit. Error bars are ±SEM. n=5.

3.2.3 The effect of pharmacological ADAM17 inhibition on soluble L-selectin and TNF-α levels *in vitro*

Previous testing of A9(B8) for its ability to inhibit ADAM17-dependent shedding of its substrates involved measuring soluble TNF-α levels in cell supernatants (Ye et al. 2017). Whilst D8P1C1 has not been tested for its role in effecting soluble ADAM17 substrate levels at all (Saha et al. 2022). Although the main aim of this work was to test the maintenance of L-selectin on the cell surface, it was also important to test soluble L-selectin and TNF-α levels in cell supernatants to validate cell surface results. Therefore, cell supernatants were collected from A9(B8), D8P1C1, 1H5 and TIMP-3 treated cells following TCR-, PMA- and LPS- induced activation of ADAM17.

There was a dose dependent reduction in soluble L-selectin levels by A9(B8) in anti-CD3/anti-CD28 activated cells detectable at 10 nM A9(B8) and maximal at ≥2 μM (Figure 3.10 A). There was also a dose dependent reduction in soluble L-selectin levels by A9(B8) in PMA activated cells, detectable at 30 nM and maximal at 7 μM (Figure 3.10 B). Higher doses of A9(B8) reduced soluble L-selectin to levels below that constitutively released in the absence of anti-CD3/CD28 or PMA activation. The dose required for this was 86 nM for anti-CD3/CD28 stimulated cells, and 777 nM for PMA treated cells (Figure 3.10 A, B).

There was a dose dependent reduction in soluble L-selectin levels by D8P1C1 in anti-CD3/CD28 activated cells detectable at 1.6 μM and maximal at 5 μM (Figure 3.11 A). However, there was no dose-dependent decrease in soluble L-selectin released from PMA activated cells treated with D8P1C1 (Figure 3.11 B), nor was there any dose-dependent changes in L-selectin levels with 1H5 (Figure 3.11 A, B). When investigating TIMP-3 treatment in lymphocytes, only 1 μM induced a reduction in soluble L-selectin levels with anti-CD3/CD28 stimulation (Figure 3.12 A). In PMA stimulated cells, all concentrations of TIMP-3 reduced soluble levels of L-selectin, however only concentrations above 400 nM resulted in reduction below basal levels (Figure 3.12 B).

Similar levels of soluble L-selectin were released from unactivated cells from anti-CD3/CD28 and PMA shedding assays, but PMA induced a greater release of soluble L-selectin upon stimulation. For example, in figure 3.11, 3.2 ng/mL and 1.1 ng/mL of L-selectin were released from unactivated cells in anti-CD3/CD28 and PMA shedding assays, respectively (Figure 3.11 A, B). However, PMA induced a 10.6x fold increase in soluble L-selectin release upon activation, compared to 2.6x fold increase upon anti-CD3/CD28 stimulation (Figure 3.11 A, B).

A9(B8) reduced levels of soluble TNF-α in a dose-dependent manner with a threshold of 10 nM and maximal inhibition at 777 nM and above (Figure 3.10 C). At concentrations above 100 nM A9(B8), levels of soluble TNF-α reached below baseline levels released by unactivated cells (Figure 3.10 C). There was a dose-dependent decrease of soluble TNF-α with D8P1C1 treatment detected at 185 nM and maximal at 2.3 μM (Figure 3.11 C). 1H5 increased soluble levels of TNF-α at concentrations above 62 nM, maximal at 185 nM (Figure 3.11C). In RAW 264.7 cells, both 333.3 nM and 1 μM TIMP-3 showed reductions in soluble TNF-α concentrations, with 1 μM causing a decrease in soluble TNF-α below LPS treatment alone (Figure 3.12 C).

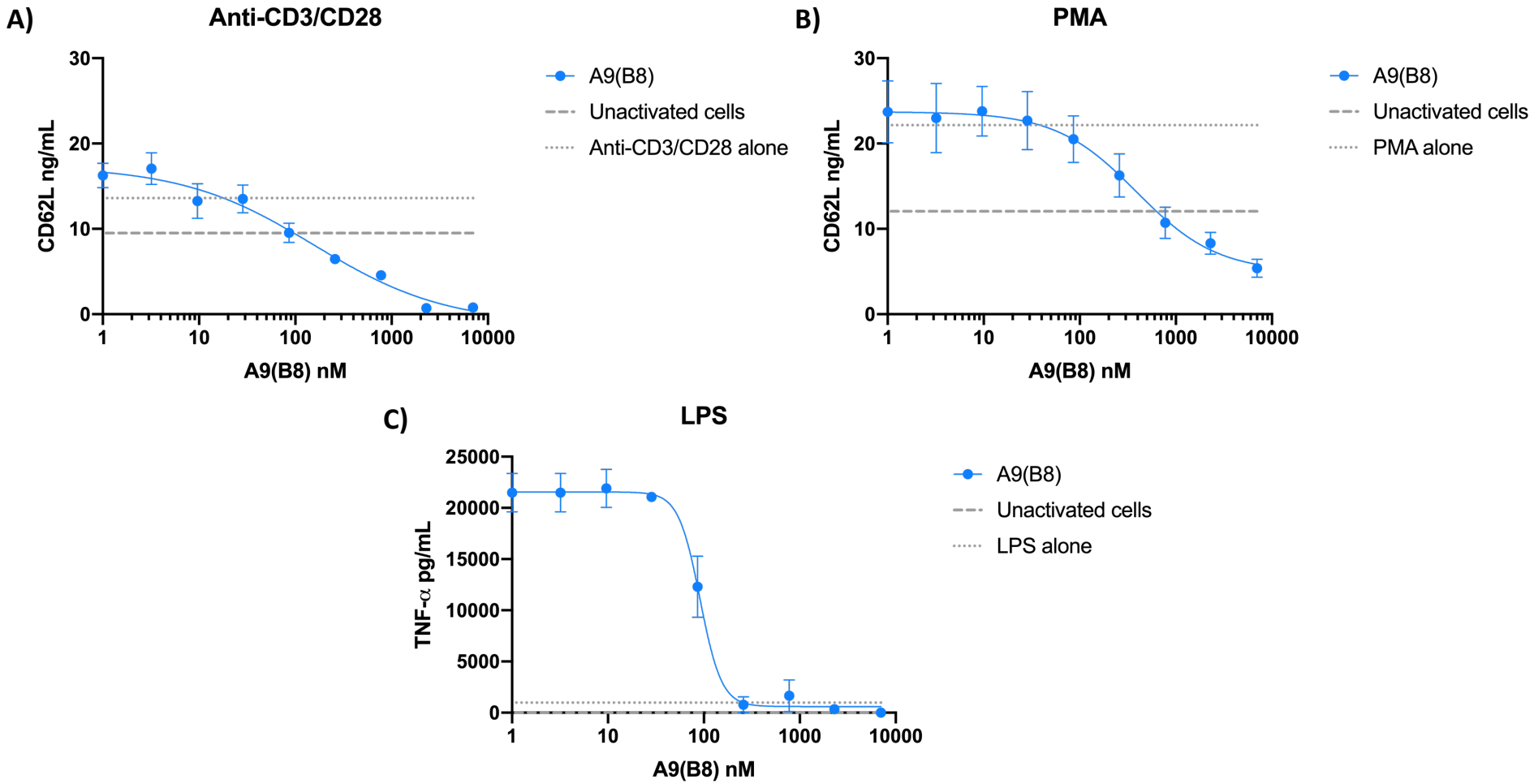

Figure 3.10. Soluble L-selectin and TNF-α levels following treatment with A9(B8). A) $5x10^5$ splenocytes were plated and treated with anti-mouse CD3 at 200 ng mL^{-1} and anti-mouse CD28 at 100 ng mL^{-1} to induce cell activation and subsequent L-selectin (CD62L) shedding via ADAM17. Cells

were also treated with varying concentrations of A9(B8) from 1 nM-7000 nM. Cell supernatants were collected for soluble L-selectin analysis 4 hours later via ELISA. Grey dotted line= L-selectin levels with anti-mouse CD3 at 200 ng mL^{-1} and anti-mouse CD28 at 100 ng mL^{-1} alone. Grey dashed line= Basal L-selectin levels on unactivated cells. X-axis shown on log_{10} scale. Nonlinear regression curve fit. Error bars are $\pm$SEM. n=3 **B)** $5x10^5$ splenocytes were plated and treated with 500 nM PMA to induce cell activation and subsequent L-selectin (CD62L) shedding via ADAM17. Cells were also treated with varying concentrations of A9(B8) from 1 nM-7000 nM. Cell supernatants were collected for soluble L-selectin analysis 30 minutes later via ELISA. Grey dotted line= L-selectin levels with 500 nM PMA activation alone. Grey dashed line= Basal L-selectin levels on unactivated cells. X-axis shown on log_{10} scale. Nonlinear regression curve fit. Error bars are $\pm$SEM. n=4. **C)** $5x10^5$ RAW 264.7 macrophages were plated and treated with 1 μg/mL lipopolysaccharide (LPS) to induce tumour necrosis factor alpha (TNF-α) expression and subsequent shedding via ADAM17. Cells were also treated with varying concentrations of A9(B8) from 1 nM-7000 nM. Cell supernatants were collected for soluble TNF-α analysis 1 hour later via ELISA. Grey dotted line= TNF-α levels on cells treated with 1 μg/mL LPS. Grey dashed line= Basal TNF-α levels on unactivated cells. X-axis shown on log_{10} scale. Nonlinear regression curve fit. Error bars are $\pm$SEM. n=4.

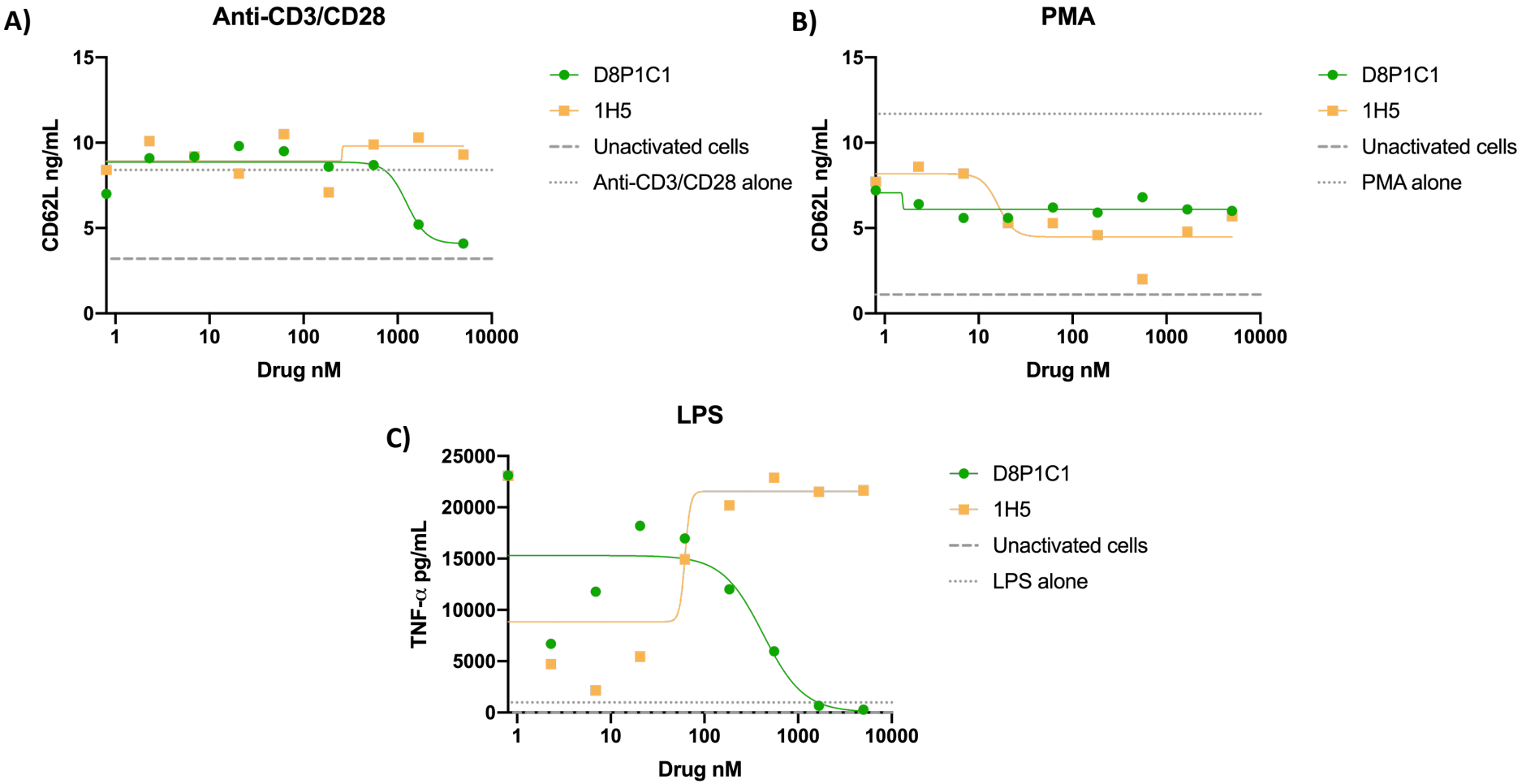

Figure 3.11. Soluble L-selectin and TNF-α levels following treatment with D8P1C1 or 1H5. A) $5x10^5$ splenocytes were plated and treated with anti-mouse CD3 at 200 ng mL^{-1} and anti-mouse CD28 at 100 ng mL^{-1} to induce cell activation and subsequent L-selectin (CD62L) shedding via ADAM17. Cells were also treated with varying concentrations of D8P1C1 or 1H5 from 0.8 nM-5000 nM. Cell supernatants were collected for soluble

L-selectin analysis 4 hours later via ELISA. Grey dotted line= L-selectin levels with anti-mouse CD3 at 200 ng mL^{-1} and anti-mouse CD28 at 100 ng mL^{-1} alone. Grey dashed line= Basal L-selectin levels on unactivated cells. X-axis shown on log_{10} scale. Nonlinear regression curve fit. n=1 **B)** $5x10^5$ splenocytes were plated and treated with 500 nM PMA to induce cell activation and subsequent L-selectin (CD62L) shedding via ADAM17. Cells were also treated with varying concentrations of D8P1C1 or 1H5 from 0.8 nM-5000 nM. Cell supernatants were collected for soluble L-selectin analysis 30 minutes later via ELISA. Grey dotted line= L-selectin levels with 500 nM PMA activation alone. Grey dashed line= Basal L-selectin levels on unactivated cells. X-axis shown on log_{10} scale. Nonlinear regression curve fit. n=1. **C)** $5x10^5$ RAW 264.7 macrophages were plated and treated with 1 μg/mL lipopolysaccharide (LPS) to induce tumour necrosis factor alpha (TNF-α) expression and subsequent shedding via ADAM17. Cells were also treated with varying concentrations of D8P1C1 from 0.8 nM-5000 nM. Cell supernatants were collected for soluble TNF-α analysis 1 hour later via ELISA. Grey dotted line= TNF-α levels on cells treated with 1 μg/mL LPS. Grey dashed line= Basal TNF-α levels on unactivated cells. X-axis shown on log_{10} scale. Nonlinear regression curve fit. n=1.

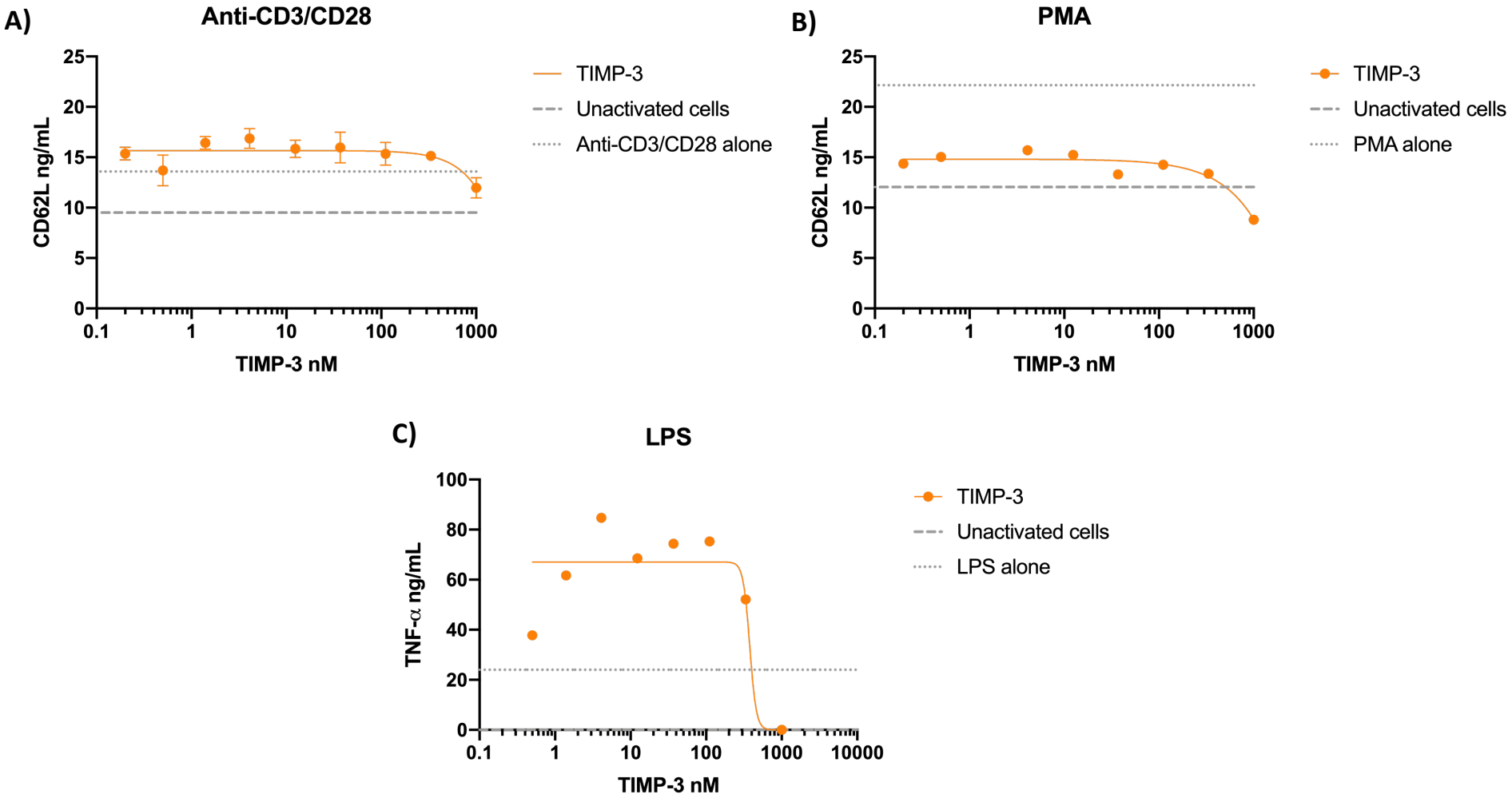

Figure 3.12. Soluble L-selectin and TNF-α levels following treatment with TIMP-3. A) 5x10^5 splenocytes were plated and treated with anti-mouse CD3 at 200 ng mL^{-1} and anti-mouse CD28 at 100 ng mL^{-1} to induce cell activation and subsequent L-selectin (CD62L) shedding via ADAM17. Cells

were also treated with varying concentrations of TIMP-3 from 0.2 nM-1000 nM. Cell supernatants were collected for soluble L-selectin analysis 4 hours later via ELISA. Grey dotted line= L-selectin levels with anti-mouse CD3 at 200 ng mL^{-1} and anti-mouse CD28 at 100 ng mL^{-1} alone. Grey dashed line= Basal L-selectin levels on unactivated cells. X-axis shown on log_{10} scale. Nonlinear regression curve fit. Error bars are $\pm$SEM. n=3 **B)** $5x10^5$ splenocytes were plated and treated with 500 nM PMA to induce cell activation and subsequent L-selectin (CD62L) shedding via ADAM17. Cells were also treated with varying concentrations of TIMP-3 from 0.2 nM-1000 nM. Cell supernatants were collected for soluble L-selectin analysis 30 minutes later via ELISA. Grey dotted line= L-selectin levels with 500 nM PMA activation alone. Grey dashed line= Basal L-selectin levels on unactivated cells. X-axis shown on log_{10} scale. Nonlinear regression curve fit. n=1. **C)** $5x10^5$ RAW 264.7 macrophages were plated and treated with 1 μg/mL lipopolysaccharide (LPS) to induce tumour necrosis factor alpha (TNF-α) expression and subsequent shedding via ADAM17. Cells were also treated with varying concentrations of TIMP-3 from 0.2 nM-1000 nM. Cell supernatants were collected for soluble TNF-α analysis 1 hour later via ELISA. Grey dotted line= TNF-α levels on cells treated with 1 μg/mL LPS alone. Grey dashed line= Basal TNF-α levels on unactivated cells. X-axis shown on log_{10} scale. Nonlinear regression curve fit. n=1.

3.2.4 Comparing A9(B8), D8P1C1 and TIMP-3 inhibition of ADAM17: differential effects on L-selectin and TNF-α shedding *in vitro*

To compare the efficacies of A9(B8), D8P1C1 and TIMP-3 as inhibitors of L-selectin and TNF-α shedding, IC_{50} values were calculated from titration curves in figures 3.1-3.12 (Table 3.1). Titration curves for inhibition of L-selectin shedding by A9(B8), D8P1C1 and TIMP-3 were carried out on primary mouse lymphocytes to analyse cell surface L-selectin levels (Figures 3.1-3.6) and soluble L-selectin levels (Figure 3.10 A, B, 3.11 A, B, 3.12 A, B). These were carried out using two different L-selectin shedding models: anti-CD3/CD28 and PMA. Titration curves for inhibition of TNF-α shedding by A9(B8), D8P1C1 and TIMP-3 were also carried out using RAW 264.7 murine macrophages to analyse cell surface TNF-α levels (Figures 3.7-3.9) and soluble TNF-α levels (Figure 3.10 C, 3.11 C, 3.12 C). Anti-ADAM10 antibody 1H5 was discarded from IC_{50} analysis as a negative control with no dose-dependent effects for blocking L-selectin or TNF-α shedding.

Firstly, regarding A9(B8), analysis of cell surface L-selectin on lymphocytes activated by anti-CD3/CD28 resulted in IC_{50} values of 261 nM and 496 nM in CD8 T cells and CD4 T cells respectively (Table 3.1). A9(B8) was most effective in CD8 T cells and least effective in B cells, as demonstrated in PMA activated lymphocytes with mean IC_{50} values of 523 nM, 684 nM, and 2837 nM for CD8 T cells, CD4 T cells and B cells respectively (Table 3.1). Analysis of soluble L-selectin released following PMA activation from T and B lymphocytes and anti-CD3/CD28 activation of T cells gave the lowest IC_{50} values for A9(B8) of 211 nM and 129 nM respectively (Table 3.1). The mean IC_{50} for inhibition of shedding of cell surface TNF-α by A9(B8) was 75 nM, whilst the IC_{50} for A9(B8) determined by measuring soluble TNF-α was 91 nM (Table 3.1).

D8P1C1 had higher IC_{50} values for inhibiting L-selectin shedding via anti-CD3/CD28 compared to A9(B8). Contrary to A9(B8), CD4 T cells had a lower IC_{50}, with values of 1304 nM and 689 nM for CD8 and CD4 T cells respectively (Table 3.1). D8P1C1 also had a much higher IC_{50} than A9(B8) for inhibiting soluble L-selectin shedding from TCR activated lymphocytes, at a value of 1243

nM (Table 3.1). As there was no inhibition of L-selectin shedding in a PMA-induced shedding assay with D8P1C1, IC_{50} values of 0 nM were calculated (Figure 3.5, Table 3.1). Regarding inhibition of TNF-α shedding, D8P1C1 had an IC_{50} value of 1468 nM for cell surface TNF-α and a reduced value of 423 nM for soluble TNF-α (Table 3.1).

TIMP-3 was less efficacious than A9(B8) at blocking L-selectin shedding via anti-CD3/CD28 activation, but mirrored the improved efficacy in CD8 T cells with IC_{50}s of 911 nM for CD8 T cells and 1857 nM for CD4 T cells (Table 3.1). TIMP-3 had lower IC_{50} values than A9(B8) for inhibiting L-selectin shedding from lymphocytes following PMA stimulation and was most effective in CD8 T cells with IC_{50} values of 488 nM, 568 nM, and 659 nM on CD8 T cells, CD4 T cells and B cells respectively (Table 3.1). TIMP-3 was less effective at inhibiting soluble L-selectin release in PMA treated cells compared to cell surface inhibition with an IC_{50} of 704 nM (Table 3.1). However, the IC_{50} for inhibiting soluble L-selectin release in anti-CD3/CD28 cells at 328 nM was much lower than that to inhibit shedding from the cell surface (Table 3.1). TIMP-3 was less effective at blocking TNF-α shedding in macrophages compared to A9(B8) when measuring either cell surface levels, with an IC_{50} of 1186 nM, or soluble levels, with an IC_{50} of 378 nM (Table 3.1).

Table 3.1. A9(B8), D8P1C1 and TIMP-3 IC_{50} values for L-selectin and TNF-α shedding. Average IC_{50} values for inhibition of L-selectin shedding via anti-CD3/anti-CD28 (TCR) or PMA stimulation, or TNF-α shedding via LPS stimulation. IC_{50}; 50% maximal inhibitory concentration, CD62L; L-selectin, TNF-α; tumour necrosis factor alpha, TIMP-3; tissue inhibitor of metalloproteinase-3. TCR; T cell receptor. PMA; phorbol 12-myristate 13-acetate. LPS; lipopolysaccharide. ±= SEM, n=5. IC_{50} values estimated using GraphPad Prism software using nonlinear regression curve fit. Values with * n=1.

Assay type	ADAM17 substrate	Cell type	Cell surface IC_{50}			Soluble IC_{50}		
			A9(B8)	D8P1C1	TIMP-3	A9(B8)	D8P1C1	TIMP-3
Anti-CD3/anti-CD28 (TCR)	CD62L	CD8 T cells	261 ± 21	1304*	911 ± 13	129 ± 21	1243*	328*
		CD4 T cells	496 ± 13	689*	1857 ± 437			
PMA	CD62L	CD8 T cells	523 ± 36	0	488 ± 32	211 ± 16	0	704 ± 40
		CD4 T cells	684 ± 61	0	568 ± 30			
		B cells	2837 ± 168	0	659 ± 23			
LPS	TNF-α	Macrophages	75 ± 21	1468*	1186 ±156	91 ± 5	423*	378*

3.3 Discussion

This chapter of work has demonstrated that A9(B8) and D8P1C1 are able to inhibit the ADAM17-mediated shedding of L-selectin from the cell surface of T and B lymphocytes *in vitro* (Figure 3.1, 3.2, 3.4, Table 3.1). This has been successfully shown for A9(B8) in T cells using two different *in vitro* L-selectin shedding assays using primary mouse lymphocytes with either TCR stimulation (Figure 3.1) or PMA stimulation (Figure 3.4). This was also successfully shown for D8P1C1 in T cells using TCR stimulation to initiate L-selectin shedding (Figure 3.2). There were clear differences between the two assays, as A9(B8) had a lower cell surface IC_{50} value in both CD8 and CD4 T cells in the anti-CD3/CD28 assay compared to PMA (Table 3.1). These differences may be attributed to how ADAM17 is activated within these assays; PMA is a direct activator of ADAM17 through protein kinase C (PKC), which is a more 'artificial' method of activation (Müllberg et al. 1992). Anti-CD3/CD28 stimulation is more physiologically relevant as it activates CD3 and CD28 co-receptors to the TCR, as with antigen presentation (Trickett and Kwan 2003). TCR stimulation results in activation of the PI3Kδ pathway, which initiates ADAM17 shedding through MAP kinases (Sinclair et al. 2008). An additional assay using peptide-pulsed APCs to activate T cells would be valuable here, to further add a physiologically relevant *in vitro* system of T cell activation and L-selectin shedding.

When CD4 T cells were treated with 7 μM A9(B8) and activated with anti-CD3/CD28, levels of cell surface L-selectin were higher than on unactivated cells (Figure 3.1 B). This suggests a role for ADAM17 in basal L-selectin shedding in CD4 T cells. Whilst this has not been investigated directly on CD4 T cells *in vitro*, Mohammed et al. have suggested that constitutive metalloproteinase-dependent L-selectin shedding by lymphocytes is non-ADAM17 and non-ADAM10 dependent (Mohammed et al. 2019). This was carried out by injecting L-selectin$^{-/-}$ mice with ADAM17 sufficient/deficient lymphocytes and detecting soluble L-selectin in peripheral blood. Levels of soluble L-selectin were slightly lowered in ADAM17$^{-/-}$ mice, but this was not statistically significant (Mohammed et al. 2019). In addition, TIMP-1 which

inhibits ADAM10 did not abrogate basal shedding of L-selectin from ADAM17 deficient T lymphocytes *ex vivo* (Mohammed et al. 2019). The mediator for basal L-selectin shedding is yet to be discovered and requires further investigation *in vitro* and *in vivo*.

D8P1C1 was unable to block PMA-induced ADAM17-mediated L-selectin shedding in CD8 T cells, CD4 T cells and B cells *in vitro* (Figure 3.5). ADAM17 is documented to exist in an 'open/active' and 'closed/inactive' structure which is the 'molecular switch' controlling ectodomain cleavage. D8P1C1 binds to the 'active' confirmation of ADAM17, as demonstrated on cancer cells (Saha et al. 2022). A potential explanation for this finding is that the open confirmation of ADAM17 does not exist long enough for sufficient D8P1C1 binding, as PMA-induced L-selectin shedding is a highly artificial, rapid interaction (Müllberg et al. 1992).

As the structure of ADAM17 can be different on each cell type (Düsterhöft et al. 2013), there is also a possibility that D8P1C1 binds more favourably to ADAM17 on tumour cells than to ADAM17 on lymphocytes. However, it should be noted that published data using D8P1C1 has all been carried out on human ADAM17. Whilst human and mouse ADAM17 are of similar structure, there are some differences. Garbers et al. has shown that ADAM17-mediated ectodomain cleavage is species specific and is not based on substrate cleavage site recognition alone (Garbers et al. 2011). A further important detail is that D8P1C1 has been investigated previously in the context of tumour cell death and reduction in proliferation; no substrates of ADAM17 have directly been investigated (Saha et al. 2022). Anti-ADAM10 antibody 1H5 was unable to block shedding of L-selectin or TNF-α in all assays carried out, confirming previous findings that there is no role for ADAM10 in the cleavage of L-selectin or TNF-α on ADAM17 insufficient cells (Figure 3.2, 3.5, 3.8) (Mohammed et al. 2019), (Reddy et al. 2000).

In the PMA shedding assay data, there were clear differences in basal levels of L-selectin on unactivated CD8 T, CD4 T and B lymphocytes prior to activation. CD8 T cells had the highest starting levels of L-selectin with an average MFI of 758, whilst CD4 T cells and B cells had average MFIs of 427 and 357

respectively (Figure 3.4). This was also observed for T cells in the anti-CD3/CD28 shedding assays (Figure 3.1, 3.2, 3.3). This validates previous findings in the literature showing CD8 T cells express the highest levels of L-selectin of all lymphocyte subsets (Tang et al. 1998).

A9(B8) was more effective at inhibiting the cell surface shedding of TNF-α compared to L-selectin with an IC_{50} of 75 nM for RAW 264.7 cells versus ≥261 nM for lymphocytes (Table 3.1). This was also true for inhibiting soluble substrate release, with an IC_{50} of 91 nM for TNF-α shedding compared to ≥129 nM for L-selectin shedding (Table 3.1). These data of TNF-α shedding support published work showing a similar soluble TNF-α IC_{50} of 72 nM for A9(B8) in the PANC-1 pancreatic cancer cell line (Ye et al. 2017). D8P1C1 was relatively ineffective at inhibiting cell surface TNF-α and L-selectin release with IC_{50} values of 1468 nM and ≥689 nM, respectively (Table 3.1). However, D8P1C1 was more effective at inhibiting release of soluble TNF-α with an IC_{50} of 423 nM, compared to 1243 nM for inhibiting release of soluble L-selectin. Unlike A9(B8), D8P1C1 was unable to reach maximal inhibition of L-selectin shedding (Figure 3.1, 3.2, 3.4, 3.5). A limitation of the D81P1C1 data collected was that titrations were only carried out as one repeat due to time constraints and limited access to compounds. To strengthen reliability of the data, further repeats are needed.

This pattern of improved efficacy against TNF-α was also seen for TIMP-3 as the IC_{50} for the inhibition of soluble TNF-α release was 378 nM compared to 704 nM for soluble L-selectin released lymphocytes with PMA activation (Table 3.1). However, TIMP-3 had a lower IC_{50} in PMA stimulated lymphocytes for L-selectin ectodomain cleavage than with anti-CD3/CD28 (Table 3.1).

This trend of requiring less ADAM17 inhibitor to block TNF-α shedding than L-selectin shedding has also been shown by Borland et al. whereby TIMP-3 had an IC_{50} value of 310-390 nM for inhibiting L-selectin shedding, and an IC_{50} value of 110 nM for inhibiting TNF-α shedding (Borland et al. 1999). These variances in IC_{50} may be attributed to the differing physiology of L-selectin and TNF-α shedding from the cell surface, however, these mechanisms are still poorly

understood. Wang et al. found that two cysteine sulfhydryl motifs in the disintegrin/cysteine rich domain of ADAM17 were indispensable for L-selectin cleavage (Wang et al. 2010). Whilst for TNF-α shedding, just the catalytic domain of ADAM17 was required (Reddy et al. 2000). To understand these mechanisms in more detail, further investigation must be carried out.

Borland et al. reported a much lower IC_{50} value for both L-selectin and TNF-α shedding compared to the values obtained in the assays used within this chapter (Borland et al. 1999). However, there are differences in the type of TIMP-3 used, as Borland et al. used a truncated N-TIMP, whereas a full-length recombinant TIMP-3 was used in this work. There are also differences in shedding assay protocols such as number of cells, incubation periods and pre-treatment with compound. A limitation to the assays used here is that 1 μM was the highest concentration of TIMP-3 that could be used due to low concentration stock solutions of TIMP-3 commercially available. Therefore, maximal inhibition and an 'S shaped curve' was not achieved with some titrations (Figure 3.3, 3.6, 3.9, 3.12).

Titrations of A9(B8) in RAW 264.7 macrophages showed that at concentrations above 778 nM, cell surface levels of TNF-α are surprisingly reduced (Figure 3.7 A). However, this was not seen with concentrations of D8P1C1 or TIMP-3 above 778 nM (Figure 3.8, 3.9). In the TNF-α ELISA analysis, there was no increase in soluble TNF-α above 778 nM A9(B8), which contradicts the flow cytometry findings (Figure 3.10). Live/dead staining from flow cytometry experiments confirm there was no increase in cell death caused with high doses of A9(B8), suggesting potential transmembrane TNF-α internalisation. However, previous studies with small molecule inhibitors have not found this result of lower cell surface TNF-α at high inhibitor concentrations (Mohler et al. 1994). ADAM17 is also documented to cleave TNF receptors; blocking ADAM17 may increase cell surface expression of TNF receptors and result in TNF-α binding on adjacent cells, which is known to result in internalisation (Fischer et al. 2011).

Within this chapter of work, A9(B8), D8P1C1 and TIMP-3 were analysed for their ability to maintain expression of ADAM17 cell surface substrates L-selectin

and TNF-α by flow cytometry, whilst their ability to inhibit the soluble release of these substrates was measured in the cell supernatants via ELISA. Single cell suspensions from whole mouse spleens were used for L-selectin shedding assays, containing a mixture of lymphocytes. Therefore, soluble L-selectin data was not available for CD8 T cells, CD4 T cells and B cells individually. An improvement to this assay would be separating these populations for individual analysis, as differences in L-selectin shedding were seen between lymphocyte subsets with cell surface data (Table 3.1). Interestingly, most IC_{50} values calculated from soluble substrate titrations are lower than those for cell surface substrate titrations (Table 3.1). Previous data on A9(B8) has been collected using soluble ADAM17 substrate levels such as TNF-α, IL-6 receptor, amphiregulin and TGF-α (Ye et al. 2017). L-selectin was not investigated when antibody clonotypes such as A9(B8) were chosen using phage display by their ability to inhibit ADAM17 (Kwok et al. 2014). Further to this, although it is known that A9(B8) binds to the extracellular domain of ADAM17, the binding epitope had not been mapped. Therefore, it is possible that A9(B8) blocks residues of ADAM17 that are dependent for TNF-α shedding, but some residues required for L-selectin shedding are not blocked. ADAM17 has been shown to have a relaxed sequence specificity for L-selectin, single amino acid residues can be changed around at the cleavage site, but cleavage still occurs (Chen et al. 1995).

One limitation to this work is that differences between the ability of A9(B8), D8P1C1 and TIMP-3 to inhibit the shedding of TNF-α and L-selectin were possibly due to differences in cells used. However, there is a lack of cell lines expressing both TNF-α and L-selectin. Several mouse cell lines including primary mouse bone marrow derived neutrophils were tested for the co-expression of TNF-α and L-selectin together, however, no cells co-expressing both substrates were found. The only cell line known to exist is a human lymphoblastic cell line, however, a further obstacle to this is finding a stimulus that will shed both L-selectin and TNF-α.

A further limitation to this work is the lack of ADAM17 inhibitors tested. There are several inhibitors of ADAM17 available such as antibody MEDI3622 (Dosch et al. 2017) and small molecule inhibitors DPC-333 (Grootveld 2003) and TMI-

005 (Thabet and Huizinga 2006). A more thorough investigation would involve testing these inhibitors in our *in vitro* shedding assays for their ability to inhibit L-selectin and TNF-α shedding. However, the ideal drug candidate for this work would be a compound which directly binds the cleavage site of L-selectin, to inhibit proteolytic shedding. Targeting ADAM17 is likely to result in widespread off-target effects on other substrates, which may abrogate the functionality of L-selectin on CD8 T cells.

The purpose of this chapter of work was to obtain a compound with the ability to maintain cell surface L-selectin on CD8 T cells to take forward to *in vivo* mouse models. D8P1C1 was unable to maintain cell surface L-selectin levels in PMA shedding assays and had high IC_{50} values for anti-CD3/CD28 shedding assays; this has rendered D8P1C1 a non-viable candidate for future mouse work (Table 3.1). A9(B8) has been shown to inhibit the shedding of L-selectin from CD8 T lymphocytes, however, high concentrations are required; much higher than for inhibiting TNF-α shedding (Table 3.1). The aim for the next chapter of work is to use A9(B8) *in vivo* to replicate previous findings in transgenic LΔP mice that maintenance of L-selectin on CTLs is beneficial for viral clearance (Mohammed et al. 2016). A9(B8) has been shown to be efficacious in a mouse model of pancreatic cancer (Ye et al. 2017). The mouse model used was *Pdx1Cre*;*Kras*^{G12D};*Trp53*$^{flox/+}$ (KP^{fl}C) whereby mice have induced *Kras* and 1 deleted allele of *Trp53* to induce spontaneous pancreatic cancer lesions from 1 month of age (Ye et al. 2017). This study did not test for the involvement of T cells in tumour eradication, nor the effect of A9(B8) on T cells, therefore the effect of A9(B8) on the immune system is still unknown and yet to be tested (Ye et al. 2017).

Overall, these data show that A9(B8) is a potential candidate to take forward to animal studies to block L-selectin shedding in CD8 T lymphocytes, however, higher doses of A9(B8) may be required to successfully block L-selectin *in vivo* than have been shown to block TNF-α in the pancreatic cancer mouse model (Ye et al. 2017).

Chapter Four

The Impact of Pharmacological ADAM17 Inhibition on the Role of L-selectin in CD8 T cell Clearance of Murine Influenza Virus

4. The Impact of Pharmacological ADAM17 Inhibition on the Role of L-selectin in CD8 T cell Clearance of Murine Influenza Virus

4.1 Introduction

The adaptive immune response is a critical defence mechanism against invading pathogens in the body. One arm of anti-viral immunity involves CD8 T cells becoming activated, migrating to sites of infection, and killing infected cells to protect the host. The effectiveness of this strategy is paramount in limiting the burden of infection (Murphy and Weaver 2017). Trafficking of CD8 T cells to LNs and the site of infection involves cell adhesion molecule interaction with endothelium (Ley et al. 2007); L-selectin is a fundamental cell adhesion molecule in this process (Arbonés et al. 1994).

Naïve CD8 T cells surveying LNs retain their L-selectin expression. Upon viral infection challenge, these naïve CD8 T cells become activated into CTLs by APCs exhibiting foreign viral peptide on MHC-I. This interaction between MHC-I/peptide and the TCR results in the cleavage of L-selectin on T cells. This cleavage is controlled by ADAM17 ectodomain shedding, a PI3Kδ-mediated process (Sinclair et al. 2008). L-selectin levels begin to increase over the following 48 hours, when the T cells egress the LNs to reach the systemic circulation (Mohammed et al. 2016). L-selectin is downregulated again, being at its lowest in infected tissues by day 8 of infection (Mohammed et al. 2016). This secondary reduction is controlled by PI3Kδ-mediated transcriptional silencing (Sinclair et al. 2008). PI3Kδ blocks the action of the transcription factor KLF2, which transcribes the L-selectin gene SELL (Sinclair et al. 2008), (Watson et al. 1990).

To explore the physiological role of cyclical L-selectin expression in activated T cells, genetically modified LΔP mice were generated in which ADAM17-resistant L-selectin is expressed on the T cells under a heterologous promoter (Galkina et al. 2003). Experiments using LΔP mice found that maintained L-selectin

expression on CTLs improved activated CD8 T cell homing to infected organs and subsequent viral clearance in murine models of influenza and vaccinia virus infections (Mohammed et al. 2016). This finding challenged the previous dogma that L-selectin is solely a LN homing molecule (Butcher and Picker 1996).

The improved CD8 T cell homing and subsequent viral clearance observed in L∆P mice has demonstrated that L-selectin is a potential therapeutic target in viral infection (Mohammed et al. 2016). Therefore, the next step for this research was to pharmacologically target L-selectin in mouse models of IAV infection to determine whether this would result in the improved viral clearance, as observed in L∆P mice (Mohammed et al. 2016). This may result in future therapeutic interventions for influenza virus for vulnerable members of the public, as current anti-virals have little impact unless taken within 36 hours of symptom onset (Stiver 2003).

As aforementioned in chapter three, there are no pharmacological agents targeting the cleavage site of L-selectin, therefore, compounds blocking the function of ADAM17 were investigated. Chapter three involved testing two anti-ADAM17 antibodies for their ability to inhibit proteolytic cleavage of L-selectin *in vitro*. Titrations of A9(B8) were carried out in *in vitro* L-selectin shedding assays, which yielded an IC_{50} of $\geq$261 nM for inhibition of L-selectin shedding, whilst the other antibody candidate D8P1C1 had an IC_{50} of $\geq$689 nM. We therefore decided upon carrying the anti-ADAM17 monoclonal antibody A9(B8) forward to our *in vivo* mouse model of X31 IAV infection. A9(B8) has previously shown efficacy in a model of murine pancreatic cancer *in vivo*, which further supports its potential use in our mouse model (Ye et al. 2017).

We hypothesise that ADAM17 inhibition *in vivo* will improve CTL recruitment to mouse lungs and viral clearance in a mouse model of IAV infection, via an L-selectin dependent mechanism.

4.1.1 Aims and Objectives

The aim of this chapter of work is to determine if treatment with anti-ADAM17 antibody A9(B8) improves virus clearance in a mouse model of

pulmonary IAV infection, and to determine whether this is dependent on L-selectin expression by CD8 T cells.

Objectives:

- To determine whether anti-ADAM17 inhibitor antibody A9(B8) inhibits the shedding of L-selectin on CD8 T cells *in vivo*.
- To examine the effects of A9(B8) on murine IAV clearance, and to determine whether virus clearance, if any, is L-selectin dependent.
- To determine effects of A9(B8) on soluble L-selectin, cytokine, and chemokine profiles in the lungs of IAV infected mice.
- To determine optimal dosing regimens and administration routes of A9(B8) in a mouse model of pulmonary IAV virus.

4.2 Results

4.2.1 The effect of pharmacological ADAM17 inhibition on the welfare of mice infected with influenza virus

Eight C57BL/6J (B6) mice from Charles River were intranasally infected with $1x10^3$ pfu of IAV X31. Four mice were treated with ADAM17 inhibitor antibody A9(B8) (gifted kindly from Professor Henry Kwok, University of Macau) 1 day before flu infection. A9(B8) was dosed at 10 mg/kg and injected i.p. in a volume of 9.5 mL/kg, in PBS. A human IgG2 isotype control antibody dosed at the same concentration and via the same method, was also administered to four mice, 1 day before infection. On day 7 of infection, mice were humanely killed, and the following were extracted: BAL, lungs, med LN, spleen, and blood (Figure 4.1). This study was ethically reviewed and carried out in accordance with the Animals (Scientific Procedures) Act 1986.

Weight loss for each mouse was recorded over the 7 days of infection. Both treatment groups showed a steady decline in weight over the 7 days, ending with an average loss of 16.5% total body weight for the A9(B8) treated group, and 15.8% for the control treated group (Figure 4.2). There was a significant difference in weight loss found between both groups at day 1 of infection, however, there was no significant difference found at any other timepoint of infection (Figure 4.2). ‘Mouse 1’ from the A9(B8) treated group retained its weight slightly better than the group average, with an average weight loss of 10% by day 7 of infection (Figure 4.2).

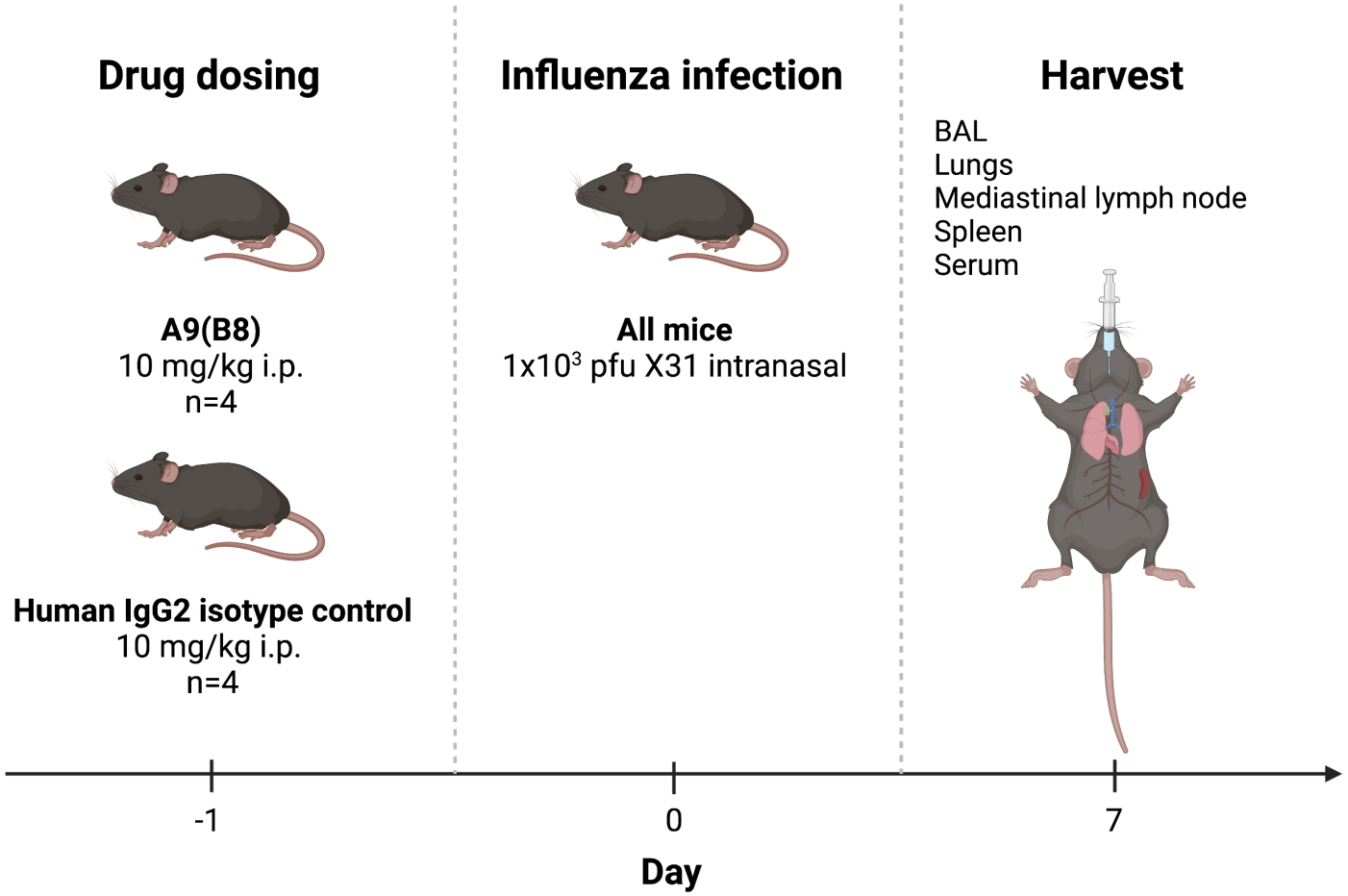

Figure 4.1. Mouse experimental plan for A9(B8) treatment in X31 influenza infection. Four female C57BL/6J mice aged 8-12 weeks received 10 mg/kg A9(B8) via 9.5 mL/kg i.p. injection in PBS. Four female C57BL/6J mice aged 8-12 weeks received 10 mg/kg human IgG2 isotype control via 9.5 mL/kg i.p. injection in PBS. 24 hours later, all eight mice received $1x10^3$ pfu X31 via 50 μL intranasal injection in PBS. Mice were weighed daily

and humanely killed on day 7 of infection. Bronchoalveolar lavage (BAL), lungs, mediastinal lymph node, spleen and serum were collected from each mouse. Figure created using Biorender.com.

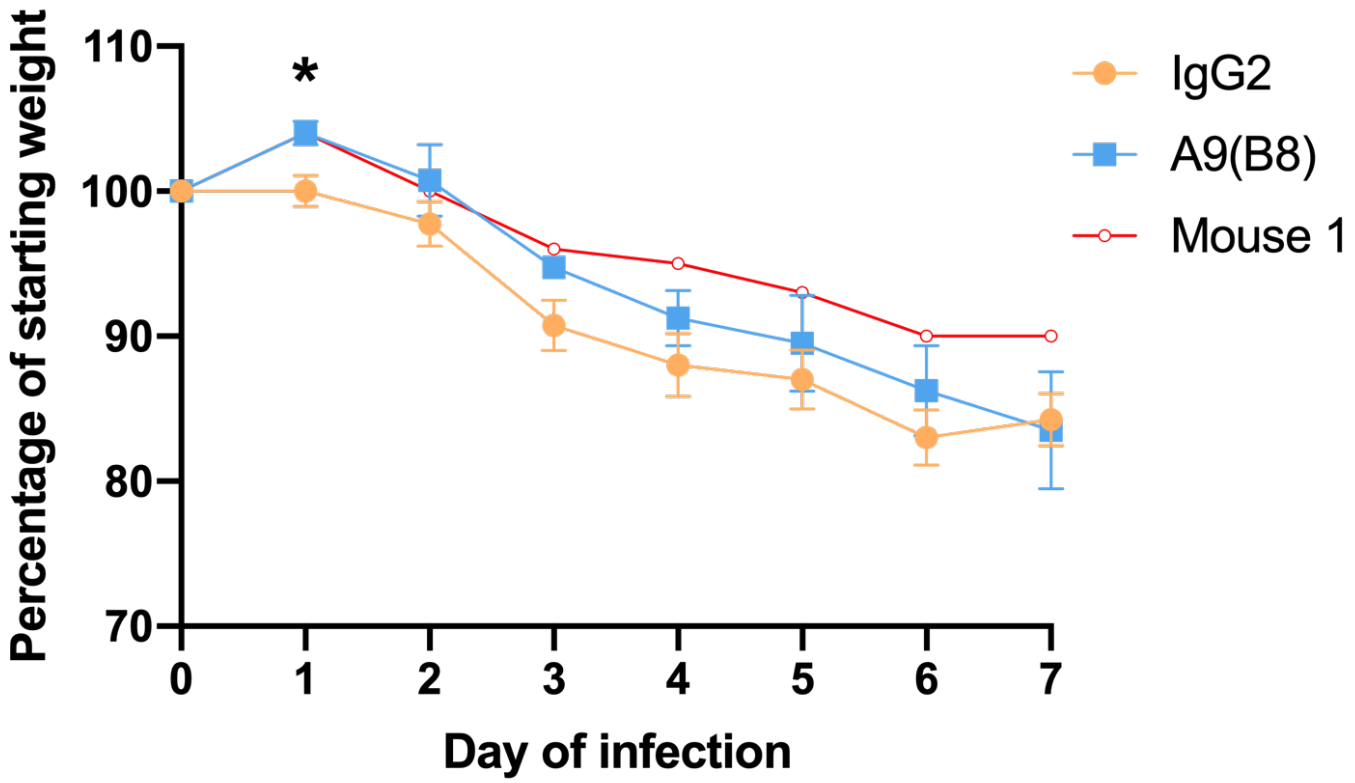

Figure 4.2. Percentage of starting body weight shown over 7 days of X31 infection. Mice were treated with 10 mg/kg of either anti-ADAM17 antibody A9(B8) or human IgG2 isotype control, via i.p. injection, 24 hours prior to $1x10^3$ pfu X31 infection. Mice were humanely killed on day 7 of infection. Red data points represent mouse number 1. Error bars are mean $\pm$ SEM, n=4. Unpaired T-test at each timepoint. *=$p \leq 0.05$.

4.2.2 The effect of pharmacological ADAM17 inhibition on influenza virus clearance in mice

To determine the effects of ADAM17 inhibition on murine influenza virus clearance, IAV titres were calculated from the lungs of mice on day 7 of X31 infection. Mice were treated with 10 mg/kg of either A9(B8) or an isotype control antibody 1 day prior to infection. There were no significant differences in the IAV titres found between treatment groups via both plaque assay and RT-qPCR analysis (Figure 4.3). However, trends in the data suggested a reduction in virus titres in mice treated with A9(B8) as measured by viral plaque assay (Figure 4.3 A). Whilst qPCR analysis suggested an increase in gene expression of X31 IAV with A9(B8) treatment (Figure 4.3 B).

Mouse 1 had notably higher titres in both assays as shown by the red data point, with 5836.6 pfu/lung and a fold change in X31 gene expression of 1.0 (Figure 4.3). These values were much larger than the other three mice within that group; removing mouse 1 from these data gave an average of 1335 pfu/lung and 0.1-fold change in X31 gene expression for the A9(B8) treated group (Figure 4.3). By removing this mouse from the data, we see a clear trend in a reduction in IAV titres in the mouse lungs when treated with A9(B8) compared to isotype (Figure 4.3 A), and a similar level of X31 gene expression between both groups (Figure 4.3 B).

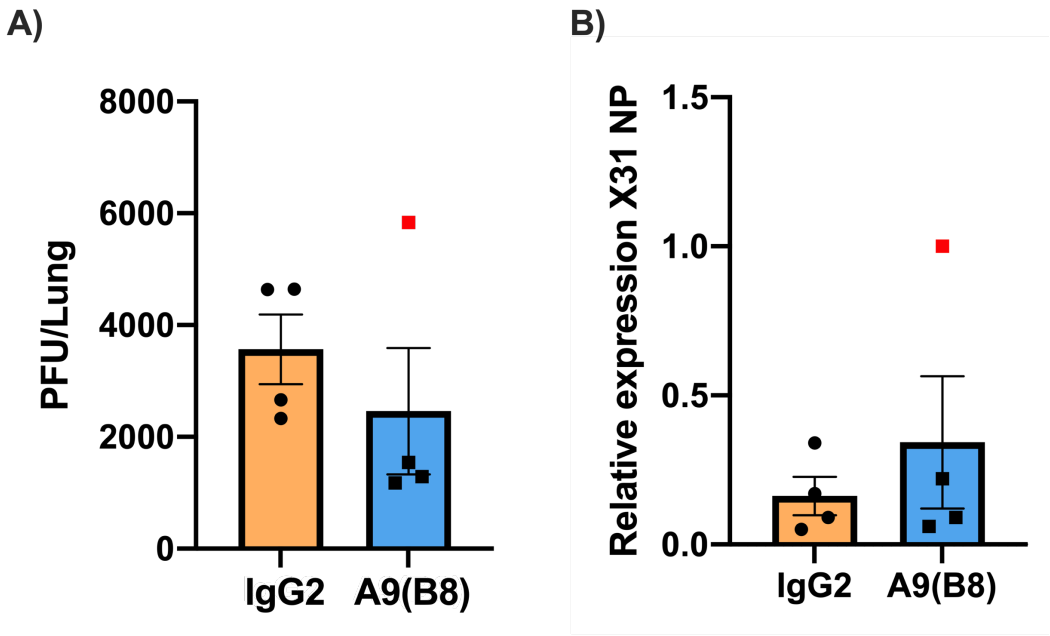

Figure 4.3. Influenza virus titres from mouse lungs on day 7 of X31 infection. Mice were treated with 10 mg/kg of either anti-ADAM17 antibody A9(B8) or human IgG2 isotype control, 24 hours prior to $1x10^3$ pfu X31 infection. Mice were humanely killed on day 7 of infection and lungs excised for analysis via plaque assay and RT-qPCR. **A)** Plaque forming unit (pfu) per whole lung calculated via plaque assay. **B)** Fold change in gene expression of X31 nucleoprotein gene (X31 NP) compared to glyceraldehyde-3-phosphate dehydrogenase (GAPDH), calculated using the $\Delta\Delta$Ct method. Red data point represents mouse number 1. Error bars are mean $\pm$ SEM, n=4. Mann-Whitney test, not significant.

4.2.3 The effect of pharmacological ADAM17 inhibition on soluble L-selectin, cytokine and chemokine and profiles in mouse lungs infected with influenza virus

To establish whether A9(B8) was able to block shedding of L-selectin in the lungs at 10 mg/kg, BALF was measured for its quantity of soluble L-selectin 8 days post-administration. There was a trend that suggested higher soluble L-selectin levels in the treated group, with an average of 527 ng/mL of soluble L-selectin in the A9(B8) treated group, compared to 400 ng/mL in the control group (Figure 4.4). However, this was not statistically significant (Figure 4.4). Mouse 1 had the highest levels of soluble L-selectin out of all mice, with 720 ng/mL (Figure 4.4).

To investigate the effects of A9(B8) on cytokine and chemokine profiles within the lungs during X31 IAV infection, BALF collected on day 7 of infection was tested using a mouse anti-virus response multiplex assay with 13 detectable analytes. Table 4.1 lists the detectable analytes with their limit of detection (LOD) values (Table 4.1). IL-12p70 (interleukin 12p70) and GM-CSF (granulocyte-macrophage colony-stimulating factor) were below the LOD and were unable to be quantified in these samples.

Interestingly, as seen with the virus titre and soluble L-selectin data, mouse 1 had a higher concentration of all analytes present in the BALF, apart from interleukin-6 (IL-6) and CXCL1 (Figure 4.5). Most striking is 2206.7 pg/mL of IFN-γ for mouse 1 compared to an average of 146.5 pg/mL for the other 3 mice in the A9(B8) treated group, and 139.7 pg/mL for the IgG2 treated group (Figure 4.5). There were no significant differences found between either treatment group with any of the analytes measured (Figure 4.5).

As TNF-α is another substrate of ADAM17, it is worth noting that this cytokine was slightly decreased on average in the A9(B8) treated group when mouse 1 was removed (Figure 4.5 C). The IgG2 treated group had an average of 161 pg/mL of TNF-α in BALF on day 7 of infection, compared to 105 pg/mL in the

A9(B8) treated group (Figure 4.5 C). However, this average is increased to 142 pg/mL when ‘mouse 1’ is considered in this group (Figure 4.5 C).

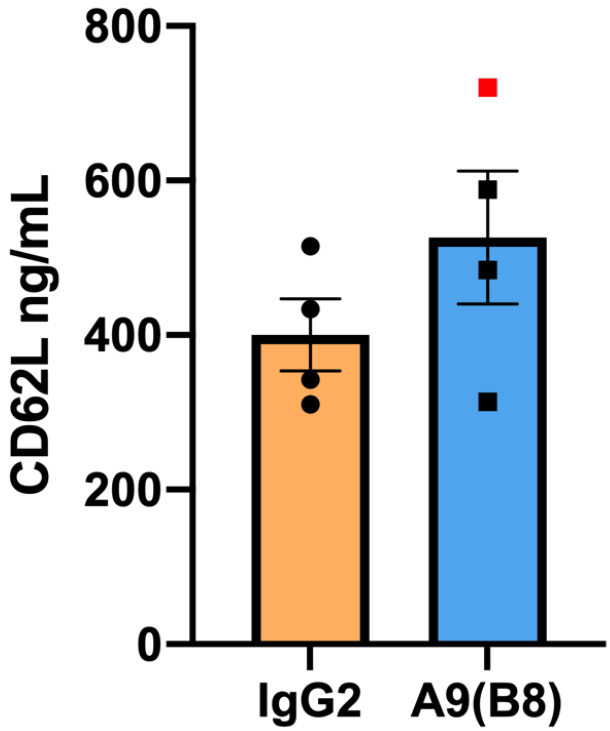

Figure 4.4. Soluble mouse L-selectin (CD62L) levels in murine bronchoalveolar lavage fluid (BALF) on day 7 of X31 influenza infection. Mice were treated with 10 mg/kg of either anti-ADAM17 antibody A9(B8) or human IgG2 isotype control, 24 hours prior to $1x10^3$ pfu X31 infection. Mice were humanely killed on day 7 of infection and BALF collected. L-selectin levels calculated in ng/mL using ELISA. Red data point represents mouse number 1. Error bars are mean ± SEM, n=4. Unpaired T-test, not significant.

Table 4.1. Limit of detection (LOD) values for each of the 13 analytes detected using LEGENDplex mouse anti-virus response panel (Biolegend). IFN-γ; interferon-gamma, CXCL1 (KC); chemokine ligand 1, TNF-α; tumour necrosis factor-alpha, CCL2 (MCP-1); chemokine ligand 2, IL-12p70; interleukin 12p70, CCL5 (RANTES); chemokine ligand 5, IL-1β; interleukin 1- beta, CXCL10 (IP-10); chemokine ligand 10, GM-CSF; granulocyte-macrophage colony-stimulating factor, IL-10; interleukin-10, IFN-β; interferon-beta, IFN-α; interferon-alpha, IL-6; interleukin-6. Limit of detection calculated using LEGENDplex software (Biolegend). Values shown in pg/mL.

Analyte	LOD pg/mL
IFN-γ	1.55
CXCL1 (KC)	6.23
TNF-α	3.68
CCL2 (MCP-1)	38.55
IL-12p70	17.23
CCL5 (RANTES)	1.71
IL-1β	5.28
CXCL10 (IP-10)	14.96
GM-CSF	19.50
IL-10	21.64
IFN-β	1.63
IFN-α	38.84
IL-6	7.38

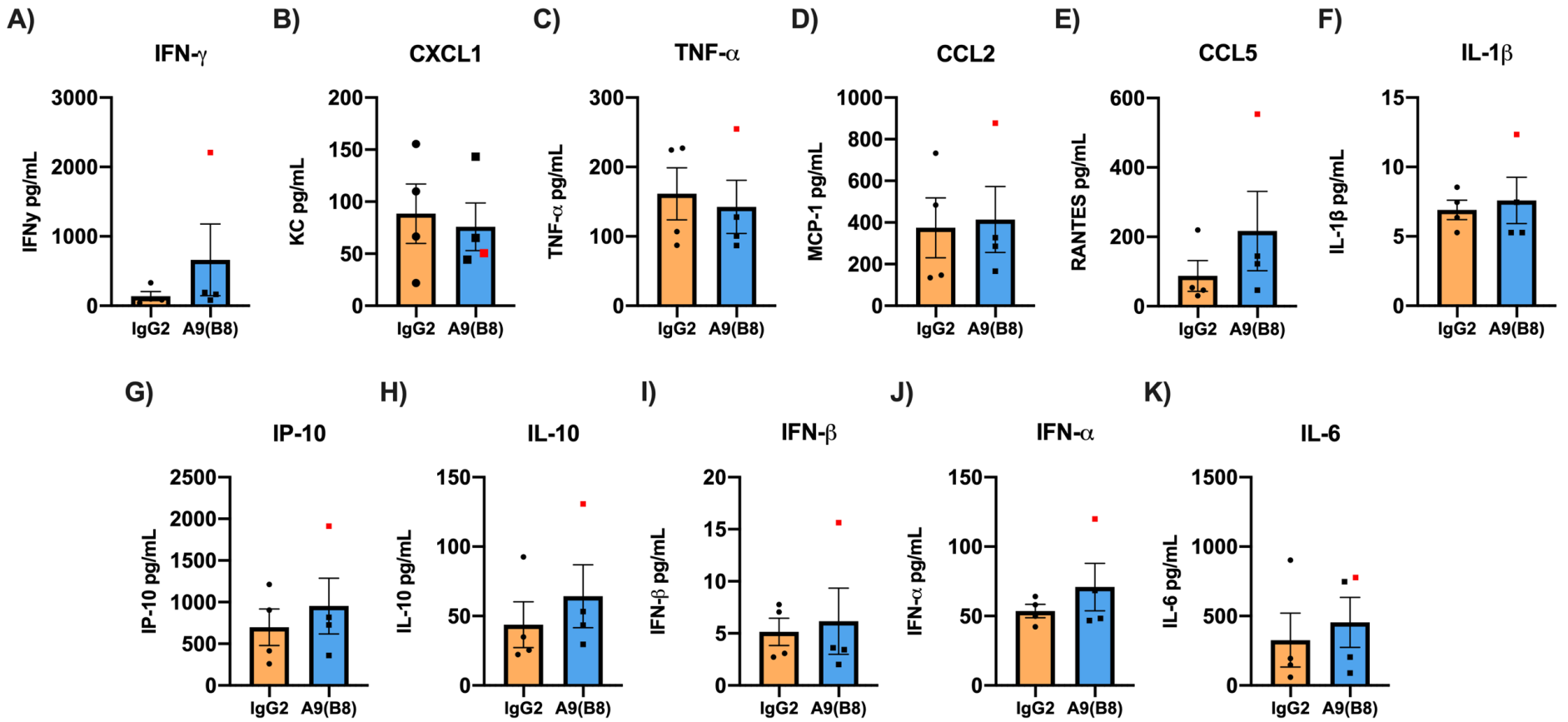

Figure 4.5. Chemokine and cytokine profiles of murine bronchoalveolar lavage fluid (BALF) on day 7 of X31 influenza infection. Mice were treated with 10 mg/kg of either anti-ADAM17 antibody A9(B8) or human IgG2 isotype control, 24 hours prior to $1x10^3$ pfu X31 infection. Mice were humanely killed on day 7 of infection and BALF collected. Analytes measured using LEGENDplex mouse anti-virus response panel (Biolegend). **A)**

IFN-γ; interferon-gamma, **B)** CXCL1 (KC); chemokine ligand 1, **C)** TNF-α; tumour necrosis factor alpha, **D)** CCL2 (MCP-1); chemokine ligand 2, **E)** CCL5 (RANTES); chemokine ligand 5, **F)** IL-1β; interleukin 1- beta, **G)** IP-10 (CXCL10); chemokine ligand 10, **H)** IL-10; interleukin-10, **I)** IFN-β; interferon-beta, **J)** IFN-α; interferon-alpha, **K)** IL-6; interleukin-6. Levels calculated in pg/mL. The following analytes were below limit of detection: IL-12p70; interleukin 12p70 and GM-CSF; granulocyte-macrophage colony-stimulating factor. Data analysed using LEGENDplex software (Biolegend). Red data points represent mouse number 1. Error bars are mean $\pm$ SEM, n=4. Mann-Whitney test (A, E, I, K) Unpaired T-test (B, C, D, F, G, H, J), not significant.

4.2.4 The effect of pharmacological ADAM17 inhibition on lymphocyte cell surface L-selectin shedding

To investigate the dose of A9(B8) circulating within the mice by day 7 of X31 IAV infection, serum was collected from both A9(B8) and IgG2 isotype control treated mice. A PMA-induced L-selectin shedding assay was utilised to assess whether there was enough A9(B8) circulating by this time point to block ADAM17-mediated L-selectin shedding. Lymphocytes from uninfected, untreated Thy1.1 mice were collected from spleens and incubated with serum from treated mice. This was compared to serum from naïve Thy1.1 mice, and serum from naïve mice with 7 μM of exogenous A9(B8). Cells were treated with 5 μM of PMA or equivalent volume of DMSO as a vehicle control, to induce L-selectin shedding. A high concentration of PMA was used with plasma and/or blood due to previous optimisation of PMA-induced L-selectin shedding (Faveeuw et al. 2001). MFI of cell surface L-selectin was measured via flow cytometry on PMA and DMSO treated cells, and a 'percentage of inhibition of L-selectin shedding' was calculated.

A9(B8) was shown to be more efficacious on T cells than B cells. 7 μM of A9(B8 inhibited L-selectin shedding in CD8 T cells by 91%, whilst on CD4 T cells, 7 μM A9(B8) completely inhibited L-selectin shedding (Figure 4.6 A, B). Interestingly, in PMA-stimulated CD4 T cells 7 μM A9(B8) resulted in cell surface L-selectin levels higher than basal (137%). In B cells, 7 μM A9(B8) only partially inhibited L-selectin shedding by 39.7% (Figure 4.6 A-C).

Sera from A9(B8) or IgG2 treated mice did not inhibit L-selectin shedding from T lymphocytes (Figure 4.6 A-C). Exogenous A9(B8) was less effective at blocking L-selectin shedding in the B cell population, so it was not possible to determine the efficacy of serum from A9(B8) treated mice on these cells (Figure 4.6 C).

In conclusion, there was no significant difference in the ability of serum from A9(B8) treated, X31 infected mice to block L-selectin shedding, compared to serum from naïve mice or serum from IgG2 treated, X31 infected mice (Figure 4.6). However, 7 μM of exogenous A9(B8) was able to cause over 90%

inhibition of L-selectin shedding in CD8 and CD4 T cells in this assay (Figure 4.6).

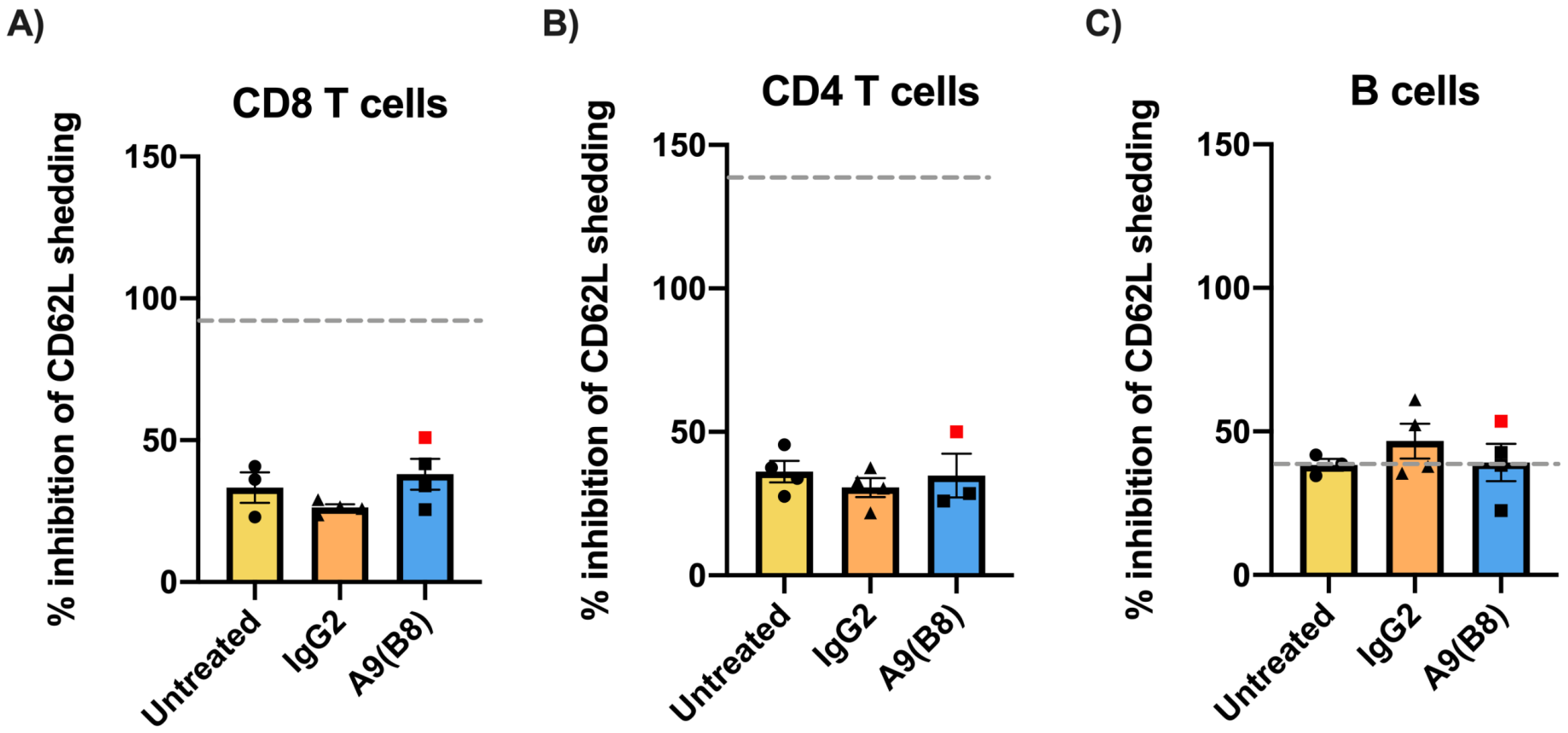

Figure 4.6. Percentage inhibition of L-selectin shedding in mice, 8 days-post A9(B8) treatment. Mice were treated with 10 mg/kg of either anti-ADAM17 antibody A9(B8) or human IgG2 isotype control, 24 hours prior to $1x10^3$ pfu X31 infection. Mice were humanely killed on day 7 of infection and serum collected. Serum was also collected from untreated, uninfected Thy1.1 mice (naïve). Splenocytes from untreated, uninfected Thy1.1 mice were prepared into a single cell suspension and incubated with collected sera, and either 5 μM PMA or equivalent volume of DMSO as vehicle control. Cell surface L-selectin (CD62L) levels were measured on lymphocytes by flow cytometric analysis. Cells gated on lymphocyte profile via

forward and side scatter, single, live cells. Exogenous A9(B8) was added to peripheral blood from naïve mice to determine maximal levels of inhibition. **A-C)** Percentage (%) inhibition of CD62L shedding. This was calculated by presenting PMA CD62L MFI as a percentage of DMSO control CD62L MFI on cells treated with either serum from untreated mice with 7 μM exogenous A9(B8) (grey dashed line), serum from untreated mice alone (yellow), serum from IgG2 treated (orange) or A9(B8) treated (blue) mice on day 7 of infection. **A)** CD8 T cell population, **B)** CD4 T cell population, **C)** B cell population. Red data points represent mouse number 1. Error bars are mean ± SEM, n=4. One-way ANOVA with Tukey's multiple comparisons test, not significant.

4.2.5 The effect of increased ADAM17 inhibitor dosage and new route of administration on welfare of mice infected with influenza virus

As shown above, there was no significant difference in IAV titres between A9(B8) and IgG2 treated mice on day 7 of infection (Figure 4.3). No clear differences were observed in soluble L-selectin and TNF-α in BALF, as well as other cytokines and chemokines associated with murine viral infection (Figure 4.4, 4.5). The levels of A9(B8) in the bloodstream were also insufficient to inhibit ADAM17-dependent L-selectin shedding at this timepoint (Figure 4.6). This suggests concentrations of A9(B8) *in vivo* were below 29 nM by day 7, as this was the level of detection of L-selectin shedding measured *in vitro* in chapter three (Figure 3.1).

To further understand these findings, a new experimental plan was devised whereby dosage of the anti-ADAM17 antibody was increased from 10 mg/kg to 15 mg/kg and administered 1 hour, rather than 24 hours, prior to X31 infection. This was done to maximise the amount of A9(B8) available to block ADAM17 and to minimise *in vivo* clearance. Three mice received A9(B8) via i.p. injection, as previously (referred to herein as i.p. group), whilst three mice received A9(B8) via i.v. tail vein injection (referred to herein as i.v. group) in 9.5 mL/kg sterile PBS. This was to determine if the administration route affected circulation and distribution of the antibody. X31 IAV dose was increased from $1x10^3$ pfu to $3x10^3$ pfu and the period of infection was shortened from 7 to 4 days to minimise clearance of the antibody before testing, whilst increasing pathogenicity of infection (Figure 4.7). Blood was also collected at 6 hours-post administration to determine functionality in blocking L-selectin rapidly after injection, whilst allowing optimal distribution around the body (Yip et al. 2014). This study was ethically reviewed and carried out in accordance with the Animals (Scientific Procedures) Act 1986.

Mice treated with A9(B8) via i.v. injection lost more weight on average, over the course of infection, compared to mice treated via i.p injection. However, this was only statistically significant on day 2 of infection. Neither group had substantial weight loss by day 4, with the i.v. group retaining an average of 93%

starting body weight, and 101% starting body weight for the i.p. group (Figure. 4.8).

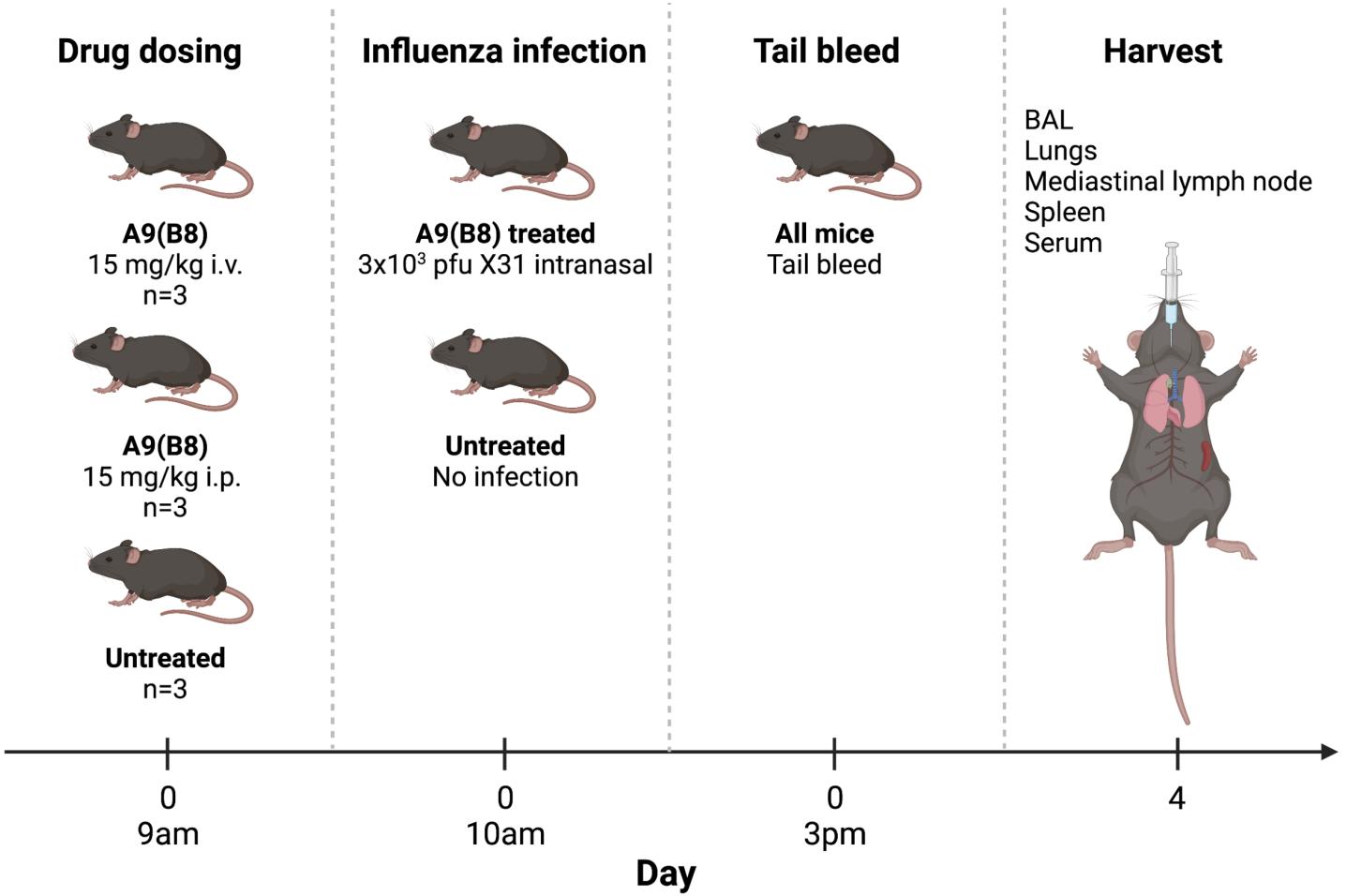

Figure 4.7. Mouse experimental plan for increased dose and new administration route of A9(B8) in X31 influenza infection. Three female Thy1.1 mice aged 8-12 weeks received 15 mg/kg A9(B8) via 9.5 mL/kg i.v. tail vein injection in PBS. Three female Thy1.1 mice aged 8-12 weeks

received 15 mg/kg A9(B8) via 9.5 mL/kg i.p. injection in PBS. 1 hour later, all six mice received $3x10^3$ pfu X31 via 50 μL intranasal injection in PBS. 6 hours post-A9(B8) administration, all treated mice and three untreated, uninfected mice (naïve) were tail bled to collect whole blood. Mice were weighed daily and humanely killed on day 4 of infection. Bronchoalveolar lavage (BAL), lungs, mediastinal lymph node, spleen and sera were collected from each mouse. Figure created using Biorender.com.

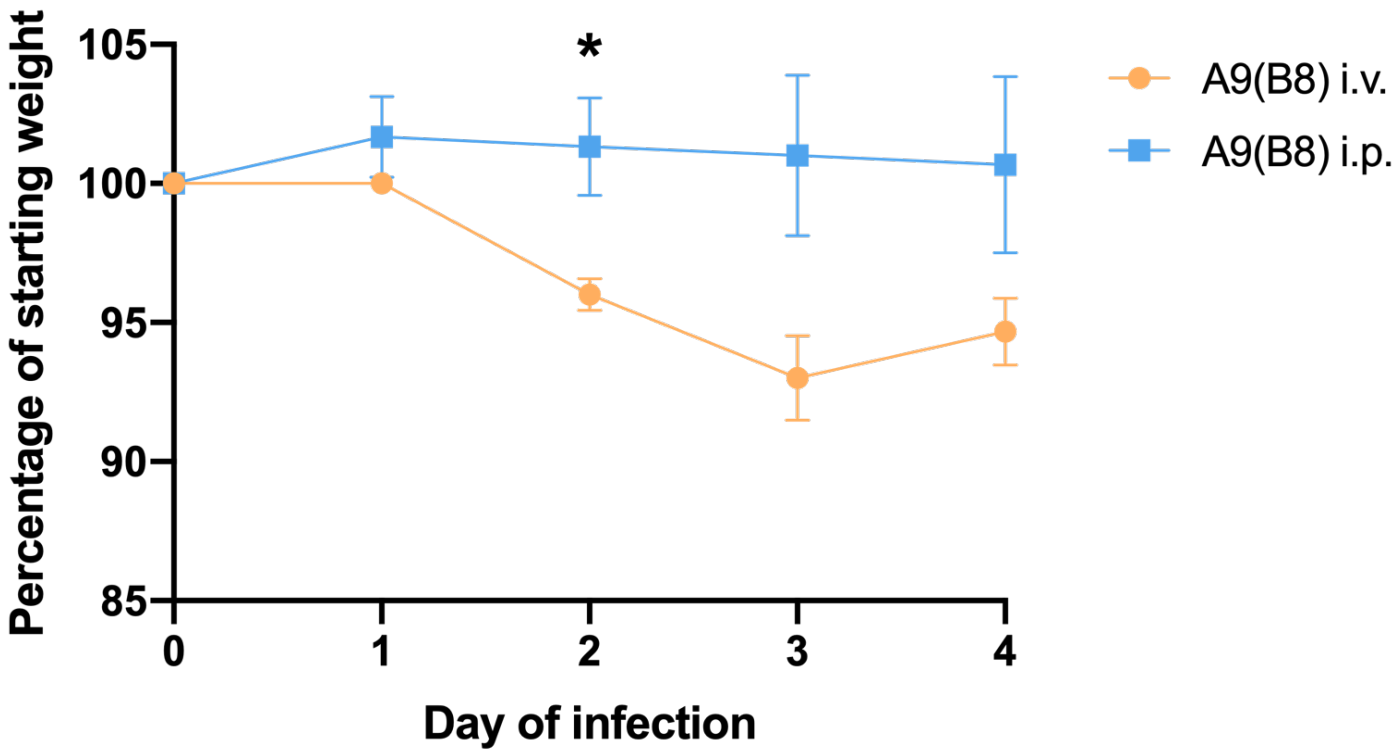

Figure 4.8. Percentage of starting body weight shown over 4 days of X31 infection. Mice were treated with 15 mg/kg of anti-ADAM17 antibody A9(B8) via i.v. or i.p. injection, 1 hour prior to $3x10^3$ pfu X31 infection. Mice were humanely killed on day 4 of infection. Error bars are mean $\pm$ SEM, n=3. Unpaired T-test at each timepoint. *=$p \leq 0.05$.

4.2.6 The effect of increased ADAM17 inhibitor dosage and new administration route, on ability to block PMA-induced L-selectin shedding on lymphocytes

To address the question of whether A9(B8) can effectively block ADAM17-mediated L-selectin shedding on lymphocytes *in vivo*, whole mouse blood was collected at two time points post-A9(B8) administration. Whole blood was tested to account for low volumes of sera which would have been yielded from tail bleeds. A PMA-induced L-selectin shedding assay was utilised on whole blood, to determine if 15 mg/kg A9(B8) was enough to block ADAM17-mediated L-selectin shedding on circulating murine lymphocytes 6 hours and 4 days post-administration. CD4 T cells were not able to be investigated in this experiment due to technical errors.

Firstly, to establish whether there was enough A9(B8) circulating to block L-selectin shedding early after dosage, a 6 hour timepoint post-A9(B8) administration was chosen, to allow for optimal antibody distribution around the body (Yip et al. 2014). The i.v. treated group had significantly higher levels of inhibition of L-selectin shedding on CD8 T cells compared to the untreated group (=$p \leq 0.001$) (Figure 4.9 A). Due to very few CD8 T cells found in two mice of the i.p. treated cohort, no statistical analysis was carried out on this group (Figure 4.9 A). However, the 1 mouse analysed in the i.p. group had levels of inhibition of L-selectin shedding higher than 7 μM exogenous A9(B8) added to untreated blood (Figure 4.9 A). Within the B cell proportion of cells, the i.p. treated and untreated groups had a significantly lower inhibition of L-selectin shedding compared to the i.v. group (*=$p \leq 0.05$) (Figure 4.9 B).

Furthermore, a 4 day timepoint after A9(B8) administration was investigated, to ascertain whether there was enough A9(B8) circulating in the bloodstream by day 4 to block L-selectin shedding (Figure 4.9 C, D). There was no significant difference between the inhibition in L-selectin shedding on CD8 T cells from untreated mice and the i.v. treated mice on day 4 (Figure 4.9 C). This was also true of the i.p. treated group (Figure 4.9 C). When analysing B cell populations, there were also no differences seen between the untreated, i.v. and i.p. groups

on day 4 (Figure 4.9 D). 7 μM of exogenous A9(B8) added to serum from untreated mice had a more efficacious effect in CD8 T cells, with 84.8% blockage of L-selectin shedding, compared to 66.0% in the B cell population (Figure 4.9 C, D).

Collectively, these findings show that levels of A9(B8) in the bloodstream 4 days post-administration were insufficient to block ADAM17-dependent shedding of L-selectin. This suggests concentrations are below 29 nM *in* vivo at this timepoint; the lowest dosage of A9(B8) with a detectable inhibition of L-selectin shedding, as demonstrated in chapter three (Figure 3.1). However, there was clear inhibition of L-selectin shedding 6 hours post-A9(B8) administration (Figure 4.9 A-D).

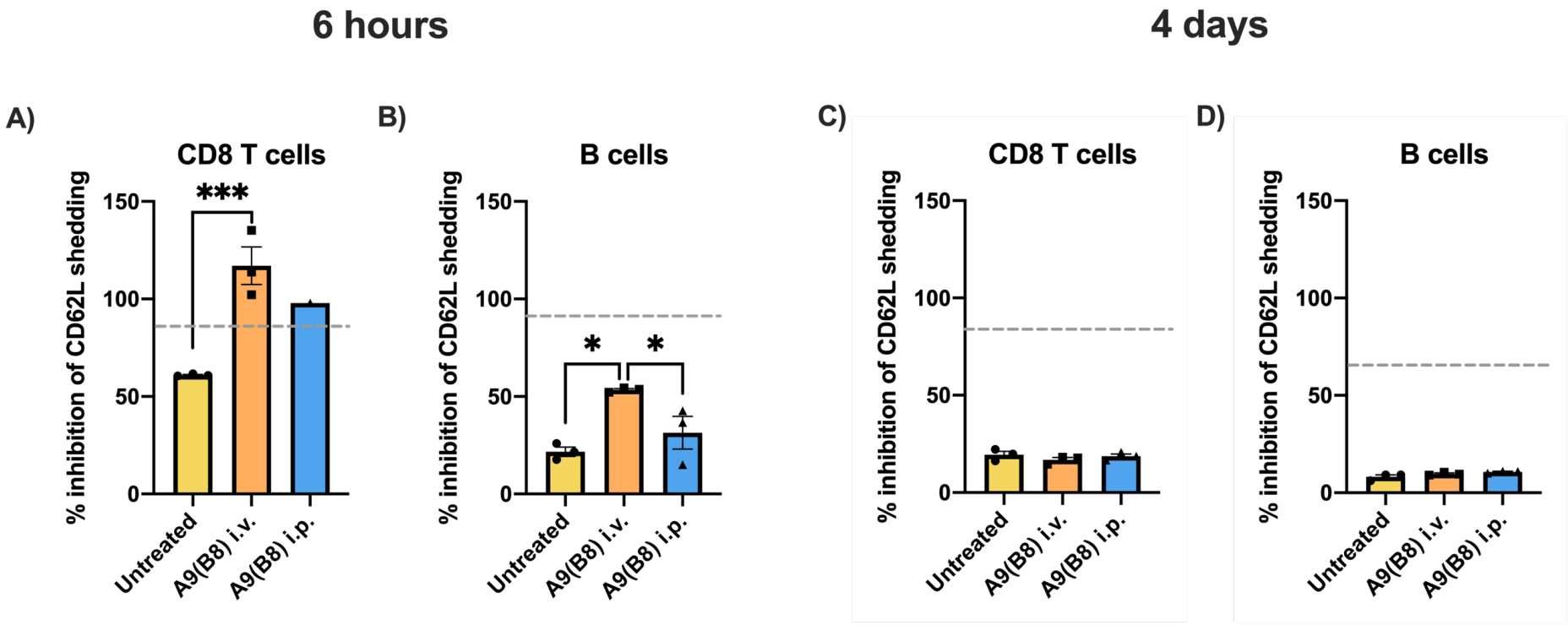

Figure 4.9. Percentage inhibition of L-selectin shedding in mice, 6 hours, and 4 days post-A9(B8) treatment. Mice were treated with 15 mg/kg of anti-ADAM17 antibody A9(B8) 1 hour prior to $3x10^3$ pfu X31 infection, either via i.v. or i.p. injection or left untreated (naïve). Mice were tail bled 6 hours-post A9(B8) administration for whole blood collection. Mice were humanely killed on day 4 of infection and blood collected via cardiac puncture. 50 μL of whole blood was treated with either 5 μM PMA or DMSO as vehicle control. Cell surface L-selectin (CD62L) was measured on lymphocytes by flow cytometric analysis. Cells gated on lymphocyte profile via forward and side scatter, single, live cells. Exogenous A9(B8) was added to peripheral blood from naïve mice to determine maximal levels of inhibition. **A)-D)** Percentage inhibition of CD62L shedding. This was calculated by presenting PMA treated CD62L MFI as a percentage of DMSO control treated CD62L MFI on blood from untreated mice with 7 μM exogenous A9(B8) (grey dashed line), blood from untreated mice alone (yellow), blood from A9(B8) i.v. treated (orange) or A9(B8) i.p. treated mice (blue). **A-B)** 6 hours-

post A9(B8) administration. **A)** CD8 T cell population, **B)** B cell population. **C-D)** 4 days-post A9(B8) administration. **C)** CD8 T cell population, **D)** B cell population. Error bars are mean ± SEM, n=4. One-way ANOVA with Tukey's multiple comparisons test. *=$p \leq 0.05$. ***=$p \leq 0.001$.

4.2.7 Detection of ADAM17 inhibitor in tissues of X31 influenza virus infected mice

A secondary antibody against A9(B8) was used in flow cytometric analysis, to determine whether A9(B8) could be detected within tissues and cells of interest following X31 IAV infection. Lungs and med LNs were prepared into single cell suspensions and stained with goat anti-human IgG-Fc-FITC (Merck) which binds A9(B8). Cells were also stained with anti-CD8a PerCP/Cyanine5.5 (Biolegend) to detect CD8 T cells. As a positive control for detection of cell surface binding of A9(B8) to CD8 T cells, 7 μM of exogenous A9(B8) was incubated with splenocytes and suspensions of lung cells from untreated, uninfected mice for 30 minutes and washed, prior to detection using anti-human IgG-Fc FITC.

When splenocytes from naïve mice were incubated with 7 μM of exogenous A9(B8) and anti-human IgG-Fc FITC, the MFI was 405 on CD8 T cells, in comparison to 167 with A9(B8) alone and 187 with IgG-Fc FITC alone (Figure 4.10 A). The MFI of IgG-Fc FITC was even lower on med LNs collected from A9(B8) treated mice on day 4 after administration. The average IgG-Fc FITC MFI was 101 in the i.v. group and 123 in the i.p. group (Figure 4.10 A). These values were comparable to the average MFI of med LNs from naïve mice treated with IgG-Fc FITC at 89 (Figure 4.10 A).

Additionally, lungs from naïve mice were incubated with 7 μM exogenous A9(B8) and anti-human IgG-Fc FITC and CD8 T cells analysed. The MFI for this sample was much higher than for the spleen at 1416, whilst control MFIs were 418 and 392 with A9(B8) alone and IgG-Fc FITC alone, respectively (Figure 4.10 B). The average lung MFIs for mice treated with A9(B8) were even lower at 301 for the i.v. treated group and 312 for the i.p. group (Figure 4.10 B).

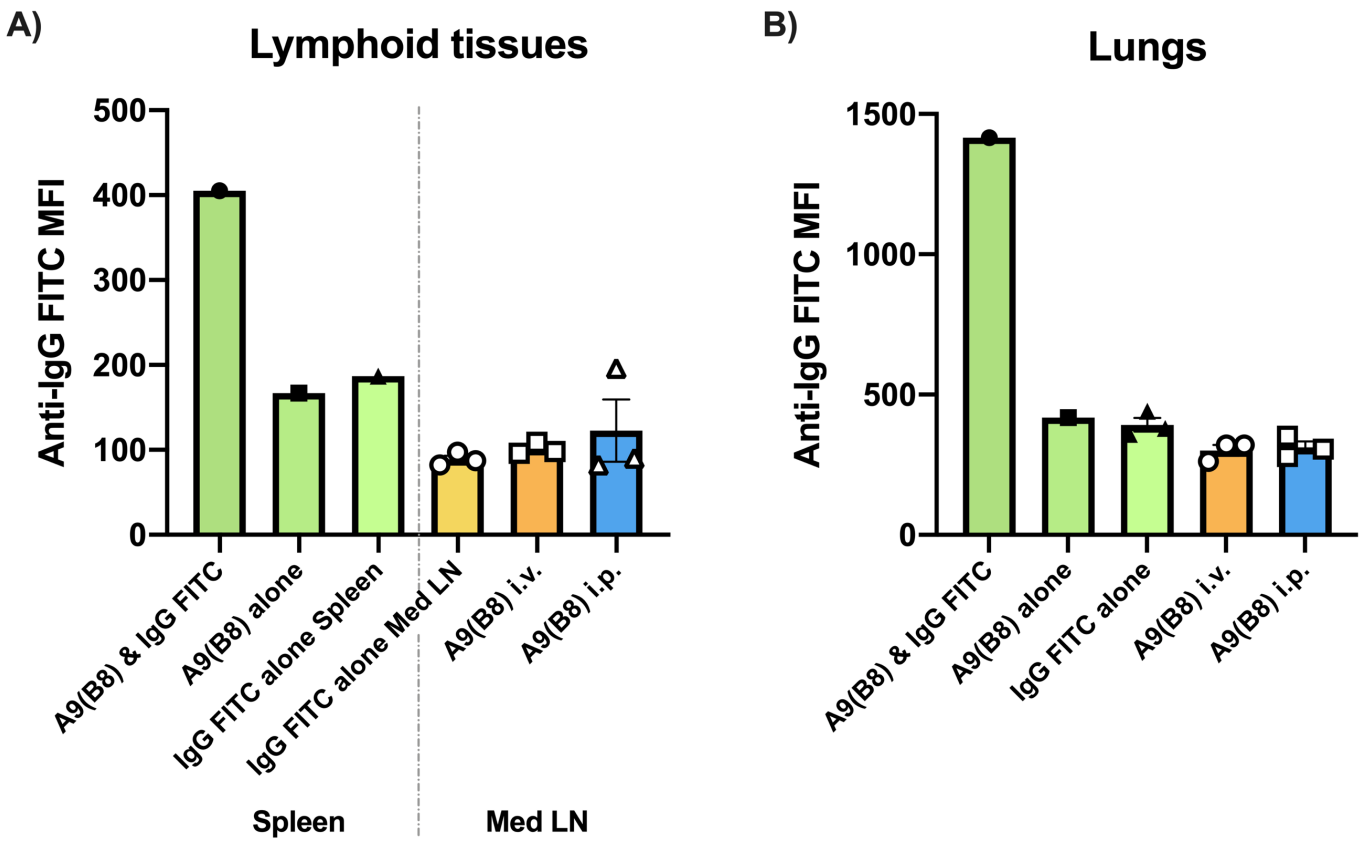

Figure 4.10. Detection of A9(B8) on CD8 T cells *ex vivo*. Mice were treated with 15 mg/kg of anti-ADAM17 antibody A9(B8) 1 hour prior to $3x10^3$ pfu X31 infection, either via i.v. or i.p. injection or left untreated and uninfected (naïve). Mice were humanely killed on day 4 of infection and lungs and mediastinal lymph nodes (med LN) were collected. A spleen was also collected from an untreated mouse. Cells gated on lymphocyte profile via forward and side scatter, single cells, live cells, CD8a positive cells. **A)** Spleen and med LN anti-human IgG-Fc-FITC MFI. Green bars: spleen CD8

cells from untreated mice treated with either 7μM exogenous A9(B8) and anti-human IgG-Fc-FITC, 7μM exogenous A9(B8) alone or anti-human IgG-Fc-FITC alone, yellow bar; med LN CD8 cells from untreated mice treated with anti-human IgG-Fc-FITC alone, orange bar; med LN from i.v. A9(B8) treated mice, blue bar; med LN from i.p. A9(B8) treated mice. Grey dashed line represents spleen to the left and med LN to the right. **B)** Lung anti-human IgG-Fc-FITC MFI. Green bars: lung CD8 cells from untreated mice treated with either 7μM exogenous A9(B8) and anti-human IgG-Fc-FITC, 7μM exogenous A9(B8) alone or anti-human IgG-Fc-FITC alone, orange bar; lungs from i.v. A9(B8) treated mice, blue bar; lungs from i.p. A9(B8) treated mice. Error bars are mean ± SEM, n=1/n=3. One-way ANOVA with Tukey's multiple comparisons test, not significant.

4.2.8 Protein concentration and purity of A9(B8)

Due to long term -80^{o}C storage, it was appropriate to re-test the protein concentration and purity of A9(B8) to confirm its use for ongoing experiments. Nanodrop protein concentration analysis demonstrated that A9(B8) was of similar concentration as when delivered, as stock was originally at 2.6 mg/mL and was re-measured at 2.2 mg/mL (Table 4.2). An SDS-PAGE of A9(B8) was also carried out, using a human IgG2 isotype antibody as a control. A fully intact human IgG2 antibody should have a single band visible at 150 kDa as seen with the non-reduced IgG2 isotype control lane (Figure 4.11). Whilst there is a strong band at 150 kDa with non-reduced A9(B8), there were some other fragments detected, mainly around 30, 55, 80 and 115 kDa (Figure 4.11). When an antibody is exposed to reducing conditions, it should separate into heavy and light chains which can be visible at 60 kDa and 30 kDa, respectively, as seen with the reduced human IgG2 control lane (Figure 4.11). There are strong bands visible for reduced A9(B8) at 30 kDa and 60 kDa, however, there were other fragments detected, mainly at 90 kDa 125 kDa (Figure 4.11).

Table 4.2. Protein concentration of human IgG2 anti-ADAM17 antibody A9(B8). Stock of A9(B8) was tested for protein concentration using NanoDrop 2000/2000c (ThermoFisher Scientific).

Original A9(B8) stock concentration	Re-tested A9(B8) stock concentration
2.6 mg/mL	2.2 mg/mL

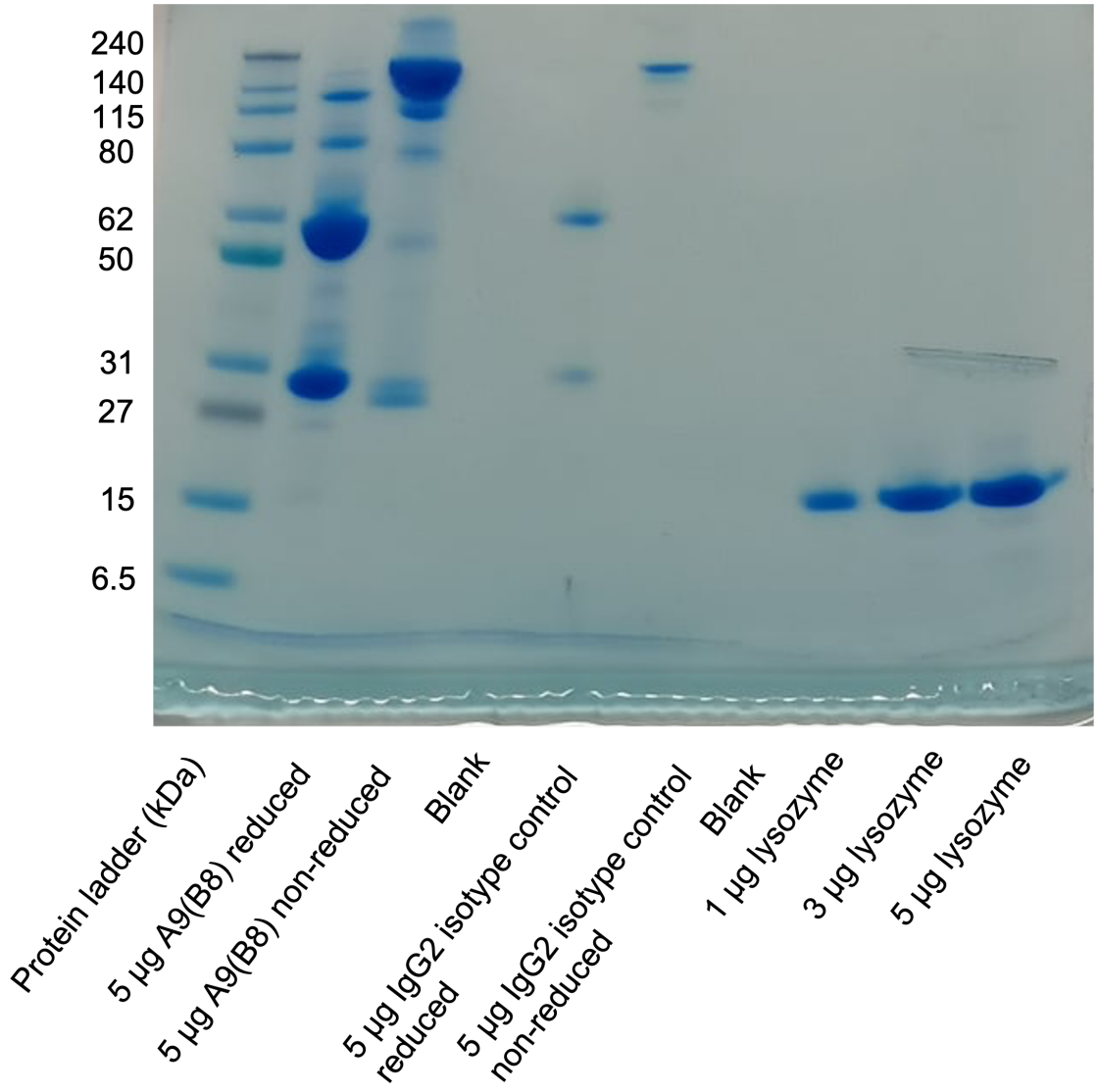

Figure 4.11. Reduced and non-reduced protein gel of human IgG2 anti-ADAM17 antibody A9(B8). 1, 3 or 5 µg of protein sample or protein ladder was mixed with sample buffer (with 0.5 M DDT for reducing conditions) and loaded onto NuPAGE™ 4-12 % Bis-Tris Plus Gel and run in NuPAGE™ MES SDS running in a Bolt Mini Gel Tank. Gel tank was powered via Bio-Rad Powerpac 200 power supply and run at 200 V for 25 minutes. Gels were removed from casing and stained for 30 minutes using quick coomassie stain. Left to right; protein ladder, 5 µg A9(B8) reduced, 5 µg A9(B8) non-reduced, 5 µg human IgG2 isotype control reduced, 5 µg human IgG2 isotype control non-reduced, 1 µg lysozyme, 3 µg lysozyme, 5 µg lysozyme.

4.3 Discussion

Initial *in vivo* findings using 10 mg/kg of anti-ADAM17 antibody A9(B8) in a mouse model of X31 IAV, suggested that this treatment did not improve virus clearance at this dose, over a 7 day infection (Figure 4.3). There was only a significant difference in weight loss on day 1 of infection (Figure 4.2), and there were no differences in levels of soluble L-selectin, cytokines, or chemokines in BALF on day 7 of infection (Figure 4.4, 4.5). Together with the inability of sera from A9(B8) treated mice to block L-selectin shedding on lymphocytes (Figure 4.6), this suggested that 10 mg/kg of A9(B8) was insufficient to inhibit ADAM17 dependent shedding of L-selectin expression on CD8 T cells throughout the period of infection studied. Consequently, viral clearance was not affected, likely because the homing of CTLs to sites of virus infection was not impacted by A9(B8) treatment.

One mouse treated with A9(B8) within this *in vivo* experiment, had consistently different results compared to the other mice within its treatment group, and mice within the control group. ‘Mouse 1’ had higher IAV titres analysed via both plaque assay and RT-qPCR (Figure 4.3). However, mouse 1 retained weight slightly better throughout the course of infection (Figure 4.2). This suggested that weight loss and pathogenicity of infection were not directly correlated.

Aside from the outlier of ‘mouse 1’, there was a trend to suggest lower X31 viral load in the lungs of mice on day 7 of infection in the A9(B8) treated group compared to the control group, when tested via plaque assay (Figure 4.3 A). However, the groups were very comparable when viral load was tested by qPCR (Figure 4.3 B). The differences between these assays may be attributed to the dead virus that could be replicated in the qPCR assay, as mRNA from dead virus may be present in the lungs. Whereas plaque assays are a measure of live replicating virus.

Soluble L-selectin in BALF measured on day 7 of infection was elevated in mouse 1 at 720 ng/mL compared to a group average of 527 ng/mL (Figure 4.4). Cytokine and chemokine profiles in BALF on day 7 of infection were also

elevated (Figure 4.5). The only cytokines not elevated were CXCL1 and IL-6 (Figure 4.5 B, K). CXCL1 is a chemokine which has roles in neutrophil recruitment and activation. Neutrophil accumulation in the lungs peaks at day 3 of X31 infection in B6 mice, therefore, due to the timepoint investigated, the peak neutrophil response may have passed, explaining the levels of CXCL1 seen in this mouse (Tate et al. 2009). IL-6 is a pro-inflammatory cytokine with important roles in T cell responses in viral infection. IL-6 deficiency in mice was previously found to increase IFN-α and TNF-α production in mouse models of IAV, as observed in this experiment (Lauder et al. 2013), (Figure 4.5 C, J). Increased levels of IFN-α, IFN-β, and IFN-γ may suggest a higher dose of X31 virus had been given to this mouse, as interferons have key roles in controlling virus infection in mice and have been correlated with virus load and virulence in mouse IAV infection (McLaren and Potter 1973).

Another possibility is that mouse 1 had an adverse reaction to A9(B8) treatment, or an existing infection. Mouse 1 sera did not exhibit any differences in the ability to block L-selectin shedding, and therefore did not suggest a higher dose of A9(B8) had been administered and caused adverse effects (Figure 4.6). However, due to the possibility of accelerated clearance of this drug *in vivo*, it is difficult to make a definitive conclusion on this.

Sera collected from mice on day 7 of infection were not able to block ADAM17-dependent L-selectin shedding on lymphocytes from naïve mice, suggesting there was not enough A9(B8) circulating by this timepoint to maintain L-selectin on the cell surface of CD8 T cells. In CD4 T cells treated with 7 µM A9(B8), there were cell surface levels of L-selectin above basal levels, suggesting a role for ADAM17 in constitutive L-selectin shedding (Figure 4.6 B). This was also observed in chapter three, whereby A9(B8) was able to block L-selectin shedding from CD4 T cells *in vitro* to levels above those on starting lymphocytes (Figure 3.1 B, 3.4 B). Published data suggests that ADAM17 does not control basal shedding of L-selectin *in vivo*, however, this has not been tested in CD4 T cells *in vitro* to date (Mohammed et al. 2019).

These initial findings led us to believe that an increased dosage of 15 mg/kg A9(B8) would be beneficial in this model, as well as shortening the course of

infection from 7 to 4 days. This was to ensure maximum chance of inhibiting L-selectin shedding *in vivo*. Further to this, an increased viral dosage of $3x10^3$ pfu X31, compared to $1x10^3$ pfu X31 in the previous experiment was chosen to increase pathogenicity across the shorter period of the experiment. Efficacy of A9(B8) had already been shown in a murine pancreatic cancer model, whereby mice were dosed with 10 mg/kg A9(B8) via i.v. injection (Ye et al. 2017). Therefore, another possibility was that A9(B8) being dosed via i.p. injection was limiting the distribution of the antibody treatment. A new *in vivo* experiment was designed to directly compare i.v. and i.p. administration routes, with increased dosage of A9(B8) given 1 hour before $3x10^3$ pfu X31 infection (Figure 4.7). Mice were then humanely killed on day 4 to assess whether this dosage and model was sufficient to block L-selectin shedding in a model of X31 IAV infection.

Mice treated with 15 mg/kg A9(B8) i.v. 6 hours prior to X31 infection showed a trend of more weight loss throughout the course of infection compared to mice administered A9(B8) via i.p. injection. However, this was only statistically significant on day 2 of infection (Figure 4.8). Nevertheless, 15 mg/kg i.p. A9(B8) appeared to protect from weight loss caused by $3x10^3$ pfu X31, which was not seen with 10 mg/kg A9(B8) and $1x10^3$ pfu X31 (Figure 4.2, 4.8). Anorexia and dehydration are the main symptoms of IAV infection which result in weight loss in mice and are thought to be caused by inflammatory mediators. There have been correlations found between levels of BALF pro-inflammatory cytokines and weight loss in IAV infection in mice (DeBerge et al. 2015). Cytokine levels were not measured in this experiment, therefore a conclusion about cytokine levels in relation to weight loss patterns cannot be drawn.

The levels of A9(B8) in the bloodstream on day 4 following administration of 15 mg/kg A9(B8) either i.v. or i.p. were insufficient to inhibit PMA-induced L-selectin shedding in lymphocytes (Figure 4.9 C, D). However, 6 hours post-treatment with 15 mg/kg A9(B8) i.v. blood levels of A9(B8) were sufficient to block L-selectin shedding in CD8 T cells but, not in B cells (Figure 4.9 A, B). Mice treated via i.p. injection did not significantly block L-selectin shedding, and within the B cell population this was significantly worse than the i.v. group (Figure 4.9 B). Notably, within the CD8 T cell population, it appears that the i.p. group sufficiently blocked PMA-induced L-selectin shedding, nevertheless, this

is n=1 due to lack of CD8 T cells detected in two of the mice in this group (Figure 4.9 A). These data suggest that 15 mg/kg A9(B8) is sufficient to maintain L-selectin on lymphocytes 6 hours post-treatment, however, this effect is better with i.v. administration and is diminished by day 4 (Figure 4.9). A further observation of this data was that i.v. blood levels of A9(B8) were sufficient to increase cell surface L-selectin above starting levels of CD8 T cells from naïve mice (4.9 A). This again suggests a role for ADAM17 in constitutive shedding of L-selectin, which has not been seen previously. A key limitation to these data is that the population of lymphocytes (notably CD8 T cells), was much lower when blood was collected via tail bleed at 6 hours, in comparison to blood collected via cardiac puncture on day 4. This smaller pool of lymphocytes analysed may not be a true representation of the whole population.

A flow cytometric assay was also utilised to indirectly detect A9(B8) in the lungs and med LN of IAV infected mice; A secondary antibody goat anti-human IgG-Fc FITC was used to detect cell bound A9(B8), in tissues. There was a clear upregulation of IgG-Fc FITC on CD8 T cells from spleens and lungs which were treated with 7 μM exogenous A9(B8), suggesting detection of ADAM17 and A9(B8) itself on these cells (Figure 4.10). Levels of A9(B8) were almost 4x higher on CD8 T cells in lungs from naïve mice compared to spleens and proposes a differential expression of ADAM17 in different tissues which is yet to be explored (Figure 4.10). There were no significant differences in anti-human IgG-Fc-FITC MFI shown between naïve, A9(B8) i.v. or A9(B8) i.p. treated mouse tissues (Figure 4.10). Overall, this assay suggests there is a lack of A9(B8) bound to CD8 T cells in the lungs and med LN of treated mice on day 4 of infection (Figure 4.10). An explanation for this finding is that the lungs contain a mucous membrane which is better penetrated by IgA antibodies, whereas A9(B8) is an IgG2 antibody. However, this could also suggest a lack of circulating antibody at this timepoint due to degradation or clearance.

Collectively, this *in vivo* experiment comparing administration routes of 15 mg/kg A9(B8) during murine X31 influenza infection, showed that A9(B8) had minimal efficacy in blocking L-selectin shedding by day 4 of infection. However, there is some efficacy 6 hours post-administration which is improved with i.v. administration (Figure 4.9).

Findings from both *in vitro* and *in vivo* experiments suggest that very high doses of A9(B8) are required to completely block ADAM17-dependent L-selectin shedding on lymphocytes, considerably higher than 200 nM required for other substrates (Ye et al. 2017). This was confirmed when A9(B8) was tested in *in vitro* models of L-selectin and TNF-α shedding in chapter three; 7 μM of A9(B8) was required for complete blockage of L-selectin shedding from CD8 T cells *in vitro* (Figure 3.1). Ye et al. carried out *in vivo* pharmacokinetic analysis of A9(B8) which showed an average concentration of 450 nM *in vivo*, 1 and 4 hours post 10 mg/kg i.v. injection (Ye et al. 2017). However, 6 hours is the optimal time to allow circulation of an antibody (Yip et al. 2014). 330 nM was measured, 24 hours-post 10 mg/kg i.v. injection (Ye et al. 2017). The initial half-life of A9(B8) was shown to be 13 hours in this study, with a terminal half-life of 10.5 days (Ye et al. 2017). 250 nM concentrations found were present in B6 mouse sera 7 days post 10 mg/kg injection (Ye et al. 2017). If this pharmacokinetic profile is true of the mice in this study, 250 nM *in vivo* is insufficient to cause any inhibition of L-selectin on lymphocytes. Nevertheless, pharmacokinetic analysis has not been carried out on IAV infected mice, which may alter drug excretion in the body. To confirm these values found by Ye et al. calculations were also carried out to determine *in vivo* whole-body molar concentrations of A9(B8) at 10 mg/kg and 15 mg/kg doses. This was carried out using published values for plasma and extracellular fluid volumes in mice (Durbin et al. 1992). 237 nM and 356 nM concentrations were calculated for 10 mg/kg and 15 mg/kg respectively, which correlates roughly with *in vivo* pharmacokinetic analyses (Ye et al. 2017).

A daily dosing approach of A9(B8) or implanted pump maybe applicable to this model; however, it seems unlikely to reach dosages capable of blocking L-selectin shedding *in vitro* due to toxicity concerns. ADAM17 targets over 80 substrates involved in several critical process such as TGF-α and EGF ligands. Inhibiting ADAM17 function *in vivo* will have widespread off-target effects which may have their own impacts on viral infection. Further to this, mouse studies carried out by Ye et al. using A9(B8) in the Pdx1Cre;$Kras^{G12D}$;$Trp53^{flox/+}$ pancreatic cancer mouse model did not contain an isotype control treated group, unlike the IAV study carried out in this chapter of

work (Ye et al. 2017). There is a possibility that reduction in tumour volume observed in the pancreatic cancer mouse model could be to do with the antibody treatment itself, or Fc receptor mediated effects rather than blockage of ADAM17 function (Ye et al. 2017). Therefore, we cannot yet confirm whether A9(B8) is a good candidate for *in vivo* mouse studies.

Another suggestion is that the antibody A9(B8) had been broken down into fragments during long term -80^{o}C storage. However, the nanodrop protein concentration analysis confirmed that A9(B8) was of a high stock concentration, similar to the original concentration when purified (Table 4.2). SDS-PAGE of A9(B8) showed some minor degradation of protein fragments, however, strong bands were still visible to show intact antibody (Figure 4.11). Therefore, purity of A9(B8) is unlikely to be the cause of the lack of efficacy seen in experiments.

Limitations to this work include the lack of an IgG2 isotype control group, infected with X31 IAV within the A9(B8) i.v. vs i.p. *in vivo* experiment. This data would have been valuable for interpreting mouse weight loss. The small number of mice in this experiment (n=3) also resulted in low power for statistical analysis. A subsequent limitation to this work is that A9(B8) was not tested in naïve mice, without IAV infection. It is possible that the strong inflammatory response seen with virus infection could be having an altered effect on drug efficacy and excretion.

An improvement to this work would be a direct comparison to the transgenic LΔP mouse strain which contains non-cleavable L-selectin on T cells, which cannot be transcriptionally silenced (Galkina et al. 2003). These mice were shown to have improved CTL homing to sites of IAV infection and subsequent viral clearance (Mohammed et al. 2016). However, LΔP mice are yet to be tested for their effects on X31 viral clearance further than day 4 of infection (Ager lab, unpublished). Therefore, it is possible that L-selectin maintenance on CD8 T cells confers no such advantage in this strain of IAV. Due to technical issues with the flow cytometer used for these experiments, no cell surface data were available to determine levels of L-selectin on CTLs in the lungs on day 7 of X31 infection. If CTLs were found to have high levels of L-selectin on their cell surface at this timepoint, it would not be applicable to continue these

studies, as the maintenance of L-selectin would be proven not to benefit X31 IAV clearance.

As pharmacological inhibition of ADAM17 has not been successful using A9(B8) *in vivo*, the next stage of work would be to determine whether inhibition of ADAM17 is a viable option for maintaining L-selectin *in vivo.* Conditional ADAM17 knockout and ADAM17 radiation chimera mice may be possible avenues for investigating this.

In conclusion, 10 mg/kg of anti-ADAM17 antibody A9(B8) did not improve virus clearance on day 7 in a murine model of X31 IAV infection. 10 mg/kg A9(B8) was insufficient to block L-selectin shedding on lymphocytes. Although, 15 mg/kg of A9(B8) was sufficient to block L-selectin shedding on lymphocytes 6 hours post-administration, however, this effect is diminished by day 4 of X31 IAV infection. A higher dose of A9(B8) is needed to block L-selectin shedding compared to other substrates such as TNF-α. In chapter three, A9(B8) had an IC_{50} of $\geq$261 nM for blocking L-selectin shedding, and $\geq$75 nM for TNF-α shedding. It's likely that doses of A9(B8) needed to effectively block L-selectin shedding on lymphocytes *in vivo*, and subsequently improve viral clearance, would be toxic to mice. Although there is a possibility that ADAM17 may control IAV infection via other substrates, independently of L-selectin. Further work is needed to fully characterise these findings.

Chapter Five

The Impact of Transgenic ADAM17 Inhibition on the role of L-selectin in CD8 T cell Clearance of Murine Influenza Virus

5. The Impact of Transgenic ADAM17 Inhibition on the role of L-selectin in CD8 T cell Clearance of Murine Influenza Virus

5.1 Introduction

As described previously, L-selectin is a homing molecule present on the cell surface of leucocytes. LΔP transgenic mice have a non-cleavable form of L-selectin on T lymphocytes, whereby the cleavage site is swapped for that of P-selectin and is maintained under a CD2 promoter to prevent transcriptional downregulation (Galkina et al. 2003). Using LΔP mice, L-selectin has been shown to improve CTL homing and clearance in mouse models of virus infection and cancer (Mohammed et al. 2016), (Watson et al. 2019). Therefore, it was hypothesised that maintaining L-selectin on the surface of CTLs pharmacologically could be of clinical benefit to patients in the future.

Although there are currently no pharmacological agents available which directly block the cleavage site of L-selectin, there are several inhibitors available which block the function of the enzyme ADAM17. ADAM17 proteolytically cleaves L-selectin from the cell surface, and previous studies have shown that blocking the function of ADAM17 inhibits the shedding of L-selectin (Peschon et al. 1998), (Le Gall et al. 2009), (Mohammed et al. 2019).

In chapters three and four, pharmacological inhibitors of ADAM17 were tested as a clinically translational route of blocking L-selectin shedding. In chapter three, two anti-ADAM17 antibodies were tested for their effects on L-selectin shedding *in vitro*; A9(B8) and D8P1C1. A9(B8) was selected for more efficacious effects in blocking L-selectin shedding with an IC_{50} of $\geq$261 nM compared to $\geq$689 nM for D8P1C1 (Table 3.1). In chapter four, A9(B8) was then tested *in vivo* and found not to improve T cell homing or viral clearance on day 7 of X31 influenza infection.

Whilst A9(B8) was not efficacious in the X31 IAV mouse model, we were still interested to discover whether ADAM17 inhibition resulted in improved CTL driven X31 virus clearance, and to determine whether this would be L-selectin dependent. Therefore, the ADAM17$^{\Delta Zn/\Delta Zn}$ (herein referred to as ADAM17$^{-/-}$) radiation chimera mouse model was chosen as a transgenic method of inhibiting ADAM17 activity *in vivo*. These mice have an exon deletion in the zinc binding catalytic domain of ADAM17 (ΔZn) which inhibits its proteolytic cleavage function. This deletion is suggested to impair protein folding and result in degradation of ADAM17, preventing its cell surface expression (Sahin et al. 2004).

Deletion of ADAM17 in mice leads to embryonic lethality and mice die between embryonic day 17.5 to 1 day post-birth (Peschon et al. 1998). However, ADAM17 radiation chimeric mice are viable and have previously been created (Mohammed et al. 2019). Heterozygous ADAM17$^{+/-}$ mice can be mated to produce ADAM17$^{-/-}$ embryos. Foetal liver stem cells can then be harvested from embryos on gestational day 16.5-17 and cryogenically preserved. Recombination activation gene 1/2 deficient (Rag$^{-/-}$) mice lack T and B lymphocytes, and when sub-lethally irradiated, there is a reduction in the haematopoietic stem cells bone marrow. Foetal liver stem cells can then be injected into the tail vein, for reconstitution 8-12 weeks later (Mohammed et al. 2019). Stromal cells are radioresistant and will not be affected. Whilst non-lymphoid haematopoietic cells will be reduced in number from sub-lethal radiation, injected stem cells are most likely to be reconstituted in the lymphoid lineage of cells. This mouse model previously utilised within the group was a prime candidate to test the effects of ADAM17 inhibition on CTL driven influenza virus clearance *in vivo*.

We hypothesise that transgenic ADAM17 inhibition in radiation chimeric mice will improve CTL recruitment and viral clearance in a mouse model of influenza virus infection, via an L-selectin dependent mechanism.

5.1.1 Aims and Objectives

The aim of this chapter of work is to determine whether transgenic inhibition of ADAM17 improves virus clearance in a mouse model of pulmonary IAV infection and to determine whether this is dependent on L-selectin expression by CD8 T cells.

Objectives:

- To generate a cohort of ADAM17 chimeric mice, that express wild-type ADAM17 ($ADAM17^{+/+}$) or inactive ADAM17 ($ADAM17^{-/-}$) in the lymphoid lineage of leucocytes.
- To generate a suitable assay for phenotyping ADAM17 chimeric mice to determine successful chimerism.
- To determine an optimal timepoint to investigate T cell dependent immunity during X31 influenza virus infection, by comparing viral clearance in wild-type mice and $Rag^{-/-}$ mice deficient in lymphocytes.
- To examine the effects of transgenic ADAM17 inhibition on murine influenza virus clearance, and to determine whether virus clearance, if any, is L-selectin dependent.

5.2 Results

5.2.1 Generation of ADAM17 radiation chimeric mice

Due to the key roles of L-selectin in CTL homing and viral clearance in mouse models of IAV infection, a method to maintain L-selectin expression on the lymphoid lineage of leucocytes was created *in vivo*. Radiation chimeric mice expressing wild-type ADAM17 ($ADAM17^{+/+}$) or inactive ADAM17 ($ADAM17^{-/-}$) on their lymphocytes were generated via sub-lethal irradiation and i.v. injection of foetal liver stem cells into $Rag^{-/-}$ mice (Figure 5.1). These studies were ethically reviewed and carried out in accordance with the Animals (Scientific Procedures) Act 1986.

Mice were phenotyped for their chimerism by testing functionality of ADAM17 8 weeks post-stem cell injection, via tail blood sampling. This was done by inducing ADAM17 activation via PMA on whole blood and detecting cell surface levels of L-selectin on lymphocytes. This was carried out to determine whether ectodomain proteolytic cleavage was functional.

Six out of eight chimeras from each group successfully generated lymphocytes with the expected phenotypes. Representative dot plots for $ADAM17^{+/+}$ and $ADAM17^{-/-}$ chimeras can be seen for CD8 T cells, CD4 T cells and B cells respectively, with non-chimeric $Rag^{-/-}$ mouse representative plots also shown for reference (Figure 5.2 A, C, E).

$ADAM17^{+/+}$ and $ADAM17^{-/-}$ mice had similar levels of L-selectin on untreated CD8 T cells from whole blood, with average MFIs of 1600 and 1629, respectively (Figure 5.2 B). This was also true of CD4 T cells, although this was slightly lower with an average L-selectin MFI of 1423 on $ADAM17^{+/+}$ cells and 1477 on $ADAM17^{-/-}$ cells (Figure 5.2 D). There was a significantly higher level of L-selectin on $ADAM17^{-/-}$ B cells, with an average L-selectin MFI of 1722 compared to 1196 on $ADAM17^{+/+}$ cells (=$p<0.05$) (Figure 5.2 F).

As predicted, ADAM17$^{-/-}$ chimeras had the same levels of L-selectin on T and B cells before and after PMA treatment (Figure 5.2 B, D, F). ADAM17$^{-/-}$ mice had an average of 9.5-fold higher cell surface L-selectin expression on CD8 T cells compared to ADAM17$^{+/+}$ chimeras when treated with PMA (Figure 5.2 B). Whilst on CD4 T cells L-selectin levels were 4.5 times higher and 16.5 times higher on B cells in ADAM17$^{-/-}$ mice (Figure 5.2 D, F). Together, these data demonstrate successful chimerism with ADAM17 deficiency (ADAM17$^{-/-}$) and sufficiency (ADAM17$^{+/+}$) phenotypes in lymphocytes.

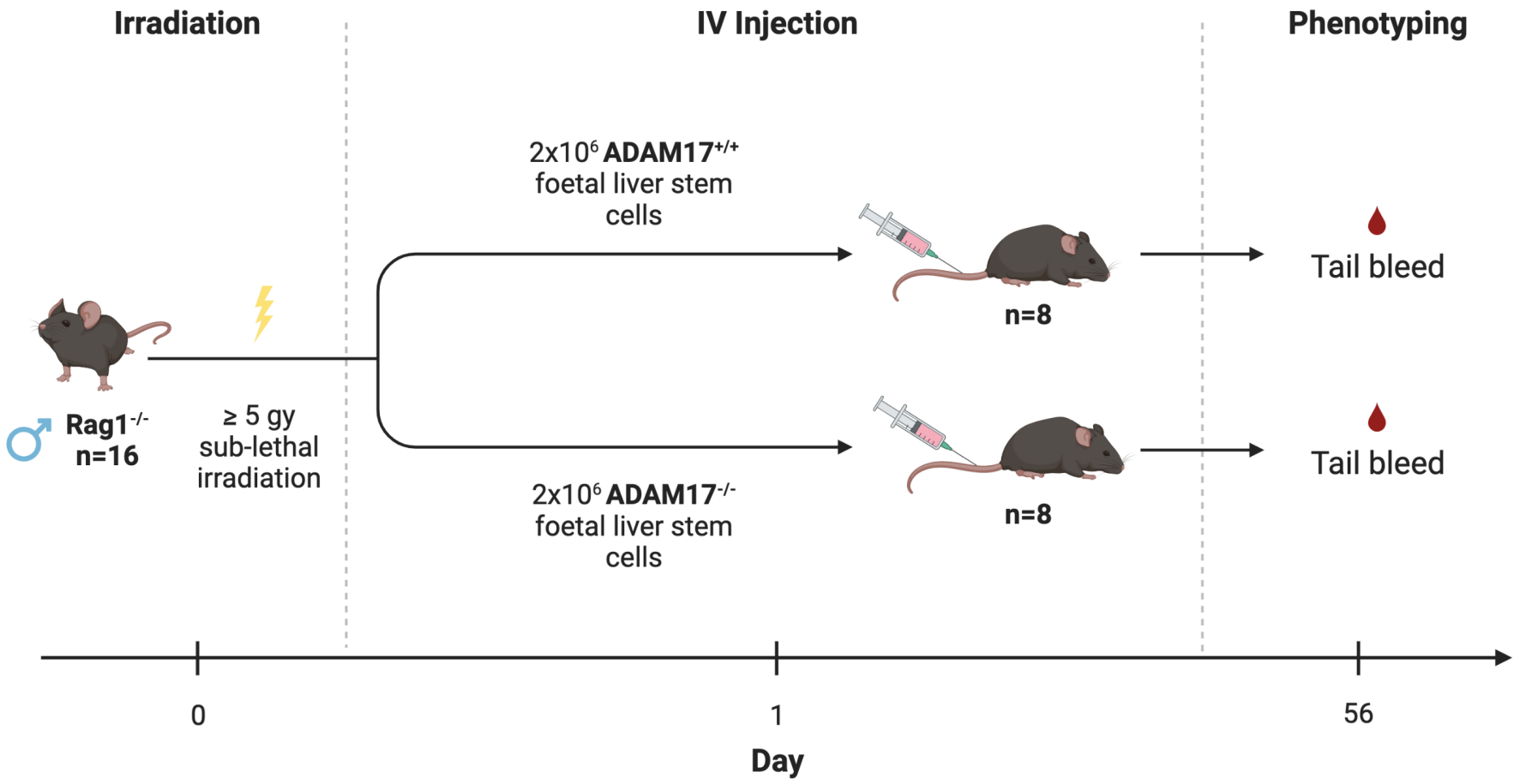

Figure 5.1. ADAM17 radiation chimeric mice experimental plan. Sixteen Rag1$^{-/-}$ mice lacking lymphocytes were sub-lethally irradiated with ≥5 Gy to create 'space' in the bone marrow. The next day mice were intravenously injected with 2x10^{6} foetal liver stem cells in a 9.5 mL/kg volume of sterile

saline; stem cells contained either wild-type $^{(+/+)}$ or inactive $^{(-/-)}$ ADAM17. 8 weeks later, mice were bled via tail-tipping to phenotype for ADAM17 activity in lymphocytes. Figure created using Biorender.com.

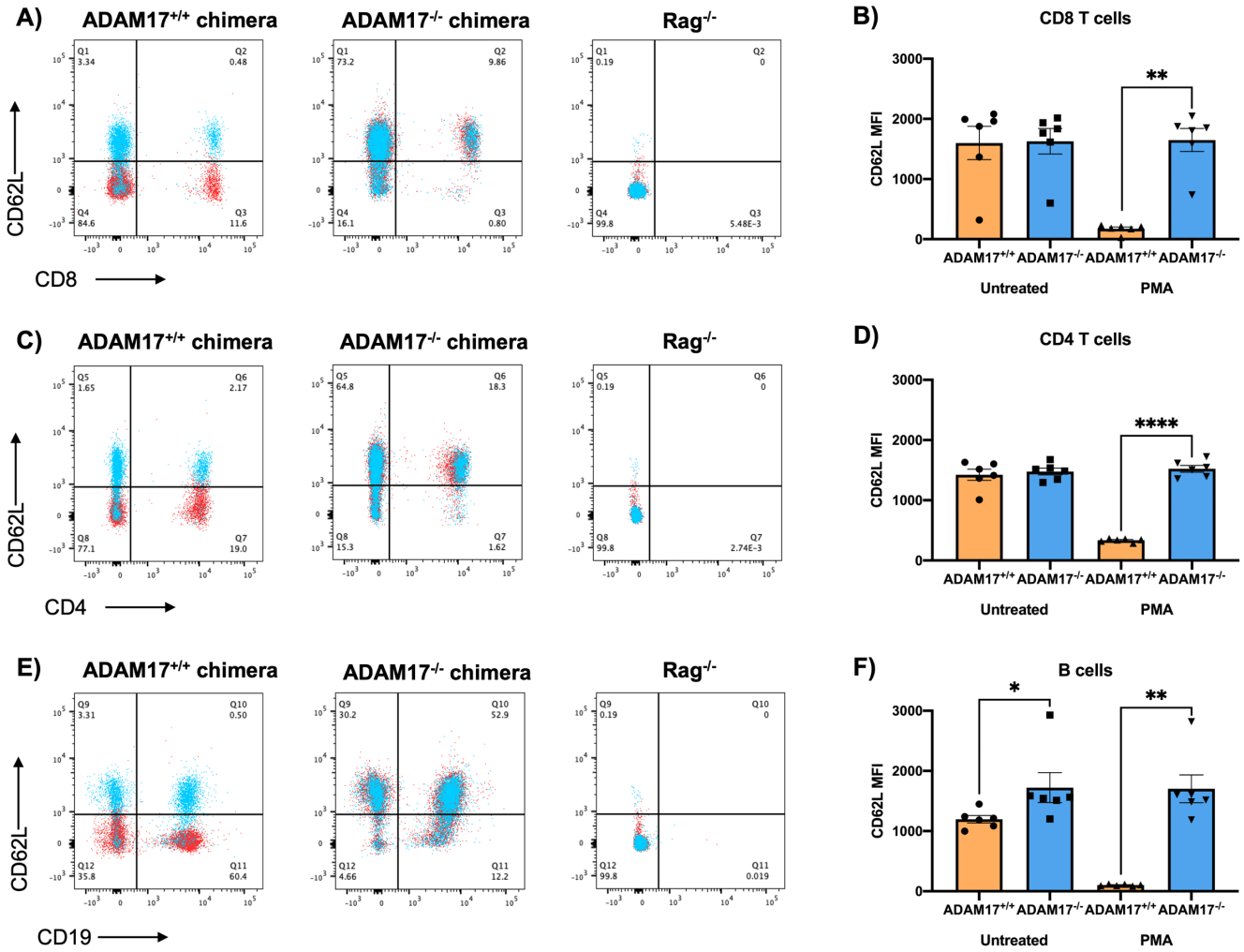

Figure 5.2. ADAM17 radiation chimeric mice phenotyping. Eight Rag1$^{-/-}$ mice injected with ADAM17$^{+/+}$ foetal liver stem cells and eight Rag1$^{-/-}$ mice injected with ADAM17$^{-/-}$ foetal liver stem cells were bled from the tail vein via tail-tipping, using ethyl chloride as local anaesthetic. Whole blood was

treated with 5 μM PMA to induce ADAM17 activation and subsequent L-selectin (CD62L) shedding, or DMSO as a vehicle control. Cell surface L-selectin was measured on lymphocytes by flow cytometric analysis. Cells gated on lymphocyte profile via forward and side scatter, single, live cells. **A)** CD8 representative dot plots X-axis; CD8, Y-axis; CD62L. Blue; untreated, red; PMA treated. **B)** Mean fluorescence intensity (MFI) of CD62L on untreated and PMA treated CD8 T cells. **C)** CD4 representative dot plots X-axis; CD4, Y-axis; CD62L. Blue; untreated, red; PMA treated. **D)** MFI of CD62L on untreated and PMA treated CD4 T cells. **E)** B cell representative dot plots X-axis; CD19, Y-axis; CD62L. Blue; untreated, red; PMA treated. **F)** MFI of CD62L on untreated or PMA treated B cells. Error bars are mean $\pm$ SEM, n=6. Mann-Whitney test (B, F), unpaired T-test (D). *=$p \leq 0.05$. **=$p \leq 0.01$. ****=$p \leq 0.0001$.

5.2.2 Determining the kinetics of T cell dependent immunity in murine influenza virus infection

Before determining the effects of ADAM17 deficient lymphocytes on IAV clearance in comparison with ADAM17 sufficient lymphocytes, an optimal timepoint for analysis of CTL driven viral clearance was investigated.

Wild-type Thy1.1 mice and lymphocyte deficient $Rag^{-/-}$ mice were infected with $1x10^3$ pfu X31 IAV and humanely killed on day 5 for tissue analysis (Figure 5.3). $Rag^{-/-}$ mice used for this experiment were subjected to ADAM17 chimera generation procedures (sub-lethal irradiation and i.v. stem cell injection) but were not reconstituted with donor stem cells, as tested via the L-selectin shedding assay on whole blood. These mice were used as they were the closest matched control to ADAM17 chimeras, which were to be subsequently tested.

$Rag^{-/-}$ mice had significantly more weight loss across the course of X31 infection than wild-type Thy1.1 mice at 1, 3, 4 and 5 days after virus inoculation (Figure 5.4). However, the effects were seen most strongly at day 4 ($p=0.0012$) and day 5 ($p=<0.0001$) (Figure 5.4). Average weight loss on day 5 of infection just was 4% for the Thy1.1 group and 14% for the $Rag^{-/-}$ group (Figure 5.4). Mice were humanely killed on day 5 to avoid reaching home office weight loss limit of 20%.

As $Rag^{-/-}$ mice have no lymphocytes, CD8 T cell numbers on day 5 of X31 infection in BAL, lungs, med LN and spleen of Thy1.1 mice were compared to previous data of Thy1.1 mice on day 7 of X31 infection at the same dose of $1x10^3$ pfu (Figure 5.5). There were no significant differences in the numbers of CD8 T cells found in mouse BAL, on day 5 compared to day 7, but there was a significantly higher number on day 7 in the lungs ($=p<0.05$) (Figure 5.5 A, B). However, there was a potential outlier in each of these graphs, and when removed this suggested a lower number of CD8 T cells in the BAL on day 7 with an average of 1967 cells compared to 12770 on day 5 (Figure 5.5 A). There were no observable differences between CD8 T cell numbers in the med LN or spleen on day 5 compared to day 7 (Figure 5.5).

Influenza virus titres between $Rag^{-/-}$ mice and Thy1.1 mice on day 5 of X31 virus infection showed a trend of lower viral load in mouse lungs of wild-type Thy1.1 with an average of 148,810 pfu/lung compared to 306,383 pfu/lung for the $Rag^{-/-}$ cohort (Figure 5.6 A). qPCR virus titre data also confirmed this trend, however, the difference between groups was less striking with a fold change in gene expression of 0.6 in the $Rag^{-/-}$ group compared to 0.5 for the Thy1.1 group (Figure 5.6 B). Although there was a trend seen, these findings were not statistically significant (Figure 5.6).

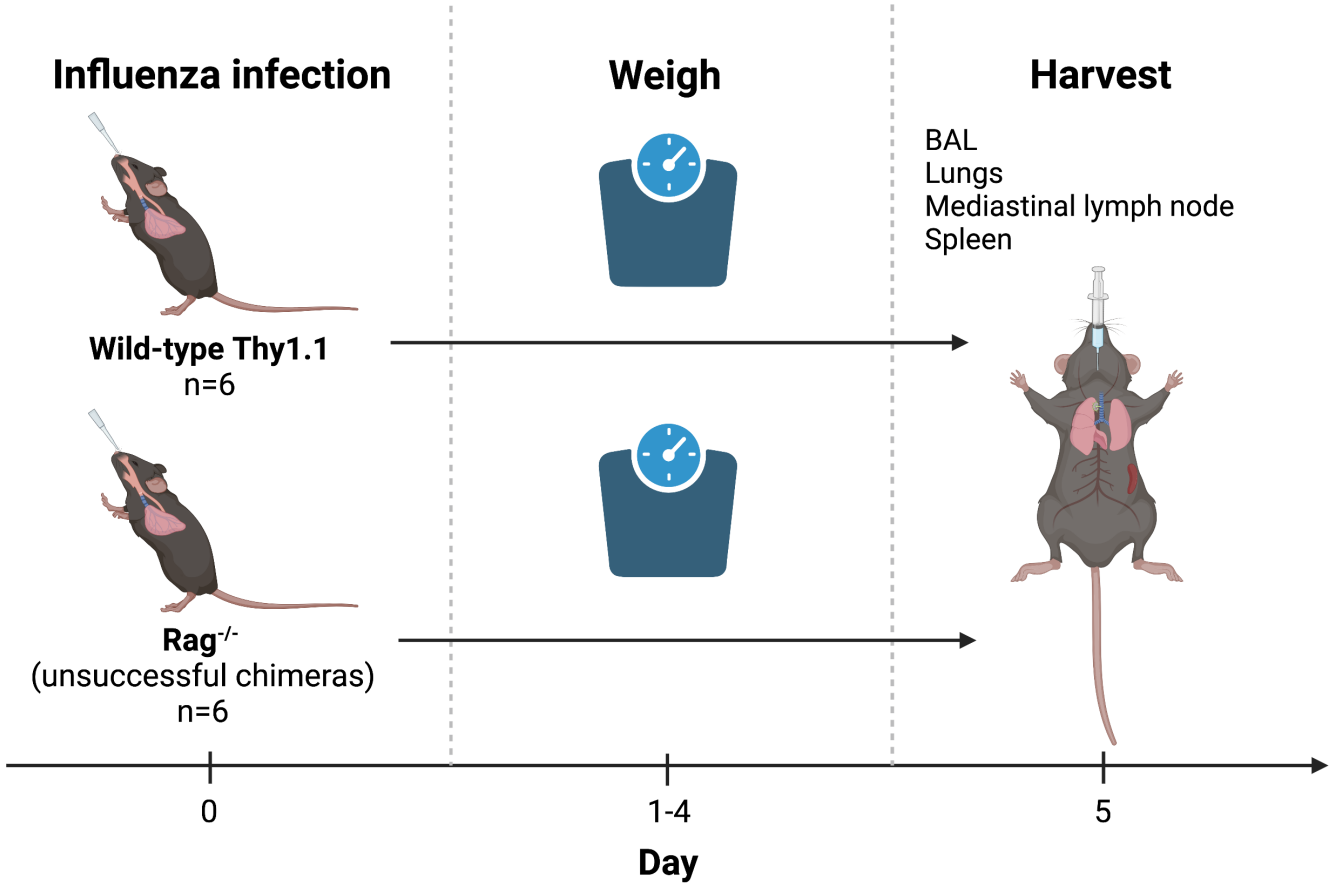

Figure 5.3. Experimental timeline for the X31 influenza virus infection of wild-type Thy1.1 and Rag$^{-/-}$ mice. Six wild-type Thy1.1 and six Rag$^{-/-}$ age-matched mice were weighed and infected with 1x10^{3} plaque forming units (pfu) of X31 influenza A virus, via intranasal administration under isoflurane anaesthesia. Mice were weighed daily and humanely killed on day 5 of infection and bronchoalveolar lavage (BAL), lungs, mediastinal lymph node and spleen excised for analysis. Figure created using Biorender.com.

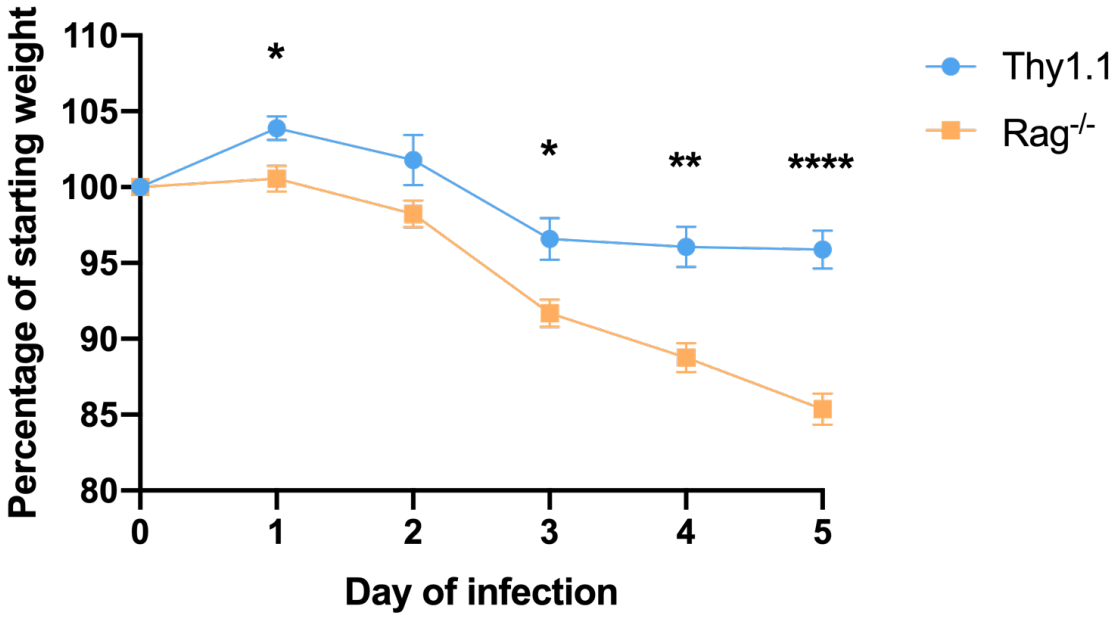

Figure 5.4. Percentage of starting weight over 5 days of X31 infection. Six Thy1.1 mice and six Rag2$^{-/-}$ mice were infected with 1x10^{3} pfu X31 influenza virus on day 0. Mice were weighed daily and humanely killed on day 5. Error bars are mean ± SEM, n=6. Unpaired T-test at each timepoint. *=p≤0.05. **=p≤0.01. ****=p≤0.0001.

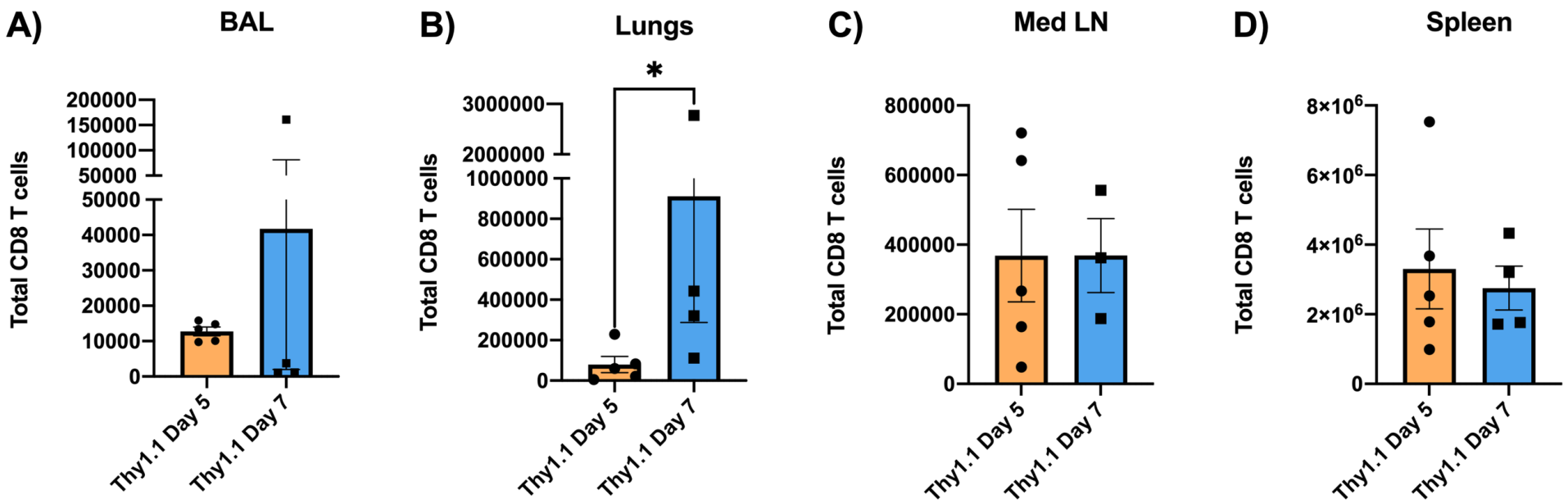

Figure 5.5. CD8 T cell numbers in wild-type mice infected with X31 influenza virus on day 5 and 7 of infection. Thy1.1 mice were infected with $1x10^3$ pfu X31 influenza virus on day 0. Mice were humanely killed on day 5 or day 7 of infection and organs collected for flow cytometric staining and analysis. Cells gated via forward and side scatter, single, live cells. **A)** Total number of CD8 T cells in mouse bronchoalveolar lavage (BAL). **B)** Total number of CD8 T cells in lungs **C)** Total number of CD8 T cells in mouse mediastinal lymph node (med LN). **D)** Total number of CD8 T cells in mouse spleens. Error bars are mean $\pm$ SEM, n=5 (day 5) n=4 (day 7). Mann-Whitney test (A, B), unpaired T-test (C, D). *=$p \leq 0.05$.

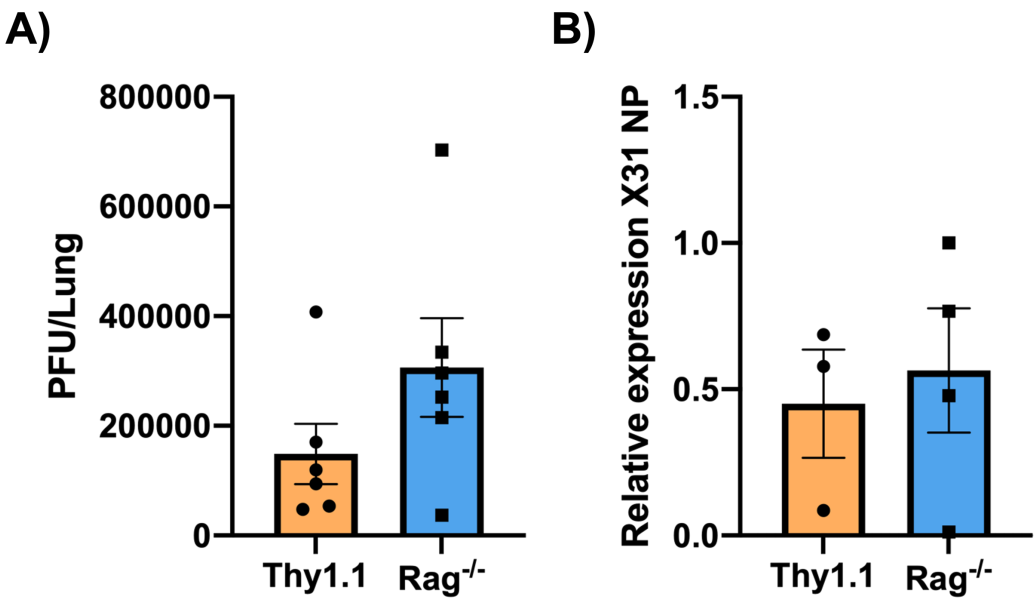

Figure 5.6. Influenza virus titres from mouse Thy1.1 and Rag$^{-/-}$ mouse lungs on day 5 of X31 infection. Six Thy1.1 mice and Six Rag$^{-/-}$ mice were infected with 1x10^{3} pfu X31 influenza virus on day 0. Mice were humanely killed on day 5 of infection and lungs excised for analysis via plaque assay and RT-qPCR. **A)** Plaque forming unit (pfu) per whole lung calculated via plaque assay. n=6. **B)** Fold change in gene expression of X31 nucleoprotein gene (X31 NP) compared to glyceraldehyde-3-phosphate dehydrogenase (GAPDH), calculated using the ΔΔCt method. n=3/4. Error bars are mean ± SEM. Unpaired T-test, not significant.

5.2.3 The effect of transgenic ADAM17 inhibition on welfare of chimeric mice infected with influenza virus

To investigate the effects of ADAM17 inhibition on X31 IAV infection, $ADAM17^{+/+}$ and $ADAM17^{-/-}$ mice were infected with $1x10^3$ pfu of X31 IAV. Mice were then humanely killed on day 5 to investigate effects on L-selectin expression, T cell homing, and viral clearance (Figure 5.7).

Weight loss was measured for 5 days over the course of infection to monitor welfare of mice and pathogenicity of infection (Figure 5.8). There was a significant difference in weight loss between $ADAM17^{+/+}$ and $ADAM17^{-/-}$ mice on day 2 of infection, however, there was no significant difference in weight loss on any other day measured (Figure 5.8). Nevertheless, there was a trend to suggest that $ADAM17^{-/-}$ mice retained weight slightly better than $ADAM17^{+/+}$ throughout the course of infection (Figure 5.8). Mice lost between 10-20% of weight by day 5 (Figure 5.8). Mice were humanely killed on day 5 of infection as several mice reached the maximum weight loss criteria of 20%, as set out by the home office.

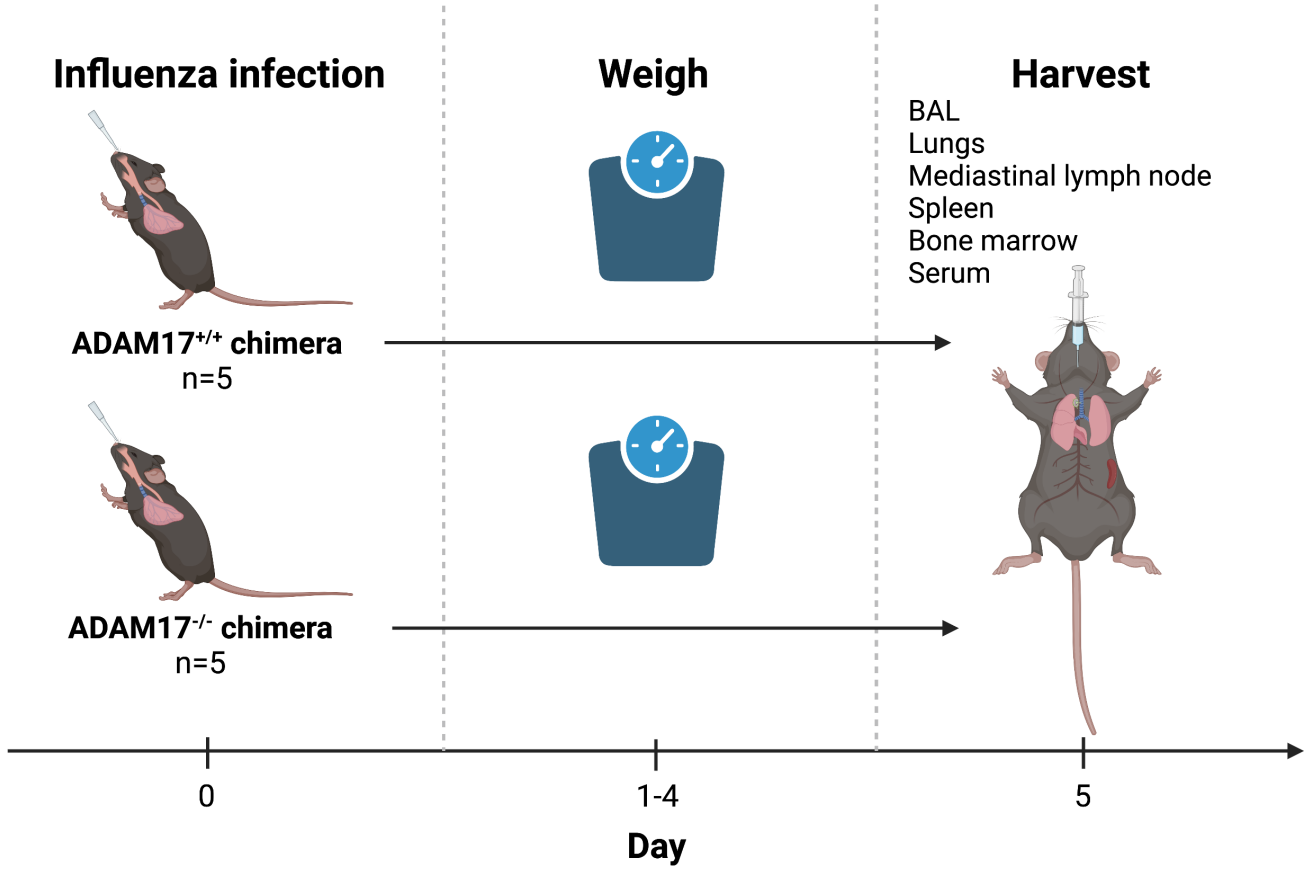

Figure 5.7. Experimental timeline for the X31 influenza virus infection of ADAM17 chimeric mice. Five ADAM17$^{+/+}$ and five ADAM17$^{-/-}$ chimeric mice were weighed and infected with 1x10^{3} plaque forming units (pfu) of X31 influenza A virus, via intranasal administration under isoflurane

anaesthesia. Mice were humanely killed on day 5 of infection and bronchoalveolar lavage (BAL), lungs, mediastinal lymph node, spleen, bone marrow and serum excised for analysis. Figure created using Biorender.com.

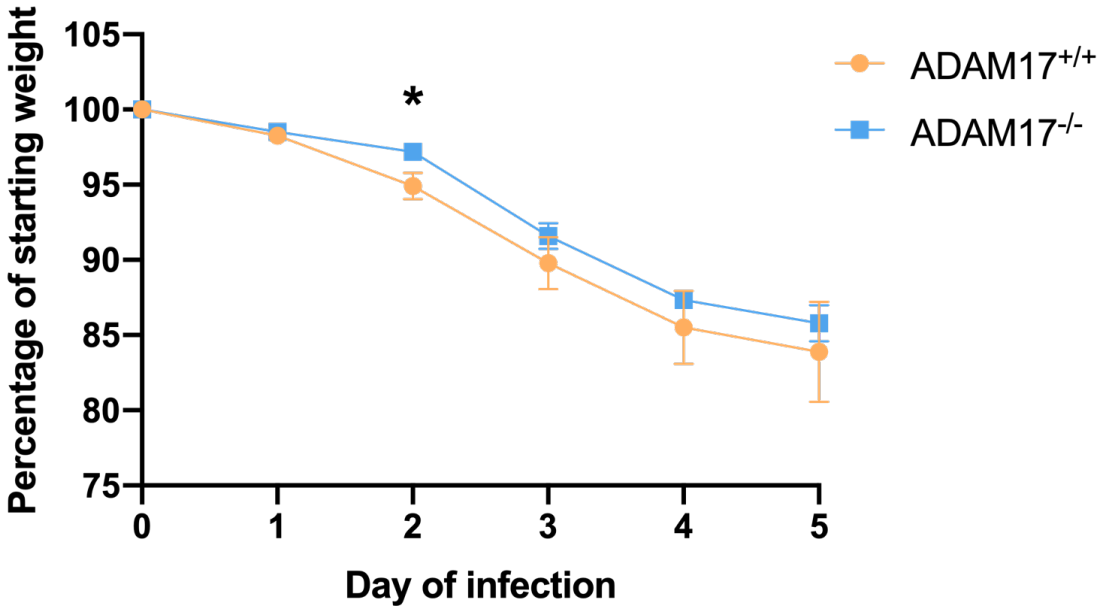

Figure 5.8. Percentage of starting body weight shown over 5 days of X31 infection. ADAM17$^{+/+}$ and ADAM17$^{-/-}$ chimeric mice were weighed and infected with 1x10^{3} pfu X31 influenza virus on day 0. Mice were weighed daily and humanely killed on day 5 of infection. Error bars are mean ± SEM, n=5. Unpaired T-test at each timepoint. *=p≤0.05.

5.2.4 The effect of transgenic ADAM17 inhibition on T cell migration and activation in X31 IAV infection

To investigate the effects of ADAM17 inhibition on T cell migration and activation on day 5 of X31 influenza infection, tissues were harvested and processed for flow cytometric staining. Numbers of CD8 and CD4 T cells were investigated, along with their cell surface levels of L-selectin and activation markers (Figure 5.9, 5.10). CD44 is an activation marker on effector and memory T cells which helps distinguish activated cells from naïve cells. CD69 is an early activation marker which can be detected very soon after lymphocyte activation. The cell surface expression of these molecules were analysed to determine activation status.

There were no significant differences in total numbers of CD8 T cells found in the BAL, lungs, med LN, spleen, or bone marrow on day 5 of infection between ADAM17 sufficient and ADAM17 deficient mice (Figure 5.9 A). Although there was a trend to suggest a higher infiltration of CD8 T cells in the BAL of ADAM17$^{-/-}$ mice (Figure 5.9 A). When analysing CD4 T cells, there were also no significant differences in any organs investigated. However, data showed a trend of increased CD4 T cells in the spleen of ADAM17$^{-/-}$ mice (Figure 5.9 B). The lungs, med LN, spleen and bone marrow had a similar number of T cells present, however the BAL had a 10x lower amount of T cells (Figure 5.9 A, B).

There were significantly increased levels of L-selectin measured on the cell surface of ADAM17$^{-/-}$ CD8 and CD4 T cells in all organs analysed (Figure 5.9 C, D). The greatest difference observed was in the med LN which drains the lungs, where ADAM17$^{-/-}$ mice had 2.8-fold higher levels of L-selectin on CD8 T cells compared to ADAM17$^{+/+}$ mice (=$p<0.0001$) (Figure 5.9 C). ADAM17-dependent shedding of L-selectin from the surface of CD8 and CD4 T cells was detectable in all tissue compartments analysed in ADAM17$^{+/+}$ chimeras, however the extent of shedding varied. For example, there was a greater amount of L-selectin shedding in BAL CD8 T cells compared to BAL CD4 T cells, as the difference between ADAM17$^{+/+}$ and ADAM17$^{-/-}$ MFI was 377 for CD8 T cells compared to 156 for CD4 T cells (Figure 5.9 C, D).

There were low levels of CD44 on CD8 T cells present in mouse lungs, med LN and spleen on day 5 of infection (Figure 5.10 A). MFI of CD44 was higher on CD8 T cells present in the BAL and bone marrow, however, this was lower for ADAM17$^{-/-}$ in the BAL compared to ADAM17$^{+/+}$ mice (Figure 5.10 A). This pattern was also seen of CD4 T cells, however, differences between ADAM17$^{+/+}$ and ADAM17$^{-/-}$ mice were not significant (Figure 5.10 B).

Levels of CD69 were lower in lungs, med LN, spleen, and bone marrow of CD8 T cells, whilst they were higher in BAL CD8 T cells, but this was similar between both groups of mice (Figure 5.10 C). This pattern was also observed in CD4 T cells, although CD69 levels were higher on ADAM17$^{-/-}$ mouse BAL CD8 T cells compared to ADAM17$^{+/+}$ (Figure 5.10 D). There were no significant differences in activation status of CD8 or CD4 T cells found in the BAL, lungs, med LN, spleen, or bone marrow on day 5 of infection between ADAM17 sufficient and ADAM17 deficient mice (Figure 5.10).

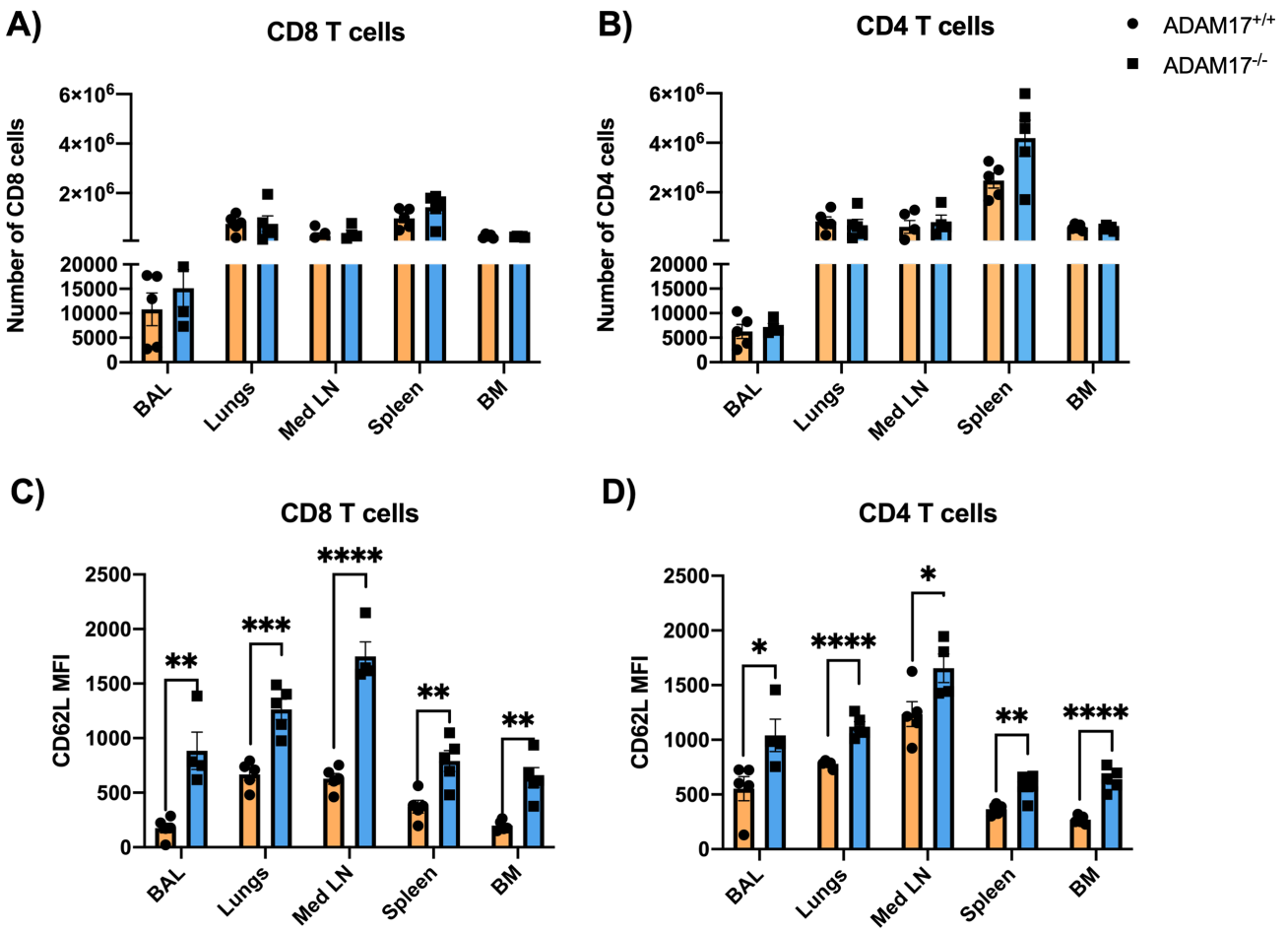

Figure 5.9. T cell numbers and L-selectin expression in ADAM17$^{+/+}$ and ADAM17$^{-/-}$ mice on day 5 of X31 infection. ADAM17$^{+/+}$ and ADAM17$^{-/-}$ chimeric mice were infected with 1x10^3 pfu X31 influenza virus on day 0. Mice were humanely killed on day 5 of infection and organs collected for flow

cytometric staining and analysis (bronchoalveolar lavage (BAL), lungs, mediastinal lymph node (med LN), spleen and bone marrow (BM)). Cells gated via forward and side scatter, single, live cells. **A)** Numbers of CD8 T cells. **B)** Numbers of CD4 T cells. **C)** L-selectin (CD62L) mean fluorescence intensity (MFI) of CD8 T cells. **D)** L-selectin MFI of CD4 T cells. Orange bars; $ADAM17^{+/+}$, blue bars; $ADAM17^{-/-}$. Error bars are mean $\pm$ SEM, n=5. Unpaired T-test. *=$p \leq 0.05$. **=$p \leq 0.01$. ***=$p \leq 0.001$. ****=$p \leq 0.0001$.

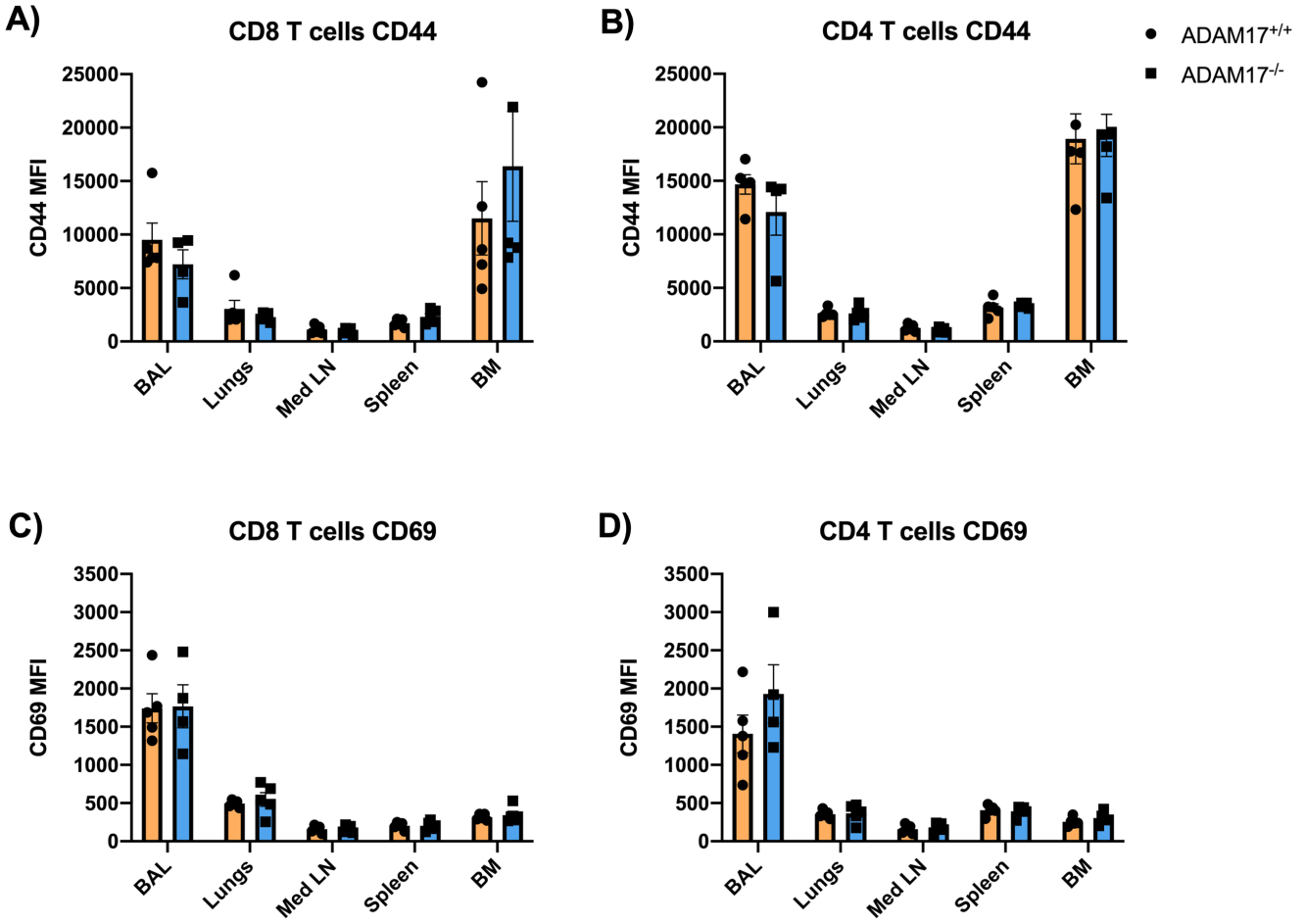

Figure 5.10. T cell activation in ADAM17$^{+/+}$ and ADAM17$^{-/-}$ mice on day 5 of X31 infection. ADAM17$^{+/+}$ and ADAM17$^{-/-}$ chimeric mice were infected with 1x10^{3} pfu X31 influenza virus on day 0. Mice were humanely killed on day 5 of infection and organs collected for flow cytometric staining

and analysis (bronchoalveolar lavage (BAL), lungs, mediastinal lymph node (med LN), spleen and bone marrow (BM)). Cells gated via forward and side scatter, single, live cells. **A)** CD44 mean fluorescence intensity (MFI) of CD8 T cells. **B)** CD44 MFI of CD4 T cells. **C)** CD69 MFI of CD8 T cells **D)** CD69 MFI of CD4 T cells. Orange bars; ADAM17$^{+/+}$, blue bars; ADAM17$^{-/-}$. Error bars are mean $\pm$ SEM, n=5. Unpaired T-test, not significant.

5.2.5 The effect of transgenic ADAM17 inhibition on influenza virus clearance in chimeric mice

ADAM17$^{+/+}$ and ADAM17$^{-/-}$ chimeric mice infected with 1x10^{3} pfu of X31 IAV were humanely killed at day 5 to investigate effects of transgenic ADAM17 inhibition on viral clearance (Figure 5.11). There were no significant differences in viral titres in the lungs of ADAM17$^{+/+}$ and ADAM17$^{-/-}$ mice on day 5 of X31 infection, measured by plaque assay (Figure 5.11 A). This was highly comparable with an average pfu/lung of 148,855 in the ADAM17$^{+/+}$ group and 157,024 pfu/lung in the ADAM17$^{-/-}$ group. There were also no significant differences between viral titres measured by qPCR (Figure 5.11 B). However, the ADAM17$^{-/-}$ group had higher X31 relative gene expression in the lungs with an average of 0.5 compared to 0.3 for the ADAM17$^{+/+}$ group (Figure 5.11 B).

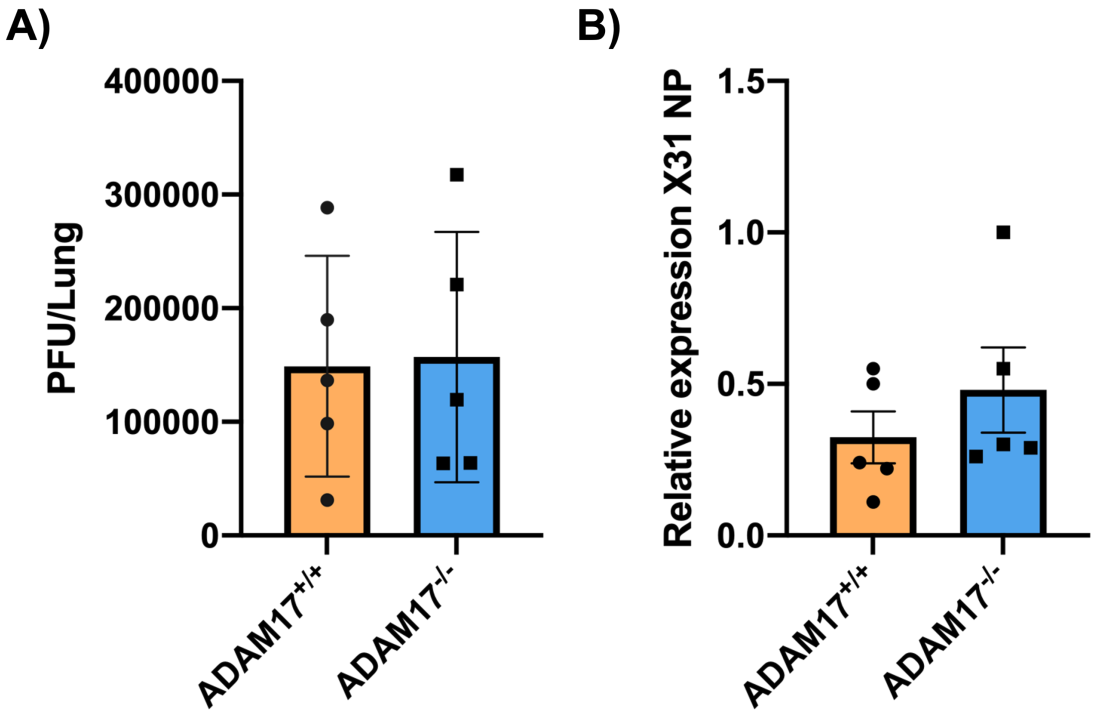

Figure 5.11. Influenza virus titres from ADAM17$^{+/+}$ and ADAM17$^{-/-}$ chimeric mouse lungs on day 5 of X31 infection. ADAM17$^{+/+}$ and ADAM17$^{-/-}$ chimeric mice were infected with 1x10^{3} pfu X31 influenza virus on day 0. Mice were humanely killed on day 5 of infection and lungs excised for analysis via plaque assay and RT-qPCR. **A)** Plaque forming unit (pfu) per whole lung calculated via plaque assay. **B)** Fold change in gene expression of X31 nucleoprotein gene (X31 NP) compared to glyceraldehyde-3-phosphate dehydrogenase (GAPDH), calculated using the ΔΔCt method. Error bars are mean ± SEM, n=5. Unpaired T-test, not significant.

5.2.6 The effect of transgenic ADAM17 inhibition on soluble L-selectin, cytokine and chemokine and profiles in chimeric mice infected with influenza virus

ADAM17 is responsible for ectodomain proteolytic shedding of several cytokines, chemokines and molecules which can be measured in their soluble form via multiplex or ELISA. Therefore, BAL fluid (BALF) and sera were collected from ADAM17 sufficient and ADAM17 deficient chimeric mice on day 5 of X31 infection for analysis of soluble factors.

Lower levels of soluble L-selectin were detected in BALF of ADAM17$^{-/-}$ mice compared to ADAM17$^{+/+}$ mice, with 168 ng/mL and 218 ng/mL respectively, however, this was not statistically significant (Figure 5.12). In sera, there was a statistically significant difference in soluble L-selectin levels with an average of 4.7 µg/mL for ADAM17$^{+/+}$ mice compared to 3.8 µg/mL for ADAM17$^{-/-}$ mice ($p=0.003$) (Figure 5.12).

Chemokine and cytokine profiles from mouse BALF and sera were analysed to determine whether there were any differences between soluble factors in the lungs or systemically between ADAM17$^{+/+}$ and ADAM17$^{-/-}$ mice on day 5 of X31 infection (Figure 5.13, 5.14). The limit of detection for each analyte are shown (Table 5.1). There were no significant differences between ADAM17$^{+/+}$ and ADAM17$^{-/-}$ mice for any of the analytes tested in BALF on day 5 of infection (Figure 5.13). However, there was a trend for lower levels of TNF-α, CXCL1 and IP-10 in ADAM17 deficient mice (Figure 5.13). In contrast, there was a trend for higher levels of IFN-α in ADAM17$^{-/-}$ mice (Figure 5.13 E, H).

In sera, only three cytokines were above the limit of detection: IFN-γ, CXCL1 and IP-10. Each of these factors show a trend of being higher in ADAM17$^{-/-}$ mice, whilst this was the opposite in the BALF (Figure 5.13, 5.14).

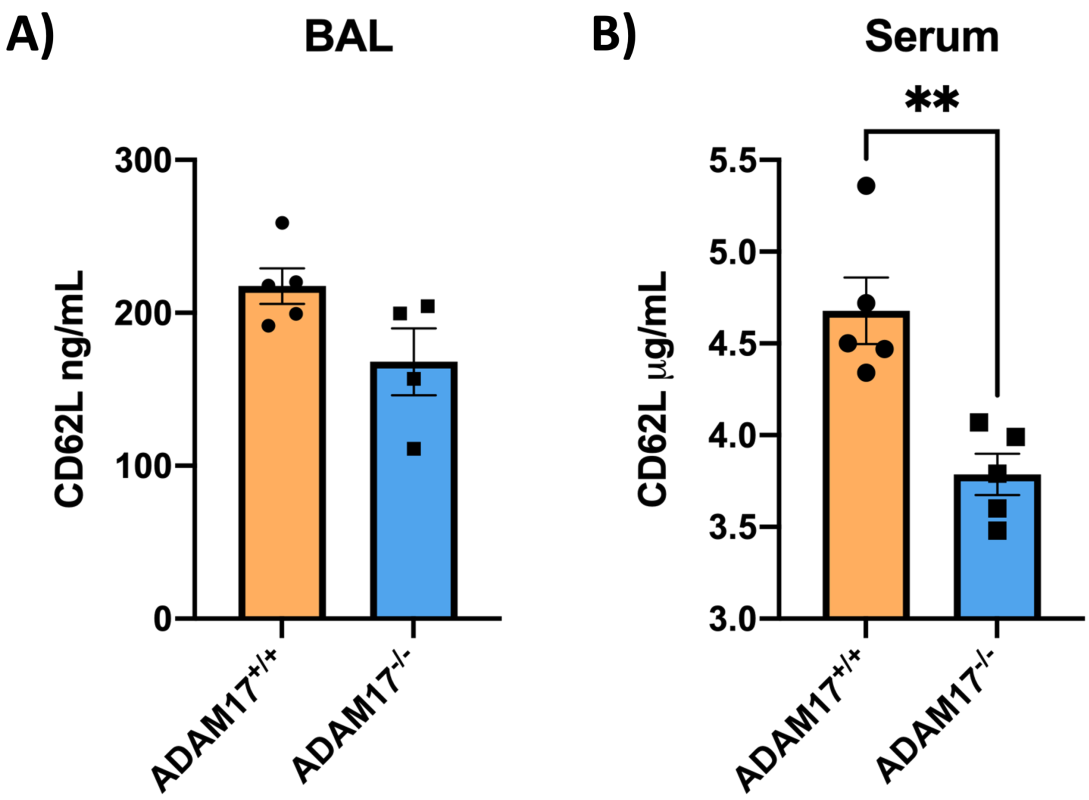

Figure 5.12. Soluble L-selectin levels in bronchoalveolar lavage fluid (BALF) and sera of ADAM17 chimeric mice on day 5 of X31 influenza virus infection. ADAM17$^{+/+}$ and ADAM17$^{-/-}$ chimeric mice were infected with 1x10^{3} pfu X31 influenza virus on day 0. Mice were humanely killed on day 5 of infection and BALF and sera collected for analysis of soluble L-selectin (CD62L) via ELISA. **A)** BALF **B)** Serum. Error bars are mean ± SEM, n=5. Unpaired T-test. **=p≤0.01.

Table 5.1. Limit of detection (LOD) values for each of the 13 analytes detected using LEGENDplex mouse anti-virus response panel (Biolegend). IFN-γ; interferon-gamma, CXCL1 (KC); chemokine ligand 1, TNF-α; tumour necrosis factor-alpha, CCL2 (MCP-1); chemokine ligand 2, IL-12p70; interleukin 12p70, CCL5 (RANTES); chemokine ligand 5, IL-1β; interleukin 1- beta, CXCL10 (IP-10); chemokine ligand 10, GM-CSF; granulocyte-macrophage colony-stimulating factor, IL-10; interleukin-10, IFN-β; interferon-beta, IFN-α; interferon-alpha, IL-6; interleukin-6. Limit of detection calculated using LEGENDplex software (Biolegend). Values shown in pg/mL.

Analyte	LOD pg/mL
IFN-γ	8.53
CXCL1 (KC)	4.13
TNF-α	5.87
CCL2 (MCP-1)	87.34
IL-12p70	2.02
CCL5 (RANTES)	13.67
IL-1β	1.21
CXCL10 (IP-10)	0.45
GM-CSF	0.02
IL-10	8.03
IFN-β	3.82
IFN-α	0.64
IL-6	1.46

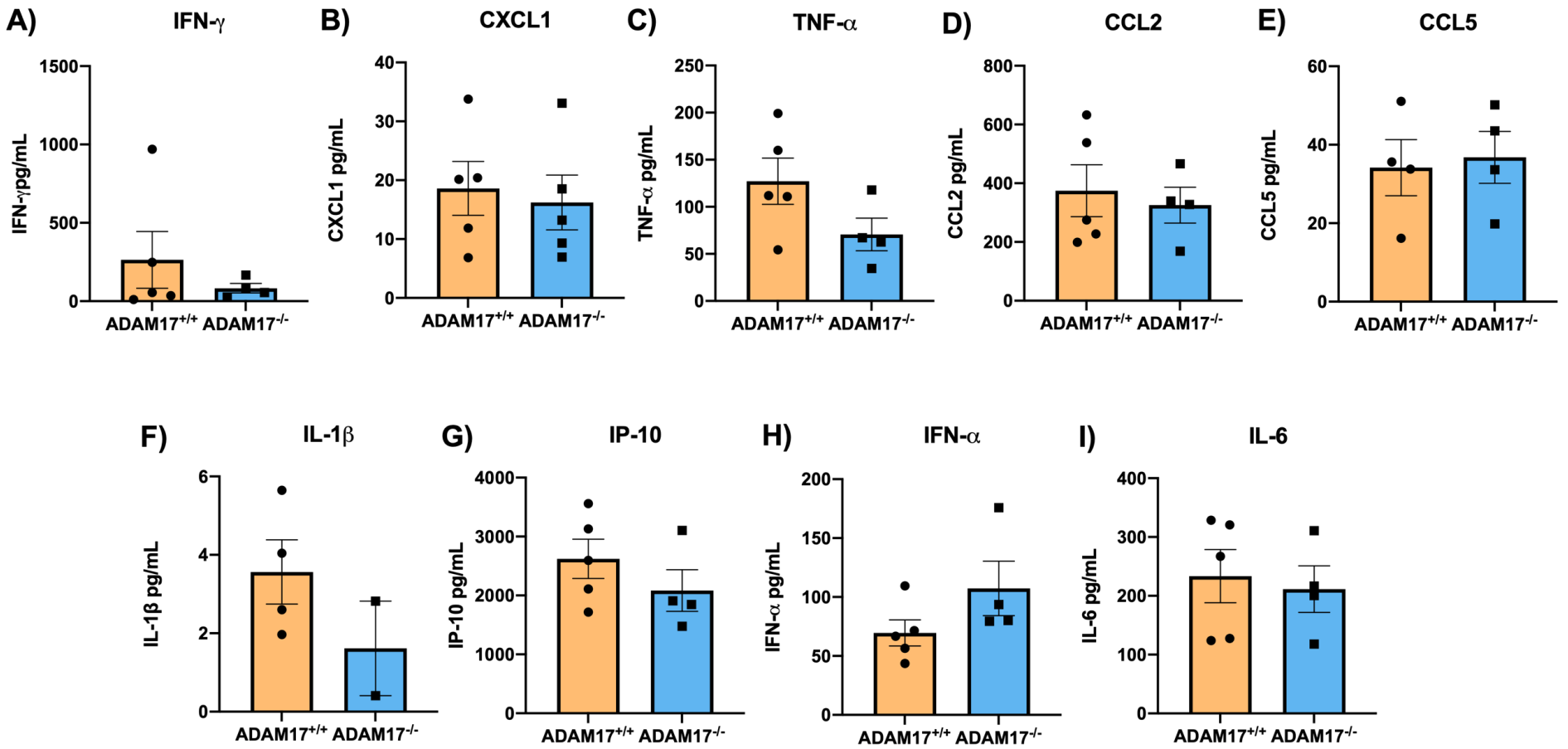

Figure 5.13. Chemokine and cytokine profiles of murine bronchoalveolar lavage fluid (BALF) on day 5 of X31 influenza infection. ADAM17$^{+/+}$ and ADAM17$^{-/-}$ chimeric mice were infected with 1x10^{3} pfu X31 influenza virus on day 0. Mice were humanely killed on day 5 of infection and BALF collected. Analytes measured using LEGENDplex mouse anti-virus response panel (Biolegend). **A)** IFN-γ; interferon-gamma, **B)** CXCL1 (KC); chemokine ligand 1, **C)** TNF-α; tumour necrosis factor alpha, **D)** CCL2 (MCP-1); chemokine ligand 2, **E)** CCL5 (RANTES); chemokine ligand 5, **F)** IL-

1β; interleukin 1 beta, n=2/4, **G)** CXCL10 (IP-10); chemokine ligand 10, **H)** IFN-α; interferon alpha, **I)** IL-6; interleukin 6. Levels calculated in pg/mL. The following analytes were below limit of detection: IL-10; interleukin 10, IFN-β; interferon beta, IL-12p70; interleukin 12p70 and GM-CSF; granulocyte-macrophage colony-stimulating factor. Data analysed using LEGENDplex software (Biolegend). Error bars are mean ± SEM, n=4/5. Mann-Whitney test (A, H), unpaired T-test (B-H, I), not significant.

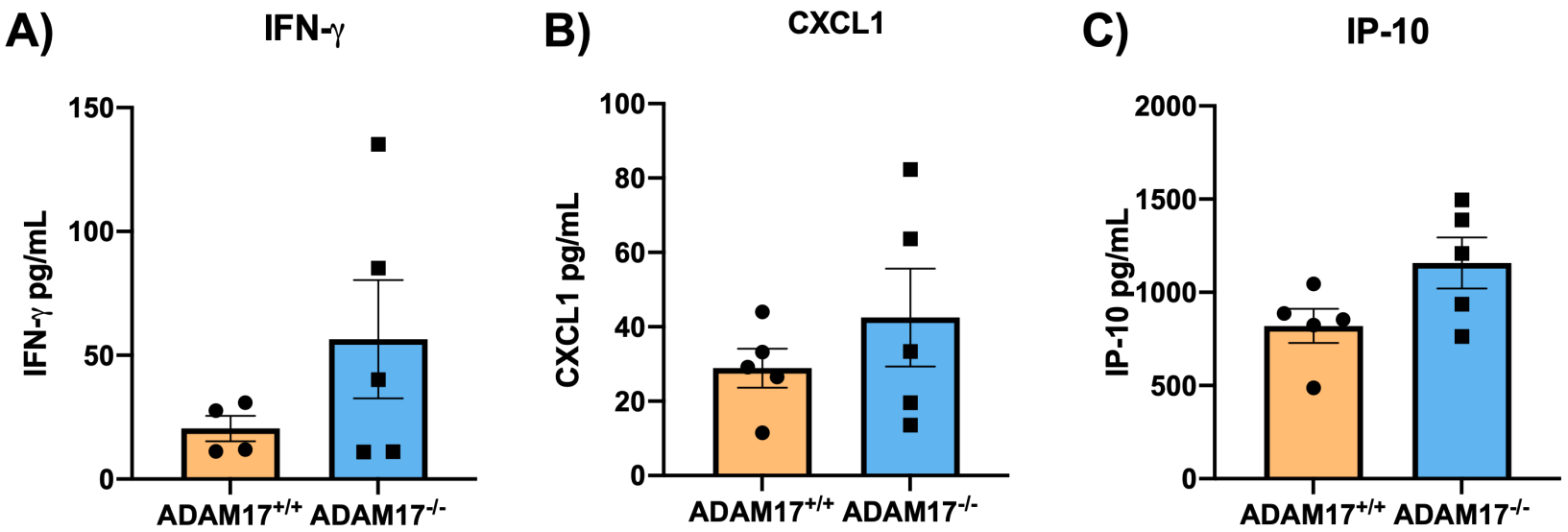

Figure 5.14. Chemokine and cytokine profiles of murine sera on day 5 of X31 influenza infection. ADAM17$^{+/+}$ and ADAM17$^{-/-}$ chimeric mice were infected with 1x10^{3} pfu X31 influenza virus on day 0. Mice were humanely killed on day 5 of infection and blood collected. Sera was prepared from whole blood. Analytes measured using LEGENDplex mouse anti-virus response panel (Biolegend). **A)** IFN-γ; interferon-gamma, **B)** CXCL1 (KC); chemokine ligand 1, **C)** CXCL10 (IP-10); chemokine ligand 10. Levels calculated in pg/mL. The following analytes were below limit of detection: TNF-α; tumour necrosis factor alpha, CCL2 (MCP-1); chemokine ligand 2 CCL2 (MCP-1); chemokine ligand 2, CCL5 (RANTES); chemokine ligand 5, IL-1β; interleukin 1 beta, IFN-α; interferon alpha, IL-6; interleukin 6, IL-10; interleukin 10, IFN-β; interferon beta, IL-12p70; interleukin 12p70 and GM-

CSF; granulocyte-macrophage colony-stimulating factor. Data analysed using LEGENDplex software (Biolegend). Error bars are mean ± SEM, n=5. Unpaired T-test, not significant.

5.3 Discussion

A cohort of radiation chimeric mice with either active ADAM17 ($ADAM17^{+/+}$) or inactive ADAM17 ($ADAM17^{-/-}$) in lymphocytes were successfully created from $Rag^{-/-}$ mice using foetal liver stem cells collected from $ADAM17^{+/+}$ or $ADAM17^{-/-}$ embryos (Figure 5.1, 5.2). Twelve out of sixteen mice successfully took up the chimerism and correct phenotype (six from each group), as demonstrated via a PMA-induced L-selectin shedding assay on whole blood (Figure 5.2). This initial testing of lymphocytes demonstrated that L-selectin was successfully maintained on activated CD8 T cells, CD4 T cells and B cells of $ADAM17^{-/-}$ mice and could be used to investigate effects on CD8 T cell homing to sites of virus infection and viral clearance *in vivo* (Figure 5.2).

There were no differences in cell surface L-selectin levels on untreated T cells from whole blood between $ADAM17^{+/+}$ and $ADAM17^{-/-}$ mice, suggesting no role for ADAM17 in basal L-selectin shedding in T cells (Figure 5.2 B, D). However, as in chapter three, data from *in vitro* L-selectin shedding assays showed that CD8 T cells had the highest cell surface expression of L-selectin out of all lymphocyte subsets, followed by CD4 T cells, with the lowest on B cells (Figure 3.1-3.4). This also agreed with previously published findings (Tang et al. 1998). This result was true of L-selectin levels in $ADAM17^{+/+}$ lymphocytes in this study, however, surprisingly $ADAM17^{-/-}$ mice had the highest levels of L-selectin on B cells (Figure 5.2 F). Furthermore, there was a significantly higher level of L-selectin on $ADAM17^{-/-}$ B cells compared to $ADAM17^{+/+}$ B cells, with an average L-selectin MFI of 1722 compared to 1196 (Figure 5.2 F). This suggests that ADAM17 may contribute to basal L-selectin shedding on B cells, which is a novel finding.

Several X31 IAV mouse experiments have previously resulted in early termination due to excessive weight loss up to 20% seen in mice. Therefore, it was practical to determine the earliest timepoint at which T cell responses could be measured in X31 IAV infection, to minimise harm and risk of excessive weight loss to mice. $Rag^{-/-}$ mice which had been through the chimera generation process, but had not taken up chimerism, were infected with $1x10^3$ pfu X31,

along with age-matched Thy1.1 wild-type mice (Figure 5.3). $Rag^{-/-}$ mice lost significantly more weight over the course of the X31 virus infection than Thy1.1 mice and were humanely killed on day 5, where there was a 10% difference in average weight loss per group (=$p \leq 0.0001$) (Figure 5.4). This suggested a role for the adaptive immune system by day 5 of X31 IAV infection.

When comparing CD8 T cell numbers in BAL on day 5 and 7 of X31 infection in Thy1.1 mice, there were no significant differences seen (Figure 5.5 A). However, these data may have been skewed due to low numbers of mice in each group and an outlier in the day 7 cohort (Figure 5.5). When the outlier is removed, there is a trend in the BAL samples to suggest lower CD8 T cell numbers on day 7 compared to day 5, however, this is the opposite in the lungs (Figure 5.5 A, B). There was a significant increase in CD8 T cells in the lungs on day 7 compared to day 5 (=$p<0.05$) (Figure 5.5 B). This increase in CD8 T cells suggests that there may be a greater effect of CTL dependent viral clearance on day 7 of IAV infection. A possibility for the differences seen is that these experiments were carried out separately, on different days, rather than analysed together. The volume of BALF that is collected upon administration of 0.5 mL sterile PBS into the lung cavity may also differ per mouse. If a substantial amount of fluid is not returned, this can skew total cell number counts. Effective cardiac perfusion must also be performed prior to lung harvest, to minimise detection of circulating CD8 T cells in the bloodstream. However, reports have shown that cardiac perfusion does not effectively remove all circulating CD8 T cells during an anti-viral responses (Anderson et al. 2012). An improvement to prevent this would be to use a technique pioneered by Anderson et al. This technique involves injecting an anti-CD8 antibody into the bloodstream almost immediately before culling, which allows labelling of circulating CD8 T cells, but not those in tissues (Anderson et al. 2012). These cells can then be gated out of flow cytometric analysis.

CD8 T cell numbers in the med LN and spleen did not change between day 5 and day 7 of X31 IAV infection (Figure 5.5 C, D). Overall, data suggest that there may be a greater role for CD8 T cells in IAV clearance in the lungs on day 7, than day 5 of infection (Figure 5.5 B). However, this finding was not observed in BAL (Figure 5.5).

A trend showed lower IAV titres in Thy1.1 mice compared to $Rag^{-/-}$ mice on day 5 of infection via plaque assay and qPCR (Figure 5.6). This also proposed a role for the adaptive immune system at this timepoint of infection. However, due to low group numbers, this was not found to be significant (Figure 5.6). A limitation to these data was that there were lower group numbers in the qPCR data due to poor quality RNA yielded from several samples. Based on these data, it was difficult to conclude whether a day 5 timepoint was acceptable for investigating the role of T cells in murine IAV infection. Whilst minimising length of infection was important for mouse welfare reasons, ideally, investigating several timepoints during the course of infection would have gained further insight into the T cell response to X31 IAV infection.

Studies of X31 IAV infection in mice have demonstrated that CD8 T cells begin to reach the lungs on day 5-6 of infection (Miao et al. 2010), (Keating et al. 2018). However, there is a clear trend of reduction in viral titres correlating with increased antigen-specific CD8 T cells in the lungs starting at day 5-6. Mathematical modelling by Miao et al. using X31 H3N2 IAV infected mice, showed that IAV specific CD8 T cells began to accumulate in the lungs on day 5, peaking at day 10 (Miao et al. 2010). Viral titres also began to decrease on day 5 of infection, with no detectable virus by day 10 (Miao et al. 2010). They described the 'adaptive phase' as day 5-14 (Miao et al. 2010). However, Keating et al. could not detect antigen-specific CD8 T cells in the lungs on day 5 of X31 infection but found peak accumulation on day 7 (Keating et al. 2018). However, viral titres were not measured in this study, so it was not possible to correlate the CTL response with viral clearance (Keating et al. 2018). Therefore, taking into account previous studies, a day 5 timepoint may be too early to investigate the adaptive immune response to murine IAV infection.

$ADAM17^{+/+}$ and $ADAM17^{-/-}$ chimeric mice were infected with $1x10^3$ pfu X31 IAV and humanely killed on day 5 to investigate the role of L-selectin on CD8 T cell homing to sites of virus infection and viral clearance (Figure 5.7). There was a trend to suggest that $ADAM17^{-/-}$ mice retained weight slightly better than $ADAM17^{+/+}$ throughout the course of infection, although this was only statistically significant on day 2 (Figure 5.8).

When comparing weight loss from both X31 mouse experiments in this chapter, there is a very similar weight loss pattern between $Rag^{-/-}$, $ADAM17^{+/+}$ and $ADAM17^{-/-}$ mice (Figure 5.4, 5.8). Average weight loss on day 5 of infection was 14% for the $Rag^{-/-}$ group, 16% for the $ADAM17^{+/+}$ group and 14% for the $ADAM17^{-/-}$ group (Figure 5.4, 5.8). This suggests that lymphocyte reconstitution and chimerism did not protect greatly against weight loss in IAV infection. However, wild-type Thy1.1 mice appeared to retain weight better throughout the 5 days of infection with an average weight loss on day 5 of infection of just 4% (Figure 5.4). This may suggest that whilst lymphocytes protect against weight loss in IAV infection, chimerism procedures (irradiation and stem cell injection) may attenuate this.

There was no significant difference in the infiltration of CD8 or CD4 T cells into mouse lungs of $ADAM17^{+/+}$ and $ADAM17^{-/-}$ chimeras on day 5 of X31 infection (Figure 5.9 A, B). Although there was a trend to show an increased number of CD8 T cells in the BAL of $ADAM17^{-/-}$ mice, potentially suggesting improved CD8 T cell homing when ADAM17 function is inhibited (Figure 5.9 A, B).

When comparing separate X31 experiments between Thy1.1 mice and ADAM17 radiation chimeras, CD8 T cell numbers are relatively comparable in BAL and lungs on day 5 of infection (Figure 5.5, 5.9). Total CD8 T cells in BAL were calculated to be between $1.0x10^4$-$1.5x10^4$, and $7.6x10^5$-$8.0x10^5$ in the lungs (Figure 5.5, 5.9). A contributing factor for this is that each of these mouse strains were of C57/BL6 background; previous research in mouse models of asthma showed disparities in BAL leucocyte content between different mouse strains (de Vooght et al. 2010). The number of CD8 T cells present in the BAL at this timepoint of infection suggested a robust T cell response has begun, as BAL from naïve, uninfected mice has few to no detectable CD8 T cells (Keating et al. 2018). This strongly suggests that the CD8 T cells present are recruited due to the pulmonary infection, however, phenotyping of these cells would conclusively reveal if they were differentiated CTLs.

CD8 T cell counts in the med LN on day 5 of infection were also highly comparable at $2.7x10^5$-$3.7x10^5$, whereas spleen CD8 T cell counts were slightly

more varied at $1x10^6$-$3x10^6$ cells (Figure 5.5, 5.9). Overall, this comparison suggests that the X31 strain of IAV is a robust model to use to investigate anti-viral responses in mice.

Previous research using L-selectin$^{-/-}$ mice found higher numbers of T cells in the spleen compared to wild-type mice, but lower numbers of T cells in LNs (Arbonés et al. 1994). Furthermore, T cell recruitment to peripheral LNs in mice was shown to be L-selectin dependent, whilst T cell recruitment to the spleen was L-selectin independent (Arbonés et al. 1994). Other studies have also shown that genetically maintained L-selectin on T cells (LΔP) does not change spleen and LN cellularity in mice and that there is a saturable density of L-selectin on T cells which will reach maximal LN homing (Galkina et al. 2003). (Galkina et al. 2007). The data presented in this thesis shows no increase in T cells in ADAM17$^{-/-}$ med LNs, but an increased number of T cells found in the spleen (Figure 5.9 A, B). This contradicts previous findings and suggests a potential role for ADAM17 in T cell trafficking to the spleen.

There were significantly increased levels of L-selectin seen on the surface of both CD8 and CD4 T cells in all organs of ADAM17$^{-/-}$ mice on day 5 of infection (Figure 5.9 C, D). Interestingly, X31 was found to reduce levels of L-selectin on T cells with ADAM17 (Figure 5.2, 5.9). Unactivated T cells in whole blood from ADAM17 chimeric mice had an MFI of L-selectin between 1423-1629 (Figure 5.2). Whilst in ADAM17$^{+/+}$ infected mice, this reduced to between 176-667 on CD8 T cells and 269-1235 on CD4 T cells, dependent on the tissue being analysed (Figure 5.9). Although peripheral blood T cells were not tested for their L-selectin levels during infection, so this is not directly comparable. Nevertheless, this implies a strong activation of ADAM17 during infection, which has been shown previously by others (Shimoda et al. 2016), (Ohta et al. 2001), (Ju et al. 2007). Whilst ADAM17-dependent shedding of L-selectin was observed in both IAV infected ADAM17$^{+/+}$ CD8 and CD4 T cells, there was a greater amount of L-selectin shedding seen in CD8 T cells (Figure 5.9 C, D). ADAM17$^{+/+}$ CD8 T cells had lower L-selectin MFI than CD4 T cells in the equivalent organ (Figure 5.9 C, D). For example, ADAM17$^{+/+}$ CD8 T cell L-selectin MFI was 177 on average compared to 553 in CD4 T cells (Figure 5.9 C,

D). This may suggest a stronger stimulation or activation of ADAM17 in CD8 T cells in IAV infection, which is likely TCR-mediated.

However, these data demonstrating high levels of L-selectin on CD8 T cells of ADAM17$^{-/-}$ mice show that L-selectin maintenance did not significantly improve CD8 T cell homing to the site of virus infection by day 5 of infection. However, a minor increase in CD8 T cells was found in the BAL of ADAM17$^{-/-}$ mice (Figure 5.9).

There were no significant changes in T cell activation levels between ADAM17$^{+/+}$ and ADAM17$^{-/-}$ mice on day 5 of IAV infection (Figure 5.10). This was measured via cell surface CD44 and CD69 expression. BAL CD8 and CD4 T cells had the highest levels of both activation markers compared to other organs, along with CD44 levels in bone marrow (Figure 5.10). CD4 T cells in the BAL showed a trend of higher levels of early activation marker CD69 in ADAM17$^{-/-}$ mice (Figure 5.10 C, D). Interestingly, upregulation of CD69 was associated with CD8 T cells which contain the shedding-resistant mutant of L-selectin (LΔP), which conferred improved tumour killing in a mouse model of melanoma (Watson et al. 2019). However, this finding has not been seen to date with virus infection. Higher levels of activation in BAL T cells may suggest that these are influenza-specific CTLs which are primed to target IAV in the lungs. However, this cannot be proven due to lack of tetramer or dextramer staining which can be used identify antigen specific T cell clones via flow cytometry. Dextramer staining was attempted using the ASNENMETM X31 peptide-MHC complex, however, high non-specific binding made this difficult to interpret.

Viral titres in ADAM17$^{-/-}$ and ADAM17$^{+/+}$ mouse lungs also showed no differences on day 5 of X31 infection measured by plaque assay or qPCR (Figure 5.11). This demonstrates that inhibiting the function of ADAM17 on lymphocytes did not improve viral clearance on day 5 in a mouse model of X31 IAV infection. However, this is likely too early of a timepoint to determine the role of ADAM17 in the adaptive immune response to murine IAV infection.

Soluble levels of L-selectin were reduced in the BALF, from an average of 218 ng/mL in ADAM17$^{+/+}$ mice to 168 ng/mL in ADAM17$^{-/-}$ mice (Figure 5.12 A). This was also seen in mouse sera, with 4.7 µg/mL for ADAM17$^{+/+}$ mice compared to 3.8 µg/mL for ADAM17$^{-/-}$ mice, which was statistically significant (=$p \leq 0.01$) (Figure 5.12). A suggestion for the higher quantity of soluble L-selectin in the sera, is that there are more cells which release L-selectin circulating in the bloodstream compared to in the lungs during IAV infection. As the chimeric mice have ADAM17 and L-selectin present on non-lymphoid cells, it is plausible that soluble L-selectin in ADAM17$^{-/-}$ chimeras is being released from innate myeloid cells. However, these levels were not investigated in non-IAV infected mice, so the effect of viral infection on soluble L-selectin production cannot be fully concluded.

Regarding the cytokine and chemokine analysis in the BAL, there was a reduction in soluble TNF-α in ADAM17 deficient mice (Figure 5.13 C). This further supports the successful inactivation of ADAM17 in this model, as TNF-α is a key substrate of ADAM17. However, there was still an average of 71 pg/mL of TNF-α measured in BALF of ADAM17$^{-/-}$ mice, suggesting that cells other than lymphocytes present in the lungs are releasing TNF-α at this timepoint. This is likely from innate immune cells such as pro-inflammatory monocytes and neutrophils which are known to peak in the lungs at day 5 of IAV infection (Lin et al. 2008), (Tate et al. 2008). Innate immune cells in chimeras are likely host derived and subsequently contain active ADAM17. Therefore, soluble TNF-α will be released from myeloid cells activated in IAV infection.

Almost all multiplex analytes were equally expressed in both chimeric mouse groups, apart from TNF-α, CXCL1 and IP-10 which were slightly lower in ADAM17$^{-/-}$ mice (Figure 5.13). IFN-α was the only cytokine upregulated in ADAM17$^{-/-}$ mice (Figure 5.13). IFN-α is a type I IFN and anti-viral cytokine with direct roles in viral replication, therefore it can also be used as a surrogate marker for viral load (McLaren and Potter 1973). This increased level of IFN-α in infected ADAM17$^{-/-}$ mice suggests higher viral replication than ADAM17$^{+/+}$ mice, which supports qPCR data, but contradicts plaque assay data (Figure 5.11).

Interestingly, whilst the majority of analytes in the BAL were unchanged or lower in ADAM17 deficient mice, this was the opposite for sera, whereby IFN-γ, CXCL1 and IP-10 were upregulated compared to ADAM17 sufficient mice (Figure 5.14). IP-10 is a chemokine which induces IFN-γ production; IFN-γ is an anti-viral cytokine with effects on improving viral clearance and reducing pathogenesis in IAV infection (Cao et al. 2006). This may suggest that ADAM17$^{-/-}$ mice had improved anti-viral responses compared to wild-type ADAM17 mice, although there is conflicting evidence to the role of IFN-γ in murine IAV infection. One study has found IFN-γ to be detrimental to survival of IAV infection in mice and can contribute to lung injury (Califano et al. 2017).

CXCL1 (also known as KC) is a neutrophil chemoattractant which was also upregulated by ADAM17$^{-/-}$ mouse sera on day 5 of X31 IAV infection. CXCL1 can be associated with recruitment of neutrophils to the lungs in IAV infection, cytotoxic functions and increased viral load in mice (Tavares et al. 2017). This may suggest increased neutrophil trafficking to the lungs in ADAM17$^{-/-}$ mice. Neutrophils also express L-selectin and its cell surface expression has been shown to impact homing to sites of infection *in vivo* (Arbonés et al. 1994). If ADAM17$^{-/-}$ foetal liver stem cells reconstituted the myeloid compartment of leucocytes in chimeric mice, there is a possibility that neutrophils could exhibit improved recruitment to the lungs in IAV infection via maintained L-selectin. However, neither neutrophils nor other cells in the myeloid compartment were tested in these mice for potential ADAM17 deficiency. Whole blood phenotyping carried out on chimeras was only tested for T and B lymphocytes (Figure 5.2). An improvement would be to include myeloid cell markers in this assay to assess if this compartment was also sufficient or deficient in ADAM17. This could rule out whether the myeloid compartment may have altered effects on homing and IAV infection seen in this chapter of work. If the myeloid compartment of cells were found to have taken up chimerism, we could conclude that there is no role for ADAM17 in overall leucocyte driven IAV clearance by day 5 of infection.

A day 5 timepoint was chosen due to erratic weight loss patterns seen in X31 IAV infection mice, however, this may be too early to see a significant

involvement of CD8 T cells in this model. As described, antigen-specific CD8 T cells are found to accumulate in the lungs on day 5-6 of IAV infection in mice, and peak between day 7-10 (Miao et al. 2010), (Keating et al. 2018). This accumulation correlated with reduction in viral titres (Miao et al. 2010). Therefore, future experiments investigating T cell recruitment to the lungs and IAV titres at days 6-10 of infection may provide an answer as to whether ADAM17 inhibition improves viral homing and clearance in a mouse model of influenza infection.

In ADAM17$^{-/-}$ mice the enzymatic activity of ADAM17 is blocked by a mutation in the zinc binding domain of ADAM17. As it is a metalloproteinase, a non-functional zinc-binding domain will render the protein inactive. However, there are no data available to show whether mutant ADAM17 can still reach the cell surface. Sahin et al. suggests that ADAM17 will be retained in the endoplasmic reticulum of the cell, become degraded and therefore not traffic to the cell surface, but this has not been proven (Sahin et al. 2004). Therefore, a CRISPR knockout of ADAM17 may be an improvement to the radiation chimera mouse model, as inactive ADAM17 protein at the cell surface may have altered biological effects. ADAM17 has other roles beside ectodomain proteolytic cleavage, such as contributing to intercellular adhesion via its disintegrin domain (Trad et al. 2013). ADAM17 has over 80 known substrates such as TNF-α, IL-6R, TGF-α and EGFR ligands and is likely to cause many unwanted changes to biological function. Secondly to this, as ADAM17 is being inhibited on all lymphocytes, this may also cause unwanted effects on CD4 T cells and B cells. CD8 T cells are the only lymphocyte subset which have been found to confer protection against murine IAV infection when L-selectin is maintained on their cell surface. Therefore, a CD8 T cell conditional ADAM17 knockout mouse would be a better mouse model to use for a more precise approach.

As with the experiments carried out in chapter four, an improvement to this work would include a comparison to an LΔP mouse group. X31 IAV is yet to be tested in LΔP mice at a day 5 timepoint, whilst at day 4 there was no improvement in viral clearance found (Ager lab, unpublished). Previous IAV experiments which have found a benefit of maintained L-selectin on T cells using LΔP mice have been carried out using IAV H1N1 strain (PR8) and virus

titres measured at day 8 post-infection. Therefore, we cannot conclude as to whether L-selectin maintenance on CTLs is beneficial for clearance of the X31 strain of IAV. Due to breeding issues with the LΔP colony of mice, this comparison was not possible to carry out and remains to be tested in the future.

A further improvement on this work would be to determine the effects of ADAM17$^{-/-}$ deficiency on lymphocytes in mice not infected with IAV. Mohammed et al. confirmed that ADAM17$^{-/-}$ and ADAM17$^{+/+}$ chimeric mice had similar levels of LN cellularity, T and B cell ratios, L-selectin levels per cell and number of L-selectin positive T cells in LNs (Mohammed et al. 2019). There were also similar levels of soluble L-selectin in serum between ADAM17$^{-/-}$ and ADAM17$^{+/+}$ chimeric mice, created on an L-selectin knockout background, confirming that basal shedding is not controlled by ADAM17 on T cells (Mohammed et al. 2019).

The data presented in this chapter suggest that ADAM17 deficient chimeric mice successfully maintained L-selectin on the surface of their T cells. Although there was not a clear conclusion as to whether this improved CD8 T cell homing to sites of virus infection; there was only a minor increase in CD8 T cells in the BAL of ADAM17$^{-/-}$ on day 5 of IAV infection which was not significant (Figure 5.9 A). However, this did not confer improved viral clearance at this day 5 timepoint and may require a later timepoint to allow for a robust T cell response (Figure 5.11).

Chapter Six

Final discussion

6. Final discussion

6.1 Overall findings

Overall, the work in this thesis has demonstrated that anti-ADAM17 antibody A9(B8) was able to block ADAM17-dependent shedding of substrates L-selectin and TNF-α *in vitro* at IC_{50}s of ≥261 nM and ≥75 nM, respectively (Table 3.1). A9(B8) was better than anti-ADAM17 antibody D8P1C1 which had IC_{50}s of ≥689 nM and ≥1468 nM for blocking cell surface L-selectin and TNF-α shedding, respectively (Table 3.1). Antibody candidate A9(B8) was therefore taken forward and tested in a mouse model of pulmonary influenza virus infection. A9(B8) was found not to improve clearance of X31 IAV from the lungs at day 7 of infection (Figure 4.3). Circulating levels of antibody detectable in the bloodstream were sufficient to inhibit ADAM17 dependent shedding of L-selectin shedding at 15 mg/kg, 6 hours post-administration (Figure 4.9). However, after 4 days, the levels bloodstream were insufficient (Figure 4.9). Rapid clearance of A9(B8) in IAV infected mice limited its use to prevent L-selectin shedding during infection. Therefore, radiation chimeric mice with $ADAM17^{-/-}$ lymphocytes were explored as a transgenic alternative to investigate whether ADAM17 inhibition can maintain L-selectin expression *in vivo*, and the effects on viral clearance. These mice successfully maintained L-selectin on the cell surface of CD8 T cells (Figure 5.9 C, D), however, there was no increased CD8 T cell homing to the lungs (Figure 5.9 A, B), nor improved viral clearance on day 5 of infection (Figure 5.11).

6.2 Differences in L-selectin and TNF-α cell surface expression and ADAM17-dependent substrate shedding

6.2.1 A9(B8) blocks ADAM17-dependent TNF-α shedding better than L-selectin shedding

In vitro shedding assays suggested that A9(B8) was more efficacious at blocking ADAM17-induced TNF-α shedding than L-selectin shedding. Cell surface IC_{50}s were 261-2837 nM for inhibiting L-selectin shedding on lymphocytes, however this was 75 nM for inhibiting cell surface TNF-α shedding on macrophages (Table 3.1). This was also true of the soluble L-selectin analysis, as the IC_{50} was 129-211 nM for L-selectin shedding and 91 nM for TNF-α shedding (Table 3.1). This suggests that A9(B8) may block residues of ADAM17 that are more involved in TNF-α shedding than L-selectin shedding. It is currently unknown which specific residues of ADAM17 A9(B8) binds to, although it's known to bind to the extracellular domain outside of the catalytic cleft (Kwok et al. 2014). TIMP-3 and D8P1C1 bind directly to the ADAM17 catalytic (metalloproteinase) domain (Wisniewska et al. 2008), (Saha et al. 2022).

Borland et al. previously demonstrated a preferential inhibition of TNF-α over L-selectin shedding using TIMP-3 as an inhibitor of ADAM17 *in vitro.* TIMP-3 was able to inhibit L-selectin shedding with an IC_{50} of 310 nM in primary mouse lymphocytes and 390 nM in human monocytes, whilst TIMP-3 inhibited TNF-α shedding in human monocytes with an IC_{50} of 110 nM (Borland et al. 1999). A limitation to the shedding assays carried out in this thesis is the use of different cell types to analyse different substrates. However, Borland et al. has demonstrated this finding when analysing L-selectin and TNF-α in human monocytes (Borland et al. 1999). This further strengthens the hypothesis that different residues of ADAM17 are involved in TNF-α and L-selectin ectodomain shedding (Figure 6.1 A).

To study potential substrate specific differences in ADAM17 ectodomain shedding, inhibitors with known binding to specific residues could be utilised. For example, A9(B8) is known to bind outside of the catalytic cleft of ADAM17, while D8P1C1 binds inside the catalytic cleft. If numerous ADAM17 inhibitors with mapped binding sites were available, they could be tested to determine which epitopes of ADAM17 are responsible for proteolytic shedding of different substrates. Furthermore, this would require testing with different stimuli as stimulus-dependent effects have been seen with ADAM17 inhibitors (Figure 3.5). Previous research has shown that there are two different pathways of L-

selectin shedding, dependent on stimulus; PKC- or MAPK-mediated (Rizoli et al. 1999). Killock and Ivetić have shown that different stimuli result in different shedding mechanisms with lymphocytes capable of both PKC and MAPK-dependent L-selectin shedding, whilst TNF-α shedding in monocytes was shown to be PKC mediated (Killock and Ivetić 2010). MAPK activation led to phosphorylation of the ADAM17 cytoplasmic tail and maintained ADAM17 cell surface expression, whilst PKC activation directly phosphorylated the L-selectin cytoplastic tail (Killock and Ivetić 2010). Different stimuli leading to these distinctive pathways of ADAM17 proteolytic shedding may attribute to differences seen between substrates and cell types (Figure 6.1 B).

Others have also identified preferential shedding activity for TNF-α over other substrates (Mohan et al. 2002). However, little work has been carried out to determine whether ectodomain shedding by ADAM17 requires different residues, dependent on substrate. Phenylarsine oxidase (PAO) was found to induce L-selectin shedding from leucocytes via PDI (Bennett et al. 2000). Bennet et al. suggest a direct effect of sulfhydryl regulation of disulfide bonds in L-selectin itself, resulting in a conformational change, allowing ectodomain shedding (Bennett et al. 2000). However, analysis of ADAM17 in neutrophils revealed that two highly conserved cysteine sulfhydryl motifs (cysteine-X-X-cysteine) within its disintegrin and cysteine-rich domains were critical for L-selectin cleavage (Wang et al. 2009). This suggests that PAO and PDI may regulate L-selectin shedding through disulphide bonds on ADAM17, rather than L-selectin itself, as Bennet et al. did not investigate ADAM17 in this study (Bennett et al. 2000). Analysis of ADAM17 transfected Chinese hamster ovary cells also revealed that one of these cysteine motifs (Cys_{600}) was required for ectodomain shedding of ADAM17 substrates TNF-α and TGF-α (Li and Fan 2004). Therefore, whilst sulfhydryl regulation of disulfide bonds is required for ADAM17-dependent L-selectin shedding, it's likely to be essential for ADAM17 general proteolytic function and may not be substrate specific.

There is a relaxed sequence specificity for L-selectin shedding, as point mutations in the cleavage site do not inhibit proteolytic cleavage of human L-selectin (Chen et al. 1995), (Migaki et al. 1995). However, some L-selectin mutants with truncated length resist cleavage, suggesting confirmation or

tertiary structure constraints to ectodomain shedding (Chen et al. 1995), (Migaki et al. 1995). A TNF-α mutant with cleavage site mutations was unable to fold correctly as a trimer protein on the cell membrane and proteolytic cleavage was unsuccessful (Tang et al. 1996). A further TNF-α mutant was also incapable of ectodomain cleavage but had successful trimer protein folding (Tang et al. 1996). This suggests that whilst the cleavage site of ADAM17 substrates is a key determinant in successful shedding, protein folding and positioning in the membrane may create steric hinderance. Therefore, understanding substrate binding partners and spatial orientation may be key to understanding substrate-specific differences in ADAM17 ectodomain cleavage.

Substrate binding partners such as tetraspanins have also been shown to affect the efficacy of ADAM17-dependent proteolytic shedding (Figure 6.1 C). Tetraspanins are transmembrane proteins which are named as they span the cell membrane four times. They have roles in organising microdomains of cell membrane proteins and are crucial in leucocyte migration due to their roles in binding integrins and cell adhesion molecules. Tetraspanin 'Tspan8' was recently discovered to bind to both TNF-α and ADAM17 to facilitate ectodomain shedding, however it was unable to bind to other ADAM17 substrates such as TGF-α and TNFR-I (Müller et al. 2022). L-selectin was not studied in this experiment and therefore the role of Tspan8 in ADAM17-mediated L-selectin shedding is yet to be elucidated (Müller et al. 2022). The role of tetraspanin binding partners of L-selectin are covered further in section 6.2.4.

There are two main pathways for trafficking of molecules to be processed and released by the cell; the constitutive secretory pathway and regulated secretory pathway. Cell surface molecules are primarily trafficked by the constitutive secretory pathway whilst soluble molecules are predominantly trafficked by the regulated secretory pathway. In the majority of cell types, TNF-α uses the constitutive secretory pathway which is upregulated by stimuli such as LPS (Stow et al. 2009). Newly synthesised TNF-α localises to the Golgi, where tubulovesicular carriers (secretory vesicles) transport it to the cell membrane or to recycling endosomes for ADAM17 processing (Stow et al. 2009). The details of where ADAM17-dependent shedding of L-selectin occurs in leucocytes is currently unknown, and differences in secretory pathways may alter proteolytic

shedding. However, P-selectin has been shown to be trafficked by the regulated secretory pathway in secretory storage granules (Disdier et al. 1992). Disdier et al. discovered that the signal for this is within the cytoplasmic domain of P-selectin as when swapped for the L-selectin cytoplasmic tail, >80% of the protein still underwent regulated secretory pathway. This suggests that signals outside of the L-selectin cytoplasmic tail instruct the cell to traffic to the cell membrane (Disdier et al. 1992). The three major hypotheses for the differences in substrate specificity of ADAM17 are summarised in figure 6.1.

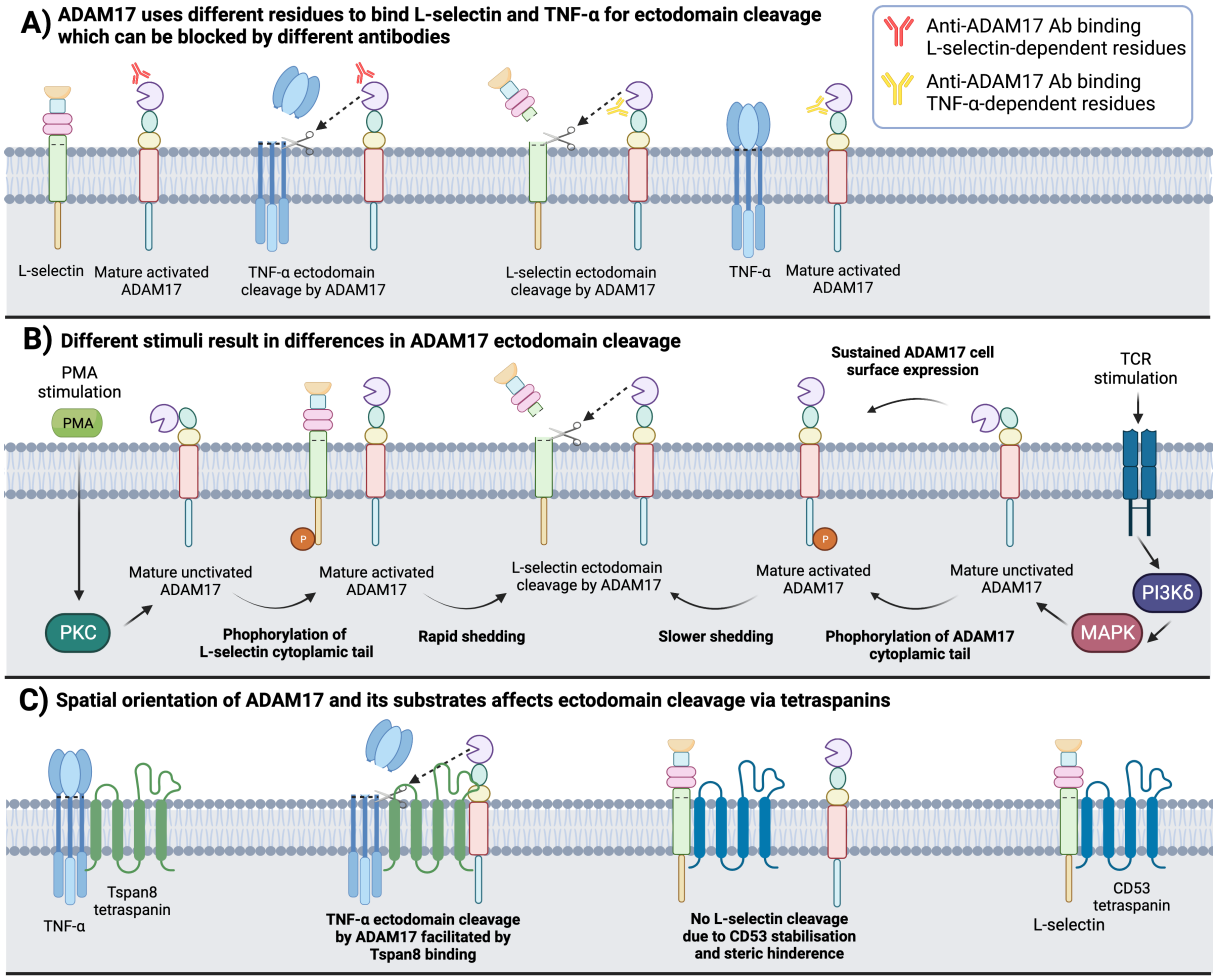

Figure 6.1. Differences in substrate specificity of ADAM17. A) ADAM17 may use different protein residues to recognise different substrates such as L-selectin and tumour necrosis factor alpha (TNF-α). Antibodies specific for different binding sites of ADAM17 may delineate this mechanism

proposed by data presented in this thesis. **B)** Different cell stimuli activate ADAM17 using different mechanisms resulting in different rates of substrate shedding. E.g., PMA rapidly activates ADAM17-dependent shedding within 30-60 minutes via a protein kinase C (PKC)-dependent mechanism (Jung and Dailey 1990), (Rizoli et al. 1999), (Frey et al. 1997), (Kilian et al. 2004). This results in phosphorylation of the L-selectin cytoplasmic tail and rapid shedding (Killock and Ivetić 2010). Whilst T cell receptor (TCR) stimulation requires 4 hours to elicit complete L-selectin shedding from T cells via a PI3Kδ, mitogen-activated protein kinase (MAPK)-dependent mechanism (Chao et al. 1997), (Sinclair et al. 2008). This results in phosphorylation of ADAM17 cytoplasmic tail, sustained ADAM17 cell surface expression and slower shedding (Killock and Ivetić 2010). **C)** Spatial orientation and the role of tetraspanins in the cell membrane may affect ADAM17 ectodomain cleavage. Tspan8 binds both TNF-α and ADAM17 to facilitate proteolytic cleavage, whereas CD53 tetraspanin may hinder ADAM17 access to binding site as this is known to stabilise L-selectin expression (Müller et al. 2022), (Demaria et al. 2020). Figure created using Biorender.com.

6.2.2 D8P1C1 blocks TCR but not PMA dependent L-selectin shedding

D8P1C1 was found to block TCR-mediated L-selectin shedding induced via anti-CD3/CD28 on CD8 and CD4 T cells with IC_{50}s of 1304 nM and 689 nM, respectively (Table 3.1). However, there was no inhibition of L-selectin shedding seen with PMA stimulation (Figure 3.5). This suggests that ADAM17 shedding activity can depend on its activation stimulus as shown by others (Killock and Ivetić 2010), (Figure 6.1 B). However, this may also depend on the binding site of D8P1C1 and how this site is activated differently by TCR and PMA stimulation. As mentioned in chapter three, ADAM17 has an 'open/active' and 'closed/inactive' confirmation which controls proteolytic activity. D8P1C1 binds to the 'active' confirmation of ADAM17, as demonstrated on cancer cells (Saha et al. 2022). It is possible that the PMA-induced interaction is too quick for sufficient D8P1C1 binding on lymphocytes and that ADAM17 exists in a closed confirmation before activation (Müllberg et al. 1992). Upon activation, the open confirmation of ADAM17 may only be available for a short time before substrate shedding is accomplished, allowing no time for D8P1C1 binding.

6.2.3 ADAM17 levels differ across cell types

A limitation to this study is that L-selectin and TNF-α were analysed on different cell types, as a murine cell that expresses both L-selectin and TNF-α that can be shed by the same stimulus was not identified. RAW 264.7 macrophages had no L-selectin expression, whilst primary mouse neutrophils tested had low levels of L-selectin, and no expression of TNF-α. CD8 T cells can express TNF-α, but this is only on effector CTLs which will have shed L-selectin during activation. This poses a question about whether ADAM17-mediated shedding may be different on each cell type. Data within chapter four suggests that ADAM17 may be expressed at different levels within cells in different tissues in mice (Figure 4.10). A9(B8) was added exogenously to single cell suspensions of mouse lungs and spleen and detected via a secondary FITC-conjugated antibody; an indirect staining method for ADAM17 (Figure 4.10). Mouse CD8 T cells in the spleen had an ADAM17 MFI of 400 compared to 1400 for CD8 T cells in mouse lungs (Figure 4.10). Data obtained from 'The Human Protein Atlas' shows that ADAM17 protein was detected in varying

amounts in different tissues in humans (Figure 6.2). Whilst most tissues expressed the same protein levels (medium), lower ADAM17 protein was detected in 9 organs including the kidney, fallopian tubes, and spleen, whilst the lungs had medium expression (Figure 6.2), which supports findings shown in figure 4.10 that ADAM17 levels are higher in the lungs than the spleen.

However, mRNA expression reveals even more variation between organs and individual cell types (Figure 6.3). The lungs are the second highest ADAM17 mRNA expressing organ after the placenta, which is 1.6x higher than the spleen (Uhlén et al. 2015), (Figure 6.3). Additionally, naïve CD4 and CD8 T cells express similar levels of ADAM17 mRNA, which is increased upon activation (Schmiedel et al. 2018), (Figure 6.4). Naïve B cells express higher ADAM17 mRNA than naïve CD4 and CD8 T cells (Schmiedel et al. 2018), (Figure 6.4). This suggests both a tissue and cell specific regulation of ADAM17 levels. This may also explain differences between L-selectin levels and ADAM17 shedding seen between different types of lymphocytes reported in this thesis.

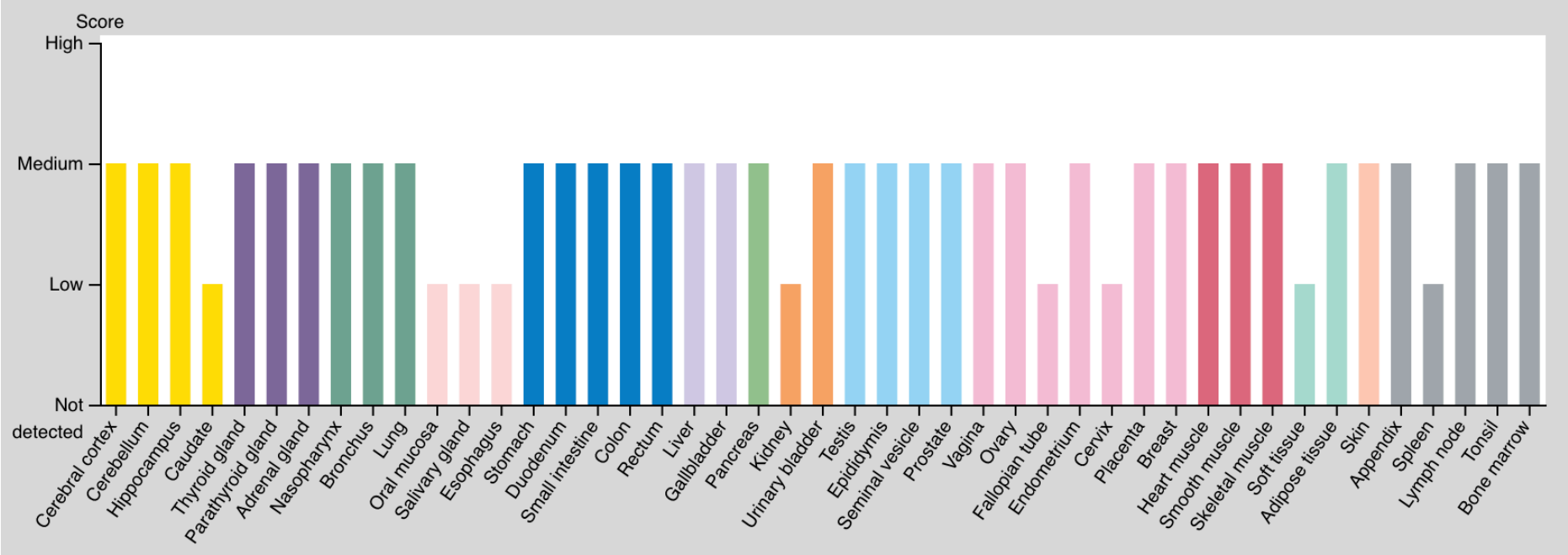

Figure 6.2. ADAM17 protein expression levels across different human tissues. Image credit: The Human Protein Atlas (https://www.proteinatlas.org/ENSG00000151694-ADAM17/tissue). (Uhlén et al. 2015).

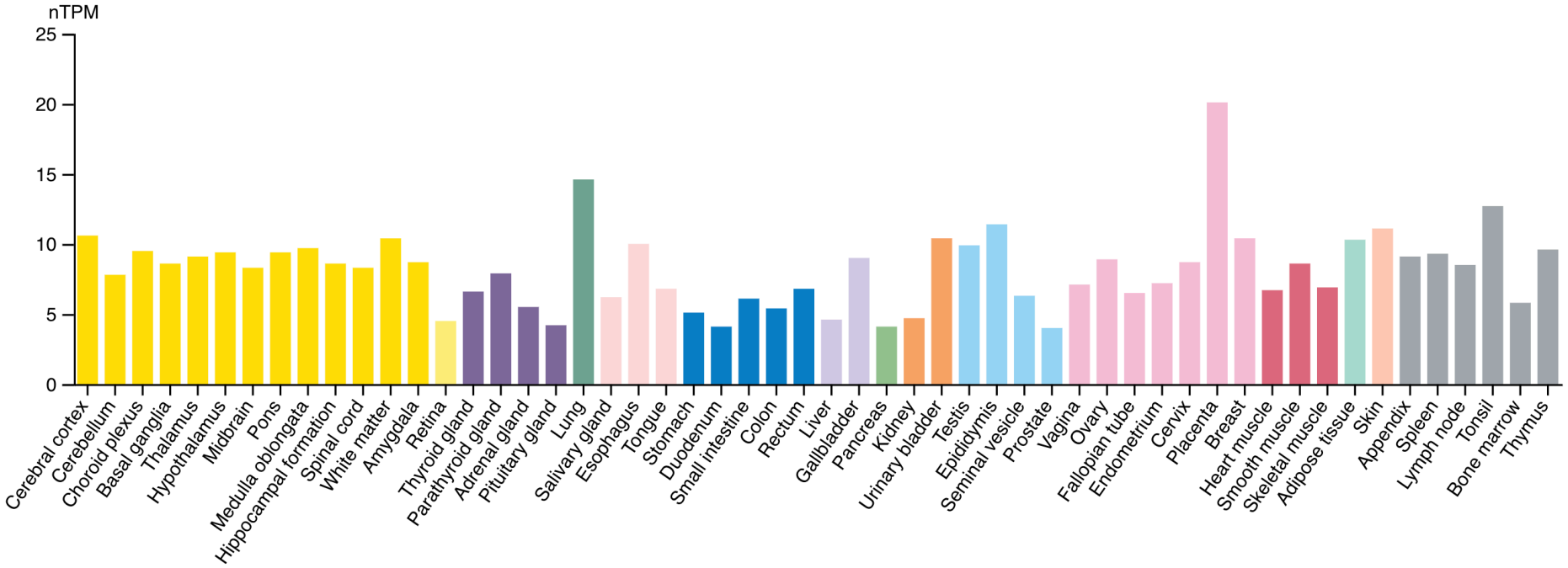

Figure 6.3. ADAM17 mRNA expression levels across different human tissues. Image credit: The Human Protein Atlas (https://www.proteinatlas.org/ENSG00000151694-ADAM17/tissue). (Uhlén et al. 2015).

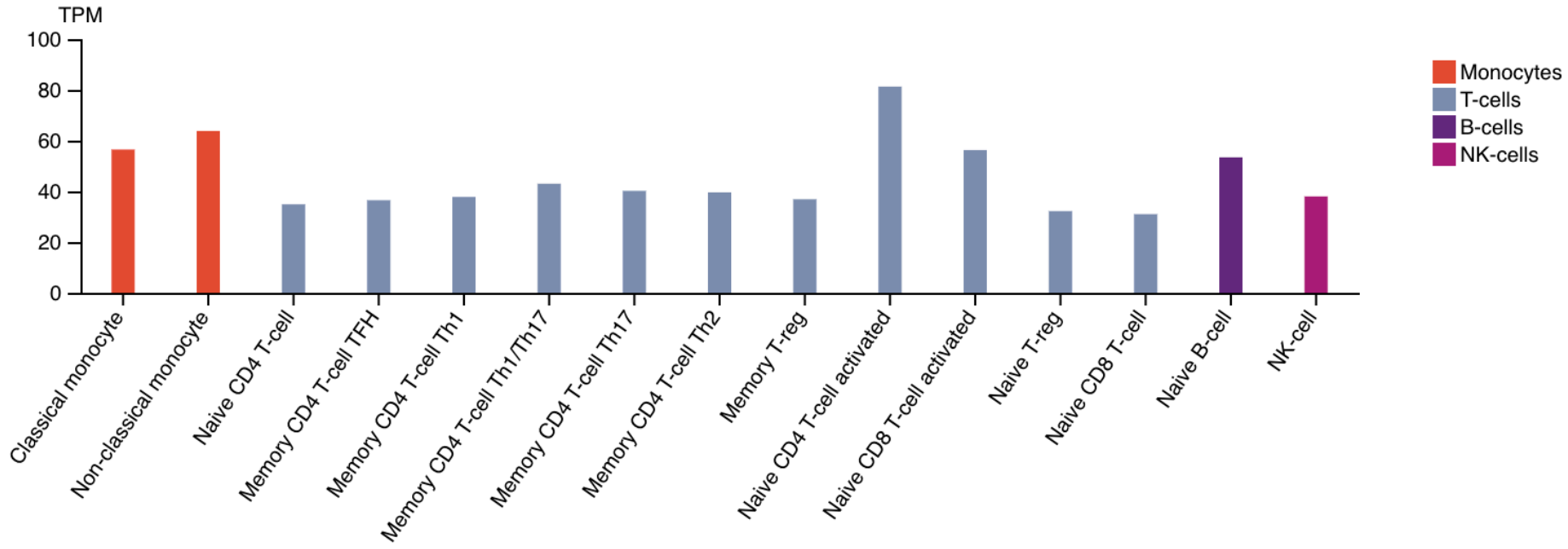

Figure 6.4. ADAM17 mRNA expression levels across different human immune cell types. Image credit: The Human Protein Atlas (https://www.proteinatlas.org/ENSG00000151694-ADAM17/immune+cell). (Schmiedel et al. 2018).

6.2.4 Differences in L-selectin expression between lymphocyte subsets

In this thesis, primary B cells from naïve mice were shown to have consistently lower levels of L-selectin than T cells. This has also been shown in previous studies (Tang et al. 1998). There are several differences between L-selectin on T and B cells that may contribute to this, such as the levels of ADAM17, the levels of the unknown 'basal sheddase' for L-selectin, or the involvement of tetraspanins (Figure 6.5).

Whilst the basal sheddase of L-selectin is still yet to be identified, it's possible that this could be ADAM17 on B cells, which may account for lower basal levels of L-selectin seen compared to T cells. ADAM17$^{-/-}$ B cells had significantly higher L-selectin levels compared to ADAM17$^{+/+}$ B cells in whole blood from uninfected mice (Figure 5.2 F). As ADAM17 mRNA levels are higher in naïve B cells, it is possible that B cells have higher levels of basal L-selectin shedding compared to T cells. This will be covered in more detail in section 6.4.

CD53 tetraspanin was found to contribute to the stability of L-selectin in leucocytes, with CD53$^{-/-}$ mice having reduced levels of L-selectin on T cells, but no L-selectin present on B cells (Demaria et al. 2020). This may suggest L-selectin on B cells is less stable than T cells or undergoes more constitutive shedding (Figure 6.5 A).

CD9 tetraspanin has been shown to directly negatively regulate ADAM17 function in endothelial cells and leucocytes (Gutiérrez-López et al. 2011). CD9 was shown to associate with ADAM17 under basal conditions, negatively regulating its function. Once PMA stimulation was induced, CD9 disassociated from ADAM17, allowing it to carry out proteolytic ectodomain shedding of TNF-α (Gutiérrez-López et al. 2011). Additionally, anti-CD9 agonist antibodies were able to block PMA-induced TNF-α shedding on monocytes, T cells, and B cells, whilst CD9 silencing induced shedding (Gutiérrez-López et al. 2011).

In this thesis anti-ADAM10 antibody 1H5 showed no effects of inhibiting L-selectin or TNF-α shedding *in vitro* (Figure 3.2, 3.5, 3.8), which confirmed previous findings that there is no role for ADAM10 in L-selectin or TNF-α

shedding (Reddy et al. 2000), (Mohammed et al. 2019). ADAM10 can shed L-selectin and TNF-α in cells where ADAM17 is knocked out (le Gall et al. 2009), (Mezyk-Kopeć et al. 2009), and ADAM10 can mediate constitutive TNF-α shedding (Arduise et al. 2008). However, this seems to be dependent on cell type and stimulus as P2X7 nucleotide receptor activation in ADAM17$^{-/-}$ fibroblasts and primary mouse B cells induced ADAM10-mediated L-selectin shedding (le Gall et al. 2009).

Gutiérrez-López et al. showed that anti-CD9 antibodies have opposite effects on ADAM10-mediated shedding compared to ADAM17-mediated shedding. Anti-CD9 antibodies induced basal TNF-α shedding from B cells, but not PMA-induced TNF-α shedding (Gutiérrez-López et al. 2011). This suggests that CD9 has stimulatory effects on ADAM10 and inhibitory effects on ADAM17 in B cells and may provide an explanation as to why naïve B cells have lower levels of L-selectin compared to T cells. Furthermore, the human protein atlas shows B cells have a higher RNA expression of CD9 compared to T cells (Uhlén et al. 2015); this increased level of CD9 may therefore exert induction of ADAM10-mediated L-selectin constitutive shedding (Figure 6.5 B). These two hypotheses for reduced L-selectin on B cells are summarised in figure 6.5.

Lower levels of L-selectin on naïve B cells compared to T cells may have functional relevance *in vivo*, as several biological processes may be affected. Whilst there is little research done on L-selectin function in B cells, B cells had reduced homing capabilities in mice compared to T cells, attributed to lower L-selectin expression (Tang et al. 1998). L-selectin$^{-/-}$ B cells also had reduced homing to LNs, and Peyer's patches compared to wild-type B cells (Tang et al. 1998). There are also reports of altered antibody production in both naïve and immunised L-selectin$^{-/-}$ mice, suggesting that L-selectin may regulate antibody production (Steeber et al. 1996). Furthermore, germinal centres in LNs were also larger in size in L-selectin$^{-/-}$ mice (Steeber et al. 1996).

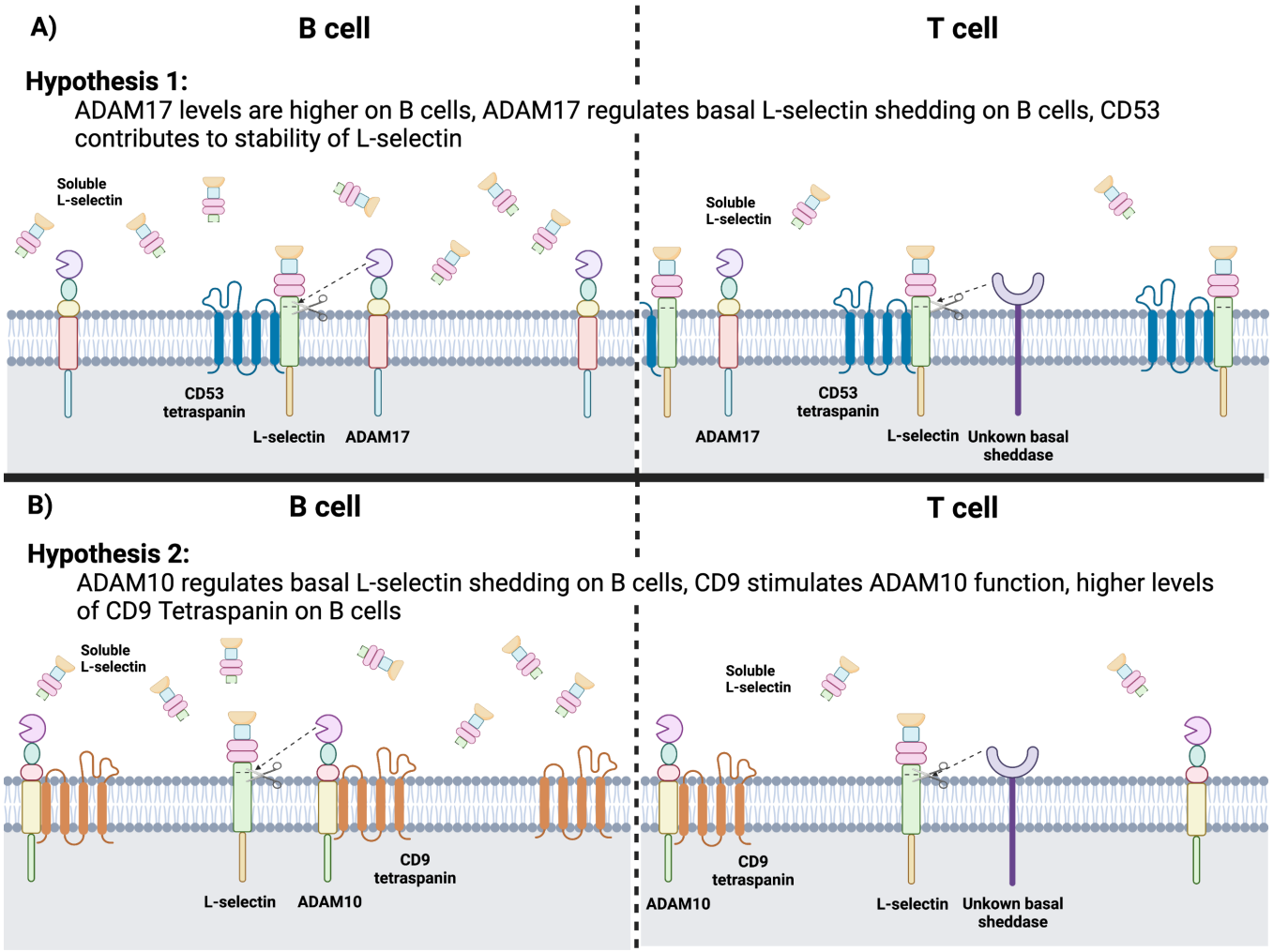

Figure 6.5. Hypotheses for lower L-selectin expression on B cells than T cells in unactivated conditions. A) Hypothesis 1; ADAM17 levels are higher on B cells than T cells. ADAM17-dependent basal shedding of L-selectin on B cells leads to lower cell surface L-selectin expression and higher

soluble L-selectin expression than T cells. CD53 tetraspanin contributes to cell surface L-selectin stability. **B)** Hypothesis 2; ADAM10-dependent basal shedding of L-selectin on B cells leads to lower cell surface L-selectin expression and higher soluble L-selectin expression than T cells. CD9 tetraspanin levels are higher on B cells than T cells, stimulating ADAM10 basal shedding function. Figure created using Biorender.com

6.3 X31 H3N2 influenza A virus model

The model of influenza virus used in this work, was the H3N2 IAV strain X31. X31 is known to be less pathogenic than commonly used H1N1 strain PR8. Mice subjected to X31 infection showed reduced weight loss and improved survival compared to mice infected with PR8 (Askovich et al. 2013). X31 was therefore chosen due to less harmful effects to mice, prioritising welfare.

Weight loss is a commonly used parameter to monitor mouse welfare during experimentation, especially during infection. Weight loss is also known as a measure of pathogenicity of infection, as it positively correlates with pro-inflammatory cytokines (DeBerge et al. 2015). There were variations in responses to X31 infection seen across different experiments in this thesis. Large error bars representing ±SEM can be seen within some groups when measuring weight loss, suggesting notable variation within treatment groups (Figure 6.6 A). Although there is a general pattern of decreasing weight observed with each individual experiment (Figure 6.6 A).

To address the concept that weight loss is a measure of pathogenicity of infection, weight loss from X31 infections in this thesis were plotted against lung viral load (Figure 6.6. B, C). Weight loss positively corresponded with viral load on day 5 of infection, with an r value of 0.2, however, this was not significant (Figure 6.6 B). On day 7 this was the opposite, with an r value of -0.4 suggesting a negative correlation. (Figure 6.6 C). This suggests that weight loss may be an unreliable measure of severity of infection, in the X31 model. Other studies have also found that weight loss does not correlate with viral titre across infection with X31 (Sanders et al. 2015), and PR8 (Kenney et al. 2019).

There were also large differences in viral titres measured in independent experiments (Figure 6.6 B, C). For example, in chapter four viral titres on day 7 of X31 infection were between $1.1x10^3$-$5.8x10^3$ pfu (Figure 4.3, 6.6 C). Whilst in chapter five on day 5 of X31 infection viral titres varied from $3.7x10^4$-$7.0x10^5$ (Figure 5.6, 5.11, 6.6 B). This suggests that viral titres may not be reproducible

across individual repeats. A limitation to the use of viral plaque assays is that counting of plaques is subjective and different individuals may count differently. A standardised method using QuPath software to count plaques has now been developed in our lab but was not used for the data presented in this work. RT-qPCR was also used to measure viral load, by detecting X31 NP mRNA in the lungs. However, mRNA does not equate to protein and there is likely to be viral RNA present in mouse lungs from dead cells which may skew data. Plaque assays are a measure of live replicating virus present in the lungs and is therefore the most widely used method.

CD8 antigen-specific T cells were not able to be detected in the mice which is a major limitation to the data presented in this thesis. Dextramers are 10-mer MHC-peptide complexes bound to a fluorophore via a dextran backbone. They can be used to detect antigen-specific T cell populations by flow cytometry. 'ASNENMDAM' dextramer from Immudex was used in these experiments, however, high levels of non-specific binding were detected in both dead and live cells, therefore a credible population of dextramer positive cells were not found. The lack of dextramer staining in this work made it difficult to detect which CD8 T cells were primed and antigen-specific, compared to unactivated circulating cells. This may suggest a lack of a robust IAV-specific CD8 T cell response. This meant a conclusion was unable to be made as to whether ADAM17 inhibition improved CTL homing in murine IAV infection.

Whilst L-selectin maintenance on CD8 T cells is protective in PR8 IAV infection, this is not true of H17 IAV infection (Mohammed et al. 2016). H17 is a non-pathogenic strain of IAV which is similar to an influenza vaccine, rather than a pathogenic infection. LΔP mice infected with H17 IAV had improved viral clearance compared to L-selectin$^{-/-}$ mice, but there was no difference compared to wild-type B6 mice (Mohammed et al. 2016). This was also true of a model whereby H17 infected Rag$^{-/-}$ mice were injected with F5 TCR transgenic T cells which recognise H17. H17 infected Rag$^{-/-}$ mice with F5LΔP T cells had improved viral clearance compared to Rag$^{-/-}$ mice supplemented with no T cells or F5L-selectin$^{-/-}$ T cells (Mohammed et al. 2016). This suggests that L-selectin maintenance on CD8 T cells is important in pathogenic IAV infection, but not in a non-pathogenic infection. As X31 is a less pathogenic strain of IAV than PR8,

it’s possible that L-selectin maintenance will provide no superior viral clearance compared to wild-type T cells.

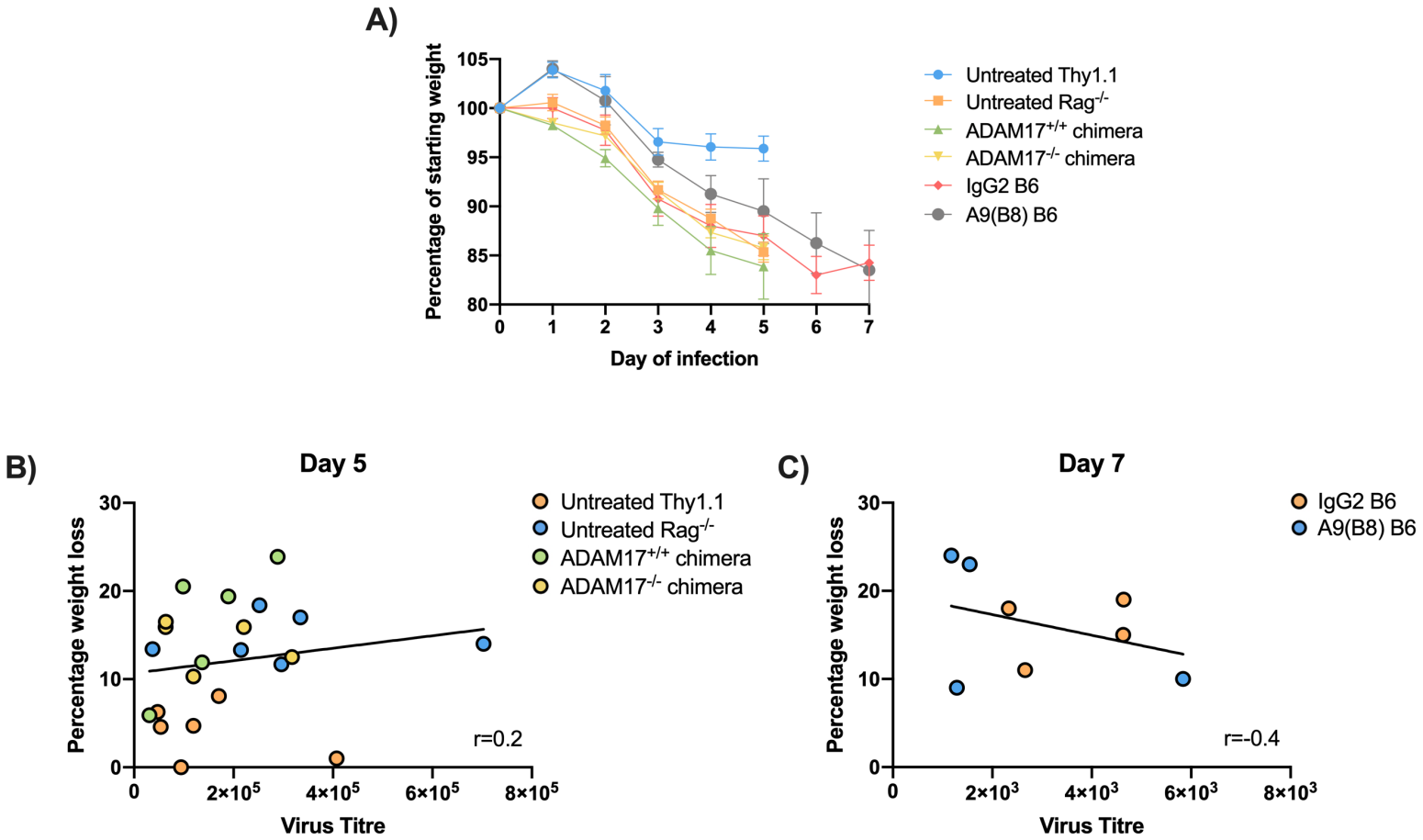

Figure 6.6. Weight loss in X31 IAV infection. All mice were intranasally infected with $1x10^3$ pfu X31 H3N2 influenza A virus. Mice were weighed daily and humanely killed on day 5 or day 7 of infection. Lungs were excised for viral load analysis via plaque assay. **A)** Percentage of starting weight

over the course of infection. Untreated Thy1.1, untreated $Rag^{-/-}$, $ADAM17^{+/+}$ radiation chimera, $ADAM17^{-/-}$ radiation chimera, IgG2 treated B6, A9(B8) treated B6. **B)** Percentage weight loss on the final day of infection (day 5) plotted against viral titre on corresponding day. M1-6 (Orange); Untreated Thy1.1 M7-12 (Blue); Untreated $Rag^{-/-}$. M13-17 (Green); $ADAM17^{+/+}$ radiation chimeras. M18-22 (Yellow); $ADAM17^{-/-}$ radiation chimeras. **C)** Percentage weight loss on the final day of infection (day 7) plotted against viral titre on corresponding day. M1-4 (Orange); IgG2 treated B6. M5-8 (Blue); A9(B8) treated B6. Simple linear regression.

6.3.1 Accelerated clearance of A9(B8) *in vivo*

Anti-ADAM17 antibody A9(B8) was unable to reduce X31 IAV burden in mouse lungs 7 days post-infection (Figure 4.3). Sera analysis revealed that concentrations of A9(B8) in the circulation at this timepoint were insufficient to block L-selectin shedding on lymphocytes (Figure 4.6). Due to this, a conclusion was unable to be made as to whether maintaining L-selectin on CTLs via ADAM17 inhibition was beneficial for virus clearance. To further determine the functionality of A9(B8) *in vivo*, 15 mg/kg of A9(B8) was administered to mice via an i.v. or i.p. injection. 6 hours post-injection, serum levels of A9(B8) were sufficient to block L-selectin shedding in CD8 T cells, however, this effect was diminished by 4 days (Figure 4.9). There was also no detection of A9(B8) in lung tissue on day 4 (Figure 4.10) However, protein analysis did confirm that A9(B8) was intact and of high concentration (Table 4.2, Figure 4.11).

These findings from chapter four suggested that A9(B8) was being cleared rapidly from the mice, or the antibody was losing its effects *in vivo*. Pharmacokinetic analysis by Ye et al. showed A9(B8) had a half-life of 13 hours *in vivo*, with a terminal half-life of 10.5 days (Ye et al. 2017). However, this was tested in naïve B6 mice and not during infection. Several studies have found that inflammation and inflammatory cytokines can affect the levels of cytochrome enzymes and transporters that play major roles in drug absorption, metabolism, and excretion (Martinez et al. 2020). Therefore, it is likely that the half-life of A9(B8) is different in mice that are fighting infection.

One potential explanation for the accelerated clearance of A9(B8) is that a human antibody would be detected as a foreign body by the murine immune system. Anti-human immunoglobin antibodies have been measured in mice and can be detected as soon as 1-week post-administration, although this was not significantly different to the PBS treated group until 10 weeks post-administration (Fülber et al. 2014).

Whilst A9(B8) was taken forward for *in vivo* studies due to its *in vitro* inhibition of L-selectin shedding, it was also chosen due to its prior success in a mouse model of pancreatic cancer (Ye et al. 2017). The model

(*P9dx1Cre*;*Kras*^{G12D};*Trp53*$^{flox/+}$(KP^{fl}C)) induces *Kras* expression and has 1 deleted allele of *Trp53* to induce spontaneous pancreatic tumour growth from 1 month of age. However, this study was carried out without an appropriate isotype control group (Ye et al. 2017). From 5 weeks of age, mice were injected twice a week with 10 mg/kg A9(B8) or PBS for 6 weeks (Ye et al. 2017). Therefore, it is difficult to conclude whether reduced tumour burden was directly due to ADAM17 inhibition, or to do with human antibody administration, especially with only 4 mice in each group (Ye et al. 2017). Whilst a reduction in soluble TNF-α and amphiregulin were seen in plasma, this was only tested after 6 weeks of treatment; A9(B8) may not have this effect after 1 dose, as used in this thesis (Ye et al. 2017). Furthermore, cell surface levels of ADAM17 substrates were not tested and function of A9(B8) was reliant on soluble substrate release.

6.3.2 ADAM17 as pharmacological target in IAV infection

Several studies have established that ADAM17 is upregulated in inflammatory conditions and cancer (Shimoda et al. 2016), (Ohta et al. 2001), (Ju et al. 2007), (Lendeckel et al. 2005). In mice infected with the PR8 strain of influenza A virus, L-selectin is reduced on activated, antigen-specific CD8 T cells in the med LN on day 2 but re-expressed by day 4 (Mohammed et al. 2016). In the peripheral blood and lungs on day 4, L-selectin expression begins to decrease, with less than 5% of CTLs in the lungs being L-selectin positive by day 8 (Mohammed et al. 2016). This suggests a critical window in which L-selectin shedding can be inhibited, prior to day 2 of infection or between days 4 and 8 following infection. *In vitro* studies in HEK and HeLa cells found that PMA caused an initial increase in mature cell surface ADAM17 levels and proteolytic cleavage, followed by internalisation and degradation (Lorenzen et al. 2016). ADAM17 activity was not restored until over 12 hours post-stimulation (Lorenzen et al. 2016). This suggests that TCR activation in CD8 T cells in IAV infection may result in an initial increase of ADAM17, which sheds L-selectin, followed by a decrease in cell surface ADAM17, allowing L-selectin re-expression. The inability of day 4 sera from A9(B8) injected mice to inhibit ADAM17-mediated shedding (Figure 4.9), suggests that bioavailability of A9(B8) is too low to block ADAM17 during the time period when activated CD8

T cells are being recruited from the bloodstream into the lungs of IAV infected mice. Further work is required to determine if ADAM17 is downregulated and re-expressed in TCR-activated T cells, as found following PMA activation of HEK cells, in order to target it therapeutically.

As pharmacological inhibition of ADAM17 using A9(B8) was redundant, radiation chimeric mice containing deficient or sufficient ADAM17 in the lymphoid lineage of leucocytes were created. Chimeras were used to determine effects of ADAM17 inhibition on T cell homing and viral clearance in a mouse model of X31 IAV infection. ADAM17$^{-/-}$ chimeric mice successfully maintained L-selectin on the surface of CD8 T cells (Figure 5.9 C), however, there was no improved CD8 T cell homing to lungs on day 5 of infection (Figure 5.9 A). There was also no significant improvement in viral clearance on day 5 compared to ADAM17$^{+/+}$ chimeric mice (Figure 5.11).

6.3.3 Day 5 of X31 IAV infection may be too early to detect a CTL response

The kinetics of murine IAV are important to understand for pharmacological intervention. In humans, current influenza drugs available are only effective if taken within a few days of symptom onset. Studies have investigated the CD8 T cell response in murine IAV infection; CTLs are found to accumulate in the lungs from day 5 of infection, peaking at day 8-10 (Miao et al. 2010), (Moskophidis and Kioussis 1998). This is also found to correlate with viral clearance (Miao et al. 2010), (Moskophidis and Kioussis 1998).

Work by Moskophidis and Kioussis using Rag$^{-/-}$ mice with F5-TCR transgenic CD8 T cells and A/NT/60/68 strain of IAV infection (recognised by F5 TCR), has given clear insight into the role of antigen-specific CTLs in murine IAV. These mice lack CD4 T cells and B cells and therefore focuses on antigen-specific CD8 T cell responses. Rag$^{-/-}$ with F5-CD8 T cells had improved survival rates at doses $\leq 10^6$ pfu compared to Rag$^{-/-}$ mice with no lymphocytes (Moskophidis and Kioussis 1998). However, there was also a pathogenic role for CTLs at high doses as Rag$^{-/-}$ with F5-CD8 T cells had significantly worse survival rates compared to Rag$^{-/-}$ at 10^7 pfu IAV (Moskophidis and Kioussis 1998). Transgenic CTLs were detected earlier in infection with higher virus inoculation doses, but

in lower doses increased lung CTLs correlated with reduction in viral load (Moskophidis and Kioussis 1998). Overall, this shows that control of IAV infection by CTLs directly correlates with viral load and survival in mice.

Our hypothesis is that maintained L-selectin on CTLs will have improved trafficking to mouse lungs and subsequent viral clearance. Therefore, if there is a role for ADAM17 in controlling L-selectin dependent homing of virus-specific CD8 T cells to the lungs during virus replication, it may not be detectable until later than day 5 post-infection measured in this study, (Figure 5.11). X31 IAV infection was carried out on $Rag^{-/-}$ and wildtype Thy1.1 mice to determine the involvement of the adaptive immune response. Whilst this was a small cohort (n=6), there was a trend suggesting lower viral titres in Thy1.1 on day 5 and no major differences in BAL CD8 infiltration compared to day 7 of X31 infection (Figure 5.5, 5.6). However, there was a significant increase in CD8 T cells in the lungs on day 7 of infection, compared to day 5 (Figure 5.5).

6.4 Basal shedding of L-selectin on lymphocytes

Several experiments have suggested roles for ADAM17 in the constitutive or basal shedding of L-selectin detected *in vitro*. Basal shedding is the homeostatic process of ectodomain cleavage in the absence of cell activation. It is currently unknown if there is a stimulus for this process, nor is the biological relevance of this process known.

In chapter three, A9(B8) was able to block L-selectin shedding from CD4 T cells *in vitro* to levels above those on starting lymphocytes (Figure 3.1 B, 3.4 B). High concentrations of A9(B8) were also able to block levels of soluble L-selectin to levels below that generated by unactivated lymphocytes (Figure 3.10). Additionally, in chapter four, CD4 T cells treated with A9(B8) had cell surface levels of L-selectin above basal (Figure 4.6 B) However, published data from the Ager lab suggests that ADAM17 does not control basal shedding of L-selectin in T cells *in vivo* or *in vitro* (Mohammed et al. 2019). In these studies, $ADAM17^{-/-}$ chimeric mice had the same levels of L-selectin on naïve T cells as $ADAM17^{+/+}$ chimeras, suggesting both had undergone the same level of

homeostatic shedding (Mohammed et al. 2019). This finding was also seen with ADAM17 chimeras generated in this thesis (Figure 5.2).

L-selectin$^{-/-}$ mice injected with ADAM17 deficient haemopoietic stem cells had serum levels of soluble L-selectin slightly lower than in mice injected with ADAM17 sufficient cells, but this was not statistically significant (Mohammed et al. 2019). This suggests ADAM17-dependent basal shedding in a small population of leucocytes, or an underpowered experiment. Furthermore, ADAM10 inhibitor TIMP-1 did not inhibit basal shedding of L-selectin from ADAM17 deficient T lymphocytes (Mohammed et al. 2019). Therefore, the basal sheddase of L-selectin on T cells is still yet to be discovered and requires further investigation.

Soluble L-selectin in the plasma of Rag$^{-/-}$ has been found to be 70% lower than wild-type mice, suggesting that a large proportion of L-selectin basal shedding is carried out on lymphocytes and only 30% is non-lymphoid derived (Tu et al. 2002). However, there is evidence that ADAM17 does control basal shedding on neutrophils, monocytes, and lymphocytes as demonstrated in ADAM17$^{-/-}$ chimeras with deficient ADAM17 in all leucocytes (Li et al. 2006). These cells sampled from peripheral blood had higher levels of cell surface L-selectin than wild-type mice (Li et al. 2006). Conversely, these ADAM17 deficient mice had similar levels of soluble L-selectin in plasma to wild-type (Li et al. 2006). Li et al. suggests that a large proportion of plasma L-selectin is generated by apoptotic neutrophils (Li et al. 2006). They found that soluble L-selectin released from neutrophils undergoing spontaneous apoptosis was similar in wild-type and ADAM17$^{-/-}$ chimeras, however this was blocked by pan-metalloproteinase inhibitors (Li et al. 2006). Additional to this finding, Wang et al. discovered that apoptotic neutrophils and Jurkat T cells released soluble L-selectin via an ADAM17-dependent mechanism in early apoptosis, but independent of ADAM17 in the later stages of cell death (Wang et al. 2010). Overall, this suggests that whilst a large proportion of basal L-selectin shedding occurs in lymphocytes, apoptotic neutrophils may account for the remaining significant portion. As neutrophils have a short life span *in vivo*, many neutrophils will undergo apoptosis every day and release soluble L-selectin. Other potential mechanisms for release of non-lymphocyte soluble L-selectin include monocyte

and neutrophil transendothelial migration (Rzeniewicz et al. 2015), (Rahman et al. 2021), (Allport et al. 1997).

B cells were not specifically investigated by Mohammed et al. or Li et al. and may have alternative constitutive shedding control mechanisms. In chapter five ADAM17$^{-/-}$ mice had higher levels of L-selectin on B cells with an average MFI of 1722 compared to 1629 and 1477 CD8 and CD4 T cells, respectively (Figure 5.2 B, D, F). There was also a significantly higher level of L-selectin on ADAM17$^{-/-}$ B cells compared to ADAM17$^{+/+}$ B cells, with an average L-selectin MFI of 1722 compared to 1196 (Figure 5.2 F). This suggests that ADAM17 may contribute to basal L-selectin shedding on B cells (Figure 6.5 A).

Overall, these findings and previous studies suggest that basal L-selectin shedding is a diverse process in mice and may have different mechanisms, depending on cell type.

6.5 Roles of soluble L-selectin and soluble TNF-α

ADAM17 ectodomain proteolytic cleavage of L-selectin and TNF-α results in the release of a soluble form of each substrate which are both documented to have their own biological effects. Soluble L-selectin was found to bind cytokine activated endothelium, inhibiting lymphocyte attachment *in vitro* in a concentration dependent manner (Schleiffenbaum et al. 1992). Soluble L-selectin was also found to reduce lymphocyte homing to lymph nodes *in vivo*, in a concentration dependent manner (Tu et al. 2002). This suggests that soluble L-selectin may negatively regulate cell homing functions. However, LΔP mice which have little soluble L-selectin exhibit no increased lymphocyte rolling velocity or recruitment to lymph nodes (Galkina et al. 2007). Therefore, soluble L-selectin may not have functional relevance *in vivo,* at least in constitutive trafficking to secondary lymphoid organs. However, reduced levels of plasma L-selectin have been linked with increased mortality rates in bacterial sepsis (Seidelin et al. 2002), although this may be a by-product of excessive leucocyte activation. To date there has not been any direct investigation into the role of soluble L-selectin in IAV infection.

Soluble TNF-α has been shown to have different biological consequences from membrane bound TNF-α such as increasing tumour growth and inflammation (Ardestani et al. 2013), (Ruuls et al. 2001). Soluble TNF-α has important roles in contributing to lung injury in IAV infection (DeBerge et al. 2013). Production of the neutrophil recruitment chemokine CXCL2 by CD8 T cells was dependent on soluble TNF-α, resulting in greater mortality in mice (DeBerge et al. 2013).

Although ADAM17$^{-/-}$ chimeric mice successfully maintained high levels of L-selectin on T lymphocytes (Figure 5.2, 5.9), there were still detectable levels of soluble L-selectin in BALF (168 ng/mL) and sera (3.8 µg/mL) (Figure 5.12). There was 71 pg/mL of TNF-α measured in BALF of ADAM17$^{-/-}$ mice (Figure 5.13 C). This suggests that other cell types are releasing soluble L-selectin and TNF-α such as innate leucocytes. Pro-inflammatory monocytes and neutrophils are known to peak in the lungs at day 5 of IAV infection and may be responsible for this (Lin et al. 2008), (Tate et al. 2008). Furthermore, a proportion of soluble L-selectin and TNF-α may still be released from lymphocytes as ADAM10 can shed L-selectin and TNF-α in cells where ADAM17 is knocked out (le Gall et al. 2009), (Mezyk-Kopeć et al. 2009).

6.6 Effects of ADAM17 inhibition other than L-selectin in lymphocytes, on IAV infection

ADAM17 was targeted in this study as the known proteolytic sheddase of L-selectin. However, ADAM17 has over 80 known substrates and blocking its function is likely to have effects on other substrates which may impact CTL development, migration and IAV clearance. For example, IL-6R is a well characterised substrate of ADAM17 which is the signalling receptor for the pro-inflammatory cytokine IL-6. An increase of IL-6R on the cell surface of leucocytes may further propagate pro-inflammatory IL-6 signalling which could result in host tissue damage. Increased sera levels of IL-6 were associated with severe disease in H1N1 IAV infection patients (Yu et al. 2011).

TNF-α and its receptors, TNFRI and TNFRII are also substrates of ADAM17 which may have profound effects in IAV infection. Soluble levels of TNF-α and TNFRII were found to be increased after IAV inoculation in mice, both systemically and in BALF (DeBerge et al. 2015). Soluble TNFRII levels positively correlated with dose of virus given, with CD8 T cells found to be a key cell to release TNFRII in the lungs (DeBerge et al. 2015). TNFRII was found to regulate levels of soluble TNF-α, as blockade or knockout of TNFRII increased BALF soluble TNF-α levels (DeBerge et al. 2015). Blocking the shedding of both TNFRII and TNF-α may reduce the propagation of pro-inflammatory TNF signalling and diminish viral clearance.

DeBerge et al. have also demonstrated that soluble TNF-α contributes to severe lung injury in IAV infection. Soluble TNF-α stimulated CXCL2 production by CD8 T cells which resulted in neutrophil accumulation in the lungs and greater mortality rates in a transgenic mouse model of H2N2 IAV pneumonia (DeBerge et al. 2013). DeBerge et al. took a similar approach to us in creating ADAM17$^{-/-}$ radiation chimeras using Rag$^{-/-}$ mice as hosts (DeBerge et al. 2013). Haemaglutinin (HA)-specific CD8 T cells isolated from ADAM17$^{-/-}$ chimeras were injected into IAV infected mice and shown to protect against IAV infection, whilst mice receiving wild-type HA-specific CD8 T cells did not survive past day 4 of infection (DeBerge et al. 2013). This suggests that a reduction in soluble TNF-α is protective in murine IAV infection. Although L-selectin levels were not analysed in this study, maintenance of L-selectin on ADAM17$^{-/-}$ CD8 T cells may also have improved IAV clearance. However, the IAV model used by DeBerge et al. was a transgenic model whereby the IAV HA gene is expressed by alveolar cells in the lungs under a promoter (DeBerge et al. 2013). A similar experiment was carried out using PR8 H1N1 virus and NP-specific CD8 T cells from ADAM17$^{-/-}$ mice (DeBerge et al. 2013). Mice receiving adoptive transfer of CD8 T cells survived infection, whilst mice receiving no CD8 T cells died by day 6 (DeBerge et al. 2013). However, this was not compared to mice receiving ADAM17$^{+/+}$ NP-specific CD8 T cells.

Undesirable effects of ADAM17 inhibition could include improved recruitment of innate inflammatory cells in infection via L-selectin. This has been demonstrated in a mouse model of peritonitis, whereby ADAM17$^{-/-}$ neutrophils had increased

recruitment to the peritoneum (Long et al. 2010), (Tang et al. 2011). Whilst this has not been investigated in IAV infection, it's a potential consequence of systemic ADAM17 inhibition which could upregulate inflammation and tissue damage.

Lymphocyte activation gene-3 (LAG-3) and T cell immunoglobulin and mucin domain-3 (TIM-3) are also substrates of ADAM17 and these function as checkpoint molecules on T cells. ADAM17 inhibition may lead to increased cell surface LAG-3 and TIM-3 expression, which could contribute to cell exhaustion and reduced CTL responses (Blackburn et al. 2009).

Due to the wide variety of substrates targeted, it is appropriate to suggest that ADAM17 may control IAV infection independently of L-selectin on CD8 T cells. Therefore, ADAM17 may be an ineffective target for increasing L-selectin dependent CTL homing and viral clearance. It may be more applicable to target L-selectin itself, due to the attenuating effects that may occur by inhibiting ADAM17 in non-CD8 T cells.

6.7 Systemic ADAM17 inhibition may result in undesirable effects

In chapters four and five, ADAM17 inhibition was not specific to CD8 T cells as desired. Anti-ADAM17 antibody A9(B8) was systemically administered either by i.p. or i.v. injection. Therefore, A9(B8) could bind to any cells expressing ADAM17. Radiation chimeras in chapter five were created with all lymphocytes deficient in ADAM17. ADAM17 inhibition in other cell types could have attenuating effects on CTLs or result in changes from other substrates. It is well characterised that mice lacking ADAM17 die *in utero* due to effects on EGF signalling (Peschon et al. 1998), whilst spontaneous ADAM17 genetic mutations in humans have all resulted in serious health issues or death (Blaydon et al. 2011), (Bandsma et al. 2015). It is well understood that ADAM17 is expressed on almost all cell types and has over 80 substrates, although we were only interested in blocking the shedding of L-selectin on CD8 T cells, due to the protective effects seen in LΔP mice (Mohammed et al. 2016). An

improvement to this work would be to use conditional ADAM17 knockout mice which would remove ADAM17 function in CD8 T cells alone (Horiuchi et al. 2007). Alternatively, an adoptive T cell model could be used whereby ADAM17$^{-/-}$ antigen-specific CD8 T cells could be isolated and injected i.v. into IAV infected mice. The most specific way to target L-selectin shedding pharmacologically, would be to design an inhibitor against the ADAM17 cleavage site of L-selectin. This would avoid the unwanted effects on other ADAM17 substrates.

As mentioned, DeBerge et al. found that IAV specific CD8 T cells isolated from ADAM17$^{-/-}$ chimeras protected from lethal IAV infection when injected into IAV infected mice (DeBerge et al. 2013). However, this was tested in a transgenic model of IAV pneumonia where the A/Japan/57 H2N2 HA gene is produced by alveolar cells under a strong promoter. This is an artificial system where HA-specific TNF-α producing CD8 T cells cause lung injury and lethality (Xu et al. 2004). Whereas antigen specific CD8 T cells in X31 IAV infection are found to be protective (Taylor and Askonas 1986). Nonetheless, this work highlights that ADAM17$^{-/-}$ CD8 T cells are protective in IAV infection, which has not been shown with any other leucocyte to date. Contrary to this, ADAM17 deficient T cells from Adam17$^{fl/fl}$×CD4cre^{+} mice which only have ADAM17 deficiency in T cells did not improve clearance of *Listeria monocytogenes* bacterial infection compared to Adam17$^{fl/fl}$×CD4cre^{-} mice (Link et al. 2017). However, this is a mouse model of bacterial infection and ADAM17 may have different roles compared to virus infection.

6.8 Future work

The key question of whether ADAM17 can be targeted for maintaining L-selectin on CD8 T cells to promote homing of CTLs during IAV infection remains to be answered. The timepoints at which this could be targeted are also yet to be answered. Unpublished work from the Ager lab shows a reduction in cell surface human ADAM17 in Molt3 T cells following peptide-MHC activation. However, there are currently no antibodies optimised for flow cytometric analysis of cell surface mouse ADAM17 within our lab, which made this work

unattainable in the timeframe. However, measuring cell surface ADAM17 on CD8 T cells across the course of X31 IAV infection could reveal optimal timepoints, if any, for anti-ADAM17 therapeutic intervention.

Adoptive transfer of antigen-specific ADAM17$^{-/-}$ CD8 T cells into IAV infected mice has been shown to be protective (DeBerge et al. 2013). Therefore, there is still scope to investigate this in the X31 IAV mouse model. DeBerge et al. see no difference in survival until day 5 in their PR8 and transgenic IAV pneumonia models. Taken together with the evidence that the CD8 T cell response to IAV infection peaks at 8-10 days, the experiment carried out in chapter five using ADAM17 radiation chimeras could be repeated with investigation at later timepoints. However, as CD8 T cells are the only ADAM17$^{-/-}$ lymphocytes to be implicated in improved IAV clearance, an adoptive transfer model may be most appropriate.

Due to the promising results seen with LΔP mice, there is a clear role for L-selectin on CTLs improving IAV clearance *in vivo* (Mohammed et al. 2016). The X31 strain of IAV is yet to be tested in LΔP mice, and we cannot be sure whether maintained L-selectin on CTLs confers protection against this strain. Therefore, having an LΔP cohort within studies on ADAM17$^{-/-}$ mice may be of benefit. However, targeting ADAM17 to achieve this may not be feasible. The most specific way to therapeutically target L-selectin would be to create a small molecule inhibitor or antibody which directly blocks the cleavage site of L-selectin. Future studies may involve immunising mice or using phage display to select antibodies against the short fragment of L-selectin which contains the ADAM17 cleavage site and screen for inhibition of L-selectin shedding.

6.9 Overall conclusion

The overarching hypothesis for this body of work is that ADAM17 inhibition in a mouse model of IAV infection will result in improved CD8 T cell homing to sites of virus infection (lungs) and subsequent viral clearance, via an L-selectin dependent mechanism. This hypothesis was unable to be proven in this body of work firstly due to ineffective ADAM17 inhibition by pharmacological

inhibitor A9(B8). Secondly due to the early timepoint of termination with IAV infected ADAM17 chimeric mice. However, data suggest that ADAM17 may not be an appropriate target to reduce viral clearance on day 5 of X31 IAV infection in mice. Maintaining L-selectin on CD8 T cells did not confer protection against X31 by day 5 of X31 infection.

Bibliography

Abdul-Careem, M.F. et al. 2012. Critical Role of Natural Killer Cells in Lung Immunopathology During Influenza Infection in Mice. *The Journal of Infectious Diseases* 206(2), pp. 167–177. doi: 10.1093/INFDIS/JIS340.

ADAM17 Inhibitor/ Rituximab After Auto HCT for DLBCL. ClinicalTrials.gov. 2014. Available at: https://clinicaltrials.gov/ct2/show/NCT02141451 [Accessed: 12 March 2021].

Ager, A. 2012. *ADAMs and Ectodomain Proteolytic Shedding in Leucocyte Migration: Focus on L-Selectin and ADAM17*. *Current Immunology Reviews* 8(2), pp. 103-117. doi: 10.2174/157339512800099657.

Akaike, T., Ando, M., Oda, T., Doi, T., Ijiri, S., Araki, S. and Maeda, H. 1990. Dependence on O2- generation by xanthine oxidase of pathogenesis of influenza virus infection in mice. *The Journal of Clinical Investigation* 85(3), pp. 739–745. doi: 10.1172/JCI114499.

Aldridge, J.R. et al. 2009. TNF/iNOS-producing dendritic cells are the necessary evil of lethal influenza virus infection. *Proceedings of the National Academy of Sciences* 106(13), pp. 5306–5311. doi: 10.1073/PNAS.0900655106.

Allport, J.R., Ding, H.T., Ager, A., Steeber, D.A., Tedder, T.F. and Luscinskas, F.W. 1997. L-selectin shedding does not regulate human neutrophil attachment, rolling, or transmigration across human vascular endothelium in vitro. *The Journal of Immunology* 158(9), pp. 4365–2372.

Alon, R. et al. 2020. Leukocyte trafficking to the lungs and beyond: lessons from influenza for COVID-19. *Nature Reviews Immunology* 21(1), pp. 49–64. doi: 10.1038/s41577-020-00470-2.

Anderson, K.G., Sung, H., Skon, C.N., Lefrancious, L., Deisinger, A., Vezys, V. and Masopust, D. 2012. Cutting Edge: Intravascular Staining Redefines Lung CD8 T Cell Responses. *The Journal of Immunology* 189(6), pp. 2702–2706.

Antunes, I. and Kassiotis, G. 2010. Suppression of Innate Immune Pathology by Regulatory T Cells during Influenza A Virus Infection of Immunodeficient Mice. *Journal of Virology* 84(24), pp. 12564–12575. doi: 10.1128/JVI.01559-10.

Arbonés, M.L. et al. 1994. Lymphocyte homing and leukocyte rolling and migration are impaired in L-selectin-deficient mice. *Immunity* 1(4), pp. 247–260.

Ardestani, S., Li, B., Deskins, D.L., Wu, H., Massion, P.P. and Young, P.P. 2013. Membrane versus Soluble Isoforms of TNF-a Exert Opposing Effects on Tumor Growth and Survival of Tumor-Associated Myeloid Cells. *American Association for Cancer Research* 73(13), pp. 3938–3950.

Arduise, C. et al. 2008. Tetraspanins Regulate ADAM10-Mediated Cleavage of TNF-α and Epidermal Growth Factor. *The Journal of Immunology* 181(10), pp. 7002–7013.
Askovich, P.S. et al. 2013. Differential Host Response, Rather Than Early Viral Replication Efficiency, Correlates with Pathogenicity Caused by Influenza Viruses. *PLoS ONE* 8(9), p. e74863. doi: 10.1371/JOURNAL.PONE.0074863.
Aversa, G., Punnonen, J. and de Vries, J.E. 1993. The 26-kD transmembrane form of tumor necrosis factor alpha on activated CD4+ T cell clones provides a costimulatory signal for human B cell activation. *Journal of Experimental Medicine* 177(6), pp. 1575–1585. doi: 10.1084/jem.177.6.1575.
Baekkevold, E.S. et al. 2001. The Ccr7 Ligand ELC (Ccl19) Is Transcytosed in High Endothelial Venules and Mediates T Cell Recruitment. *Journal of Experimental Medicine* 193(9), pp. 1105–1112. doi: 10.1084/JEM.193.9.1105.
Bandsma, R.H.J. et al. 2015. Loss of ADAM17 is associated with severe multiorgan dysfunction. *Human pathology* 46(6), p. 923-928. doi: 10.1016/j.humpath.2015.02.010.
Baumgart, A. et al. 2010. ADAM17 Regulates Epidermal Growth Factor Receptor Expression through the Activation of Notch1 in Non–Small Cell Lung Cancer. *Cancer Research* 70(13), pp. 5368–5378. doi: 10.1158/0008-5472.CAN-09-3763.
Bender, B.S., Croghan, T., Zhang, L. and Small, P.A. 1992. Transgenic mice lacking class I major histocompatibility complex-restricted T cells have delayed viral clearance and increased mortality after influenza virus challenge. *Journal of Experimental Medicine* 175(4), pp. 1143–1145. doi: 10.1084/JEM.175.4.1143.
Benechet, A.P. et al. 2016. T cell-intrinsic S1PR1 regulates endogenous effector T-cell egress dynamics from lymph nodes during infection. *Proceedings of the National Academy of Sciences of the United States of America* 113(8), pp. 2182–2187. doi: 10.1073/PNAS.1516485113.
Bennett, T.A., Edwards, B.S., Sklar, L.A. and Rogelj, S. 2000. Sulfhydryl Regulation of L-Selectin Shedding: Phenylarsine Oxide Promotes Activation-Independent L-Selectin Shedding from Leukocytes. *The Journal of Immunology* 164(8), pp. 4120–4129.
Berg, E.L., McEvoy, L.M., Berlin, C., Bargatze, R.F. and Butcher, E.C. 1993. L-selectin-mediated lymphocyte rolling on MAdCAM-1. *Nature* 366(6456), pp. 695–698. doi: 10.1038/366695a0.
Berlin, C. et al. 1993. α4β7 integrin mediates lymphocyte binding to the mucosal vascular addressin MAdCAM-1. *Cell* 74(1), pp. 185–195. doi: 10.1016/0092-8674(93)90305-A.
Berlin-Rufenach, C., Otto, F., Mathies, M., Westermann, J., Owen, M.J., Hamann, A. and Hogg, N. 1999. Lymphocyte Migration in Lymphocyte Function-associated Antigen (LFA)-1–deficient Mice. *The Journal of Experimental Medicine* 189(9), p. 1478. doi: 10.1084/JEM.189.9.1467.

Black, R.A. et al. 1997. A metalloproteinase disintegrin that releases tumour-necrosis factor-ø from cells. *Nature* 385(6618), pp. 729–733. doi: 10.1038/385729a0.
Blackburn, S.D. et al. 2009. Coregulation of CD8 + T cell exhaustion by multiple inhibitory receptors during chronic viral infection. *Nature Immunology* 10(1), pp. 29–37. doi: 10.1038/ni.1679.
Blaydon, D.C. et al. 2011. Inflammatory Skin and Bowel Disease Linked to ADAM17 Deletion. *New England Journal of Medicine* 365(16), pp. 1502–1508. doi: 10.1056/NEJMoa1100721.
Blümel, J. et al. 2009. Influenza virus. *Transfusion Medicine and Hemotherapy* 36(1), pp. 32–39. doi: 10.1159/000197314.
Borland, G., Murphy, G. and Ager, A. 1999. Tissue inhibitor of metalloproteinases-3 inhibits shedding of L-selectin from leukocytes. *Journal of Biological Chemistry* 274(5), pp. 2810–2815. doi: 10.1074/jbc.274.5.2810.
Bouvier, N.M. and Lowen, A.C. 2010. Animal Models for Influenza Virus Pathogenesis and Transmission. *Viruses 2010, Vol. 2, Pages 1530-1563* 2(8), pp. 1530–1563. doi: 10.3390/V20801530.
Brandes, M., Klauschen, F., Kuchen, S. and Germain, R.N. 2013. A Systems Analysis Identifies a Feedforward Inflammatory Circuit Leading to Lethal Influenza Infection. *Cell* 154(1), pp. 197–212. doi: 10.1016/J.CELL.2013.06.013.
Bromley, S.K., Mempel, T.R. and Luster, A.D. 2008. Orchestrating the orchestrators: chemokines in control of T cell traffic. *Nature Immunology* 9(9), pp. 970–980. doi: 10.1038/ni.f.213.
Budagian, V. et al. 2004. Natural Soluble Interleukin-15Rα Is Generated by Cleavage That Involves the Tumor Necrosis Factor-α-converting Enzyme (TACE/ADAM17). *Journal of Biological Chemistry* 279(39), pp. 40368–40375. doi: 10.1074/JBC.M404125200.
Butcher, E.C. and Picker, L.J. 1996. Lymphocyte Homing and Homeostasis. *Science* 272(5258), pp. 60–67. doi: 10.1126/science.272.5258.60.
Caiazza, F. et al. 2015. Targeting ADAM-17 with an inhibitory monoclonal antibody has antitumour effects in triple-negative breast cancer cells. *British Journal of Cancer* 112(12), pp. 1895–1903. doi: 10.1038/bjc.2015.163.
Califano, D., Furuya, Y., Roberts, S., Avram, D., McKenzie, A.N.J. and Metzger, D.W. 2017. IFN-γ increases susceptibility to influenza A infection through suppression of group II innate lymphoid cells. *Mucosal Immunology* 11(1), pp. 209–219. doi: 10.1038/mi.2017.41.
Cappenberg, A. et al. 2019. L-selectin shedding affects bacterial clearance in the lung: a new regulatory pathway for integrin outside-in signaling. *Blood* 134(17), pp. 1445–1457. doi: 10.1182/BLOOD.2019000685.

Cardani, A., Boulton, A., Kim, T.S. and Braciale, T.J. 2017. Alveolar Macrophages Prevent Lethal Influenza Pneumonia By Inhibiting Infection Of Type-1 Alveolar Epithelial Cells. *PLOS Pathogens* 13(1), p. e1006140. doi: 10.1371/journal.ppat.1006140.

Carlin, L.E., Hemann, E.A., Zacharias, Z.R., Heusel, J.W. and Legge, K.L. 2018. Natural killer cell recruitment to the lung during influenza A virus infection is dependent on CXCR3, CCR5, and virus exposure dose. *Frontiers in Immunology* 9(781), p. 781. doi: 10.3389/FIMMU.2018.00781/BIBTEX.

Cavadas, M. et al. 2017. Phosphorylation of iRhom2 Controls Stimulated Proteolytic Shedding by the Metalloprotease ADAM17/TACE. *Cell Reports* 21(3), pp. 745–757. doi: 10.1016/J.CELREP.2017.09.074.

Cella, M., Jarrossay, D., Facchetti, F., Alebardi, O., Nakajima, H., Lanzavecchia, A. and Colonna, M. 1999. Plasmacytoid monocytes migrate to inflamed lymph nodes and produce large amounts of type I interferon. *Nature medicine* 5(8), pp. 919–923. doi: 10.1038/11360.

Chao, C.C., Jensen, R. and Dailey, M.O. 1997. Mechanisms of L-selectin regulation by activated T cells. *Journal of immunology* 159(4), pp. 1686–94.

Chen, A., Engel, P. and Tedder, T.F. 1995. Structural requirements regulate endoproteolytic release of the L- selectin (CD62L) adhesion receptor from the cell surface of leukocytes. *The Journal of Experimental Medicine* 182(2), p. 530. doi: 10.1084/jem.182.2.519.

Coro, E.S., Chang, W.L.W. and Baumgarth, N. 2006. Type I IFN Receptor Signals Directly Stimulate Local B Cells Early following Influenza Virus Infection. *The Journal of Immunology* 176(7), pp. 4343–4351. doi: 10.4049/JIMMUNOL.176.7.4343.

Crowe, P.D., Walter, B.N., Mohler, K.M., Otten-Evans, C., Black, R.A. and Ware, C.F. 1995. A metalloprotease inhibitor blocks shedding of the 80-kD TNF receptor and TNF processing in T lymphocytes. *Journal of Experimental Medicine* 181(3), pp. 1205–1210. doi: 10.1084/JEM.181.3.1205.

Davies, W.L. et al. 1964. Antiviral Activity of 1-Adamantanamine (Amantadine). *Science* 144(3620), pp. 862–863. doi: 10.1126/SCIENCE.144.3620.862.

DeBerge, M.P., Ely, K.H., Cheng, G.-S. and Enelow, R.I. 2013. ADAM17-Mediated Processing of TNF-α Expressed by Antiviral Effector CD8+ T Cells Is Required for Severe T-Cell-Mediated Lung Injury. *PLoS ONE* 8(11), p. e79340. doi: 10.1371/journal.pone.0079340.

DeBerge, M.P., Ely, K.H., Wright, P.F., Thorp, E.B. and Enelow, R.I. 2015. Shedding of TNF receptor 2 by effector CD8+ T cells by ADAM17 is important for regulating TNF-α availability during influenza infection. *Journal of Leukocyte Biology* 98(3), pp. 423–434. doi: 10.1189/jlb.3A0914-432RR.

Demaria, M.C. et al. 2020. Tetraspanin CD53 Promotes Lymphocyte Recirculation by Stabilizing L-Selectin Surface Expression. *iScience* 23(5), p. 101124. doi: 10.1016/j.isci.2020.101104.
Derry, C., Mordsley, K., Preece, G. and Ager, A. 1997. Purification of L-selectin ligands synthesised by rat peripheral lymph nodes and cultured high endothelial cells. *Biochemical Society transactions* 25(2). doi: 10.1042/BST025260S.
Disdier, M., Morrissey, J.H., Fugate, R.D., Bainton, D.F. and McEver, R.P. 1992. Cytoplasmic domain of P-selectin (CD62) contains the signal for sorting into the regulated secretory pathway. *Molecular Biology of the Cell* 3(3), pp. 309–321. doi: 10.1091/MBC.3.3.309.
Doerschuk, C.M., Beyers, N., Coxson, H. 0, Wiggs, B. and Hogg, J.C. 1993. Comparison of neutrophil and capillary diameters and their relation to neutrophil sequestration in the lung. *The Journal of Applied Physiology* 74(6), pp. 3040–3045. doi: 10.1152/jappl.1993.74.6.3040.
Dosch, J. et al. 2015. Monoclonal antibody targeting of ADAM17 is an effective treatment for metastatic colorectal cancer resulting in tumor growth control and reductions of cancer stem cells. *Cancer Research* 75(15), pp. 975–975. doi: 10.1158/1538-7445.AM2015-975.
Dosch, J. et al. 2017. Targeting ADAM17 inhibits human colorectal adenocarcinoma progression and tumor-initiating cell frequency. *Oncotarget* 8(39), pp. 65090–65099. doi: 10.18632/ONCOTARGET.17780.
Dou, D., Revol, R., Östbye, H., Wang, H. and Daniels, R. 2018. Influenza A virus cell entry, replication, virion assembly and movement. *Frontiers in Immunology* 9(1581). doi: 10.3389/fimmu.2018.01581.
Dougan, S.K. et al. 2013. Antigen-specific B-cell receptor sensitizes B cells to infection by influenza virus. *Nature* 03(7476), pp. 406–409. doi: 10.1038/nature12637.
Durbin, P., Jeung, N., Kullgren, B. and Clemons, G. 1992. Gross composition and plasma and extracellular water volumes of tissues of a reference mouse. *Health physics* 63(4), pp. 427–442. doi: 10.1097/00004032-199210000-00007.
Düsterhöft, S., Jung, S., Hung, C.W., Tholey, A., Sönnichsen, F.D., Grötzinger, J. and Lorenzen, I. 2013. Membrane-proximal domain of a disintegrin and metalloprotease-17 represents the putative molecular switch of its shedding activity operated by protein-disulfide isomerase. *Journal of the American Chemical Society* 135(15), pp. 5776–5781. doi: 10.1021/ja400340u.
Edwards, D.R., Handsley, M.M. and Pennington, C.J. 2008. The ADAM metalloproteinases. *Molecular Aspects of Medicine* 29(5), pp. 258–289. doi: 10.1016/J.MAM.2008.08.001.

Effros, R.B., Doherty, P.C., Gerhard, W. and Bennink, J. 1977. Generation of both cross-reactive and virus-specific T-cell populations after immunization with serologically distinct influenza A viruses. *The Journal of Experimental Medicine* 145(3), pp. 557–568. doi: 10.1084/jem.145.3.557.

Ettensohn, D.B., Frampton, M.W., Nichols, J.E. and Roberts, N.J. 2016. Human Alveolar Macrophages May Not Be Susceptible to Direct Infection by a Human Influenza Virus. *The Journal of Infectious Diseases* 214(11), pp. 1658–1665. doi: 10.1093/INFDIS/JIW413.

Faveeuw, C., Preece, G. and Ager, A. 2001. Transendothelial migration of lymphocytes across high endothelial venules into lymph nodes is affected by metalloproteinases. *Blood* 98(3), pp. 688–695. doi: 10.1182/BLOOD.V98.3.688.

Fiege, J.K. et al. 2021. Mice with diverse microbial exposure histories as a model for preclinical vaccine testing. *Cell Host & Microbe* 29, pp. 1–13. doi: 10.1016/J.CHOM.2021.10.001.

Fischer, R., Maier, O., Naumer, M., Krippner-Heidenreich, A., Scheurich, P. and Pfizenmaier, K. 2011. Ligand-induced internalization of TNF receptor 2 mediated by a di-leucin motif is dispensable for activation of the NFκB pathway. *Cellular signalling* 23(1), pp. 161–170. doi: 10.1016/J.CELLSIG.2010.08.016.

Förster, R., Schubel, A., Breitfeld, D., Kremmer, E., Renner-Müller, I., Wolf, E. and Lipp, M. 1999. CCR7 Coordinates the Primary Immune Response by Establishing Functional Microenvironments in Secondary Lymphoid Organs. *Cell* 99(1), pp. 23–33. doi: 10.1016/S0092-8674(00)80059-8.

Franke, M. et al. 2016. Human and Murine Interleukin 23 Receptors Are Novel Substrates for A Disintegrin and Metalloproteases ADAM10 and ADAM17. *Journal of Biological Chemistry* 291(20), pp. 10551–10561. doi: 10.1074/JBC.M115.710541.

Frey, M., Appenheimer, M.M. and Evans, S.S. 1997. Tyrosine kinase-dependent regulation of L-selectin expression through the Leu-13 signal transduction molecule: evidence for a protein kinase C-independent mechanism of L-selectin shedding. The Journal of Immunology 158(11), pp. 5424–5434.

Friedman, S. et al. 2010. Clinical benefit of INCB7839, a potent and selective ADAM inhibitor, in combination with trastuzumab in patients with metastatic HER2+ breast cancer. *Cancer Research* 69(24), pp. 3025–3025. doi: 10.1200/jco.2010.28.15_suppl.3025.

Fülber, I., Bacher, M., Dodeu, R. and Roskam, S. 2014. Evaluating The Murine Anti-Human Antibody Response And Assessment Of General Activity And Cognition After Treatment With Human Intravenous Immunoglobulins In Healthy Adult C57/B6J Mice. *European Journal of Inflammation* 12(3), pp. 489–497. doi: 10.1177/1721727X1401200310.

Galkina, E. et al. 2003. L-selectin shedding does not regulate constitutive T cell trafficking but controls the migration pathways of antigen-activated T lymphocytes. *The Journal of experimental medicine* 198(9), pp. 1323–35. doi: 10.1084/jem.20030485.
Galkina, E. et al. 2007. T lymphocyte rolling and recruitment into peripheral lymph nodes is regulated by a saturable density of L-selectin (CD62L). *European Journal of Immunology* 37(5), pp. 1243–1253. doi: 10.1002/EJI.200636481.
Le Gall, S.M. et al. 2009. ADAMs 10 and 17 Represent Differentially Regulated Components of a General Shedding Machinery for Membrane Proteins Such as Transforming Growth Factor, L-Selectin, and Tumor Necrosis Factor. *Molecular Biology of the Cell* 20, pp. 1785–1794. doi: 10.1091/mbc.E08.
Gallatin, W.M., Weissman, I.L. and Butcher, E.C. 1983. A cell-surface molecule involved in organ-specific homing of lymphocytes. *Nature* 304(5921), pp. 30–34. doi: 10.1038/304030a0.
Garbers, C. et al. 2011. Species Specificity of ADAM10 and ADAM17 Proteins in Interleukin-6 (IL-6) Trans-signaling and Novel Role of ADAM10 in Inducible IL-6 Receptor Shedding. *The Journal of Biological Chemistry* 286(17), p. 14811. doi: 10.1074/jbc.M111.229393.
Garton, K.J. et al. 2003. Stimulated shedding of vascular cell adhesion molecule 1 (VCAM-1) is mediated by tumor necrosis factor-alpha-converting enzyme (ADAM17). *The Journal of biological chemistry* 278(39), pp. 37459–37464. doi: 10.1074/JBC.M305877200.
Gattinoni, L. et al. 2011. A human memory T cell subset with stem cell–like properties. *Nature Medicine* 17(10), pp. 1290–1297. doi: 10.1038/nm.2446.
Ge, M.Q., Ho, A.W.S., Tang, Y., Wong, K.H.S., Chua, B.Y.L., Gasser, S. and Kemeny, D.M. 2012. NK Cells Regulate CD8+ T Cell Priming and Dendritic Cell Migration during Influenza A Infection by IFN-γ and Perforin-Dependent Mechanisms. *The Journal of Immunology* 189(5), pp. 2099–2109. doi: 10.4049/JIMMUNOL.1103474.
Gelderblom, H.R. 1996. *Structure and Classification of Viruses*. Medical Microbiology 4th Ed. Galveston: University of Texas Medical Branch.
Giuliani, E., Vassena, L., Galardi, S., Michienzi, A., Desimio, M.G. and Doria, M. 2018. Dual regulation of L-selectin (CD62L) by HIV-1: Enhanced expression by Vpr in contrast with cell-surface down-modulation by Nef and Vpu. *Virology* 523, pp. 121–128. doi: 10.1016/J.VIROL.2018.07.031.
Gómez-Gaviro, M. et al. 2007. Expression and Regulation of the Metalloproteinase ADAM-8 during Human Neutrophil Pathophysiological Activation and Its Catalytic Activity on L-Selectin Shedding. *The Journal of Immunology* 178(12), pp. 8053–8063. doi: 10.4049/jimmunol.178.12.8053.

Gooz, M.B. et al. 2014. ADAM17 promotes proliferation of collecting duct kidney epithelial cells through ERK activation and increased glycolysis in polycystic kidney disease. *American Journal of Physiology* 307(5), pp. 551-559. doi: 10.1152/ajprenal.00218.2014.
Govorkova, E.A. et al. 2005. Lethality to Ferrets of H5N1 Influenza Viruses Isolated from Humans and Poultry in 2004. *Journal of Virology* 79(4), pp. 2191–2198. doi: 10.1128/JVI.79.4.2191-2198.2005.
Grell, M. et al. 1995. The Transmembrane Form of Tumor Necrosis Factor Is the Prime Activating Ligand of the 80 kDa Tumor Necrosis Factor Receptor. *Cell* 83(5), pp. 793–802. doi: 10.1016/0092-8674(95)90192-2.
Griffin, J.D., Spertini, O., Ernst, T.J., Belvin, M.P., Levine, H.B., Kanakura, Y. and Tedder, T.F. 1990. Granulocyte-macrophage colony-stimulating factor and other cytokines regulate surface expression of the leukocyte adhesion molecule-1 on human neutrophils, monocytes, and their precursors. *The Journal of Immunology* 145(2), pp. 576-584.
Grootveld, M. 2003. BMS-561392. Bristol-Myers Squibb. *Current Opinion in Investigational Drugs* 4(5), pp. 598–602.
Gunn, M.D., Tangemann, K., Tam, C., Cyster, J.G., Rosen, S.D. and Williams, L.T. 1998. A chemokine expressed in lymphoid high endothelial venules promotes the adhesion and chemotaxis of naive T lymphocytes. *Immunology* 95(1), pp. 258–263. doi: 10.1073/pnas.95.1.258.
Guo, H., Kumar, P., Moran, T.M., Garcia-Sastre, A., Zhou, Y. and Malarkannan, S. 2009. The functional impairment of natural killer cells during influenza virus infection. *Immunology and Cell Biology* 87(8), pp. 579–589. doi: 10.1038/ICB.2009.60.
Gutiérrez-López, M.D. et al. 2011. The sheddase activity of ADAM17/TACE is regulated by the tetraspanin CD9. *Cellular and Molecular Life Sciences* 68(19), pp. 3275–3292. doi: 10.1007/s00018-011-0639-0.
Haddad, W. et al. 2003. P-Selectin and P-Selectin Glycoprotein Ligand 1 Are Major Determinants for Th1 Cell Recruitment to Nonlymphoid Effector Sites in the Intestinal Lamina Propria. *Journal of Experimental Medicine* 198(3), pp. 369–377. doi: 10.1084/JEM.20020691.
Hafezi-Moghadam, A., Thomas, K.L., Prorock, A.J., Huo, Y. and Ley, K. 2001. L-Selectin Shedding Regulates Leukocyte Recruitment. *Journal of Experimental Medicine* 193(7), pp. 863–872. doi: 10.1084/JEM.193.7.863.
Hao, X., Kim, T.S. and Braciale, T.J. 2008. Differential Response of Respiratory Dendritic Cell Subsets to Influenza Virus Infection. *Journal of Virology* 82(10), pp. 4908–4919. doi: 10.1128/JVI.02367-07.

Hashimoto, Y., Moki, T., Takizawa, T., Shiratsuchi, A. and Nakanishi, Y. 2007. Evidence for Phagocytosis of Influenza Virus-Infected, Apoptotic Cells by Neutrophils and Macrophages in Mice. *The Journal of Immunology* 178(4), pp. 2448–2457. doi: 10.4049/JIMMUNOL.178.4.2448.
Horiuchi, K., Kimura, T., Miyamoto, T., Takaishi, H., Okada, Y., Toyama, Y. and Blobel, C.P. 2007. Cutting Edge: TNF-α-Converting Enzyme (TACE/ADAM17) Inactivation in Mouse Myeloid Cells Prevents Lethality from Endotoxin Shock. *The Journal of Immunology* 179(5), pp. 2686–2689. doi: 10.4049/jimmunol.179.5.2686.
Hornick, E.E., Zacharias, Z.R. and Legge, K.L. 2019. Kinetics and Phenotype of the CD4 T Cell Response to Influenza Virus Infections. *Frontiers in Immunology* 10, p. 2351. doi: 10.3389/fimmu.2019.02351.
Hossain, M.J., Perez, S., Guo, Z., Chen, L.M. and Donis, R.O. 2010. Establishment and characterization of a Madin-Darby canine kidney reporter cell line for influenza A virus assays. *Journal of clinical microbiology* 48(7), pp. 2515–2523.
Hou, W. et al. 2012. Viral infection triggers rapid differentiation of human blood monocytes into dendritic cells. *Blood* 119(13), pp. 3128–3131. doi: 10.1182/BLOOD-2011-09-379479.
Huang, K.-Y.A. et al. 2014a. Virus-Specific Antibody Secreting Cell, Memory B-cell, and Sero-Antibody Responses in the Human Influenza Challenge Model. *The Journal of Infectious Diseases* 209(9), pp. 1354–1361. doi: 10.1093/INFDIS/JIT650.
Huang, Y., Benaich, N., Tape, C., Kwok, H.F. and Murphy, G. 2014b. Targeting the Sheddase Activity of ADAM17 by an Anti-ADAM17 Antibody D1(A12) Inhibits Head and Neck Squamous Cell Carcinoma Cell Proliferation and Motility via Blockage of Bradykinin Induced HERs Transactivation. *International Journal of Biological Sciences* 10(7), p. 702. doi: 10.7150/IJBS.9326.
Ibricevic, A. et al. 2006. Influenza virus receptor specificity and cell tropism in mouse and human airway epithelial cells. *Journal of virology* 80(15), pp. 7469–7480. doi: 10.1128/JVI.02677-05.
INCB7839 in Treating Children With Recurrent/Progressive High-Grade Gliomas. ClinicalTrials.gov. 2020. Available at: https://clinicaltrials.gov/ct2/show/NCT04295759?term=INCB7839&draw=2&rank=1 [Accessed: 12 March 2021].
Influenza (Seasonal). 2018. Available at: https://www.who.int/news-room/fact-sheets/detail/influenza-(seasonal) [Accessed: 29 September 2020].
von Itzstein, M. et al. 1993. Rational design of potent sialidase-based inhibitors of influenza virus replication. *Nature* 363(6428), pp. 418–423. doi: 10.1038/363418a0.

de Jong, M.D. et al. 2006. Fatal outcome of human influenza A (H5N1) is associated with high viral load and hypercytokinemia. *Nature Medicine* 12(10), pp. 1203–1207. doi: 10.1038/nm1477.
Ju, C., Xia, X. and Chen, R. 2007. Expressions of tumor necrosis factor-converting enzyme and ErbB3 in rats with chronic obstructive pulmonary disease. *Chinese Medical Journal* 120 (17), pp. 1505–1510.
Jung, T. and Dailey, M. 1990. Rapid modulation of homing receptors (gp90MEL-14) induced by activators of protein kinase C. Receptor shedding due to accelerated proteolytic cleavage at the cell surface. *The Journal of Immunology* 144(8), pp. 3130–3136.
Kaldjian, E.P. and Stoolman, L.M. 1995. Regulation of L-selectin mRNA in Jurkat cells. Opposing influences of calcium- and protein kinase C-dependent signaling pathways. *The Journal of Immunology* 154(9), pp. 4351-4362.
Keating, R. et al. 2018. Potential killers exposed: tracking endogenous influenza-specific CD8+ T cells. *Immunology and Cell Biology* 96(10), pp. 1104-1119. doi: 10.1111/imcb.12189.
Kenney, A.D. et al. 2019. IFITM3 protects the heart during influenza virus infection. *Proceedings of the National Academy of Sciences of the United States of America* 116(37), pp. 18607–18612. doi: 10.1073/pnas.1900784116.
Kilian, K., Dernedde, J., Mueller, E.C., Bahr, I. and Tauber, R. 2004. The interaction of protein kinase C isozymes α, ι, and θ with the cytoplasmic domain of L-selectin is modulated by phosphorylation of the receptor. *Journal of Biological Chemistry* 279(33), pp. 34472–34480. doi: 10.1074/jbc.M405916200.
Killock, D.J. and Ivetić, A. 2010. The cytoplasmic domains of TNFα-converting enzyme (TACE/ADAM17) and L-selectin are regulated differently by p38 MAPK and PKC to promote ectodomain shedding. *Biochemical Journal* 428(2), pp. 293–304. doi: 10.1042/BJ20091611.
Kim, M.L., Zhang, B., Mills, I.P., Milla, M.E., Brunden, K.R. and Lee, V.M.-Y. 2008. Effects of TNFα-Converting Enzyme Inhibition on Amyloid β Production and APP Processing In Vitro and In Vivo. *Journal of Neuroscience* 28(46), pp. 12052–12061. doi: 10.1523/JNEUROSCI.2913-08.2008.
Koenen, R.R. et al. 2009. Regulated release and functional modulation of junctional adhesion molecule A by disintegrin metalloproteinases. *Blood* 113(19), pp. 4799–4809. doi: 10.1182/BLOOD-2008-04-152330.
Kollmus, H., Pilzner, C., Leist, S.R., Heise, M., Geffers, R. and Schughart, K. 2018. Of mice and men: the host response to influenza virus infection. *Mammalian Genome* 29(7), p. 446. doi: 10.1007/S00335-018-9750-Y.

Kos, F.J. and Engleman, E.G. 1996. Role of Natural Killer Cells in the Generation of Influenza Virus-Specific Cytotoxic T Cells. *Cellular Immunology* 173(1), pp. 1–6. doi: 10.1006/CIMM.1996.0245.
Kosik, I. and Yewdell, J.W. 2019. Influenza Hemagglutinin and Neuraminidase: Yin–Yang Proteins Coevolving to Thwart Immunity. Viruses 11(4), p. 346. doi: 10.3390/v11040346.
Kumamoto, Y., Mattei, L.M., Sellers, S., Payne, G.W. and Iwasaki, A. 2011. CD4+ T cells support cytotoxic T lymphocyte priming by controlling lymph node input. *Proceedings of the National Academy of Sciences* 108(21), pp. 8749–8754. doi: 10.1073/PNAS.1100567108.
Kunkel, E.J., Ramos, C.L., Steeber, D.A., Müller, W., Wagner, N., Tedder, T.F. and Ley, K. 1998. The roles of L-selectin, beta 7 integrins, and P selectin in leukocyte rolling and adhesion in high endothelial venules of Peyer's Patches. *The Journal of Immunology* 161(5), pp. 2449–2456.
Kwok, H.F., Botkjaer, K.A., Tape, C.J., Huang, Y., McCafferty, J. and Murphy, G. 2014. Development of a 'mouse and human cross-reactive' affinity-matured exosite inhibitory human antibody specific to TACE (ADAM17) for cancer immunotherapy. *Protein Engineering, Design and Selection* 27(6), pp. 179–190. doi: 10.1093/protein/gzu010.
Lam, J.H. and Baumgarth, N. 2019. The Multifaceted B Cell Response to Influenza Virus. *Journal of immunology* 202(2), p. 351. doi: 10.4049/JIMMUNOL.1801208.
Lambert, D.W. et al. 2005. Tumor Necrosis Factor-α Convertase (ADAM17) Mediates Regulated Ectodomain Shedding of the Severe-acute Respiratory Syndrome-Coronavirus (SARS-CoV) Receptor, Angiotensin-converting Enzyme-2 (ACE2). *Journal of Biological Chemistry* 280(34), pp. 30113–30119. doi: 10.1074/JBC.M505111200.
Langjahr, P. et al. 2014. Metalloproteinase-Dependent TLR2 Ectodomain Shedding is Involved in Soluble Toll-Like Receptor 2 (sTLR2) Production. *PLOS ONE* 9(12), p. e104624. doi: 10.1371/JOURNAL.PONE.0104624.
Lartey, N.L. et al. 2022. ADAM17/MMP inhibition prevents neutrophilia and lung injury in a mouse model of Covid-19. *The Journal of Leukocyte Biology* 111(6). p. 1147-1158. doi: 10.1002/JLB.3COVA0421-195RR.
Lauder, S.N. et al. 2013. Interleukin-6 limits influenza-induced inflammation and protects against fatal lung pathology. *European Journal of Immunology* 43(10), pp. 2613–2625. doi: 10.1002/EJI.201243018.
Lee, L.Y.H. et al. 2008. Memory T cells established by seasonal human influenza A infection cross-react with avian influenza A (H5N1) in healthy individuals. *The Journal of Clinical Investigation* 118(10), pp. 3478–3490. doi: 10.1172/JCI32460.
Lehmann, J.C.U., Jablonski-Westrich, D., Haubold, U., Gutierrez-Ramos, J.-C., Springer, T. and Hamann, A. 2003. Overlapping and Selective Roles of Endothelial

Intercellular Adhesion Molecule-1 (ICAM-1) and ICAM-2 in Lymphocyte Trafficking. *The Journal of Immunology* 171(5), pp. 2588–2593. doi: 10.4049/JIMMUNOL.171.5.2588.
Lendeckel, U., Kohl, J., Marco, A., Carl-Mcgrath, S., Donat, H. and Christoph, R. 2005. Increased expression of ADAM family members in human breast cancer and breast cancer cell lines. *Journal of Cancer Research and Clinical Oncology* 131, pp. 41–48. doi: 10.1007/s00432-004-0619-y.
Leung, K.N. and Leung, G.L. 1981. Induction of natural killer cells during murine influenza virus infection. *Immunobiology* 160(3–4), pp. 352–366. doi: 10.1016/S0171-2985(81)80061-7.
Ley, K., Laudanna, C., Cybulsky, M.I. and Nourshargh, S. 2007. Getting to the site of inflammation: The leukocyte adhesion cascade updated. *Nature Reviews Immunology* 7(9), pp. 678–689. doi: 10.1038/nri2156.
Ley, K., Tedder, T. and Kansas, G. 1993. L-selectin can mediate leukocyte rolling in untreated mesenteric venules in vivo independent of E- or P-selectin. *Blood* 82(5), pp. 1632–1638. doi: 10.1182/BLOOD.V82.5.1632.1632.
Li, N. et al. 2007. Metalloproteases regulate T-cell proliferation and effector function via LAG-3. *EMBO Journal* 26(2), pp. 494–504. doi: 10.1038/sj.emboj.7601520.
Li, X. and Fan, H. 2004. Loss of ectodomain shedding due to mutations in the metalloprotease and cysteine-rich/disintegrin domains of the tumor necrosis factor-alpha converting enzyme (TACE). *The Journal of biological chemistry* 279(26), pp. 27365–27375. doi: 10.1074/jbc.M401690200.
Li, Y., Brazzell, J., Herrera, A. and Walcheck, B. 2006. ADAM17 deficiency by mature neutrophils has differential effects on L-selectin shedding. *Blood* 108(7), pp. 2275-2279. doi: 10.1182/blood-2006-02-005827.
Lim, K. et al. 2015. Neutrophil trails guide influenza specific CD8+ T cells in the airways. *Science* 349(6252), pp.4352. doi: 10.1126/science.aaa4352.
Lin, K.L., Suzuki, Y., Nakano, H., Ramsburg, E. and Gunn, M.D. 2008. CCR2+ Monocyte-Derived Dendritic Cells and Exudate Macrophages Produce Influenza-Induced Pulmonary Immune Pathology and Mortality. *The Journal of Immunology* 180(4), pp. 2562–2572. doi: 10.4049/jimmunol.180.4.2562.
Lin, S.J. et al. 2014. The pathological effects of CCR2+ inflammatory monocytes are amplified by an IFNAR1-triggered chemokine feedback loop in highly pathogenic influenza infection. *Journal of Biomedical Science* 21(1), pp. 1–18. doi: 10.1186/S12929-014-0099-6.
Link, M.A., Lücke, K., Schmid, J., Schumacher, V., Eden, T., Rose-John, S. and Mittrücker, H.W. 2017. The role of ADAM17 in the T-cell response against bacterial pathogens. *PLOS ONE* 12(9), p. e0184320. doi: 10.1371/journal.pone.0184320.

Liu, X. et al. 2006. Selective inhibition of ADAM metalloproteases blocks HER-2 extracellular domain (ECD) cleavage and potentiates the anti-tumor effects of trastuzumab. *Cancer Biology & Therapy* 5(6), pp. 648-656. doi: 10.4161/cbt.5.6.2707.
Londrigan, S.L., Short, K.R., Ma, J., Gillespie, L., Rockman, S.P., Brooks, A.G. and Reading, P.C. 2015. Infection of Mouse Macrophages by Seasonal Influenza Viruses Can Be Restricted at the Level of Virus Entry and at a Late Stage in the Virus Life Cycle. *Journal of Virology* 89(24), pp. 12319–12329. doi: 10.1128/JVI.01455-15.
Long, C., Hosseinkhani, M.R., Wang, Y., Sriramarao, P. and Walcheck, B. 2012. ADAM17 activation in circulating neutrophils following bacterial challenge impairs their recruitment. *Journal of Leukocyte Biology* 92(3), pp. 667–672. doi: 10.1189/JLB.0312112.
Long, C., Wang, Y., Herrera, A.H., Horiuchi, K. and Walcheck, B. 2010. In vivo role of leukocyte ADAM17 in the inflammatory and host responses during E. coli-mediated peritonitis. *Journal of Leukocyte Biology* 87(6), pp. 1097–1101. doi: 10.1189/jlb.1109763.
Lorenzen, I. et al. 2016. Control of ADAM17 activity by regulation of its cellular localisation. *Scientific Reports* 6(1), pp. 1–15. doi: 10.1038/srep35067.
Luther, S.A., Tang, H.L., Hyman, P.L., Farr, A.G. and Cyster, J.G. 2000. Coexpression of the chemokines ELC and SLC by T zone stromal cells and deletion of the ELC gene in the plt/plt mouse. *Proceedings of the National Academy of Sciences* 97(23), pp. 12694–12699. doi: 10.1073/PNAS.97.23.12694.
Maddox, B. 2015. *Tumor Necrosis Factor Alpha Converting Enzyme Inhibition during Tumor Necrosis Factor Alpha Converting Enzyme Inhibition during Acute Colitis in Mice: A Regional Analysis Acute Colitis in Mice: A Regional Analysis*. MSc Thesis. Missouri State University.
Maekawa, M. et al. 2019. A Novel TNF-α Converting Enzyme (TACE) Selective Inhibitor JTP-96193 Prevents Insulin Resistance in KK-A y Type 2 Diabetic Mice and Diabetic Peripheral Neuropathy in Type 1 Diabetic Mice. *Biol Pharm Bull* 42(11), pp. 1906–1912. doi: 10.1248/bpb.b19-00526.
Mao, H. et al. 2009. Influenza Virus Directly Infects Human Natural Killer Cells and Induces Cell Apoptosis. *Journal of Virology* 83(18), pp. 9215–9222. doi: 10.1128/JVI.00805-09
Martinez, M.N., Greene, J., Kenna, L., Kissell, L. and Kuhn, M. 2020. The Impact of Infection and Inflammation on Drug Metabolism, Active Transport, and Systemic Drug Concentrations in Veterinary Species. *Drug Metabolism and Disposition* 48(8), pp. 631–644. doi: 10.1124/dmd.120.090704.

Matthews, V. et al. 2003. Cellular cholesterol depletion triggers shedding of the human interleukin-6 receptor by ADAM10 and ADAM17 (TACE). *The Journal of biological chemistry* 278(40), pp. 38829–38839. doi: 10.1074/JBC.M210584200.
McLaren, C. and Potter, C.W. 1973. The relationship between interferon and virus virulence in influenza virus infections of the mouse. *Journal of medical microbiology* 6(1), pp. 21–32. doi: 10.1099/00222615-6-1-21.
Mendel, D.B. et al. 1998. Oral administration of a prodrug of the influenza virus neuraminidase inhibitor GS 4071 protects mice and ferrets against influenza infection. *Antimicrobial Agents and Chemotherapy* 42(3), pp. 640–646. doi: 10.1128/AAC.42.3.640.
Mezyk-Kopeć, R. et al. 2009. Identification of ADAM10 as a major TNF sheddase in ADAM17-deficient fibroblasts. *Cytokine* 46(3), pp. 309–315. doi: 10.1016/J.CYTO.2009.03.002.
Miao, H. et al. 2010. Quantifying the Early Immune Response and Adaptive Immune Response Kinetics in Mice Infected with Influenza A Virus. *Journal of Virology* 84(13), pp. 6687–6698. doi: 10.1128/JVI.00266-10.
Migaki, G.I., Kahn, J. and Kishimoto, T.K. 1995. Mutational Analysis of the Membrane-proximal Cleavage Site of L-Selectin: Relaxed Sequence Specificity Surrounding the Cleavage Site. *The Journal of Experimental Medicine* 182(2), pp. 549–557.
Mishra, H.K., Ma, J., Mendez, D., Hullsiek, R., Pore, N. and Walcheck, B. 2020. Blocking adam17 function with a monoclonal antibody improves sepsis survival in a murine model of polymicrobial sepsis. *International Journal of Molecular Sciences* 21(18), pp. 1–10. doi: 10.3390/ijms21186688.
Mishra, H.K., Pore, N., Michelotti, E.F. and Walcheck, B. 2018. Anti-ADAM17 monoclonal antibody MEDI3622 increases IFNγ production by human NK cells in the presence of antibody-bound tumor cells. *Cancer Immunology, Immunotherapy* 67(9), pp. 1407–1416. doi: 10.1007/s00262-018-2193-1.
Mobley, J.L. and Dailey, M.O. 1992. Regulation of adhesion molecule expression by CD8 T cells in vivo. I. Differential regulation of gp90MEL-14 (LECAM-1), Pgp-1, LFA-1, and VLA-4 alpha during the differentiation of cytotoxic T lymphocytes induced by allografts. *The Journal of Immunology* 148(8), pp. 2348–2356.
Mobley, J.L., Rigby, S.M. and Dailey, M.O. 1994. Regulation of adhesion molecule expression by CD8 T cells in vivo. II. Expression of L-selectin (CD62L) by memory cytolytic T cells responding to minor histocompatibility antigens. *Journal of immunology* 153(12), pp. 5443–52.
Mohammed, R.N. et al. 2019. ADAM17-dependent proteolysis of L-selectin promotes early clonal expansion of cytotoxic T cells. *Scientific Reports* 9(1), pp. 1–12. doi: 10.1038/s41598-019-41811-z.

Mohammed, R.N., Watson, H.A., Vigar, M., Ohme, J., Thomson, A., Humphreys, I.R. and Ager, A. 2016. L-selectin Is Essential for Delivery of Activated CD8+ T Cells to Virus-Infected Organs for Protective Immunity. *Cell Reports* 14(4), pp. 760–771. doi: 10.1016/j.celrep.2015.12.090.
Mohan, M.J. et al. 2002. The tumor necrosis factor-α converting enzyme (TACE): A unique metalloproteinase with highly defined substrate selectivity. *Biochemistry* 41(30), pp. 9462–9469. doi: 10.1021/bi0260132.
Mohler, K.M. et al. 1994. Protection against a lethal dose of endotoxin by an inhibitor of tumour necrosis factor processing. *Nature* 370(6486), pp. 218–220. doi: 10.1038/370218a0.
Möller-Hackbarth, K., Dewitz, C., Schweigert, O., Trad, A., Garbers, C., Rose-John, S. and Scheller, J. 2013. A Disintegrin and Metalloprotease (ADAM) 10 and ADAM17 Are Major Sheddases of T Cell Immunoglobulin and Mucin Domain 3 (Tim-3). *Journal of Biological Chemistry* 288(48), pp. 34529–34544. doi: 10.1074/JBC.M113.488478.
Monteiro, J.M., Harvey, C. and Trinchieri, G. 1998. Role of Interleukin-12 in Primary Influenza Virus Infection. *Journal of Virology* 72(6), pp. 4825–4831. doi: 10.1128/jvi.72.6.4825-4831.1998.
Moser, B. 2015. CXCR5, the Defining Marker for Follicular B Helper T (TFH) Cells. *Frontiers in Immunology* 6, p. 296. doi: 10.3389/fimmu.2015.00296.
Moskophidis, D. and Kioussis, D. 1998. Contribution of Virus-specific CD8+ Cytotoxic T Cells to Virus Clearance or Pathologic Manifestations of Influenza Virus Infection in a T Cell Receptor Transgenic Mouse Model. *The Journal of Experimental Medicine* 188(2), p. 223. doi: 10.1084/JEM.188.2.223.
Moss, M.L. et al. 1997. Cloning of a disintegrin metalloproteinase that processes precursor tumour-necrosis factor-α. *Nature* 385(6618), pp. 733–736. doi: 10.1038/385733a0.
Moss, M.L. and Minond, D. 2017. Recent Advances in ADAM17 Research: A Promising Target for Cancer and Inflammation. doi: 10.1155/2017/9673537.
Müllberg, J., Schooltink, H., Stoyan, T., Heinrich, P.C. and Rose-John, S. 1992. Protein kinase C activity is rate limiting for shedding of the interleukin-6 receptor. *Biochemical and Biophysical Research Communications* 189(2), pp. 794–800. doi: 10.1016/0006-291X(92)92272-Y.
Müller, M. et al. 2022. Tetraspanin 8 Subfamily Members Regulate Substrate-Specificity of a Disintegrin and Metalloprotease 17. *Cells* 11(17), p. 2683. doi: 10.3390/cells11172683.
Murphy, K. and Weaver, C. 2017. *Janeway's Immunobiology*. 9th ed. New York: Garland Science.

Nagano, O. et al. 2004. Cell–matrix interaction via CD44 is independently regulated by different metalloproteinases activated in response to extracellular Ca2+ influx and PKC activation. *Journal of Cell Biology* 165(6), pp. 893–902. doi: 10.1083/JCB.200310024.
Nakanishi Yumi Hashimoto, Y., Moki, T. and Takizawa, T. 2007. Neutrophils and Macrophages in Mice Virus-Infected, Apoptotic Cells by Evidence for Phagocytosis of Influenza. *J Immunol References* 178, pp. 2448–2457. doi: 10.4049/jimmunol.178.4.2448.
Nguyen-Van-Tam, J.S. 2010. 2009 Pandemic Influenza A (H1N1): Pathology and Pathogenesis of 100 Fatal Cases in the United States. *The American Journal of Pathology* 177(1), pp. 166–175. doi: 10.2353/ajpath.2010.100115.
Nicol, M.Q. et al. 2019. Lack of IFNγ signaling attenuates spread of influenza A virus in vivo and leads to reduced pathogenesis. *Virology* 526, pp. 155–164. doi: 10.1016/j.virol.2018.10.017.
Nielsen, M.A. et al. 2016. A disintegrin and metalloprotease-17 and galectin-9 are important regulators of local 4-1BB activity and disease outcome in rheumatoid arthritis. *Rheumatology* 55(10), pp. 1871–1879. doi: 10.1093/rheumatology/kew237.
Ohta, S. et al. 2001. Tumor necrosis factor-alpha (TNF-alpha) converting enzyme contributes to production of TNF-alpha in synovial tissues from patients with rheumatoid arthritis. *The Journal of Rheumatology* 28(8), pp. 1756–1763.
Österlund, P. et al. 2010. Pandemic H1N1 2009 Influenza A Virus Induces Weak Cytokine Responses in Human Macrophages and Dendritic Cells and Is Highly Sensitive to the Antiviral Actions of Interferons. *Journal of Virology* 84(3), pp. 1414–1422. doi: 10.1128/jvi.01619-09.
Padilla-Quirarte, H.O., Lopez-Guerrero, D. V., Gutierrez-Xicotencatl, L. and Esquivel-Guadarrama, F. 2019. Protective Antibodies Against Influenza Proteins. *Frontiers in Immunology* 10, p. 1677. doi: 10.3389/fimmu.2019.01677.
Peng, M., Guo, S., Yin, N., Xue, J., Shen, L., Zhao, Q. and Zhang, W. 2010. Ectodomain shedding of Fcα receptor is mediated by ADAM10 and ADAM17. *Immunology* 130(1), pp. 83–91. doi: 10.1111/J.1365-2567.2009.03215.X.
Perez, C., Albert, I., Defay, K., Zachariades, N., Gooding, L. and Kriegler', M. 1990. A Nonsecretable Cell Surface Mutant of Tumor Necrosis Factor (TNF) Kills by Cell-to-Cell Contact. *Cell* 63(2), pp. 251–258. doi: 10.1016/0092-8674(90)90158-b.
Peschon, J.J. et al. 1998. An essential role for ectodomain shedding in mammalian development. *Science* 282(5392), pp. 1281–1284. doi: 10.1126/science.282.5392.1281.
Puri, K.D., Finger, E.B., Gaudernack, G. and Springer, T.A. 1995. Sialomucin CD34 is the major L-selectin ligand in human tonsil high endothelial venules. *Journal of Cell Biology* 131(1), pp. 261–270. doi: 10.1083/JCB.131.1.261.

Qian, M. et al. 2007. Pharmacokinetics and pharmacodynamics of DPC 333 ((2R)-2-((3R)-3-amino-3{4- [2-methyl-4-quinolinyl) methoxy] phenyl}-2-oxopyrrolidinyl)-N-hydroxy-4- methylpentanamide, a potent and selective inhibitor of tumor necrosis factor α-converting enzyme in rodents, dogs, chimpanzees, and humans. *Drug Metabolism and Disposition* 35(10), pp. 1916–1925. doi: 10.1124/dmd.107.015933.
Rabinovich, S. 1972. Rimantadine therapy of influenza A infection in mice. *Antimicrobial agents and chemotherapy* 1(5), pp. 408–411. doi: 10.1128/AAC.1.5.408.
Rahman, I. et al. 2021. L-selectin regulates human neutrophil transendothelial migration. *Journal of Cell Science* 134(3), pp. 1–17. doi: 10.1242/jcs.250340.
Rangel-Moreno, J. et al. 2008. B Cells Promote Resistance to Heterosubtypic Strains of Influenza via Multiple Mechanisms. *The Journal of Immunology* 180(1), pp. 454–463. doi: 10.4049/jimmunol.180.1.454.
Reddy, P. et al. 2000. Functional Analysis of the Domain Structure of Tumor Necrosis Factor-α Converting Enzyme. *Journal of Biological Chemistry* 275(19), pp. 14608–14614. doi: 10.1074/jbc.275.19.14608.
Richards, F.M., Tape, C.J., Jodrell, D.I. and Murphy, G. 2012. Anti-tumour effects of a specific anti-ADAM17 antibody in an ovarian cancer model in vivo. *PLoS ONE* 7(7), p. 40597. doi: 10.1371/journal.pone.0040597.
Richards, H., Longhi, M.P., Wright, K., Gallimore, A. and Ager, A. 2008. CD62L (L-Selectin) Down-Regulation Does Not Affect Memory T Cell Distribution but Failure to Shed Compromises Anti-Viral Immunity. *The Journal of Immunology* 180(1), pp. 198–206. doi: 10.4049/jimmunol.180.1.198.
Van Riel, D., Munster, V.J., De Wit, E., Rimmelzwaan, G.F., Fouchier, R.A.M., Osterhaus, A.D.M.E. and Kuiken, T. 2007. Human and Avian Influenza Viruses Target Different Cells in the Lower Respiratory Tract of Humans and Other Mammals. *The American Journal of Pathology* 171(4), pp. 1215–1223. doi: 10.2353/ajpath.2007.070248.
Rios-Doria, J. et al. 2015. Amonoclonal antibody to ADAM17 inhibits tumor growth by inhibiting EGFR and non-EGFR-mediated pathways. *Molecular Cancer Therapeutics* 14(7), pp. 1637–1649. doi: 10.1158/1535-7163.mct-14-1040.
Rizoli, S.B., Rotstein, O.D. and Kapus, A. 1999. Cell Volume-dependent Regulation of L-selectin Shedding in Neutrophils. *Journal of Biological Chemistry* 274(31), pp. 22072–22080. doi: 10.1074/jbc.274.31.22072.
Romee, R. et al. 2013. NK cell CD16 surface expression and function is regulated by a disintegrin and metalloprotease-17 (ADAM17). *Blood* 121(18), pp. 3599–3608. doi: 10.1182/blood-2012-04-425397.

Rosshart, S.P. et al. 2019. Laboratory mice born to wild mice have natural microbiota and model human immune responses. *Science* 365(6452), p. 444. doi: 10.1126/science.aaw4361.
Ruuls, S.R. et al. 2001. Membrane-Bound TNF Supports Secondary Lymphoid Organ Structure but Is Subservient to Secreted TNF in Driving Autoimmune Inflammation. *Immunity* 15(4), pp. 533–543. doi: 10.1016/S1074-7613(01)00215-1.
Rzeniewicz, K. et al. 2015. L-selectin shedding is activated specifically within transmigrating pseudopods of monocytes to regulate cell polarity in vitro. *Proceedings of the National Academy of Sciences of the United States of America* 112(12), pp. E1461–E1470. doi: 10.1073/pnas.1417100112.
Saha, N. et al. 2022. Inhibitory monoclonal antibody targeting ADAM17 expressed on cancer cells. *Translational oncology* 15(1), p. 101265. doi: 10.1016/j.tranon.2021.101265.
Sahin, U. et al. 2004. Distinct roles for ADAM10 and ADAM17 in ectodomain shedding of six EGFR ligands. *Journal of Cell Biology* 164(5), pp. 769–779. doi: 10.1083/jcb.200307137.
Sallusto, F., Lenig, D., Förster, R., Lipp, M. and Lanzavecchia, A. 1999. Two subsets of memory T lymphocytes with distinct homing potentials and effector functions. *Nature 1999 401:6754* 401(6754), pp. 708–712. doi: 10.1038/44385.
Samarasinghe, A.E. et al. 2017. Eosinophils Promote Antiviral Immunity in Mice Infected with Influenza A Virus. *The Journal of Immunology* 198(8), pp. 3214–3226. doi: 10.4049/jimmunol.1600787.
Sanders, R.D. et al. 2015. Immune cell expression of GABAA receptors and the effects of diazepam on influenza infection. *Journal of Neuroimmunology* 282, pp. 97–103. doi: 10.1016/J.jneuroim.2015.04.001.
Sassetti, C., Tangemann, K., Singer, M.S., Kershaw, D.B. and Rosen, S.D. 1998. Identification of Podocalyxin-like Protein as a High Endothelial Venule Ligand for L-selectin: Parallels to CD34. *Journal of Experimental Medicine* 187(12), pp. 1965–1975. doi: 10.1084/jem.187.12.1965.
Schleiffenbaum, B., Spertini, O. and Tedder, T.F. 1992. Soluble L-selectin Is Present in Human Plasma at High Levels and Retains Functional Activity. *The Journal of Cell Biology* 119(1), pp. 229–238. doi: 10.1083/jcb.119.1.229.
Schlöndorff, J., Becherer, J.D. and Blobel, C.P. 2000. Intracellular maturation and localization of the tumour necrosis factor α convertase (TACE). *Biochemical Journal* 347(1), pp. 131–138.
Schmiedel, B.J. et al. 2018. Impact of Genetic Polymorphisms on Human Immune Cell Gene Expression. *Cell* 175(6), pp. 1701-1715. doi: 10.1016/j.cell.2018.10.022.

Schmittgen, T.D. and Livak, K.J. 2008. Analyzing real-time PCR data by the comparative CT method. *Nature Protocols* 3(6), pp. 1101–1108. doi: 10.1038/nprot.2008.73.
Schweigert, O., Dewitz, C., Möller-Hackbarth, K., Trad, A., Garbers, C., Rose-John, S. and Scheller, J. 2014. Soluble T cell immunoglobulin and mucin domain (TIM)-1 and -4 generated by A Disintegrin And Metalloprotease (ADAM)-10 and -17 bind to phosphatidylserine. *Biochimica et biophysica acta* 1843(2), pp. 275–287. doi: 10.1016/j.bbamcr.2013.11.014.
Seidelin, J.B., Nielsen, O.H. and Strøm, J. 2002. Soluble L-selectin levels predict survival in sepsis. *Intensive Care Med* 28, pp. 1613–1618. doi: 10.1007/s00134-002-1501-5.
Sellers, S.A., Hagan, R.S., Hayden, F.G. and Fischer, W.A. 2017. The hidden burden of influenza: A review of the extra-pulmonary complications of influenza infection. *Influenza and Other Respiratory Viruses* 11(5), pp. 372–393. doi: 10.1111/irv.12470.
Sharma, A., Bender, S., Zimmermann, M., Riesterer, O., Broggini-Tenzer, A. and Pruschy, M.N. 2016. Secretome Signature Identifies ADAM17 as Novel Target for Radiosensitization of Non–Small Cell Lung Cancer. *Clinical Cancer Research* 22(17), pp. 4428–4439. doi: 10.1158/1078-0432.CCR-15-2449.
Sharma, M. et al. 2013. Selective inhibition of tumor necrosis factor-α converting enzyme attenuates liver toxicity in a murine model of concanavalin A induced auto-immune hepatitis. *International Immunopharmacology* 17(2), pp. 229–236. doi: 10.1016/j.intimp.2013.06.014.
Shimoda, M. et al. 2016. Epithelial Cell-Derived a Disintegrin and Metalloproteinase-17 Confers Resistance to Colonic Inflammation Through EGFR Activation. *EBioMedicine* 5, pp. 114–124. doi: 10.1016/j.ebiom.2016.02.007.
Shope, R.E. 1935. The infection of mice with swine influenza virus. *Journal of Experimental Medicine* 62(4), pp. 561–572. doi: 10.1084/JEM.62.4.561.
Sidwell, R.W., Smee, D.F., Huffman, J.H., Barnard, D.L., Bailey, K.W., Morrey, J.D. and Babu, Y.S. 2001. In vivo influenza virus-inhibitory effects of the cyclopentane neuraminidase inhibitor RWJ-270201. *Antimicrobial Agents and Chemotherapy* 45(3), pp. 749–757. doi: 10.1128/AAC.45.3.749-757.2001.
Sinclair, L. v. et al. 2008. Phosphatidylinositol-3-OH kinase and nutrient-sensing mTOR pathways control T lymphocyte trafficking. *Nature Immunology* 9(5), pp. 513–521. doi: 10.1038/ni.1603.
Snelgrove, R.J. et al. 2008. A critical function for CD200 in lung immune homeostasis and the severity of influenza infection. *Nature Immunology* 9(9), pp. 1074-1083. doi: 10.1038/ni.1637.

Solomon, N.K.A., Covington, M.B. and Decicco, C.P. 1997. The fate of pro-TNF-alpha following inhibition of metalloprotease-dependent processing to soluble TNF-alpha in human monocytes. *The Journal of Immunology* 159(9), pp. 4524–4531.
Spertini, O., Cordey, A.S., Monai, N., Giuffrè, L. and Schapira, M. 1996. P-selectin glycoprotein ligand 1 is a ligand for L-selectin on neutrophils, monocytes, and CD34+ hematopoietic progenitor cells. *Journal of Cell Biology* 135(2), pp. 523–531. doi: 10.1083/JCB.135.2.523.
Sprenger, H., Meyer, R.G., Kaufmann, A., Bußfeld, D., Rischkowsky, E. and Gemsa, D. 1996. Selective induction of monocyte and not neutrophil-attracting chemokines after influenza A virus infection. *Journal of Experimental Medicine* 184(3), pp. 1191–1196. doi: 10.1084/JEM.184.3.1191.
Springer, T.A. 1994. Traffic signals for lymphocyte recirculation and leukocyte emigration: The multistep paradigm. *Cell* 76(2), pp. 301–314. doi: 10.1016/0092-8674(94)90337-9.
Srivastava, B. et al. 2009. Host Genetic Background Strongly Influences the Response to Influenza A Virus Infections. *PLOS ONE* 4(3), p. e4857. doi: 10.1371/journal.pone.0004857.
Steeber, D.A., Green, N.E., Sato, S. and Tedder, T.F. 1996. Humoral immune responses in L-selectin-deficient mice. *The Journal of Immunology* 157(11), pp. 4899–4907.
Stein, J. V. et al. 2000. The Cc Chemokine Thymus-Derived Chemotactic Agent 4 (Tca-4, Secondary Lymphoid Tissue Chemokine, 6ckine, Exodus-2) Triggers Lymphocyte Function–Associated Antigen 1–Mediated Arrest of Rolling T Lymphocytes in Peripheral Lymph Node High Endothelial Venules. *Journal of Experimental Medicine* 191(1), pp. 61–76. doi: 10.1084/jem.191.1.61.
Stevens, J., Blixt, O., Glaser, L., Taubenberger, J.K., Palese, P., Paulson, J.C. and Wilson, I.A. 2006. Glycan Microarray Analysis of the Hemagglutinins from Modern and Pandemic Influenza Viruses Reveals Different Receptor Specificities. *Journal of Molecular Biology* 355(5), pp. 1143–1155. doi: 10.1016/j.jmb.2005.11.002.
Stiver, G. 2003. The treatment of influenza with antiviral drugs. *Canadian Medical Association Journal* 168(1), pp. 49–57.
Stow, J.L., Ching Low, P., Offenhäuser, C. and Sangermani, D. 2009. Cytokine secretion in macrophages and other cells: Pathways and mediators. *Immunobiology* 214(7), pp. 601–612. doi: 10.1016/j.imbio.2008.11.005.
Streeter, P.R., Rouse, B.T. and Butcher, E.C. 1988. Immunohistologic and functional characterization of a vascular addressin involved in lymphocyte homing into peripheral lymph nodes. *Journal of Cell Biology* 107(5), pp. 1853–1862. doi: 10.1083/jcb.107.5.1853.

Sun, J., Madan, R., Karp, C.L. and Braciale, T.J. 2009. Effector T cells control lung inflammation during acute influenza virus infection by producing IL-10. *Nature Medicine 2009 15:3* 15(3), pp. 277–284. doi: 10.1038/nm.1929.
Szabo, S.J., Kim, S.T., Costa, G.L., Zhang, X., Fathman, C.G. and Glimcher, L.H. 2000. A Novel Transcription Factor, T-bet, Directs Th1 Lineage Commitment. *Cell* 100(6), pp. 655–669. doi: 10.1016/S0092-8674(00)80702-3.
Takeda, S., Igarashi, T., Mori, H. and Araki, S. 2006. Crystal structures of VAP1 reveal ADAMs' MDC domain architecture and its unique C-shaped scaffold. *The EMBO Journal* 25(11), pp. 2388–2396. doi: 10.1038/sj.emboj.7601131.
Tang, J. et al. 2011. Adam17-dependent shedding limits early neutrophil influx but does not alter early monocyte recruitment to inflammatory sites. *Blood* 118(3), pp. 786–794. doi: 10.1182/blood-2010-11-321406.
Tang, P., Hung, M.C. and Klostergaard, J. 1996. Human pro-tumor necrosis factor is a homotrimer. *Biochemistry* 35(25), pp. 8216–8225. doi: 10.1021/bi952182t.
Tape, C.J. et al. 2011. Cross-domain inhibition of TACE ectodomain. *Proceedings of the National Academy of Sciences of the United States of America* 108(14), pp. 5578–5583. doi: 10.1073/pnas.1017067108.
Tate, M., Brooks, A. and Reading, P. 2008. The role of neutrophils in the upper and lower respiratory tract during influenza virus infection of mice. *Respiratory research* 9(1), pp. 1–13. doi: 10.1186/1465-9921-9-57.
Tate, M.D., Deng, Y.-M., Jones, J.E., Anderson, G.P., Brooks, A.G. and Reading, P.C. 2009. Neutrophils Ameliorate Lung Injury and the Development of Severe Disease during Influenza Infection. *The Journal of Immunology* 183(11), pp. 7441–7450. doi: 10.4049/jimmunol.0902497.
Tavares, L.P. et al. 2017. CXCR1/2 antagonism is protective during influenza and post-influenza pneumococcal infection. *Frontiers in Immunology* 8, p. 1799. doi: 10.3389/fimmu.2017.01799.
Taylor, P.M. and Askonas, B.A. 1986. Influenza nucleoprotein-specific cytotoxic T-cell clones are protective in vivo. *Immunology* 58(3), pp. 417-420.
Tedder, T.F., Isdaacs, C.M., Ernst, T.J., Demetri, G.D., Adler, D.A. and Disteche, C.M. 1989. Isolation and chromosomal localization of cDNAs encoding a novel human lymphocyte cell surface molecule, LAM-1. Homology with the mouse lymphocyte homing receptor and other human adhesion proteins. *The Journal of experimental medicine* 170(1), pp. 123–133. doi: 10.1084/jem.170.1.123.
Tedder, T.F., Steeber, D.A. and Pizcueta, P. 1995. L-selectin-deficient mice have impaired leukocyte recruitment into inflammatory sites. *The Journal of experimental medicine* 181(6), pp. 2259–2264. doi: 10.1084/jem.181.6.2259.

Tedder, T.F., Tang, M.L.K., Steeber, D.A. and Zhang, X.-Q. 1998. Intrinsic Differences In L-selectin Expression Levels Affect T and B Lymphocyte Subset-Specific Recirculation Pathways. *J Immunol* 160(10), pp. 5113–5121.

Thabet, M.M. and Huizinga, T.W.J. 2006. Drug evaluation: Apratastat, a novel TACE/MMP inhibitor for rheumatoid arthritis. *Current Opinion in Investigational Drugs* 7(11), pp. 1014–1019.

Topham, D.J., Tripp, R.A. and Doherty, P.C. 1997. CD8+ T cells Clear Influenza Virus by Perforin or Fas-dependent processes. *The Journal of Immunology* 159(11), pp. 5197–5200.

Trad, A., Riese, M., Shomali, M., Hedeman, N., Effenberger, T., Grötzinger, J. and Lorenzen, I. 2013. The disintegrin domain of ADAM17 antagonises fibroblast carcinoma cell interactions. *International Journal of Oncology* 42(5), pp. 1793–1800. doi: 0.3892/ijo.2013.1864.

Travanty, E. et al. 2015. Differential Susceptibilities of Human Lung Primary Cells to H1N1 Influenza Viruses. *Journal of Virology* 89(23), p. 11935. doi: 10.1128/jvi.01792-15.

Trickett, A. and Kwan, Y.L. 2003. T cell stimulation and expansion using anti-CD3/CD28 beads. *Journal of Immunological Methods* 275(1–2), pp. 251–255. doi: 10.1016/S0022-1759(03)00010-3.

Tripathi, S., Verma, A., Kim, E.-J., White, M.R. and Hartshorn, K.L. 2014. LL-37 modulates human neutrophil responses to influenza A virus. *Journal of leukocyte biology* 96(5), pp. 931–938. doi: 10.1189/jlb.4a1113-604rr.

Tsakadze, N.L., Sithu, S.D., Sen, U., English, W.R., Murphy, G. and D'Souza, S.E. 2006. Tumor necrosis factor-alpha-converting enzyme (TACE/ADAM-17) mediates the ectodomain cleavage of intercellular adhesion molecule-1 (ICAM-1). *The Journal of biological chemistry* 281(6), pp. 3157–3164. doi: 10.1074/jbc.m510797200.

Tu, L., Poe, J.C., Kadono, T., Venturi, G.M., Bullard, D.C., Tedder, T.F. and Steeber, D.A. 2002. A functional role for circulating mouse L-selectin in regulating leukocyte/endothelial cell interactions in vivo. *Journal of immunology* 169(4), pp. 2034–2043. doi: 10.4049/jimmunol.169.4.2034.

Tumpey, T.M. et al. 2005. Pathogenicity of Influenza Viruses with Genes from the 1918 Pandemic Virus: Functional Roles of Alveolar Macrophages and Neutrophils in Limiting Virus Replication and Mortality in Mice. *Journal of Virology* 79(23), pp. 14933–14944. doi: 10.1128/jvi.79.23.14933-14944.2005.

Uchikawa, S., Yoda, M., Tohmonda, T., Kanaji, A., Matsumoto, M., Toyama, Y. and Horiuchi, K. 2015. ADAM17 regulates IL-1 signaling by selectively releasing IL-1 receptor type 2 from the cell surface. *Cytokine* 71(2), pp. 238–245. doi: 10.1016/j.cyto.2014.10.032.

Uhlén, M. et al. 2015. Tissue-based map of the human proteome. *Science* 347(6220). doi: 10.1126/science.1260419.
Venkatesh, H.S. et al. 2017. Targeting neuronal activity-regulated neuroligin-3 dependency in high-grade glioma. *Nature* 549(7673), pp. 533–537. doi: 10.1038/nature24014.
Vidal, P.M., Lemmens, E., Avila, A., Vangansewinkel, T., Chalaris, A., Rose-John, S. and Hendrix, S. 2013. ADAM17 is a survival factor for microglial cells in vitro and in vivo after spinal cord injury in mice. *Cell Death & Disease* 4(12), pp. e954–e954. doi: 10.1038/cddis.2013.466.
de Vooght, V., Vanoirbeek, J.A.J., Luyts, K., Haenen, S., Nemery, B. and Hoet, P.H.M. 2010. Choice of Mouse Strain Influences the Outcome in a Mouse Model of Chemical-Induced Asthma. *PLOS ONE* 5(9), p. e12581. doi: 10.1371/journal.pone.0012581.
Wagner, N., Löhler, J., Tedder, T.F., Rajewsky, K., Müller, W. and Steeber, D.A. 1998. L-selectin and β7 integrin synergistically mediate lymphocyte migration to mesenteric lymph nodes. *European Journal of Immunology* 28(11), pp. 3832–3839. doi: 10.1002/(sici)1521-4141(199811)28:11.
Wang, Y., Herrera, A.H., Li, Y., Belani, K.K. and Walcheck, B. 2009. Regulation of mature ADAM17 by redox agents for L-selectin shedding. *Journal of immunology.* 182(4), pp. 2449–2457. doi: 10.4049/jimmunol.0802770.
Wang, Y., Zhang, A.C., Ni, Z., Herrera, A. and Walcheck, B. 2010a. ADAM17 Activity and Other Mechanisms of Soluble L-selectin Production during Death Receptor-Induced Leukocyte Apoptosis. *The Journal of Immunology* 184(8), pp. 4447–4454. doi: 10.4049/jimmunol.0902925.
Warnock, R.A., Askari, S., Butcher, E.C. and Andrian, U.H. von 1998. Molecular Mechanisms of Lymphocyte Homing to Peripheral Lymph Nodes. *The Journal of Experimental Medicine* 187(2), p. 205. doi: 10.1084/jem.187.2.205.
Warnock, R.A., Campbell, J.J., Dorf, M.E., Matsuzawa, A., McEvoy, L.M. and Butcher, E.C. 2000. The Role of Chemokines in the Microenvironmental Control of T versus B Cell Arrest in Peyer's Patch High Endothelial Venules. *Journal of Experimental Medicine* 191(1), pp. 77–88. doi: 10.1084/jem.191.1.77.
Watson, H.A. et al. 2019. L-Selectin Enhanced T Cells Improve the Efficacy of Cancer Immunotherapy. *Frontiers in Immunology* 10, p. 1321. doi: 10.3389/fimmu.2019.01321.
Watson, M.L. et al. 1990. Genomic organization of the selectin family of leukocyte adhesion molecules on human and mouse chromosome 1. *Journal of Experimental Medicine* 172(1), pp. 263–272. doi: 10.1084/jem.172.1.263.
Weber, S. and Saftig, P. 2012. Ectodomain shedding and ADAMs in development. *Development* 139(20), pp. 3693–3709. doi: 10.1242/dev.076398.

Weinheimer, V.K. et al. 2012. Influenza A Viruses Target Type II Pneumocytes in the Human Lung. *The Journal of Infectious Diseases* 206(11), pp. 1685–1694. doi: 10.1093/infdis/jis455.
Wisniewska, M. et al. 2008. Structural Determinants of the ADAM Inhibition by TIMP-3: Crystal Structure of the TACE-N-TIMP-3 Complex. *Journal of Molecular Biology* 381(5), pp. 1307–1319. doi: 10.1016/j.jmb.2008.06.088.
Wu, H., Haist, V., Baumgärtner, W. and Schughart, K. 2010. Sustained viral load and late death in Rag2-/- mice after influenza A virus infection. *Virology Journal* 7(1), pp. 1–6. doi: 10.1186/1743-422x-7-172.
Wu, T., Hu, Y., Lee, Y.-T., Bouchard, K.R., Benechet, A., Khanna, K. and Cauley, L.S. 2014. Lung-resident memory CD8 T cells (TRM) are indispensable for optimal cross-protection against pulmonary virus infection. *Journal of Leukocyte Biology* 95(2), pp. 215–224. doi: 10.1189/jlb.0313180.
Xu, L., Yoon, H., Zhao, M.Q., Liu, J., Ramana, C. v. and Enelow, R.I. 2004. Cutting Edge: Pulmonary Immunopathology Mediated by Antigen-Specific Expression of TNF-α by Antiviral CD8+ T Cells. *The Journal of Immunology* 173(2), pp. 721–725. doi: 10.4049/jimmunol.173.2.721.
Yacoub, D., Benslimane, N., Al-Zoobi, L., Hassan, G., Nadiri, A. and Mourad, W. 2013. CD154 Is Released from T-cells by a Disintegrin and Metalloproteinase Domain-containing Protein 10 (ADAM10) and ADAM17 in a CD40 Protein-dependent Manner. *Journal of Biological Chemistry* 288(50), pp. 36083–36093. doi: 10.1074/jbc.m113.506220.
Yan, I. et al. 2016. ADAM17 controls IL-6 signaling by cleavage of the murine IL-6Rα from the cell surface of leukocytes during inflammatory responses. *Journal of Leukocyte Biology* 99(5), pp. 749–760. doi: 10.1189/jlb.3a0515-207r/-/dc1.
Yang, W.S., Kim, J.J., Lee, M.J., Lee, E.K. and Park, S.K. 2018. ADAM17-Mediated Ectodomain Shedding of Toll-Like Receptor 4 as a Negative Feedback Regulation in Lipopolysaccharide-Activated Aortic Endothelial Cells. *Cellular Physiology and Biochemistry* 45(5), pp. 1851–1862. doi: 10.1159/000487876.
Yang, Z., Chan, K.I., Kwok, H.F. and Tam, K.Y. 2019. Novel Therapeutic Anti-ADAM17 Antibody A9(B8) Enhances EGFR-TKI–Mediated Anticancer Activity in NSCLC. *Translational Oncology* 12(11), pp. 1516–1524. doi: 10.1016/j.tranon.2019.08.003.
Ye, J., Yuen, S.M., Murphy, G., Xie, R. and Kwok, H.F. 2017. Anti-tumor effects of a 'human & mouse cross-reactive' anti-ADAM17 antibody in a pancreatic cancer model in vivo. *European Journal of Pharmaceutical Sciences* 110, pp. 62–69. doi: 10.1016/j.ejps.2017.05.057.

Yip, V. et al. 2014. Quantitative cumulative biodistribution of antibodies in mice: Effect of modulating binding affinity to the neonatal Fc receptor. *mAbs* 6(3), pp. 689–696. doi: 10.4161/mabs.28254.
Young, J. et al. 2010. Lymphotoxin-αβ heterotrimers are cleaved by metalloproteinases and contribute to synovitis in rheumatoid arthritis. *Cytokine* 51(1), pp. 78–86. doi: 10.1016/j.cyto.2010.03.003.
Yu, X. et al. 2011. Intensive Cytokine induction in Pandemic H1N1 Influenza Virus Infection Accompanied by Robust Production of IL-10 and IL-6. *Plos One* 6(12), p. e28680. doi: 10.1371/journal.pone.0028680.
Zanin, M., Baviskar, P., Webster, R. and Webby, R. 2016. The Interaction between Respiratory Pathogens and Mucus. *Cell Host and Microbe* 19(2), pp. 159–168. doi: 10.1016/j.chom.2016.01.001.
Zhao, Y. et al. 2008. Neutrophils may be a vehicle for viral replication and dissemination in human h5n1 avian influenza. *Clinical Infectious Diseases* 47(12), pp. 1575–1578. doi: 10.1086/593196.